ACADEMIC
REPORT

2024-2025

शैक्षणिक प्रतिवेदन
2024-2025

होमी भाभा राष्ट्रीय संस्थान
HOMI BHABHA NATIONAL INSTITUTE

(यूजीसी अधिनियम 1956 की धारा 3 के तहत एक मानद विश्वविद्यालय एवं
परमाणु ऊर्जा विभाग की एक सहायता प्राप्त संस्था)

(A Deemed to be University u/s 3 of UGC Act 1956 and a Grant-in-Aid
Institute of the Department of Atomic Energy, Govt. of India)

Location of HBNI Central Office, Constituent Institutions & Off Campus Centres

HBCH & RC, New Chandigarh

HBCH & MPMMCC Varanasi

VECC, Kolkata

HRI, Prayagraj

SINP, Kolkata

RRCAT, Indore

NISER, Bhubaneswar

IPR, Gandhinagar

IoP, Bhubaneswar

BARC, Mumbai

IMSc, Chennai

TMC, Mumbai

HBNI Central Office, Mumbai

IGCAR, Kalpakkam

Academic Report

(August 2024 to July 2025)

Contents

I am pleased to present to the Academic Report of the Institute for the year 2024-25 to all the stakeholders of HBNI with joy and pride. HBNI has emerged as one of the best Research University in the country that offers a variety of academic programs in frontier areas of national interest in Nuclear Science & Engineering and Cancer Healthcare. The excellent academic performance of the Institute is appropriately reflected in the latest rankings by the Ministry of Education (MoE). HBNI secured 7th rank in the Research Category, 12th rank in the University Category and 20th rank in Overall Category in NIRF-2025 rankings. I, hereby extend, heartiest congratulations as well as sincere thanks to all the contributors who helped us in achieving this feat par excellence.

During the Academic Year 2024-25, HBNI offered 46 programs in different disciplines. A total of 1158 new enrolments took place across all Cis and OCCS in these 46 programs. In the first ever held University Convocation on June 02, 2025, 293 students received doctoral degrees and during the Foundation Day on June 03, 2025, 131 students received M.Tech. degrees in this period. The academic output of our students of HBNI is well-reflected in the Nature-Index 2025 rank which is based on the publications in all subjects in Nature Group of Journals. I am pleased to inform you that HBNI was placed at 1st position with respect to publications in Physical Sciences and at 3rd position in overall category.

We are continuously striving to implement the recommendations of NEP 2020 to facilitate our students and cater to innovation, placement and academic flexibility. Several of such recommendations such as Institutional Innovation Council, Industry Linkage Centre, Placement Cell, Alumni Cell, Multiple Entry and Exit, Academic Bank of Credits, Research & Development Cell, Academic Break etc. have already been implemented at HBNI.

In order to expand our academic wings, we are adding new programs as well as new centres under our ambit. I am happy to share that Homi Bhabha Cancer Hospital & Research Centre, New Chandigarh, Punjab became our 13th OCC in April, 2025. We are also initiating 2 new programs from the next academic session i.e M.Sc. (Mathematics) and Ph.D. (Environmental Science and Engineering).

In this Academic Report, we are showcasing selected Ph.D. thesis highlights from all the disciplines, to give the readers a brief idea about the variety of scientific pursuits being undertaken by HBNI students as their research topics.

A comprehensive list of Ph.D., M.Tech., DM, MD and MCh students who have completed their program during this period is also presented at the end.

The continued support from all the stake holders of HBNI will ensure a smooth academic journey for our faculty and students. I, once again, thank one and all and look forward to the times ahead.

Thanking you and with best regards

U Kamachi Mudali

(U. Kamachi Mudali)

Introduction

Homi Bhabha National Institute (HBNI), the academic wing of DAE, was setup in 2005 as a deemed-to-be university under section 3 of the UGC act 1956, to boost and accelerate the academic programs in DAE institutions. Today, HBNI has grown into a highly reputed research university with valuable contributions to DAE as well as society. HBNI's excellent performance in the last 20 years is reflected in its National Assessment and Accreditation Council (NAAC, 2021) CGPA of 3.4 and a grade of A^+ as well as National Institutional Ranking Framework (NIRF) 2024 rank of 6^{th} in the Research Institution category. Since February 2014, HBNI is a fully funded grant-in-aid institute of the Department of Atomic Energy (DAE).

As on July 31, 2025, HBNI has the following 13 centres as its Constituent Institution (CI; 10 No.) and Off-Campus Centres (OCCs; 3 No.):

1. Bhabha Atomic Research Centre (BARC), Mumbai
2. Indira Gandhi Centre for Atomic Research (IGCAR), Kalpakkam
3. Raja Ramanna Centre for Advanced Technology (RRCAT), Indore
4. Variable Energy Cyclotron Centre (VECC), Kolkata
5. Saha Institute of Nuclear Physics (SINP), Kolkata
6. Institute for Plasma Research (IPR), Gandhinagar
7. Institute of Physics (IoP), Bhubaneswar
8. Harish-Chandra Research Institute (HRI), Prayagraj
9. Tata Memorial Centre (TMC), Mumbai
10. The Institute of Mathematical Sciences (IMSc), Chennai
11. National Institute of Science, Education and Research (NISER), Bhubaneswar
12. Homi Bhabha Cancer Hospital and Mahamana Pandit Madan Mohan Malaviya Cancer Centre (HBCH & MPMMCC), Varanasi
13. Homi Bhabha Cancer Hospital & Research Centre (HBCH & RC), New Chandigarh, Punjab

ACADEMIC PROGRAMMES OF THE INSTITUTE

The focus of HBNI is on research-based quality education programmes in Chemical Sciences, Engineering Sciences, Life Sciences, Medical and Health Sciences, Physical Sciences, Mathematical Sciences and Applied Systems Analysis, including Humanities & Social Sciences.

HBNI offered 46 academic programs during academic year 2024-25 under its 13 institutions and all the programmes were being conducted under the aegis of HBNI.

The range of academic programmes in various disciplines of science offered by HBNI are given below:

- **Ph.D.** degrees in varied disciplines (Applied System Analysis, Chemical Sciences, Computer Science, Computational Biology, Earth & Planetary Science, Engineering Sciences, Humanities & Social Sciences, Life Sciences, Mathematical Sciences, Medical & Health Sciences, Physical Sciences and Theoretical Computer Science)
- **Integrated Ph.D.** in Applied System Analysis, Chemical Sciences, Computational Biology, Engineering Sciences, Life Sciences, Mathematical Sciences and Theoretical Computer Science
- **M.Sc**. (Engineering Sciences), **M.Sc.** (Physics)
- **M.Sc**. (Nursing) and **M.Sc.** (Clinical Research)
- **M.Sc.** (Public Health in Epidemiology) and **Masters in Occupational Therapy in Oncology**
- **M.Sc.** (Nuclear Medicine and Molecular Imaging Technology)**, M.Sc. (Patient Navigation) and M.Sc.** (Nuclear Medicine Technology and Hospital Radio pharmacy)
- **M.Sc.** (Medical and Radiological Physics)
- **Integrated M.Sc.** (five-year duration in Chemical Sciences, Life Sciences, Mathematical Sciences and Physical Sciences)
- **Post-Graduate Medical Degree, M.D.** in various broad domains of Oncology
- **Super Specialty Medical Degree, D.M**., **M.Ch**. and **certified fellowships** in specialised domains of Oncology
- **Post graduate (PG) Diploma** in Nuclear Science and Engineering (**PGDNSE)**
- **PG Diploma** in Radiological Physics (**DipRP**)

More details about the courses and admission requirements are available on HBNI website: http://www.hbni.ac.in/.

ACADEMIC COLLABORATIONS

HBNI has signed Memorandum of Understanding (MoU) with several eminent academic institutions in the country and overseas to obtain the benefits from the mutual expertise in various research areas, teaching, learning, to facilitate collaborative research for the faculty and to enrich the knowledge of the students. The list of MoU institutions is given below:

1. Indian Institute of Science, Bangalore
2. Indian Institute of Technology, Bombay
3. Indian Institute of Technology, Kharagpur
4. Indian Institute of Technology, Kanpur

5. Indian Institute of Technology, Madras
6. Indian Institute of Technology, Indore
7. Indian Institute of Technology, Roorkee
8. Institute of Chemical Technology, Mumbai
9. Chennai Mathematical Institute, Chennai
10. Jadavpur University, Kolkata
11. Jawaharlal Nehru University, New Delhi
12. Panjab University, Chandigarh
13. Tata Institute of Fundamental Research, Mumbai
14. University of Calicut, Calicut
15. The Commissariat a I'energie atomique et aux energies alternatives, France*
16. Ghent University, Belgium*
17. Defence Institute of Advanced Technology, Pune
18. Indian Institute of Management (IIM), Ahmedabad
19. Confederation of Indian Industry (CII), Mumbai
20. Indian Institute of Technology, Delhi
21. Indian Institute of Technology, Jammu
22. Indian Institute of Technology, Guwahati
23. Jawaharlal Nehru Centre for Advanced Scientific Research (JNCASR), Bangalore
24. AIC RRCAT PI-Hub Foundation (AIC π-Hub), Indore
25. Indian Institute of Technology, Hyderabad
26. AIC-IPR Plasmatech Innovation Foundation, Gandhinagar

The MoUs from S. No.'s 21-26 were signed during the Academic Year 2024-25. These MoUs enable HBNI students to attend courses at above mentioned institutes and earn course credits. Research collaborations are also possible between HBNI and institutes under MoU. HBNI students can avail research facilities of these institutes. Faculty of such institutes can also be co-guides of HBNI students and vice versa.

*Under Renewal

COURSES CONDUCTED BY HBNI DURING 2024-25

1) Online course on Research Methodology & Research and Publication Ethics

University Grants Commission in its 53rd meeting held on August 9, 2019 approved a two-credit course for awareness about the publication ethics and publication misconducts entitled "Research and Publication Ethics (RPE)" to be made mandatory for all Ph.D. students for pre-registration course work. Accordingly, a course on Research Methodology encompassing the RPE course has been developed and being offered to the students of all the CIs and OCC of HBNI since 2021-2022 academic session.

The course consists of 45 lectures and has three modules: (a) Module A: Research design and methods (18 lectures); (b) Module B: Research and Publication Ethics (12 lectures); (c) Module C: Computational and Experimental Methods (15 lectures). During FY 2024-25, lectures on Module A and B were delivered by Prof. B. K. Nayak, Prof. Prabuddha Ganguli and Prof. V. Siruguri. Total 300 students from different CI and OCC attended the course during February to April 2024.

2) Online Course on Advanced Materials Chemistry

An online course on "Advanced Materials Chemistry" was conducted by HBNI from October 14-December 23, 2024. Prof. Vinita G. Gupta, BARC was the Course Director. The broad topics covered under the course included general materials chemistry, characterization techniques, major trace and ultra-trace chemical analysis techniques, and functional materials. Twenty-nine students from CIs/OCC of HBNI and other educational institutes from all over India attended the course and benefitted from it.

3) Nuclear Leadership Development Programme

HBNI has entered into a Memorandum of Understanding (MoU) with Indian Institute of Management, Ahmedabad [IIM (A)]. The objective of this MoU is to create a framework for HBNI to avail the services of IIM (A) in providing a customized Management Development Programme (MDP) for the senior executives of DAE organizations.

A Nuclear Leadership Development Programme was conducted during March 22-27, 2025 at Indian Institute of Management(A) for 30 participants from NPCIL. The training programme consisted of three sessions in a day and covered topics on effective project management approaches, uncertainty and risk management in nuclear project, financial analysis using ratios, Mapping and influencing difficult stakeholders in Nuclear Projects etc.

Council of Management

(As on July 31, 2025)

Prof. A. K. Mohanty, Secretary DAE & Chairman, AEC	**Chairman**
Prof. U. Kamachi Mudali, Vice Chancellor, HBNI	Member
Shri Vivek Bhasin, Director, BARC	Member
Ms. Seema Jain, Member (Finance), AEC	Member
Dr. Sumit Som, Director, VECC	Member
Dr. Sudeep Gupta, Director, TMC	Member
Prof. H. N. Ghosh, Director, NISER	Member
Prof. Ujjwal Sen, Director, HRI	Member
Dr. V. S. Ramamurthy, Emeritus Professor, NIAS, Bengaluru	Member
Dr. S. Sivaram, Emeritus Professor, IISER Pune & Hon. Professor, IISER, Kolkata	Member
Prof. A. K. Tyagi, Dean, HBNI	Member
Shri Hari Narayan Sahu	Non-Member Secretary

Academic Council

(As on July 31, 2025)

Prof. U. Kamachi Mudali, Vice Chancellor, HBNI	**Chairperson**
Prof. A. K. Tyagi, Dean, HBNI	Member
Shri Vivek Bhasin, Director, BARC	Member
Shri C. G. Karhadkar, Director, IGCAR	Member
Shri Unmesh D. Malshe, Director, RRCAT	Member
Prof. Sumit Som, Director, VECC	Member
Prof. Gautam Bhattacharyya, Director, SINP	Member
Prof. Shashank Chaturvedi, Director, IPR	Member
Prof. Karuna Kar Nanda, Director IoP	Member
Prof. V. Ravindran, Director, IMSc	Member
Prof. Ujjwal Sen, Director, HRI	Member
Prof. Sudeep Gupta, Director, TMC	Member
Dr. Satyajit Pradhan, Director, HBCH & MPMMCC	Member
Prof. H. N. Ghosh, Director, NISER	Member
Prof. Siva Umapathy, IISc, Bengaluru	Member
Prof. Manoj K. Tiwari, IIM, Mumbai	Member
Prof. Devang V. Khakhar, IIT, Bombay	Member
Prof. D. V. Udupa, BARC	Member
Prof. Pankaj Chaturvedi, TMC	Member
Dr. Ashish Gulia, Director, HBCH & RC, New Chandigarh, Punjab	Member
Prof. A. Srinivasan, NISER	Member
Prof. Pranay Kumar Swain, Convenor, BoS (Applied Systems Analysis)	Member
Prof. Bedangadas Mohanty, Convenor, BoS (Physical Sciences)	Member
Prof. R. Tewari, Convenor, BoS (Engineering Sciences)	Member
Prof. S. Gautam, Convenor, BoS (Life Sciences)	Member
Prof. Manoj Kumar Yadav, Convenor, BoS (Mathematical Sciences)	Member
Prof. S. D. Banavali, Convenor, BoS (Medical & Health Sciences)	Member
Prof. Chandra Nath Patra, Convenor, BoS (Chemical Sciences)	Member
Prof. C. Gunanathan, Convenor, BoS (Int. Master's Programme)	Member
Prof. Mainak Bandyopadhyay, Convenor, BoS (Interdisciplinary Science & Engineering)	Member
Shri Hari Narayan Sahu, Registrar, HBNI	Secretary

Planning & Monitoring Board

(As on June 30, 2025)

Prof. U. Kamachi Mudali, Vice Chancellor, HBNI	**Chairperson**
Shri Vivek Bhasin, Director, BARC	Member
Prof. A. K. Tyagi, Dean, HBNI	Member
Prof. R. B. Grover, Member, AEC	Member
Shri C. G. Karhadkar, Director, IGCAR	Member
Prof. S. Chaturvedi, Director, IPR	Member
Prof. G. Bhattacharyya, Director, SINP	Member
Prof. Devang Khakhar, IIT Bombay	Member
Prof. Amlan J. Pal, Director, UGC-DAE Consortium for Scientific Research, Indore	Member
Prof. Jayaram N. Chengalur, Director, TIFR	Member
Shri Hari Narayan Sahu, Registrar, HBNI	Secretary

Officers of the Institute

(As on July 31, 2025)

Academic	
Prof. U. Kamachi Mudali	Vice Chancellor
Prof. A. K. Tyagi	Dean
Prof. Naveen Kumar	Associate Dean
Prof. Dipanwita Dutta	Associate Dean
Prof. Madhumita Goswami	Associate Dean
Dr. Rachna Agarwal	Assistant Dean
Administrative & Accounts	
Shri Hari Narayan Sahu	Registrar
Shri S. Jakhotiya	Finance Officer
Shri K. K. Dange	Dy. Registrar
Ms. Pramila M. Rani	Sr. Accounts Officer
Ms. Preeti Ubale	Asst. Accounts Officer
Ms. Gomti Iyer	Asst. Personal Officer

Boards of Studies
(As on July 31, 2025)

BoS, Chemical Sciences	**Balancing Members:**
1. Prof. C. N. Patra, BARC - Convener	1. Dr. Manjusha Vagal, TMC
2. Prof. V. Sudarsan, BARC - Co-Convener	2. Prof. Madhumita Goswami, HBNI
3. Prof. A. Dutta, IIT Bombay	
4. Prof. Tapas Das, BARC	**BoS, Life Sciences**
5. Prof. Madhumita Goswami, HBNI	1. Prof. S. Gautam, BARC - Convener
6. Prof. K. A. Venkatesan, IGCAR	2. Prof. Harapriya Mohapatra, NISER - Co-Convener
7. Prof. A. Srinivasan, NISER	3. Prof. Praful Singru, SBS, NISER
8. Prof. H. S. Biswal, NISER	4. Prof. Rahul Siddharthan, IMSc
9. Prof. Deepa Khushalani, TIFR	5. Prof. Sorab Dalal, ACTREC
10. Prof. Avinash Kumbhar, SPPU	6. Prof. Chandrima Das, SINP
Balancing Members:	7. Prof. B. S. Patro, BARC
1. Prof. B. S. Patro, BARC	8. Prof. B. N. Pandey, BARC
	9. Prof. Y. V. Nancharaiah, BARC-Kalpakkam
BoS, Engineering Sciences	10. Prof. Sharmila Bapat, NCCS, Pune
1. Prof. R. Tewari, BARC - Convener	**Balancing Members:**
2. Prof. J. Chattopadhyay, BARC - Co-Convener	1. Prof. Shovan Majumder, RRCAT
3. Prof. G. Sugilal, BARC	2. Dr. Rachna Agarwal, HBNI
4. Prof. Paritosh Nanekar, BARC	
5. Prof. V. G. Gaikar, ICT, Mumbai	**BoS, Mathematical Sciences**
6. Prof. P. Y. Nabhiraj, VECC	1. Prof. Manoj Kumar Yadav, HRI - Convener
7. Prof. C. P. Paul, RRCAT	2. Prof. Sanoli Gun, IMSc - Co-Convener
8. Prof. B. Dikshit, BARC	3. Prof. Brundaban Sahu, NISER
9. Prof. Alphonsa Joseph, IPR	4. Prof. K. Sandeep, TIFR, Bengaluru
10. Prof. Anish Kumar, IGCAR	5. Prof. K. V. Subrahmanyam, CMI, Chennai
Balancing Members:	6. Prof. Anil Kumar Karn, NISER
1. Prof. Gopika Vinod, BARC	7. Prof. Saket Sourabh, IMSc
2. Prof. Naveen Kumar, HBNI	8. Prof. Umesh V. Dubey, HRI
3. Prof. A. K. Dureja, BARC	9. Prof. Dishant Mayurbhai Pancholi, IMSc
	10. Prof. Aritra Banik, NISER
BoS, Medical & Health Sciences	**Balancing Members:**
1. Prof. S. D. Banavali, TMC - Convener	1. Prof. Naveen Kumar, HBNI
2. Prof. Sandeep Basu, RMC-Co-Convener	
3. Prof. Sudeep Gupta, Director, TMC	**BoS, Physical Sciences**
4. Dr. Nithya Gogtay, KEM Hospital, Mumbai	1. Prof. B. Mohanty, NISER - Convener
5. Dr. Ashutoshnath Agarwal, PGIMER, Chandigarh	2. Prof. V. K. Aswal, BARC- Co-Convener
6. Dr. Manisha Pawar, TMH	3. Prof. Anushuman Maharana, HRI
7. Prof. Siddhartha Laskar, TMC	4. Prof. Awadhesh Mani, IGCAR
8. Dr. Ajay Puri, TMC	5. Prof. D. Indumathi, IMSc
9. Dr. J. P. Agarwal, TMC	6. Prof. Arijit Saha, loP
10. Dr. Suyash Kulkarni, TMC	7. Prof. Sudip Sengupta, IPR

8. Prof. Shovan Majumder, RRCAT	**BoS, Interdisciplinary Science and Engineering**
9. Prof. Gopal Mukherjee, VECC	1. Prof. Mainak Bandyopadhyay, IPR - Convener
10. Prof. Amit Ghosh, SINP	2. Prof. P. A. Hassan, BARC – Co-Convener
Balancing Members:	3. Prof. Anish Kumar, IGCAR
1. Prof. D. Dutta, HBNI	4. Prof. Balchandra M. Bhanage, ICT, Mumbai
	5. Prof. Awadhesh Mani, IGCAR
BoS, Studies for Applied Systems Analysis	6. Prof. Gopika Vinod, BARC
1. Prof. Pranay Swain, HBNI-Convener	7. Prof. C. P. Paul, RRCAT
2. Prof. Karuna Jain, IIT Bombay	8. Prof. P.Y. Nabhiraj, VECC
3. Prof. A. K. Dureja, HBNI/BARC	9. Prof. Siddhartha Laskar, TMC
4. Prof. Surinder Jaswal, TISS	10. Prof. Harapriya Mohapatra, NISER
5. Prof. Amit Garg, IIM Ahmedabad	**Balancing Members:**
6. Prof. Jyotirmayee Mohanty, BARC	1. Dr. Rachna Agarwal, HBNI
7. Prof. A. K. Nayak, NCPW	
8. Dr. Garima Sharma, NCPW	
Balancing Members:	
1. Prof. D. Dutta, HBNI	

BoS, Integrated Masters Programme
1. Prof. Chidambaram Gunanathan, NISER – Convener
2. Prof. Pranay Swain, NISER – Co-Convener
3. Chair, School of Life Sciences, NISER (Ex-Officio)
4. Chair, School of Chemical Sciences, NISER (Ex-Officio)
5. Chair, School of Mathematics, NISER (Ex-Officio)
6. Chair, School of Physical Sciences, NISER (Ex-Officio)
7. Chair, School of Undergraduate Studies Committee, NISER (Ex-Officio)
8. Prof. Anirban Basu, HRI
9. Prof. Arijit Saha, loP
10. Prof. Sujit Roy, IIT Bhubaneswar
Balancing Members:
1. Prof. D. Dutta, HBNI
2. Prof. Manoj Kumar Yadav, HRI

Deans (Academics) at Constituent Institutes (CIs) and Off-Campus Centres (OCCs)
(As on July 31, 2025)

CI/ OCC	Discipline	Dean-Academic
Bhabha Atomic Research Centre (BARC)	Chemical Sciences	Prof. Chandra Nath Patra
	Engineering Sciences I	Prof. (Smt.) Sulekha Mukhopadhyay
	Engineering Sciences II	Prof. Gopika Vinod
	Life Sciences	Prof. Birija Sankar Patro
	Medical & Health Sciences	Prof. Sandip Basu
	Physical & Mathematical Sciences	Prof. Dinesh Udupa
Indira Gandhi Centre for Atomic Research	Chemical Sciences	Prof. C. V. S. Brahmananda Rao
	Engineering Sciences	Prof. A. Nagesha
	Physical Sciences	Prof. Awadhesh Mani
Raja Ramanna Centre for Advanced Technology	All Disciplines	Prof. Shovan K. Majumder
Variable Energy Cyclotron Centre	Engineering Sciences	Prof. Nabhiraj P. Yalagoud
	Physical Sciences	Prof. Parnika Das
Saha Institute of Nuclear Physics	Chemical & Life Sciences	Prof. Oishee Chakrabarti
	Physical Sciences	Prof. Harvendra Singh
Institute for Plasma Research	All Disciplines	Prof. Raju Daniel
Institute of Physics	Physical Sciences	Prof. Arijit Saha
Harish-Chandra Research Institute	All Disciplines	Prof. Punita Batra
The Institute of Mathematical Sciences	Life Sciences	Prof. Sitabhra Sinha
	Mathematical Sciences	Prof. Anirban Mukhopadhyay
	Physical Sciences	Prof. R. Rajesh
Tata Memorial Centre	All Disciplines	Prof. Shripad Banavali
National Institute of Science, Education and Research	All Disciplines	Prof. Pranay Swain
Homi Bhabha Cancer Hospital and Mahamana Pandit Madan Mohan Malaviya Cancer Centre	All Disciplines	Dr. Shashikant C. U. Patne

BoS Wise List of Faculty Members at CIs and OCCs of HBNI

HBNI, Central Office, Mumbai	
S. No.	Faculty Name
1	Prof. U. Kamachi Mudali
2	Prof. A. K. Tyagi
3	Prof. Dipanwita Dutta
4	Prof. Naveen Kumar
5	Prof. Madhumita Goswami
6	Dr. Rachna Agarwal

Applied Systems Analysis	
NISER, Bhubaneswar	
S. No.	Faculty Name
7	Dr. Amarendra Das
8	Dr. Amarjeet Nayak
9	Dr. Debashis Pattanaik
10	Dr. Joe Varghese Yeldho
11	Dr. Pranaya Kumar Swain
12	Dr. Rooplekha Khuntia

Chemical Sciences	
BARC	
S. No.	Faculty Name
13	Prof. Ashis Kumar Satpati
14	Prof. Chiranjib Majumder
15	Prof. Hari Prasad Upadhyaya
16	Prof. Hassan P. A.
17	Prof. Hirendra Nath Ghosh
18	Prof. Jyotirmayee Mohanty
19	Prof. K. Dash
20	Prof. Kallola Kumar Swain
21	Prof. Kathi Sudarshan
22	Prof. M. C. Rath
23	Prof. Madhava B. Mallia
24	Prof. Mrinal R. Pai
25	Prof. Niharendu Choudhury
26	Prof. Puspalata Rajesh
27	Prof. R. Mishra
28	Prof. Raghunath Acharya
29	Prof. Rajesh V. Pai
30	Prof. S. Jeyakumar
31	Prof. S. N. Achary
32	Prof. Salil Varma
33	Prof. Sangita D. Kumar
34	Prof. Sanjukta A. Kumar
35	Prof. Shilpa N. Sawant
36	Prof. Subir Kumar Ghosh
37	Prof. Sudarsan V.
38	Prof. Sukhendu Nath

39	Prof. Suparna Sodaye
40	Prof. Suresh Chandra Parida
41	Prof. Tapas Das
42	Prof. Tirumalesh Keesari
43	Prof. Vandana Pulhani
44	Prof. Vinita Grover Gupta
45	Prof. Virendra Kumar
46	Prof. Y. K. Bhardwaj
47	Dr. A. C. Bhasikuttan
48	Dr. A. Jahur Mondal
49	Dr. Adish Tyagi
50	Dr. Aditi Chakrabarty Patra
51	Dr. Adya Prasad Mishra
52	Dr. Aishwarya Soumitra Kar
53	Dr. Ajay K. Singh
54	Dr. Ajish Kumar K. S.
55	Dr. Amit Kunwar
56	Dr. Ankita Rao
57	Dr. Ankur Saha
58	Dr. Anupkumar B.
59	Dr. Apurav Guleria
60	Dr. Arijit Sengupta
61	Dr. Arnab Sarkar
62	Dr. Aruna Kumar M.
63	Dr. Arunasis Bhattacharyya
64	Dr. Arup Kumar Pathak
65	Dr. Asim Kumar Ghosh
66	Dr. Atanu Barik
67	Dr. Atindra Banerjee

68	Dr. Bal Govind Vats
69	Dr. Balaji Prasad Mandal
70	Dr. Beena G. Singh
71	Dr. Bholanath Mahanty
72	Dr. Biswajit Sadhu
73	Dr. Brindaban Modak
74	Dr. Chhavi Agarwal
75	Dr. Dayamoy Banerjee
76	Dr. Debashis Banerjee
77	Dr. Dhanadeep Dutta
78	Dr. Dibakar Goswami
79	Dr. Dimple Dutta
80	Dr. Drishty Satpati
81	Dr. Goutam Chakraborty
82	Dr. Gunjan Verma
83	Dr. Hemant Shivram Sodaye
84	Dr. Hirakendu Basu
85	Dr. J. Selvakumar
86	Dr. Jayashree Biswal
87	Dr. Jayshree Ramkumar
88	Dr. Juby K. Ajish
89	Dr. Jyoti Prakash
90	Dr. K. C. Barick
91	Dr. K. R. S. Chandrakumar
92	Dr. Kaushik Sanyal
93	Dr. Kaustava Bhattacharyya
94	Dr. Kedarnath G.
95	Dr. Kumar Abhinav Dubey
96	Dr. Mahesh Sundararajan

97	Dr. Mahesh Tiwari
98	Dr. Mainak Roy
99	Dr. Malaya Kumar Nayak
100	Dr. Manidipa Basu
101	Dr. Manjulata Sahu
102	Dr. Manoj Kumar Sharma
103	Dr. Manoj Kumbhakar
104	Dr. Manoj Mohapatra
105	Dr. Mhejabeen Sayed
106	Dr. Mohini Guleria
107	Dr. Musharaf Ali S. K.
108	Dr. N. N. Meeravali
109	Dr. Naina Raje
110	Dr. Nandita Maiti
111	Dr. Neetika Rawat
112	Dr. Nilanjal Misra
113	Dr. Nilotpal Barooah
114	Dr. Nimai Pathak
115	Dr. Ningthougam Raghumani Singh
116	Dr. P. Chandramohan
117	Dr. P. Mathi
118	Dr. P. S. Ramanjaneyulu
119	Dr. Pallavi Singhal
120	Dr. Pankaj Kumar Patro
121	Dr. Parveen Kumar Verma
122	Dr. Patra Chandra Nath
123	Dr. Prabhat Kumar Singh
124	Dr. Pradeep Kumar

125	Dr. Pramod Sharma
126	Dr. Prasad Padmakar Phadnis
127	Dr. Priya Maheshwari
128	Dr. R. Ganguly
129	Dr. Raghunath Chowdhury
130	Dr. Rahul Tripathi
131	Dr. Rajib Ghosh
132	Dr. Rajini P. Antony
133	Dr. Rama Mohana Rao Dumpala
134	Dr. Ravi Joshi
135	Dr. Remya Devi P. S.
136	Dr. Rimpi Dawar
137	Dr. Ritesh Ruhela
138	Dr. Ritu M. Shrivastav
139	Dr. Rubel Chakravarty
140	Dr. Ruma Gupta
141	Dr. Sabyasachi Patra
142	Dr. Sabyasachi Rout
143	Dr. Sajeev Y.
144	Dr. Sandeep Kumar Sharma
145	Dr. Sandeep Nigam
146	Dr. Sandip Dey
147	Dr. Sangita D. Lenka
148	Dr. Sanhita Chaudhury
149	Dr. Sanjay Kumar
150	Dr. Santosh Kumar Gupta
151	Dr. Saurav Kumar Guin
152	Dr. Seemita Banerjee

153	Dr. Seraj Ahmad Ansari
154	Dr. Sharmistha Dutta Choudhury
155	Dr. Sipra Choudhury
156	Dr. Soumyaditya Mula
157	Dr. Srinivasu Kancharlapalli
158	Dr. Suchandra Chatterjee
159	Dr. Suchismita Mishra
160	Dr. Sumana Sengupta
161	Dr. Sumit Kumar
162	Dr. Surajit Panja
163	Dr. Tijo Joseph V.
164	Dr. Usha Pandey
165	Dr. V. Kusum Vats
166	Dr. Veena Subramanian
IGCAR	
167	Dr. A. S. Suneesh
168	Dr. A. Sree Rama Murthy
169	Dr. Arindam Das
170	Dr. Ashish Jain
171	Dr. B. Anandkumar
172	Dr. B. Sreenivasulu
173	Dr. C.V.S. Brahmmananda Rao
174	Dr. Chowdari Jagadeeswara Rao
175	Dr. G. Gopakumar
176	Dr. Hrudananda Jena
177	Dr. K. A. Venkatesan
178	Dr. K. I. Gnanasekar
179	Dr. K. Sundararajan
180	Dr. N. Ramanathan
181	Dr. Pavan Kumar Narayanam
182	Dr. R. Kumar
183	Dr. R. Kumaresan
184	Dr. R. Venkata Krishnan
185	Dr. Rajesh Ganesan
186	Dr. Satendra Kumar
187	Dr. Sublime Ningshen
188	Dr. V. Jayaraman
NISER	
189	Dr. Alagar Srinivasan
190	Dr. Arindam Ghosh
191	Dr. Bhargava B. L.
192	Dr. Bidraha Bagh
193	Dr. Bishnu Prasad Biswal
194	Dr. Chandra Shekhar Purohit
195	Dr. Chidambaram Gunanathan
196	Dr. Dipak Samanta
197	Dr. Himansu Sekhar Biswal
198	Dr. Jogendra Nath Behera
199	Dr. Moloy Sarkar
200	Dr. Nagendra Kumar Sharma
201	Dr. Nembenna Sharanappa
202	Dr. P. C. Ravikumar
203	Dr. Prasenjit Mal
204	Dr. Sanjib Kar
205	Dr. Saravanan Peruncheralathan

206	Dr. Subhadip Ghosh
207	Dr. Sudip Barman
208	Dr. Upakarasamy Lourderaj
209	Dr. Venkatasubbaiah Krishnan
RRCAT	
210	Dr. Dipankar Nanda
SINP	
211	Dr. Barun Kumar Maity
212	Dr. Dulal Senapati
213	Dr. Montu K. Hazra
214	Dr. Padmaja Prasad Mishra
215	Dr. Srestha Basu

Engineering Sciences	
BARC	
216	Prof. A. Vinod Kumar
217	Prof. Adarsh Kumar Dureja
218	Prof. Alok Awasthi
219	Prof. Amit Sinha
220	Prof. Aniruddha Biswas
221	Prof. Arijit Laik
222	Prof. Biswaranjan Dikshit
223	Prof. D. C. Kar
224	Prof. Deep Prakash
225	Prof. Dinesh Kumar Chandraker
226	Prof. Geogy Jiju Abraham
227	Prof. Gopalakrishnan Sugilal
228	Prof. Gopika Vinod

229	Prof. Imran Ali Khan
230	Prof. Jayanta Chattopadhyay
231	Prof. Joydipta Banerjee
232	Prof. Jung Bahadur Singh
233	Prof. K. Anand Rao
234	Prof. Kapilesh Bhargava
235	Prof. Kinshuk Dasgupta
236	Prof. Kulwant Singh
237	Prof. M. K. Samal
238	Prof. Manoj Kumar
239	Prof. Paritosh Prabhakar Nanekar
240	Prof. R. Karthikeyan
241	Prof. Raghvendra Tewari
242	Prof. Rajeev Kapoor
243	Prof. Rajesh Kumar
244	Prof. Ram Niwas Singh
245	Prof. Rishi Verma
246	Prof. S. K. Satpati
247	Prof. S. R. Shimjith
248	Prof. Samiran Sengupta
249	Prof. Sanjib Majumdar
250	Prof. Sudipta Chakraborty
251	Prof. Sulekha Mukhopadhyay
252	Prof. Suneel Kumar Gupta
253	Prof. Supratik Roychowdhury
254	Prof. Tarasankar Mahata
255	Prof. Tessy Vincent
256	Prof. Yogita Parulekar

257	Dr. Abhijeet Mohan Vaidya
258	Dr. Abhijit Raha
259	Dr. Abhishek Mukherjee
260	Dr. Anil Kumar Tiwari
261	Dr. Anindya Chakravarty
262	Dr. Bhaskar Paul
263	Dr. Chiradeep C. Gupta
264	Dr. Dauji Saha
265	Dr. Debanik Roy
266	Dr. Gaurav Bhutani
267	Dr. K. K. Singh
268	Dr. Kamal Sharma
269	Dr. Kamlesh Chandra
270	Dr. Karri Venkata Mani Krishna
271	Dr. M. Hari Prasad
272	Dr. Maha Nand Jha
273	Dr. Mahendra Prasad
274	Dr. Mithilesh Kumar
275	Dr. Nirvik Sen
276	Dr. Noble Jacob
277	Dr. Onkar Suresh Gokhale
278	Dr. Poulami Chakraborty Srivastava
279	Dr. Prabhat Ranjan
280	Dr. Pranesh Sengupta
281	Dr. Praveen Kumar
282	Dr. Punit Arora
283	Dr. Ranjan Kumar
284	Dr. Sabyasachi Mitra
285	Dr. Sangita Pal
286	Dr. Soumitra Kar
287	Dr. Suman Neogy
288	Dr. Surender Kumar Sharma
289	Dr. Tammana Sree Rama Chandra Murthy
290	Dr. Vishwanadh Bathula
IGCAR	
291	Prof. A. Nagesha
292	Prof. Aniruddha Moitra
293	Prof. Anish Kumar
294	Prof. M. Vasudevan
295	Prof. Mahadevan S.
296	Prof. R. Suresh Kumar
297	Prof. V. Karthik
298	Dr. A. Jasmin Sudha
299	Dr. A. Ravi Shankar
300	Dr. B. Arivazhagan
301	Dr. C. Sudha
302	Dr. Chitta Ranjan Das
303	Dr. D. Sornadurai
304	Dr. David Vijayanand V.
305	Dr. Diptimayee Samantaray
306	Dr. G.V. Prasad Reddy
307	Dr. Matcha Nani Babu
308	Dr. P. Mangarjuna Rao
309	Dr. R. Mythili
310	Dr. R. Priya
311	Dr. S. Thirunavukkarasu

312	Dr. T. Sakthivel
313	Dr. Vani Shankar
314	Dr. Venkata Satyamu Sanapala
IPR	
315	Prof. Paritosh Chaudhuri
316	Prof. Vipulkumar L. Tanna
317	Dr. Alphonsa Joseph
318	Dr. Manoj Kumar Gupta
319	Dr. Nirav I. Jamnapara
320	Dr. Rajesh Kumar
321	Dr. Rana Pratap Yadav
322	Dr. Ritesh Sugandhi
323	Dr. Suryakant B. Gupta
324	Dr. Vishal Jain
NISER	
325	Dr. Anup Kumar Bhattacharya
326	Dr. Sabyasachi Karati
RRCAT	
327	Prof. Christ Prakash Paul
328	Prof. Mangesh Balkrishna Borage
329	Dr. Ajit Upadhyay
330	Dr. Prabhat Kumar Gupta
331	Dr. Rahul Shukla
332	Dr. Vikas Kumar Jain
VECC	
333	Prof. P. Y. Nabhiraj
334	Prof. Paramita Mukherjee
335	Prof. Sandip Pal
336	Prof. Tapatee Kundu Roy
337	Dr. Hemendra Kumar Pandey

Life Sciences	
BARC	
338	Prof. Anand D. Ballal
339	Prof. Anand M. Badigannavar
340	Prof. Anu Ghosh
341	Prof. Archana Mukherjee
342	Prof. B. K. Das
343	Prof. B. N. Pandey
344	Prof. Bhavani S. Shankar
345	Prof. Birija Sankar Patro
346	Prof. Deepak Sharma
347	Prof. Joy G. Manjaya
348	Prof. Mahesh Subramanian
349	Prof. Nagesh Bhat
350	Prof. Ravindra D. Makde
351	Prof. S. N. Jamdar
352	Prof. Sandur Santosh Kumar
353	Prof. Satyendra Gautam
354	Prof. Sheetal Uppal
355	Prof. Y. V. Nancharaiah
356	Dr. Ajay Saini
357	Dr. Aman Kumar Ujaoney
358	Dr. Amit Das
359	Dr. Amit Kumar
360	Dr. Ananganti Narasimha
361	Dr. Archana Joshi Saha

362	Dr. Archana N. Rai
363	Dr. Aruna Jyothi Kora
364	Dr. Ashish Kumar Srivastava
365	Dr. Avik Chakraborty
366	Dr. Bhakti Basu
367	Dr. Bhaskar Sanyal
368	Dr. Bibhuti Bhusan Mishra
369	Dr. Celin Acharya
370	Dr. Chandan Kumar
371	Dr. Chitra Seetharam Misra
372	Dr. Dharmendra Kumar Maurya
373	Dr. Gagan Deep Gupta
374	Dr. Hema Rajaram
375	Dr. Himanshi N. Mishra
376	Dr. Himanshu Tak
377	Dr. Hiren Joshi
378	Dr. J. Souframanien
379	Dr. Jayakumar Sundarraj
380	Dr. Jitendra Kumar
381	Dr. Jyoti Tripathi
382	Dr. Manisha Banerjee
383	Dr. Mrityunjay Tyagi
384	Dr. Murali M. S. Balla
385	Dr. P. Sriyutha Murthy
386	Dr. Pramod Kumar Gupta
387	Dr. R. Shashidhar
388	Dr. Raghvendra Shridharrao Patwardhan
389	Dr. Rahul Checker
390	Dr. Rajani Kant Chittela
391	Dr. Rajesh Kumar
392	Dr. Ramesh Hire
393	Dr. Rath Devashish
394	Dr. S. T. Mehetre
395	Dr. Sachin Nandkumar Hajare
396	Dr. Sanjeev Kumar
397	Dr. Shraddha Singh
398	Dr. Sonia Chadha
399	Dr. Subhash Chandra Bihani
400	Dr. Sudhanshu Saxena
401	Dr. Sudhir Kumar Gupta
402	Dr. Sudhir Kumar Shukla
403	Dr. Sudhir Singh
404	Dr. Suman Bakshi
405	Dr. Sumit Gupta
406	Dr. Suvendu Mondal
407	Dr. Swathi Kota
408	Dr. Sweetie R. Kanatt
409	Dr. Vandan Nagar
410	Dr. Vinay Jain
411	Dr. Vishal Prashar
412	Dr. Yogendra Singh Rajpurohit
IMSc	
413	Dr. Areejit Samal
414	Dr. Rahul Siddharthan
415	Dr. Sandeep Choubey
NISER	

416	Prof. Konkimalla Venkatsai Badireenath
417	Dr. Aniruddha Datta Roy
418	Dr. Asima Bhattacharyya
419	Dr. Chandan Goswami
420	Dr. Debasmita Pankaj Alone
421	Dr. Harapriya Mohapatra
422	Dr. Himabindu Vasuki Kilambi
423	Dr. Kishore Chandrasekhar Panigrahi
424	Dr. Manjusha Dixit
425	Dr. Mohammed Saleem
426	Dr. Palok Aich
427	Dr. Pankaj Vidyadhar Alone
428	Dr. Praful S. Singru
429	Dr. Renjith Mathew
430	Dr. Rudresh Acharya
431	Dr. Srinivasan Ramanujam
432	Dr. Subhasis Chattopadhyay
433	Dr. Swagata Ghatak
434	Dr. Tirumala Kumar Chowdary
RRCAT	
435	Dr. Ashwani Kumar
436	Dr. Khageswar Sahu
437	Dr. Rashmi Shrivastava
SINP	
438	Prof. Debashis Mukhopadhyay
439	Dr. Aditi Chandra
440	Dr. Chandrima Das
441	Dr. H. Raghuraman
442	Dr. Kaushik Sengupta
443	Dr. Oishee Chakrabarti
444	Dr. Sangram Bagh
445	Dr. Soumen Kanti Manna
446	Dr. Subhabrata Majumder
447	Dr. Subhendu Roy
448	Dr. Tofayel Ahmed
449	Dr. Udayaditya Sen
TMC	
450	Prof. Arvind D. Ingle
451	Prof. Manoj Balkrishna Mahimkar
452	Prof. Sorab Nariman Dalal
453	Dr. Abhijit De
454	Dr. Ashok Varma
455	Dr. Chilakapati Murali Krishna
456	Dr. Dibyendu Bhattacharyya
457	Dr. Jyoti Anand Kode
458	Dr. Kakoli Bose
459	Dr. Khizer Hasan Syed
460	Dr. Nandini Verma
461	Dr. Pritha Ray
462	Dr. Rohan Jayant Khadilkar
463	Dr. Sanjay Gupta
464	Dr. Sanjeev Waghmare
465	Dr. Sejal Patwardhan
466	Dr. Sharath Chandra Arandkar
467	Dr. Sonam Mehrotra
468	Dr. Subir Biswas

469	Dr. Sunil S. Kumar Shetty
470	Dr. Venkatraman Prasanna
471	Dr. Vikram Suryaprakash Gota

Mathematical Sciences	
HRI	
472	Prof. Manoj Kumar
473	Prof. P. K. Ratnakumar
474	Prof. Punita Batra
475	Prof. Ravindranathan Thangadurai
476	Prof. Surya D. Ramana
477	Dr. Anirban Mukhopadhyay
478	Dr. Brundaban Sahu
479	Dr. Indrava Roy
480	Dr. Panchugopal Bikram
481	Dr. Pralay Chatterjee
482	Dr. Tuhin Ghosh
483	Dr. Umesh Kumar Vanktesh Dubey
484	Dr. Vikram Sharma
IMSc	
485	Prof. Amritanshu Prasad
486	Prof. Jaya N. Iyer
487	Prof. Saket Saurabh
488	Prof. Sankaran Viswanath
489	Prof. Sanoli Gun
490	Prof. Vijay Kodiyalam
491	Dr. Anil Kumar Karn
492	Dr. Anisur Rahaman Molla

493	Dr. Anup Biswanath Dixit
494	Dr. Aprameyo Pal
495	Dr. Aritra Banik
496	Dr. C. Ramya
497	Dr. Dishant Mayurbhai Pancholi
498	Dr. Gyan Prakash
499	Dr. Hemangi Madhusudan Shah
500	Dr. Nabin Kumar Jana
501	Dr. Subhankar Mishra
502	Dr. Sudhir Kumar Pujahari
NISER	
503	Dr. Amrita Ghosh
504	Dr. Anupam Pal Choudhary
505	Dr. Bhamidi Sai Somanjana Sreedhar
506	Dr. Binod Kumar Sahoo
507	Dr. Chitrabhanu Chaudhuri
508	Dr. Deepak Kumar Dalai
509	Dr. Dinesh Kumar Keshari
510	Dr. Jishnu Ray
511	Dr. Kamal Lochan Patra
512	Dr. Kaushik Majumder
513	Dr. Krishanu Dan
514	Dr. Manas Ranjan Sahoo
515	Dr. Manoj Mishra
516	Dr. Meher Jaban
517	Dr. Prakash Saivasan
518	Dr. Rahul Gupta

519	Dr. Ramesh Manna
520	Dr. Rishiraj Bhattacharyya
521	Dr. Ritwik Mukherjee
522	Dr. Roy Sutanu
523	Dr. S. Sundar
524	Dr. Sanjay Parui
525	Dr. Senthil Kumar K.
526	Dr. Sumana Hatui
527	Dr. Sushmita Gupta
528	Dr. Sushmita Venugopal
529	Dr. Tushar Kanta Naik

Medical & Health Sciences	
BARC	
530	Prof. Gaurav Malhotra
531	Prof. Priyanka Verma
532	Prof. Rahul Vithalrao Parghane
533	Prof. Sandip Basu
534	Prof. Sunil Dutt Sharma
535	Prof. Sunita Nitin Sonavane
536	Dr. Ashwini Kalshetty
537	Dr. J. G. Kalbhande
538	Dr. Satish C. Mishra
539	Dr. Swapna Nabar
HBCH & MPMMCC	
540	Prof. Gulia Seema
541	Dr. Abhishek Shinghal
542	Dr. Ajay Kumar Choubey
543	Dr. Ajay S. Krishnan

544	Dr. Ankita Chaurasia
545	Dr. Ankita Rungta Kapoor
546	Dr. Anwita Mishra
547	Dr. Arvind Suresh
548	Dr. Bal Krishna Mishra
549	Dr. Bipinesh Sansar
550	Dr. Dhiraj Kandpal
551	Dr. Kunal Ranjan Vinayak
552	Dr. Monotosh Pramanik
553	Dr. Nikhil Kumar Singh
554	Dr. Ninad H. Patil
555	Dr. Parichay Singh
556	Dr. Prashanth G.
557	Dr. Praveen L.
558	Dr. Rajesh Bahadur Singh
559	Dr. Revathy Nair K.
560	Dr. Roma Jethani
561	Dr. Sadaf Haiyat
562	Dr. Sambit Swarup Nanda
563	Dr. Sandipan Banerjee
564	Dr. Sashank Saini
565	Dr. Shalini Chaudhuri
566	Dr. Shashank Tiwari
567	Dr. Shreya Shukla
568	Dr. Soumitra Saha
569	Dr. Sunayana R. Sarkar
570	Dr. Syed Sadaqat Hussain
571	Dr. Vijeta Bajpai Batra
572	Dr. Vishakha Anu

TMC	
573	Prof. Ajay Puri
574	Prof. Aliasgar V. Moiyadi
575	Prof. Amit Prakashchandra Joshi
576	Prof. Amita Maheshwari
577	Prof. Amol Trymbakrao Kothekar
578	Prof. Anant Gokarn
579	Prof. Anant Ramaswamy
580	Prof. Aparna Sanjay Chatterjee
581	Prof. Archi Ramesh Agrawal
582	Prof. Ashwin Luis Desouza
583	Prof. Ashwini Narsingrao Budrukkar
584	Prof. Atul M Budukh
585	Prof. Atul Prabhakar Kulkarni
586	Prof. Avanish Parmesh Saklani
587	Prof. Ayushi Sahay
588	Prof. Bharat Rekhi
589	Prof. Bhausaheb Pandurang Bagal
590	Prof. Conjeevaram Shanmugham Pramesh
591	Prof. Deepa Ravindranathan Nair
592	Prof. Dushyant Jaiswal
593	Prof. Gagan Prakash
594	Prof. Gaurav Narula
595	Prof. Gauravi Ashish Mishra
596	Prof. Girish Chinnaswamy
597	Prof. Goda Jayant Sastri
598	Prof. Gouri Himalaya Pantvaidya
599	Prof. Hasmukh Kantilal Jain
600	Prof. Jaya Ghosh
601	Prof. Jayita Kedar Deodhar
602	Prof. Jeson Rajan Doctor
603	Prof. Kedar Kamalakar Deodhar
604	Prof. Madhavi Gopalkrishna Shetmahajan
605	Prof. Mahendra Pal
606	Prof. Mahesh Goel
607	Prof. Malini Premkumar Joshi
608	Prof. Manish Suresh Bhandare
609	Prof. Manisha Nandkumar Pawar
610	Prof. Manju Sengar
611	Prof. Maya Prasad
612	Prof. Mukta Ravindra Ramdwar
613	Prof. Munita Meenu Bal
614	Prof. Murthy Vedang
615	Prof. Navin Khattry
616	Prof. Nayana Shekar Amin
617	Prof. Neha Mittal
618	Prof. Nehal Rishi Khanna
619	Prof. Nikhil Vijay Patkar
620	Prof. Nilendu Chandrakant Purandare
621	Prof. Nilesh Pandurang Sable

622	Prof. Nitin Sudhakar Shetty
623	Prof. Pankaj Chaturvedi
624	Prof. Papagudi Ganesan Subramanian
625	Prof. Poonam K. Panjwani
626	Prof. Prabhash Kumar
627	Prof. Prachi Sunil Patil
628	Prof. Prakash Shetty
629	Prof. Prashant Ramesh Tembhare
630	Prof. Priti Dhansukhbhai Desai
631	Prof. Priya Ranganathan
632	Prof. Raghu Sudarshan Thota
633	Prof. Rajiv Kumar
634	Prof. Reshma Ambulkar
635	Prof. Sabita Shambhulal Jiwnani
636	Prof. Sachin Punatar
637	Prof. Sajid Shafique Quresh
638	Prof. Sandeep Vivek Gurav
639	Prof. Sanjay Biswas
640	Prof. Santosh Menon
641	Prof. Sarbani Ghosh Laskar
642	Prof. Shaesta Abdulaziz Mehta
643	Prof. Shailesh Vinayak Shrikhande
646	Prof. Shalaka Prakash Joshi
648	Prof. Sharmila Anil Pimple
649	Prof. Shashank Ojha
650	Prof. Sheela Prashant Sawant
651	Prof. Sheila Nainan Myatra
652	Prof. Shilpushp Jagannath Bhosale
653	Prof. Shraddha Patkar
654	Prof. Siddhartha Sankar Laskar
655	Prof. Sneha Shah
656	Prof. Sohan Lal Solanki
657	Prof. Sridhar Epari
658	Prof. Subhash Chotelal Yadav
659	Prof. Sudeep Gupta
660	Prof. Sudhir Vasudevan Nair R.
661	Prof. Sumitra Ganesh Bakshi
662	Prof. Supriya Jayant Sastri
663	Prof. Suyash Sureshchandra Kulkarni
664	Prof. Swapnil Ulhas Rane
665	Prof. Swapnil Yeshwant Parab
666	Prof. Tabassum Abdulwahid Wadasadawala
667	Prof. Tejpal Gupta
668	Prof. Vandana Agarwal
669	Prof. Vijay Maruti Patil
670	Prof. Vijaya Prakash Patil
671	Prof. Vikas Sureshchand Ostwal
672	Prof. Vikram Anil Chaudhari
673	Prof. Vinay Kant Shankhdhar
674	Prof. Vivek Gajanan Bhat
675	Dr. Abhishek Chatterjee
676	Dr. Aekta Shah
677	Dr. Akanksha Chichra

678	Dr. Akshay Dwarkadas Baheti
679	Dr. Amandeep Manjeet Singh Arora
680	Dr. Ameya Dattatraya Puranik
681	Dr. Ameya Rajan Bindu
682	Dr. Amit Kumar Jayant Choudhari
683	Dr. Amrita Guha
684	Dr. Anisha A. Navkudkar
685	Dr. Anjana S. Wajekar
686	Dr. Anuja Dhananjay Deshmukh
687	Dr. Anuprita Dilip Daddi
688	Dr. Aparna Katdare
689	Dr. Archya Dasgupta
690	Dr. Arpita Sahu
691	Dr. Asawari Jingonda Patil
692	Dr. Ashwini D. Rane
693	Dr. Atanu Bhattacharjee
694	Dr. Badira Cheriyalinkal Parambil
695	Dr. Bhakti Dushyant Trivedi
696	Dr. Chetan Anil Dhamne
697	Dr. Dhanlaxmi L. Shetty
698	Dr. Gaurav Vijay Salunke
699	Dr. Gauri Raman Gangakhedkar
700	Dr. Gauri Rohan Deshpande
701	Dr. Gurukaran Preet Singh
702	Dr. Indraja Devidas Dev
703	Dr. Janu Amit Kumar

704	Dr. Jifmi Jose Manjali
705	Dr. Kajari Bhattacharya
706	Dr. Katha Nikhil Rabade
707	Dr. Kinjalka Ghosh
708	Dr. Kunal B. Gala
709	Dr. Lingaraj Nayak
710	Dr. Madhavi Dattatraya Desai
711	Dr. Manish Pruthi
712	Dr. Meenakshi Singh
713	Dr. Nandini Sharrel Menon
714	Dr. Nivedita Chakrabarty
715	Dr. Nupur Suresh Kenkre
716	Dr. Omshree Shetty
717	Dr. Pagdhune Avinash Rameshrao
718	Dr. Palak Bhavesh Popat
719	Dr. Pankaj Chaturvedi
720	Dr. Parthiban K. Velayutham
721	Dr. Poonam Joshi
722	Dr. Prabhat Bhargava
723	Dr. Prachi Mittal
724	Dr. Pradip Ramdas Chaudhari
725	Dr. Prakash R. Nayak
726	Dr. Pratik Chandrani
727	Dr. Priyamvada Maitre
728	Dr. Purvi Haria
729	Dr. Rahul Krishnatry
730	Dr. Revathy Krishnamurthy
731	Dr. Ritu Raj Upreti

732	Dr. S. Anbarasan
733	Dr. Sangeeta Kakoti
734	Dr. Shamali Poojary
735	Dr. Sheetal Vidyadhar Gaikwad
736	Dr. Shiva Kumar Thiagarajan
737	Dr. Shivakumar Gudi
738	Dr. Shrikant C. Raut
739	Dr. Shruti Gairola
740	Dr. Shwetabh Sinha
741	Dr. Shyam Srinivasan
742	Dr. Suchismita Ghosh
743	Dr. Sudivya Prashast Sharma
744	Dr. Sujata Lall
745	Dr. Sukhada D. Savarkar
746	Dr. Sumathi S Hiregoudar
747	Dr. Sumeet Prakash Mirgh
748	Dr. Suryatapa Saha
749	Dr. Sushmita Rath
750	Dr. Trupti Pai
751	Dr. Uma M. Sakhadeo
752	Dr. Vasundhara Patil
753	Dr. Veer Deepak Thakkar
754	Dr. Vidisha Vipin Tuljapurkar
755	Dr. Vikas Singh
Physical Sciences	
BARC	
756	Prof. Aditi Ray
757	Prof. Ajay Singh
758	Prof. Alka B. Garg

759	Prof. Amitava Roy
760	Prof. Anil Kumar Chauhan
761	Prof. Anurag Gupta
762	Prof. Aradhana Shrivastava
763	Prof. Arup Biswas
764	Prof. Asavari Santosh Dhavale
765	Prof. B. K. Sapra
766	Prof. Debasis Sen
767	Prof. Dibyendu Bhattacharyya
768	Prof. Dinesh Venkatesh Udupa
769	Prof. J. Padma Nilaya
770	Prof. Jagannath
771	Prof. K. K. Yadav
772	Prof. Keshaw D. Joshi
773	Prof. Kripamay Mahata
774	Prof. M. V. Suryanarayana
775	Prof. Mala N. Rao
776	Prof. Manoj Kumar Warrier
777	Prof. Mukesh Kumar
778	Prof. N. Padma
779	Prof. Nandini Garg
780	Prof. Paritosh Modak
781	Prof. Prashant Shukla
782	Prof. Priyamvada M Dighe
783	Prof. Ranjan Mittal
784	Prof. Rekha Rao
785	Prof. Renju George Thomas
786	Prof. S. Anand
787	Prof. Sakuntala T.

788	Prof. Samrath Lal Chaplot
789	Prof. Satyaranjan Santra
790	Prof. Shashwati Sen Yeram
791	Prof. Srikumar Ghorui
792	Prof. Subhankur Mitra
793	Prof. Sukanta Karmakar
794	Prof. Surendra Singh
795	Prof. T. Palani Selvam
796	Prof. Tej Singh
797	Prof. Usha Pal
798	Prof. V. Jha
799	Prof. V. K. Aswal
800	Prof. Vyaghri Lalitha Sanyasirao Sista
801	Dr. Ajay Kumar Mishra
802	Dr. Amit Kumar
803	Dr. Amit P. Srivastava
804	Dr. Amit Verma
805	Dr. Anil Jain
806	Dr. Anup Kumar Bera
807	Dr. Aparna Shastri
808	Dr. Apu Sarkar
809	Dr. Arundhati Bute
810	Dr. Asawari D. Rath
811	Dr. Ashish Kumar Agrawal
812	Dr. Ashok Kumar Bakshi
813	Dr. Ashok Kumar Verma
814	Dr. Ashok Kumar Yadav
815	Dr. Asim Pal

816	Dr. B. Sunder Sahayanathan
817	Dr. Babita Tiwari
818	Dr. Bhushan Dhabekar
819	Dr. Bhushan Nishikant Joshi
820	Dr. Bijay Kumar Sahoo
821	Dr. Biplab Ghosh
822	Dr. Brahmananda Chakraborty
823	Dr. C. D. Sijoy
824	Dr. C. L. Prajapat
825	Dr. Chandrani Nayak
826	Dr. D. R. Mishra
827	Dr. Debarati Bhattacharya
828	Dr. Debdutta Lahiri
829	Dr. Debjani Karmakar
830	Dr. Deodatta Shinde
831	Dr. Dipak Kumar Mishra
832	Dr. G. Laxmi Narasimha Reddy
833	Dr. G. Sridhar
834	Dr. Gayatri Mohanto
835	Dr. Giri Dhari Patra
836	Dr. Goutam Dev Mukherjee
837	Dr. H. Kumawat
838	Dr. Himal Bhatt
839	Dr. Himanshu Kumar Poswal
840	Dr. Jayanta Mondal
841	Dr. Jitendra Bahadur
842	Dr. Jose V. Mathew
843	Dr. Kiran R. M.
844	Dr. Krishan Kumar Pandey

845	Dr. Krishna Kumar Singh
846	Dr. Manish Joshi
847	Dr. Manmeet Kaur
848	Dr. Mayanak Kumar Gupta
849	Dr. Mayank Shukla
850	Dr. Minal Y. Nadar
851	Dr. Mohit Tyagi
852	Dr. Munish Kumar
853	Dr. Narender Singh Rawat
854	Dr. Niranjan Suryakant Ramgir
855	Dr. Nishant Chaudhary
856	Dr. Param Jeet Singh
857	Dr. Parasmani Rajput
858	Dr. Partha Sarathi Ghosh
859	Dr. Partha Sarathi Sarkar
860	Dr. Prakash Chandra Rout
861	Dr. Pramod Bhatt
862	Dr. Pratap Baburao Wagh
863	Dr. Purnananda Nandi
864	Dr. Purushottam Jha
865	Dr. Raghwendra Kumar
866	Dr. Raj Bahadur Tokas
867	Dr. Rajeev Kumar
868	Dr. Rajesh Kumar
869	Dr. Rajib Kar
870	Dr. Rajul Ranjan Choudhury
871	Dr. Ram Niranjan
872	Dr. Ramesh Chandra Das
873	Dr. Ranita Basu
874	Dr. Ranu Bhatt
875	Dr. Rohit Shukla
876	Dr. Rosaline Mishra
877	Dr. S. K. Pandit
878	Dr. S. P. Behera
879	Dr. S. P. Tripathy
880	Dr. Sabyasachi Paul
881	Dr. Sambaran Pahari
882	Dr. Sanjay Kumar Mishra
883	Dr. Sanjay Kumar Sahu
884	Dr. Santanu Bera
885	Dr. Saroj Bishnoi
886	Dr. Shankar Prasad Koiry
887	Dr. Shilpa Tripathi
888	Dr. Shiv Govind Singh
889	Dr. Shivanand Chaurasia
890	Dr. Shovit Bhattacharya
891	Dr. Shuvendu Jena
892	Dr. Sk Maidul Haque
893	Dr. Sohrab Abbas
894	Dr. Somsundar Mukhopadhyay
895	Dr. Soumen Bhattacharyya
896	Dr. Subir Bhattacharyya
897	Dr. Sugam Kumar
898	Dr. Suhail Ahmad Khan
899	Dr. Sunita Kedia
900	Dr. Swarupananda Pradhan
901	Dr. Tushar Roy
902	Dr. V. V. Parkar

903	Dr. Veerendra Kumar Sharma
904	Dr. Venkata Ramana Ikkurthi
905	Dr. Vibha Saxena
906	Dr. Vinayak Mishra
907	Dr. Vineet Kumar
908	Dr. Vinod Singh Rawat
909	Dr. Vir Krishen Dhar
910	Dr. Yogesh K. Gupta
911	Dr. Yogesh Kashyap
912	Prof. Aniruddha Kumar
HRI	
913	Prof. Aditi Sen De
914	Prof. Asesh Krishna Datta
915	Prof. Prasenjit Sen
916	Prof. Ujjwal Sen
917	Dr. Anirban Basu
918	Dr. Anshuman Maharana
919	Dr. Debraj Rakshit
920	Dr. Santosh Kumar Rai
921	Dr. Sayan Choudhury
922	Dr. Sudip Chakraborty
923	Dr. T. P. Pareek
924	Dr. Tapas Kumar Das
925	Dr. Tathagata Ghosh
IGCAR	
926	Prof. Arup Dasgupta
927	Prof. Awadhesh Mani
928	Prof. Christopher David
929	Prof. N Subramanian

930	Prof. S Ganesamoorthy
931	Prof. Sharat Chandra
932	Dr. Amit Kumar
933	Dr. Anees P.
934	Dr. Arun K. Prasad
935	Dr. B. Sundaravel
936	Dr. Balmukund Shukla
937	Dr. Barid Baran Lahiri
938	Dr. Ch. Kishan Singh
939	Dr. Chanchal Ghosh
940	Dr. Deepak Kumar Gupta
941	Dr. Dipak Kumar Baisnab
942	Dr. Edward Prabu Amaladass
943	Dr. Gurpreet Kaur
944	Dr. Haraprasanna Tripathy
945	Dr. K. Ganesan
946	Dr. K. Prabhakar
947	Dr. Kishore Kumar Madapu
948	Dr. M. Manohari
949	Dr. N. R. Sanjay Kumar
950	Dr. O. Annalakshmi
951	Dr. R. Ramaseshan
952	Dr. Rajendra Ganpat Joshi
953	Dr. Ramanathaswamy Pandian
954	Dr. Ravi Chinnappan
955	Dr. Renjith Ramachandran
956	Dr. S. Abhaya
957	Dr. S. Amirthapandian
958	Dr. S. C. Vanithakumari

959	Dr. S. Tripura Sundari
960	Dr. Sainath G.
961	Dr. Soumee Chakraborty
962	Dr. Syamalarao Polaki
963	Dr. T Sathyanarayana Annam
964	Dr. Vinod K.
IMSc	
965	Prof. Raghib Hassan Syed
966	Prof. Rajesh R.
967	Prof. Satyavani Vemparala
968	Prof. Sibasish Ghosh
969	Prof. Sitabhra Sinha
970	Prof. V. Ravindran
971	Dr. Ajit Coimbatore Balram
972	Dr. Arnab Pal
973	Dr. Chandrashekar C. M.
974	Dr. Debayan Chakraborty
975	Dr. Dhiraj Kumar Hazra
976	Dr. Ganesh Ramchandran
977	Dr. Gopalakrishna Shrihari
978	Dr. Manjari Bagchi
979	Dr. Mukul S. Laad
980	Dr. Padmanath Madanagopalan
981	Dr. Partha Mukhopadhyay
982	Dr. Pinaki Chaudhuri
983	Dr. Roji Pius
984	Dr. Ronojoy Adhikari
985	Dr. Sanatan Digal
986	Dr. Sayantan Sharma
987	Dr. Shankha Banerjee
988	Dr. Sujay K. Ashok
989	Dr. Venkata Suryanarayana Nemani
IoP	
990	Prof. Karuna Kar Nanda
991	Prof. Pradip Kumar Sahu
992	Prof. Som Tapobrata
993	Prof. Sudipta Mukherji
994	Dr. Arijit Saha
995	Dr. Aruna Kumar Nayak
996	Dr. Debasish Chaudhuri
997	Dr. Debottam Das
998	Dr. Dinesh Topwal
999	Dr. Goutam Tripathy
1000	Dr. Kirtiman Ghosh
1001	Dr. Manimala Mitra
1002	Dr. Samal Debakanta
1003	Dr. Sanjib Kumar Agarwalla
1004	Dr. Saptarshi Mandal
1005	Dr. Satyaprakash Sahoo
IPR	
1006	Prof. Anitha V. P.
1007	Prof. Indranil Bandyopadhyay
1008	Prof. Mahendrajit Singh
1009	Prof. Mainak Bandyopadhyay
1010	Prof. Raju Daniel
1011	Prof. Subrata Pradhan
1012	Prof. Sudip Sengupta

1013	Dr. Amreen Ara Hussain
1014	Dr. Amulya Kumar Sanyasi
1015	Dr. C. Balasubramanian
1016	Dr. Debasis Chandra
1017	Dr. Devendra Sharma
1018	Dr. Ganesh Rajaraman
1019	Dr. Gourab Bansal
1020	Dr. Harshita Raj
1021	Dr. Hiteshkumar B. Pandya
1022	Dr. Jinto Thomas
1023	Dr. Joydeep Ghosh
1024	Dr. Jugal Chowdhury
1025	Dr. Jyoti Shankar Mishra
1026	Dr. Kishore Kanti Mishra
1027	Dr. Malay Bikas Chowdhuri
1028	Dr. Mrityunjay Kundu
1029	Dr. Mukesh Ranjan
1030	Dr. N. Ramasubramanian
1031	Dr. Ngangom Aomoa
1032	Dr. Pintu Bandyopadhyay
1033	Dr. Pratipalsinh A. Rayjada
1034	Dr. Rajendraprasad Bhattacharyay
1035	Dr. Rakesh Moulick
1036	Dr. Ramkrishna Rane
1037	Dr. Ravi G.
1038	Dr. Saikia Bipul
1039	Dr. Samir Khirwadkar
1040	Dr. Sanjeev Kumar Sharma
1041	Dr. Sanjeev Kumar Varshney
1042	Dr. Sarveshwar Sharma
1043	Dr. Sejal Shah
1044	Dr. Shantanu Kumar Karkari
1045	Dr. Shekar Goud Thatipamula
1046	Dr. Shishir Purohit
1047	Dr. Smruti R. Mohanty
1048	Dr. Subhash P. V.
1049	Dr. Ziauddin Khan
NISER	
1050	Prof. Bedangadas Mohanty
1051	Dr. A.V. Anil Kumar
1052	Dr. Abdur Rahman
1053	Dr. Ajaya Kumar Nayak
1054	Dr. Amaresh Kumar Jaiswal
1055	Dr. Anamitra Mukherjee
1056	Dr. Ashis Kumar Nandy
1057	Dr. Ashok Kumar Mohapatra
1058	Dr. Chethan N. Gowdigere
1059	Dr. Colin Benjamin
1060	Dr. Guneshwar Thangjam
1061	Dr. Jaya Khanna
1062	Dr. Jayesh M. Goyal
1063	Dr. Joydeep Bhattacharjee
1064	Dr. Kartikeswar Senapati
1065	Dr. Kush Saha
1066	Dr. Liton Majumdar
1067	Dr. Luke Chamandy
1068	Dr. Najmul Haque

1069	Dr. Narayan Rana
1070	Dr. Nishikanta Khandai
1071	Dr. Pathikrit Bhattacharya
1072	Dr. Prasanjit Samal
1073	Dr. Pratap Kumar Sahoo
1074	Dr. Priyadarshi Chowdhury
1075	Dr. Prolay Kumar Mal
1076	Dr. Ritwick Das
1077	Dr. Sanjay Kumar Swain
1078	Dr. Satyaprasad P. Senanayak
1079	Dr. Sayantani Bhattacharyya
1080	Dr. Shamik Banerjee
1081	Dr. Shovon Pal
1082	Dr. Subhankar Bedanta
1083	Dr. Subhasish Basak
1084	Dr. Sumedha
1085	Dr. Surya Snata Rout
1086	Dr. Tapan Mishra
1087	Dr. Tuhin Ghosh
1088	Dr. V. Ravi Chandra
1089	Dr. Victor Roy
1090	Dr. Yogesh Kumar Srivastava
RRCAT	
1091	Prof. Anand Moorti
1092	Prof. Gurvinderjit Singh
1093	Prof. Indranil Bhaumik
1094	Prof. J. A. Chakera
1095	Prof. Maulindu Kumar Chattopadhyay
1096	Prof. Mohammed Hussein Modi
1097	Prof. Om Prakash
1098	Prof. Pankaj Misra
1099	Prof. Sanjay Kumar Rai
1100	Prof. Shovan K. Majumder
1101	Prof. Srinibas Satapathy
1102	Prof. Sunil Verma
1103	Prof. Tapas Ganguli
1104	Prof. Tarun Kumar Sharma
1105	Prof. Vibhuti Bhushan Tiwari
1106	Prof. Vinit Kumar
1107	Dr. Archana Sagdeo
1108	Dr. Arun Kumar Rai
1109	Dr. Avnish K. Sharma
1110	Dr. Brahma Nand Upadhyaya
1111	Dr. C. Kamal
1112	Dr. Chandra Pal Singh
1113	Dr. Chandrachur Mukherjee
1114	Dr. Haranath Ghosh
1115	Dr. Himanshu Singhal
1116	Dr. Himanshu Srivastava
1117	Dr. J. Jayabalan
1118	Dr. Jitendra Kumar
1119	Dr. L. S. Sharath Chandra
1120	Dr. Maheswar Nayak
1121	Dr. Manoj Kumar Singh
1122	Dr. Manoj Kumar Tiwari
1123	Dr. P. K. Mukhopadhyay

1124	Dr. Pooja Gupta
1125	Dr. Pragya Tiwari
1126	Dr. Rajeev Bhatt
1127	Dr. Raktim Dasgupta
1128	Dr. Ramakanta Biswal
1129	Dr. Ravindra Jangir
1130	Dr. Sachin Kumar Srivastava
1131	Dr. Salahuddin Khan
1132	Dr. Sanyasi Rao Bobbili
1133	Dr. Shailesh Kumar Khamari
1134	Dr. Shankar Lal
1135	Dr. Shreyashkar Dev Singh
1136	Dr. Soma Banik
1137	Dr. Suman Bagchi
1138	Dr. Suparna Pal
1139	Dr. Surya Mohan Gupta
1140	Dr. Uday Chakravarty
1141	Dr. Vijay Kumar Dixit
1142	Dr. Vishnu Kumar Sharma
1143	Dr. Yogesh Verma
SINP	
1144	Prof. Abhik Basu
1145	Prof. Chandan Mazumdar
1146	Prof. Gautam Bhattacharyya
1147	Prof. Harvendra Singh
1148	Prof. Krishnakumar S. R. Menon
1149	Prof. Pradip Kumar Roy
1150	Prof. Satyajit Hazra

1151	Prof. Ushasi Datta
1152	Dr. Akashrup Banerjee
1153	Dr. Amit Ghosh
1154	Dr. Ananya Kundu
1155	Dr. Anirban Das
1156	Dr. Anjali Mukherjee
1157	Dr. Arka Santra
1158	Dr. Arnab Kundu
1159	Dr. Arti Garg
1160	Dr. Arunava Mukherjee
1161	Dr. Ashish Shukla
1162	Dr. Augustine Kshetrimayum
1163	Dr. Biswajit Karmakar
1164	Dr. Biswarup Satpati
1165	Dr. Chinmay Basu
1166	Dr. Debasish Banerjee
1167	Dr. Debasish Das
1168	Dr. Kalpataru Pradhan
1169	Dr. Krishanu Roychowdhury
1170	Dr. Maitreyee Nandy
1171	Dr. Mala Das
1172	Dr. Mrinmay Kumar Mukhopadhyay
1173	Dr. Nayana Majumdar
1174	Dr. Pratik Majumdar
1175	Dr. Samik Duttagupta
1176	Dr. Sankar De
1177	Dr. Satyaban Bhunia
1178	Dr. Satyaki Bhattacharya

1179	Dr. Shilpa Kastha
1180	Dr. Srijani Mallik
1181	Dr. Subir Sarkar
1182	Dr. Suchandra Dutta
1183	Dr. Sudipto Chakrabarti
1184	Dr. Supratic Chakraborty
1185	Dr. Swarup Deb
1186	Dr. Tinku Sinha Sarkar
VECC	
1187	Prof. Arup Bandyopadhyay
1188	Prof. Gayathri N Banerjee
1189	Prof. Parnika Das
1190	Prof. Sarmishtha Bhattacharyya
1191	Prof. Sourav Sarkar
1192	Dr. Ajay Kumar Himanshu
1193	Dr. Anand Kumar Dubey
1194	Dr. Animesh Goswami
1195	Dr. Arindam Kumar Sikdar
1196	Dr. Ayan Ray
1197	Dr. Debasish Mondal
1198	Dr. Deepak Pandit
1199	Dr. Gargi Chaudhri
1200	Dr. Gopal Mukherjee
1201	Dr. Jajati Kesari Nayak
1202	Dr. Jedidiah Pradhan
1203	Dr. Jhilam Sadhukhan
1204	Dr. Kaushik Banerjee
1205	Dr. Partha Pratim Bhaduri
1206	Dr. Prasanta Karmakar
1207	Dr. Pratap Roy
1208	Dr. Rupa Chatterjee
1209	Dr. Samir Kundu
1210	Dr. Sanjib Muhuri
1211	Dr. Sanyal Dirtha
1212	Dr. Shashi C. L. Srivastava
1213	Dr. Siddhartha De choudhury
1214	Dr. Soumik Bhattacharya
1215	Dr. Supriya Mukhopadhyay
1216	Dr. Swagata Mallik
1217	Dr. Tapan Kumar Rana
1218	Dr. Tilak Kumar Ghosh
1219	Dr. Tumpa Bhattacharjee
1220	Dr. Uttam Bhunia
1221	Dr. Vaishali Naik
1222	Dr. Zubayer Ahammed

ACADEMIC DATA OF HBNI

Total New Enrollments during FY 2024-25: 1158

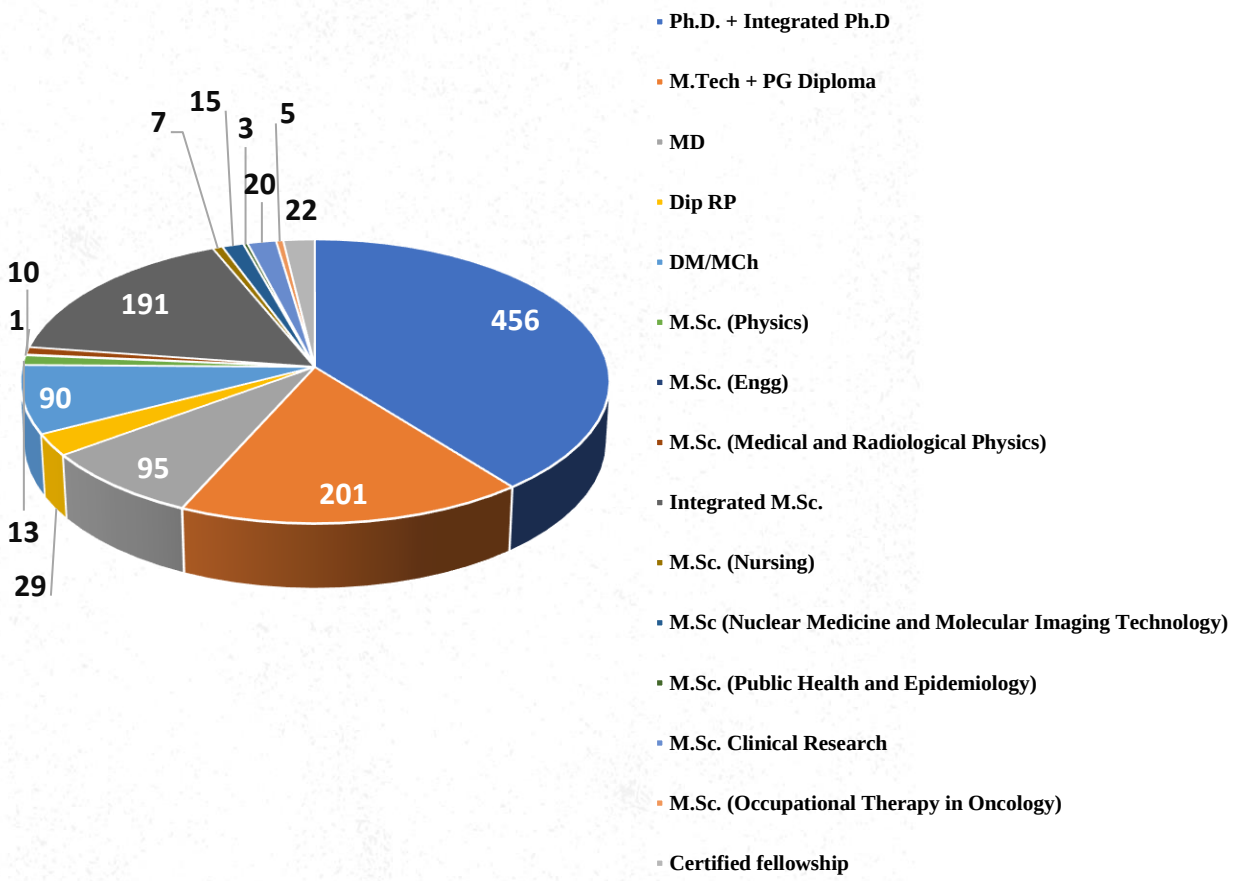

Total new enrolments during FY 2024-25 (Institute Wise)

Academic Programme	BARC	IGCAR	RRCAT	VECC	SINP	IPR	TMC	IoP	IMSc	HRI	NISER	Total
Ph.D. + Integrated Ph.D	128	48	19	14	40	14	36	7	18	10	122	456
M.Tech + PG Diploma	201	….	….	….	….	…	….	…	….	….	….	201
MD	6	….	….	….	….	…	89	…	….	….	….	95
Dip RP	29	….	….	….	….	…	….	…	….	….	….	29
DM/MCh	….	….	….	….	….	…	90	…	….	….	….	90
M.Sc. (Physics)	….	….	….	….	….	…	….	…	….	13	….	13
M.Sc. (Engg)	1	….	….	….	….	…	….	…	….	….	….	1
M.Sc. (Medical and Radiological Physics)	….	….	….	….	….	…	….	…	….	….	10	10

Integrated M.Sc.	….	….	….	….	….	…	….	…	….	….	191	191
M.Sc. (Nursing)	….	….	….	….	….	…	7	…	….	….	….	7
M.Sc (Nuclear Medicine and Molecular Imaging Technology)	….	….	….	….	….	…	15	…	….	….	….	15
M.Sc. (Public Health and Epidemiology)	….	….	….	….	….	…	3	…	….	….	….	3
M.Sc. Clinical Research	….	….	….	….	….	…	20	…	….	….	….	20
M.Sc. (Occupational Therapy in Oncology)	….	….	….	….	….	…	5	…	….	….	….	5
Certified fellowship	….	….	….	….	….	…	22	…	….	….	….	22
Total	**365**	**48**	**19**	**14**	**40**	**14**	**287**	**7**	**18**	**23**	**323**	**1158**

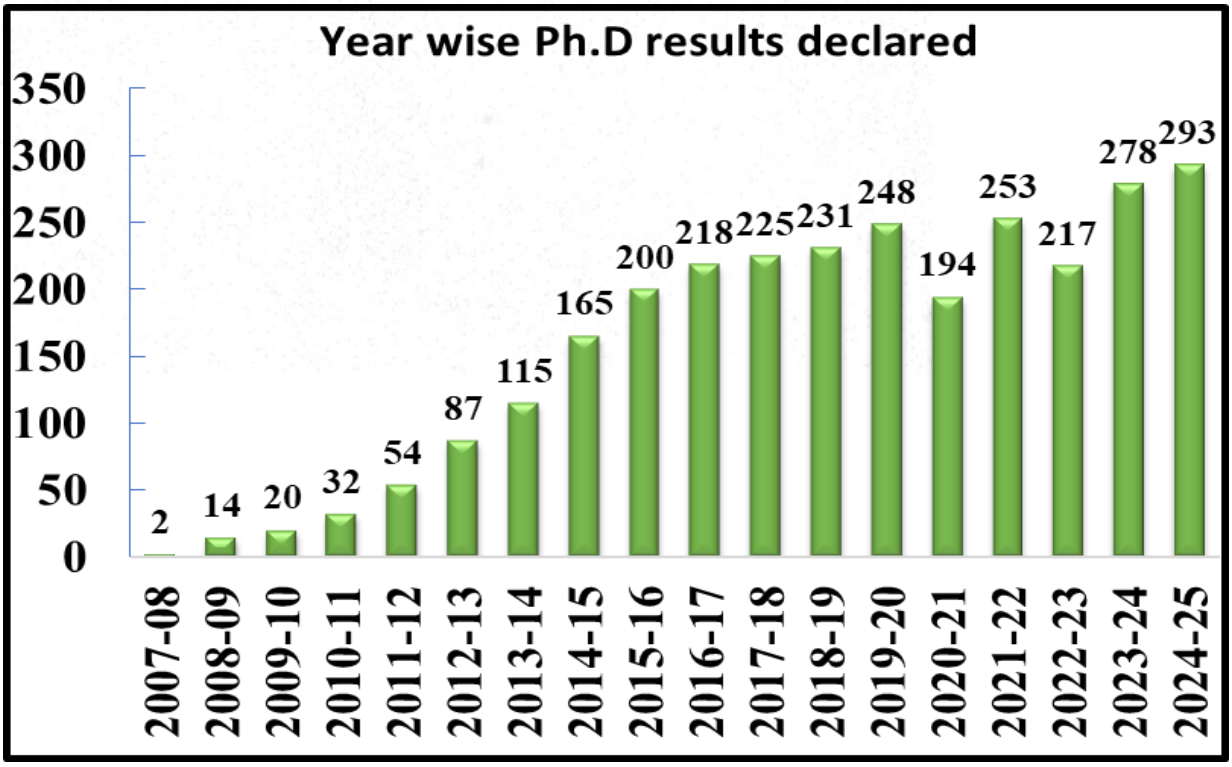

Total no. of results declared (9227) for various academic programs of HBNI till March 31, 2025

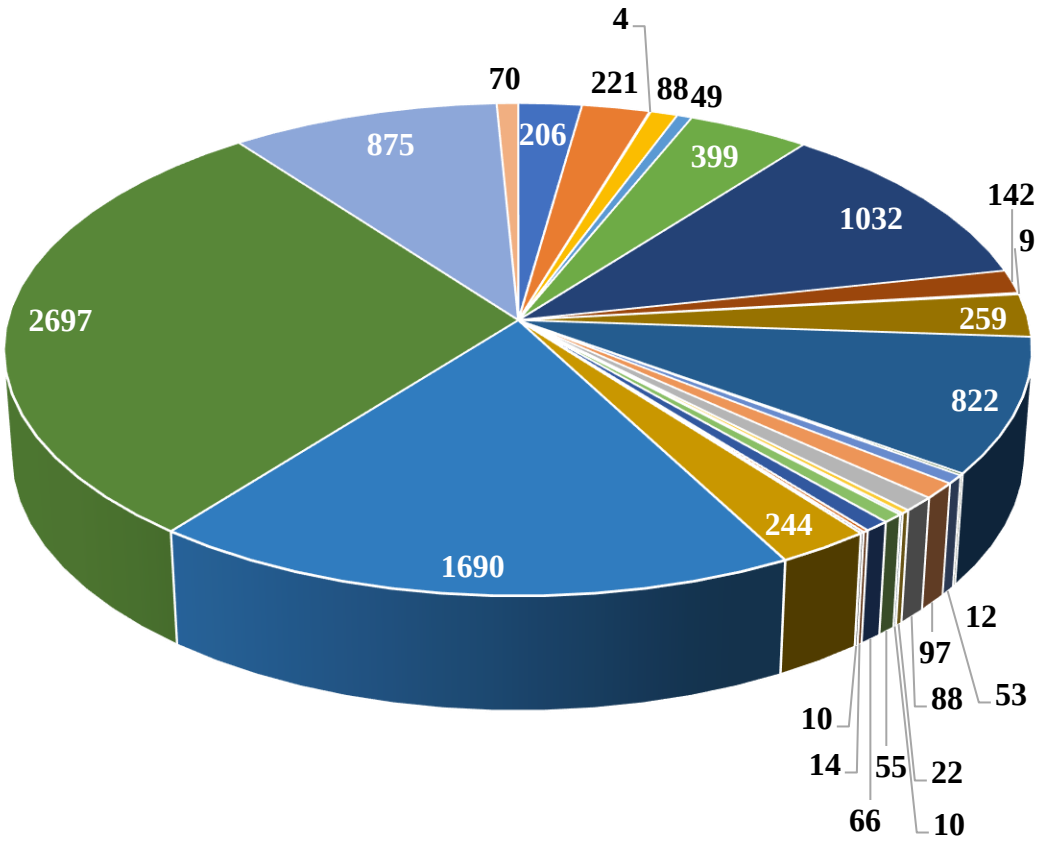

- Certified Fellowship
- D.M.
- DA-Dip. In Medicine(Anaesthesia)
- Diploma in Medical Radio-Isotope Tehniques (DMRIT)
- Diploma in Radiation Medicine (DRM)
- Diploma in Radiological Physics (Dip.RP)
- Integrated M.Sc. (Five Years)
- Integrated Ph.D. (Dual Degree)
- Integrated Ph.D. (Single Degree)
- M.Ch.
- M.D.
- M.Phil.
- M.Sc.
- M.Sc. (Clinical Research)
- M.Sc. (Engg)
- M.Sc. (Hospital Radiopharmacy)
- M.Sc. (Medical and Radiological Physics)
- M.Sc. (Nuclear Medicine and Molecular Imaging Technology)
- M.Sc. (Nursing)
- M.Sc. (Occupational Therapy in Oncology)
- M.Sc. (Public Health at Epidemiology)
- M.Sc. Degree of Int Ph.D. (Dual Degree)
- M.Tech.
- Ph.D.
- Post Graduate Diploma (PGD)
- Post Graduate Diploma in Fusion Imaging Technology

Discipline wise distribution of Total (2846) Ph.D. results declared since inception

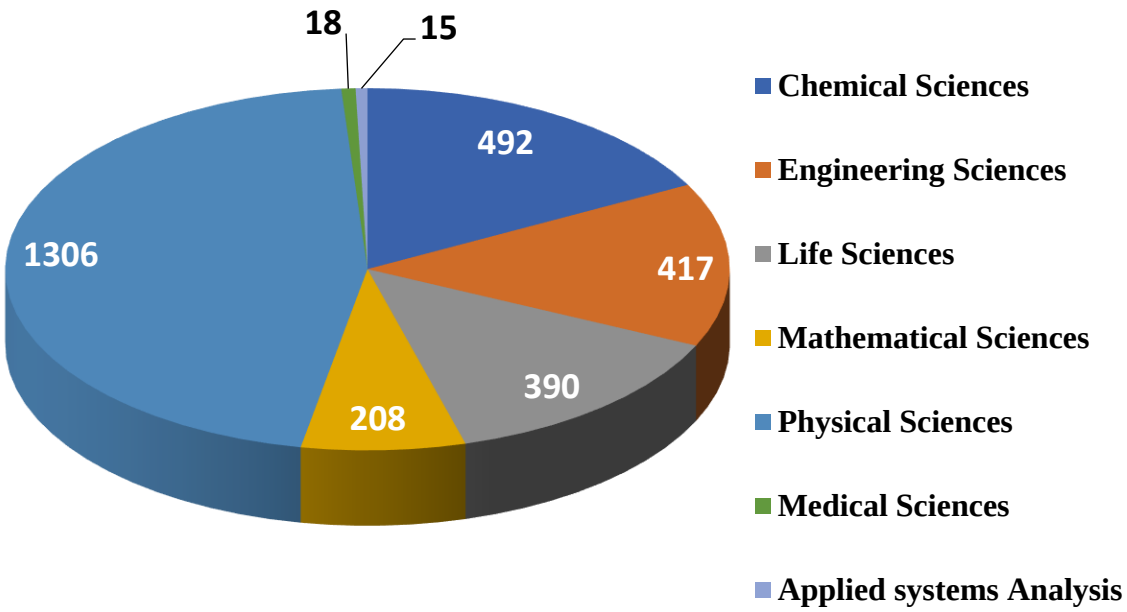

Discipline-wise Ph.D. Degrees Awarded by HBNI for the Period April 2024-March 2025 (293)

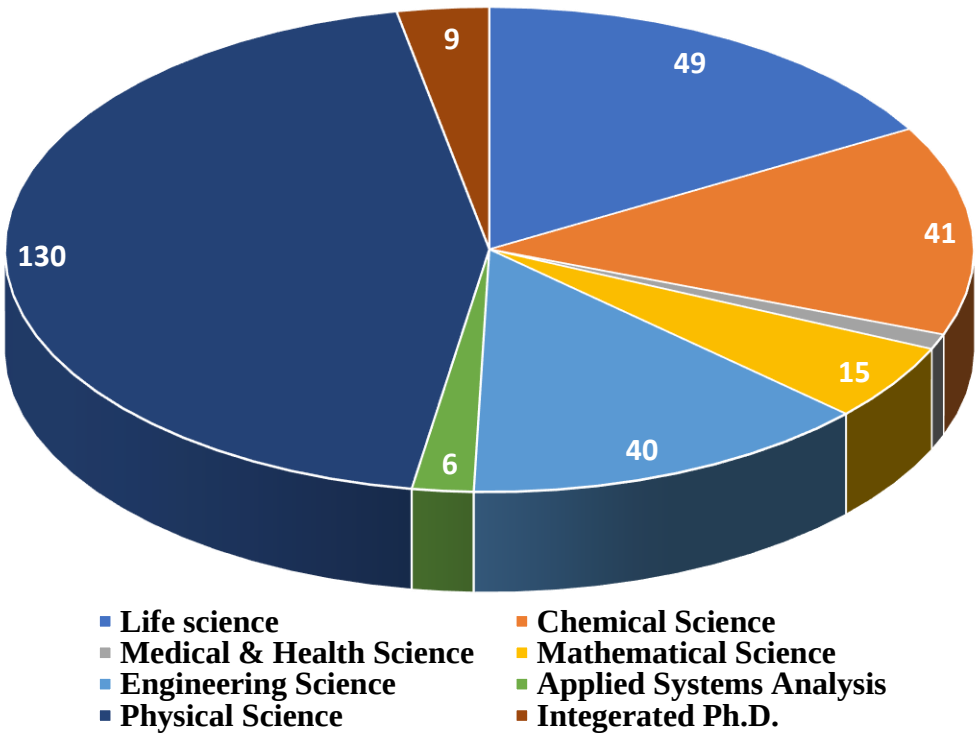

The data represents the period from April 1 of the preceding year to March 31 of the ending year.

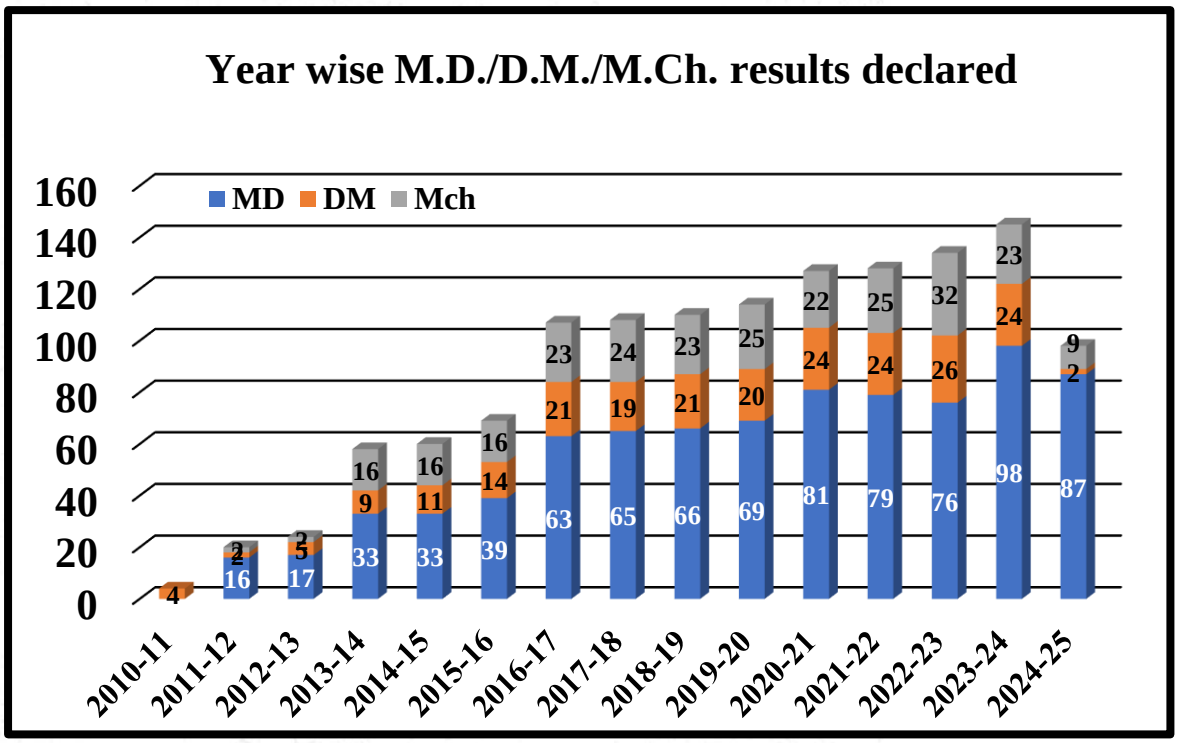

The data represents the period from April 1 of the preceding year to March 31 of the ending year.

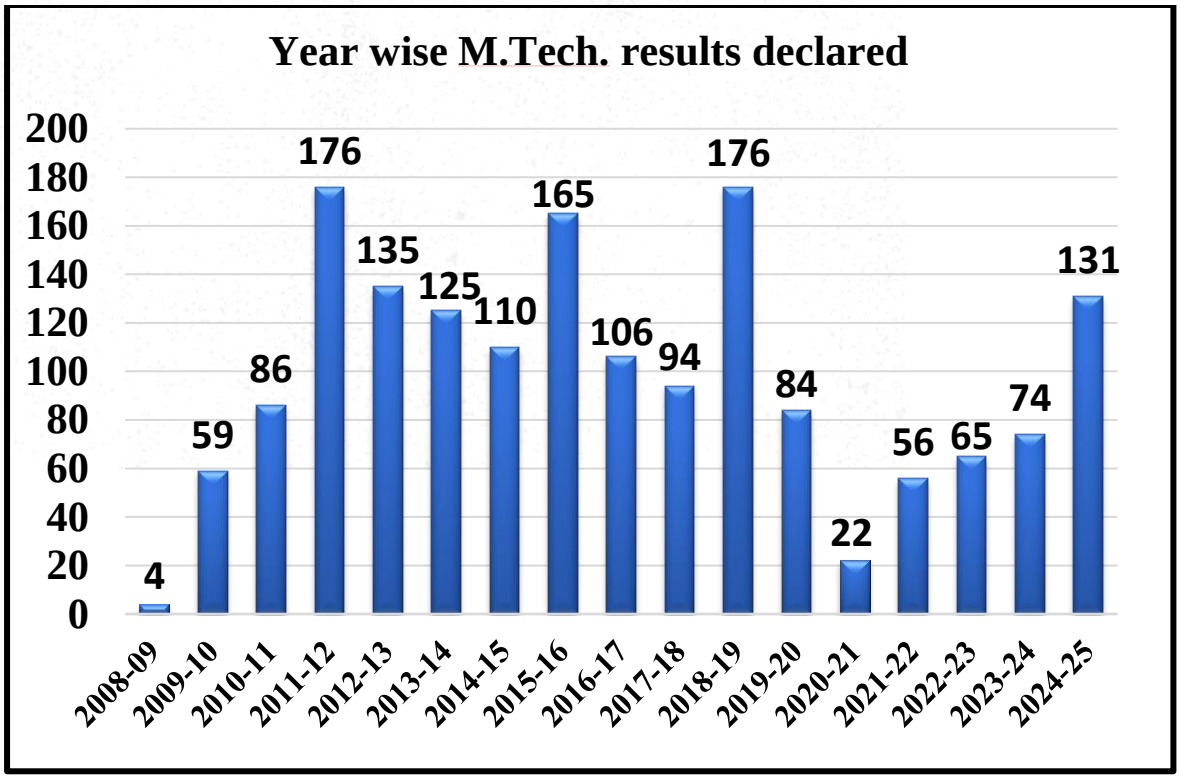

The data represents the period from April 1 of the preceding year to March 31 of the ending year.

Discipline and CI/ OCC wise details of the students who have been awarded Ph.D./ Integrated Ph.D. degree during August 01, 2024-July 31, 2025

Studies for Applied Systems Analysis

BARC, Mumbai

S. No.	Student Name	Enrollment No.	Title of the thesis
1	Rupsha Bhattacharyya	APSA01202104001	A Quantitative Assessment of the Role of Nuclear Power Reactors in a Low Carbon Energy Mix
NISER, Bhubaneswar			
2	Laxmikanta Gual	APSA11201904002	Institutions and Intra-State Development Disparity within Democracy: Evidence from an Indian State
3	Asmita Nayak	APSA11201704001	A Behavioural Profile and Social-emotional Reciprocity of Children with Autism Spectrum Disorder
4	Monika Mishra	APSA11201904004	Narrating Unstable Futures and the Complexit(ies) of Being: the Cognitive Dynamics of Second-Person Narration in N.K. Jemisin's Broken Earth Trilogy
5	Suchismita Pramanik	APSA11201904005	Development of a Psychometric Instrument for Unconditional Self-acceptance and Exploring its Correlates

Chemical Sciences

S. No.	Student Name	Enrollment No.	Title of the Thesis
BARC, Mumbai			
6	Koushik Bhandari	CHEM01201704003	Complex Oxides as Host in Inert Matrix Fuel: Structural and Thermo-physical Investigations
7	Atanu Jha	CHEM01201704006	Surface and Interface Modification of Single/Multi-Component Polymeric Systems by Radiation Technology for Industrial and Environmental Applications
8	Sreeja Raj Menon	CHEM01201804001	Formulation and Dosimetry of ^{177}Lu Labeled Monoclonal Antibodies and ^{177}Lu/^{68}Ga Labeled Peptides for Theranostic Applications in the Management of Specific Cancers.
9	Barendra Kumar Rana	CHEM01201804011	Behaviour and Assessment of Uranium

			Tailings Generated from Dolostone Uranium Mineralised Ore at Tummalapalle Site
10	Abhishek Sharma	CHEM01201804016	Electrochemical Investigation of Iron, Bismuth and Vanadium Oxide-Based Composites for Photoelectrochemical Splitting of Water
11	Pratik Das	CHEM01202004001	Investigations on Fluorapatite as a Matrix to Immobilize High Level Wastes of Advance Reactors
12	Pampa Modak	CHEM01202104009	Computational Studies on Fluoride and Phosphate Based Phosphor Materials for Radiation Dosimetry Applications
13	Aranyak Sarkar	CHEM01201904005	Investigation of Molecular Interaction with Advanced Fluorescence Correlation Spectroscopy and Super-resolution Orientation Imaging
14	Pasupati Nath Khan	CHEM01201904007	Development of Supramolecule Based Extractants and Suitable Diluents for the Separation of Radio Toxic Elements
15	Saparya Chattaraj	CHEM01201904009	Evaluation of Soft Donor Ligands for the Separation of Alpha Emitting Nuclides from Nuclear Waste
16	Prabhath Ravi K.	CHEM01201904011	Chemical and Chronological Characterization of Some Nuclear and Other Radioactive Materials for Nuclear Forensic Applications
17	Annadasankar Roy	CHEM01201904016	Hydrological Investigation of Regional Aquifer Systems in Contrasting Climatic Regions of North West India using Isotope–Geochemical Modeling Approaches
18	Kanagala Sandeep Rao	CHEM01202004004	Development of High Energy Density Electrode Materials for Advanced Lithium Based Batteries
19	Sushil Maruti Patil	CHEM01202004005	Synthesis and Characterization of Novel Deep Eutectic Solvent for Studying Dissolution, Co-ordination and Redox Chemistry of Lanthanides and Actinides
IGCR, Kalpakkam			
20	Muthukumaran T.	CHEM02201604013	Preparation, Characterization and Applications of Silicon Carbide and Phosphate- Capped Magnetic Nanoparticles

21	Srinivas Manepalli	CHEM02201604014	Pitting Corrosion Studies on as Welded and Thermally Aged 316SS Weld with Different Nitrogen and 316LN SS
22	Biranchi Narayan Mohanty	CHEM02201804013	Studies on Adsorption of Ruthenium on Carbon Based Nano Materials
23	Mohd Sufiyan Khan	CHEM02201904002	Studies on Preparation of Alloys and Intermetallic Compounds by High Temperature Electrochemical De-Oxidation of Metal Oxides
24	S. Shyam Kumar	CHEM02201904009	Setting up of Isopiestic Experimental Facility towards Thermodynamic Studies on Pr-Cd and RE-Te (RE: La, Ce, Pr, Nd, Gd) Systems
25	Rongali Hareesh	CHEM02201704010	High Temperature Oxidation and Corrosion Behavior of Pyrolytic Graphite under Simulated Pyrochemical Reprocessing Conditions.
26	Abiram Senapati	CHEM02201804011	Evaluation of Structural and Thermo-Physical Properties of Sodium Niobium Phosphate Glass for Nuclear Waste Immobilization Application with CeO_2 as an Actinide Simulant
27	Anushree Chintaparthi	CHEM02201804012	Synthesis of Bifunctional Magnetic Nanostructures and Their Applications in Dye and Oil Removal
28	Gopinath Shit	CHEM02201804014	Corrosion Assessment of Type 304L SS in Simulated Spent Fuel Reprocessing Environment
29	Nair Afijith Ravindranath	CHEM02201804015	Investigation on the Influence of Polarization Resistance for Low Temperature Operation of Multilayered Thin Film YSZ Oxygen Sensors
30	Nandalal Mahapatra	CHEM02201904005	Nitrogen as a Pnicogen in π-hole Driven Pnicogen Bonding: Matrix Isolation Infrared Spectroscopic and Computational Studies
31	Parvathy Narayanan	CHEM02201904006	Probing and Maneuvering the Third Phase Formation in Diglycolamide/n-dodecane Systems
NISER, Bhubaneswar			

32	Ayendrila Das	CHEM11201804012	Ultrafast and Single-Molecule Studies of Photo-Physical Processes in Quantum-Confined Materials
33	Priyanka Ghosh	CHEM11201704022	Synthesis and Application of Supramolecular Architectures and Biologically Active Molecules having Heterocyclic Moiety
34	Chinmay Kumar Jena	CHEM11201704030	Synthesis and Biochemical Evaluation of Unnatural Amino Acids/Peptides Comprising Aminotropone /Kynurenine /Proline
35	Sushanta Kumar Meher	CHEM11201804026	Pd, Ru, Mg Complexes for CO_2 Utilisation, Crosscoupling/Transfer-hydrogenation Reactions: Base-Mediated Synthesis of Isothiazole
36	R. Vijaya Sankar	CHEM11201904007	Ruthenium Pincer Catalyzed Organic Transformations
37	Sourav Ranjan Pradhan	CHEM11201904009	Synthesis, Spectral, Structural Analyses, Coordination and Binding Studies of Triaryl-Embedded Expanded Porphyrin and Calixphyrin Analogues.
38	Subhra Jyoti Panda	CHEM11201904011	Exploring the Chemistry of N7-Purine Derivatives: From Synthesis to Functional Metal-Organic Frameworks (MOFs)
39	Rajib Samanta	CHEM11202004003	Carbon Supported Metal Composites and Heteroatom Doped Carbons for Energy Conversion Reactions and Sodium Ion Battery
40	Rosalin Bhanja	CHEM11202104018	Metal-free Approaches Towards C-N and C-O Bond Formations
41	Pradeep N.	CHEM11201804017	5-Aminopyrazoles as Versatile Building Blocks for the Synthesis of Functionalized Pyrazoles, Pyrazolines and Spiroheterocycles using Sustainable Synthetic Strategies
42	Subhashini V. S.	CHEM11201804022	Selective Functionalization of Arenes, Heteroarenes and Dinitriles using Hypervalent Iodine Reagents and Nickel Salts
43	Subhashree Subhadarshini Panda	CHEM11201804023	Synthesis and Biochemical Evaluation of Unnatural Aromatic Amino Acids/ Peptides/ DNA Comprising Salicylic-Picolamide and Aminotropone Scaffolds

44	Ratnakar Saha	CHEM11201904003	Base Metal (Ni, Cu and Fe)-Catalyzed C(sp^3)–H Alkylations with Alcohols as Coupling Partners Employing Borrowing Hydrogen Approach and Post Functionalizations
SINP, Kolkata			
45	Arpita Nandy	CHEM05201804001	Designing Electrocatalysts for Sustainable Future: Applications Toward Electrolyzers and Fuel Cells

Engineering Sciences

S. No.	Student Name	Enrollment No.	Title of the thesis
BARC, Mumbai			
46	Jadhav Pankaj Shankarrao	ENGG01201404021	Time-Frequency Domain Machine and Deep Learning Approaches for Automated Detection of Sleep Stages using EEG Recordings
47	Rakesh Kumar	ENGG01201804007	Investigations on Critical Heat Flux and Heat Transfer Coefficient Under Oscillatory Flow Conditions
48	D. Satish Kumar	ENGG01201804033	Developing Methodology for Evaluating Design Basis Flood Level for Coastal Sites of Nuclear Facilities
49	Avinash Jagannath Gaikwad	ENGG01201818006	Studies on NPP Heat Transport System Configuration for Steam Drum Level Behavior and Improvement in Safety of Multiple Loop BWR
50	Raj Kumar Singh	ENGG01201918001	Study Of Turbulence Mixing and Flow Structures in Reactor Sub-Channels Using Direct Numerical Simulation
51	Rehim N. Rajan	ENGG01201504004	Electromagnetic Interference in Accelerators
52	Hitesh Choudhary	ENGG01201604005	Studies on Pulsed Electromagnetic Expansion and Dissimilar Metal Joining
53	Sherry Rosily	ENGG01201604011	Study and Analysis of Supersonic Gas Jet Based Beam Profile Monitoring Systems for A High Intensity Linear Proton Accelerator
54	Gyanendra Kumar	ENGG01201604018	Pulse Power Application in Cell Biology and Cancer Treatment
55	Kapil Bodkha	ENGG01201704003	Investigations on Thermal-Hydraulic Characteristics of Supercritical Fluid Under Natural Circulation

56	Saurav Sunil	ENGG01201704009	Thermo-Mechanical Processing of AISI 304L to Achieve an Ultrafine Grained Microstructure and its Correlation With Mechanical Properties
57	Binu Kumar	ENGG01201704010	Interaction of Thermo-Mechanical Hydraulic Processes in Deep Geological Disposal System: Predictive Modelling and Experimental Validation
58	Harshit Jain	ENGG01201804002	Study, Simulation, Experimental Validation and Flaw Characterization Using Ultrasonic Instrumentation for Concrete Material
59	Priyanshu Gupta	ENGG01201804003	Multiscale Processing of Seismic Ambient Noise with Application to Imaging Earth's Interior
60	Md. Serajjudin	ENGG01201804013	Studies on Optimization of Processing Parameters of Grinding and Solid Liquid Separation for Limestone Ore
61	Sourav Sarkar	ENGG01201804015	Experimental and Computational Studies on Hydrodynamics and Mass Transfer in Liquid-Liquid Pulsatile Flow in Column Contactors
62	Shrishma Paik	ENGG01201804017	Study on Ultrasound Assisted Precipitation of Yellow Cakes
63	Kanchi Sunil	ENGG01201804024	Study, Design and Experimental Verification of Plasma Opening Switch for High Current Applications
64	Rajnesh Kumar Chaurasiya	ENGG01201804030	Experimental and Computational Studies on Microfluidic Solvent Extraction
65	Nida Khan	ENGG01201804031	Synthesis and Characterisation of Lithium Titanate for Tritium Breeding Application
66	Swetha K.	ENGG01201804032	Identification of Contaminant Sources in Groundwater using Simulation Optimization Models with Uncertainty Analysis
67	Priti Singh	ENGG01201904031	Investigation and Characterisation of Electron Beam Generated High Density Plasma and Separations of Ions from Plasma
IGCAR, Kalpakkam			
68	Satya Prakash Pathak	ENGG02201604005	Investigations into Water Flow Instability and Thermo-Mechanical Damage of Once-Through Steam Generators Used in SFR

69	Aditya Gour	ENGG02201504014	Novel Approach towards Qualification of COTS Components for Distributed Digital Control Architecture of Nuclear Reactors
70	E. Hemanth Rao	ENGG02201518002	Molten Fuel Sodium Interaction Studies Using Simulated Corium
71	E. Vetrivendan	ENGG02201704016	Development, Testing, and Characterization of Highly Oriented Pyrolytic Graphite Coatings for Pyroprocessing
72	Vivek Kumar Mishra	ENGG02201804007	Analysis for Performance Optimization of a Fast Reactor Fuel Vault Ventilation System
73	D. Sujish	ENGG02201804008	Separation of Fission Products from Electro-refiner Spent Salt
74	Sneha M.	ENGG02201804012	Organic Electrochemical Transistor-based Biosensing of Salt Stress in Plants
75	Ramesh Sanga	ENGG02201604008	Studies on Development of Quasi Digital Sensors and Instrumentation for Online Analysis of the Lubricant Oil Quality of Rotating Machinery
76	Parthkumar Rajendrabhai Patel	ENGG02201604019	Severe Accident Source Term Mechanistic Model Development for SFR
77	N. V. Adinarayana Karibandi	ENGG02201904010	Numerical Investigations on the Performance of Coupled Natural Circulation Loops with Application to Nuclear Reactor Safety
IPR, Gandhinagar			
78	Piyush Prajapati	ENGG06201604001	An Engineering Study of Concepts for Heat Extraction and Power Conversion from Tokamak Fusion Reactors
79	Debrup Mukhopadhyay	ENGG06201604002	Comparative Study of Negative Hydrogen Ion Density Measurement through Enhancing Technical Competency of Various Diagnostics in RF Plasma
80	Vyom Ajaybhai Desai	ENGG06201804013	Synthesis and Application Studies of Ti_3AlC_2 Max Phase Material
81	Patel Harsh Bhikhubhai	ENGG06201904004	Experimental and Simulation Studies of Effective Thermal Conductivity of Compressed and Uncompressed Pebble Beds for Fusion Blankets
82	Patel Kirankumar Ganeshbhai	ENGG06201804010	FPGA Based Real Time Density Feedback Contol System for ADITYA-U Tokamak

RRCAT, Indore			
83	Saurav Kumar Nayak	ENGG03201704001	Laser Based Thick Layered Powder Bed Fusion of Material for Building Smart Engineering Components
84	Sunil Yadav	ENGG03201804003	Investigating on Laser Directed Energy Deposition based Multi-material Additive Manufacturing of Copper and Stainless-Steel

Medical and Health Sciences

S. No.	Student Name	Enrollment No.	Title of the thesis
TMC, Mumbai			
85	Vaishakhi Sharadkumar Trivedi	HLTH09201504003	Characterization of Therapeutically Relevant Alterations in Human Thyroid Cancers
86	Harshini Sriram	HLTH09201804003	Evaluation of Role of miRNA Dysregulation in the Prognostication of Newly Diagnosed Multiple Myeloma
87	Smriti Sharma	HLTH09201804006	Quality Audit in Flattening Filter Free Beams of High Precision Radiotherapy

Life Science

S. No.	Student Name	Enrollment No	Title of the Thesis
BARC, Mumbai			
88	Babita Singh	LIFE01201504003	Identification of Druggable Targets and New Therapeutics for Improving the Outcome of Radiotherapy
89	Poonam Gajanan Bhad	LIFE01201704001	Genetic and molecular characterization of large seed mutant in groundnut (*Arachis hypogaea L.*)
90	Navamani Mallikarjunan	LIFE01201804003	Radiation Processed *Psyllium* for Development of Fortified Functional Foods
91	Mahesh Kumar Padwal	LIFE01201804004	Development of Diagnostic and Prognostic Algorithms for Neuroendocrine Tumors from RNA-Sequencing Profiles of Peripheral Blood Cells
92	Golu Misra	LIFE01201804007	Characterization of Leaf Developmental Mutant and its Response to Salt Stress in Chickpea (*Cicer arietinum L.*)

93	Devanshi Khare	LIFE01201904002	Molecular Physiology of Metal Tolerance and Transport in *Chryseobacterium* sp. Strain PMSZPI Isolated from a Uranium Ore Deposit
94	Shruti Mishra	LIFE01201904005	Molecular Studies on Interaction Between FtsK and Tyrosine Recombinases in *Deinococcus radiodurans*
95	Vikash Kumar	LIFE01201504010	Studies on the Stage-specific Mechanisms of Salt Tolerance and Contribution of Signaling Pathway Components in Rice (*Oryza sativa L.*)
96	Gautam Vishwakarma	LIFE01201504011	Identification and Analysis of Stem Rust Responsive Genes in Wheat
97	Megha Sodani	LIFE01201704005	A CRISPR Based Analysis of Essential Genes in Mycobacteria
98	Rohit Sharma	LIFE01201804005	Studies on Development of Radioimmunotherapy Agents and Understanding their Mechanism of Action
99	Pooja Negi	LIFE01201804008	Physiological and Molecular Insights into Radiation Induced Salt Tolerant Mutant of Sugarcane
100	Ganesh Pai B.	LIFE01201804009	Interplay of DNA Damage Repair, Replication Stress and Autophagy under the Functional Deficiency of PARPs in Cancers
101	Archita Rai	LIFE01201804010	Modification of Nrf-2 Activity in Radio-resistance and Inflammatory Responses
IMSc, Chennai			
102	T. S. Sreevidya	LIFE10201704001	Effects of Charged Mutations and Phosphorylation on Binding Pocket Dynamics in Proteins
103	Chandrani Kumari	LIFE10201704003	Machine Learning and Predicting Clinical Outcomes
104	S. Pavitra	LIFE10201704004	Evolution and its Role in DNA, Centromeres and Speciation
105	Ajaya Kumar Sahoo	LIFE10201904002	Computational Data-driven Investigation of Chemical Exposome and its Links to Human and Ecosystem Health
NISER, Bhubaneswar			
106	Aranyadip Gayen	LIFE11201604002	Exploring the Function of Zinc-binding Domain of eIF2 Complex in Translation Initiation Fidelity
107	Indrajit Poirah	LIFE11201604001	Understanding Hypoxic Gastric Cancer Microenvironment

108	Nishant Kumar Dubey	LIFE11201704009	Importance of Steroids on Atypical Ca^{2+} - Channels: Implications in Health and Diseases
109	Somlata Khamaru	LIFE11201804009	Analysis of Altered Cell-mediated Immune Responses during Modulation of Melanoma driven Immunosuppression
110	Sakshi Mahesh Poddar	LIFE11201804016	Characterization of *Escherichia coli* cell division protein FtsZ: Insights from ring assembly defective mutants and FtsZ inhibitor PC190723 binding
111	Tathagata Mukherjee	LIFE11201604008	Regulation of Cell-Mediated Immune (CMI) Responses Associated with Experimental Immunosuppression
112	Deep Shikha	LIFE11201804004	Importance of TRPM8 Ion Channel in Cellular, Sub-Cellular-Organelle Functions in Neuronal and Immune Cells, and its Implications in Health as well as Diseases
113	Patel Saket Awadhesbhai	LIFE11201804007	Unlocking the Therapeutic Potential of EEF1A2 in Breast Cancer: Unravelling Molecular Mechanisms, Crosstalk, and Small Molecule Inhibitors for Effective Treatment Strategies
114	Ananya Palo	LIFE11201804011	Investigating the Regulatory Dynamics of FRG1: Characterization of cis-acting Regions, Downstream Pathways, and its Role in Nonsense-Mediated Decay
115	Avrajjal Ghosh	LIFE11201904004	Biogeography and Systematics of Three Wet-zone Skink Genera (Family: Scincidae) from the Indian Subcontinent
116	Swati Sagarika Panda	LIFE11201904013	The Role of Gut Microbiota in Maintaining Health via Gut-Adipose-Brain Axis
RRCAT, Indore			
117	Kinkar Omkar Umesh	LIFE03201704001	Molecular Characterization of Bacterial Insecticidal Proteins
SINP, Kolkata			
118	Sk. Ramiz Islam	LIFE05201704001	Understanding Metabolic and Epitranscriptomic Reprogramming Associated with Nutritional and Therapeutic Stress Response in Liver Cancer Cells
119	Vipin Singh	LIFE05201804003	Reprogramming of Epigenetic Landscape of Chromatin by E3 Ubiquitin Ligase in Oncogenesis and infection

120	Priyanka Sengupta	LIFE05201804007	Deciphering the Role of Insulin Signaling in Neurodegenration and its regulatory mechanism
121	Farhana Islam	LIFE05201904001	Architectural Roles of IHF and Tfam in Genome Organization: A Single-Molecule Spectroscopic Approach to Study Holliday Junction Dynamics and Mitochondrial DNA Bending
122	Debasish Prusty	LIFE05201904005	Analysis of Metabolomic Changes Associated with Wearing Face-mask and COVID-19.
123	Manorama Ghosal	LIFE05201904009	Designing Plasmonic Nanoparticles for Theranostics and Multiscale Biophysical Investigations at Nano-Bio Interfaces
124	Aditya Singha Roy	LIFE05201704002	Post-transcriptional Regulation of Gene Expression in Eukaryotes by RNA Sequence and Structural Elements
125	Palamou Das	LIFE05201804002	Mitochondrial Fission-fusion Dynamics and Effect on mtDNA Release
126	Rupasree Brahma	LIFE05201804004	Gating-related Structural Dynamics of MgtE Homologs from *Thermus thermophilus* and *Bacillus firmus*
127	Swagata Adhikari	LIFE05201804008	Remodelling of Extracellular Matrix by Chromatin Regulator UBR7 in Triple-negative Breast cancer: Insight into Chemoresistance
TMC, Mumbai			
128	Dipti Kamalkant Sharma	LIFE09201504009	Assessment of Cellular and Molecular Alteration Associated with Acquirement of Radiation Resistance in Oral Cancers
129	Lonare Amol Moreshwar	LIFE09201704003	The Role of 14-3-3σ in Regulation of Tumor Progression, Chemo and Radio Resistance
130	Phadte Pratham Prakash	LIFE09201804001	Investigating Role of MAPK-ERK & PIK3CA-AKT Signalling on Autophagic Flux in Ovarian Cancer Stem Cells
131	Madhura Vishwas Ketkar	LIFE09201804013	Discovering the Molecular Mechanisms Governing Cellular Senescence in Glioblastoma
132	Shaikh Zaid Muneef Shaheen	LIFE09201804016	Molecular Studies on Chemoprevention using Polymeric Black-tea Polyphenols (PBP's) on Experimental Lung Carcinogenesis.

133	Sayoni Roy	LIFE09201604007	Understanding the Role of Wnt Signaling pathways in Epidermal Homeostasis and Stem Cell regulation
134	Shreosi Chatterjee	LIFE09201604009	Study of Size, Shape and Dynamics of the Nucleolus
135	Sushant Shirish Navarange	LIFE09201604010	Molecular Profiling to Understand the Regulation and Maintenance of Oral Cancer Stem Cell
136	Neha Mishra	LIFE09201704016	Structural and Functional Characterization of Different Domains of BRCA1 and its Interacting Proteins
137	Kalyani Abhiram Natu	LIFE09201704018	Investigating the Molecular Basis of c-FLIP/Calmodulin Interaction for Modulating Apoptosis
138	Shubhashish Chakraborty	LIFE09201804005	Structural Basis of Eph Receptor and Ephrin Ligand to Understand Cell-Cell Signalling and Pathogenicity of Mutations Identified in Cancer
139	Bhawna Singh	LIFE09201804008	Elucidating the Role of BCCIP in Cancer Pathogenesis and Development of Resistance

Mathematical Science

S. No.	Student Name	Enrollment No.	Title of the thesis
HRI, Prayagraj			
140	Parul Keshari	MATH08201704006	Invariants of Moduli Spaces and (Semi) Tannakian Categories of Twisted Quiver Bundles
141	Srijonee Shabnam Chaudhury	MATH08201804005	Some Problems in Quadratic Forms Over Number Fields and Related Topics
IMSc, Chennai			
142	Piyasa Sarkar	MATH10201704003	On Multi-Parameter CCR Flows
143	Tanmoy Bera	MATH10201804002	Poissonian Pair Correlation in Higher Dimensions
144	Ratheesh T V	MATH10201704001	On Combinatorial Models for q-Whittaker and Modified Hall–Littlewood Polynomials
145	Namitha C H	MATH10201904004	Some Results on Multiparameter Decomposable Product Systems and CAR Flows
146	Manas Mandal	MATH10201804004	Cohomology of Generalized Dold Manifolds
147	Siddheswar Kundu	MATH10201804007	Demazure Crystal Structure for Flagged Skew Tableau and Flagged Reverse Plane Partitions
148	Dhananjaya Sahu	MATH10201904002	On Holomorphy and Special Values of Artin L-Functions
NISER, Bhubaneswar			

149	Rucha Bhalchandra Joshi	MATH11201904003	Graph Neural Networks: Privacy and Applications
150	Suman Mukherjee	MATH11201904009	Weighted Inequalities for Multilinear Operators in Dunkl Setting
151	Susobhan Bandopadhyay	MATH11202004002	Parameterized Algorithms for Constrained Graph Problems

Physical Sciences

S. No.	Student Name	Enrollment No.	Title of the thesis
BARC, Mumbai			
152	Nilesh Subhash Tawade	PHYS01201704013	Measurement of Fast Neutron Induced Reaction Cross-Section for Elements Relevant to Reactor Technologies
153	Deepak Raikwal	PHYS01201804001	Neutrino Mass Ordering, Earth Tomography and Lorentz Invariance Violation Study in ICAL@INO, Long Baseline and Reactor Experiments
154	Tanmay Sarkar	PHYS01201804012	Studies of Near-source Aerosol Dynamics and Microphysics: Impacts on Optical Properties in Standalone Mie Models and Atmospheric General Circulation Models
155	Anurup Das	PHYS01201904012	Development of Doped Nasicon-Type Glass ceramics Systems as SolidState Electrolyte For Lithium Ion Battery
156	Raj Bhupen Shah	PHYS01201904024	Feasibility Study of Cosmic Muon Veto Detector and Measurement of Muon Charge Ratio Near Equator
157	Gaurav Mukherjee	PHYS01202004006	QCD Matter under Rotation and Magnetic Field
158	Jim M. John	PHYS01201704015	Improvements to INO-RPC Detector and the Charge Dependent Muon Flux at Madurai
159	Rathod Tejas Damjibhai	PHYS01201804005	Optical Properties of Carbonaceous Aerosol and its Radiative forcing Potential at an Urban Site in Mumbai, India
160	Deepa Sathian	PHYS01201804014	Design and Development of New Neutron Detectors for Criticality Accident Dosimetry
161	Subodha Sahoo	PHYS01201904017	High Pressure Magnetic, Transport and Spectroscopic Investigations on some Cu Based Insulators and Layered Metallic Systems.

162	Swati Mehta	PHYS01201904020	Electrostatic Complexation of Charged Nanoparticle-Polyelectrolytes and their Evaporation-Induced Assembly
163	Vidha Bhasin	PHYS01201904021	Investigations on Thin Film Electrode Based Lithium-Ion Battery
164	Raj Kumar	PHYS01202004001	Characterizing the Spectral and Timing Properties of Black Hole Systems in High Energies
165	Abharana N	PHYS01202004013	In-Situ Structural investigation on Novel Electrode Materials for Rechargeable Lithium-Ion Battery
HRI, Prayagraj			
166	Divyansh Shrimali	PHYS08201804005	Tight Bounds with Capacity of Entanglement and for Charging of Quantum Battery
167	Sankha Subhra Bakshi	PHYS08201605002	Nonequilibrium Dynamics of Photo-Pumped Correlated Insulators
168	Abhay Srivastav	PHYS08201804001	Quantum Speed Limits for Arbitrary Time-Continuous Processes
169	Anjan Kumar Barik	PHYS08201804003	Studies on Aerosol Transport Through Various Leak Pathways
170	Ratul Banerjee	PHYS08201804011	Measurement - Based Entanglement Generation in Quantum Network
171	Sachin Grover	PHYS08201804012	Unitary/Non-Unitary Correspondence, and Defects in 2D CFTS.
172	Lakkaraju Leela Ganesh Chandra	PHYS08201904002	Exploring Variable-Range and Non-Hermitian Systems: From Entanglement Distribution to Quantum Battery
173	Rivu Gupta	PHYS08201904004	Quantum information Processing with Random States
IGCAR, Kalpakkam			
174	Usha Pujala	PHYS02201504004	Effect of Aerosol Morphology and Charging Over the Dynamics of Aerosols in a Closed Chamber in the Context of Sodium Cooled Fast Reactor (SFR) Safety analysis
175	Sujatha Pavan Narayanam	PHYS02201604003	Studies on Aerosol Transport Through Various Leak Pathways
176	V. Madhav Kumar	PHYS02201604017	Transition Metal Oxides Decorated Vertical Graphene Nanosheets for Supercapacitor Application
177	Shakti Singh	PHYS02201904003	Atomistic Models of Iron Phosphate Glasses - Development, Structural Characteristics and Properties through Simulations

178	Julie S.	PHYS02201704003	The Impact of Ion Irradiation on the Texture, Grain Boundary Characteristics, Void Swelling Behavior and Surface Morphology of Nanocrystalline Ni
179	Sreelakshmi N.	PHYS02201704008	Ion Irradiation Induced Defect Production, Recovery and Blistering Mechanism in 3C-SiC
180	R. S. Mrinaleni	PHYS02201804005	Studies on Magnetic and Magnetotransport Properties of $Nd0.6Sr0.4MnO_3$ Thin Films and $Nd0.6Sr0.4MnO_3/SrRuO_3$ Heterostructures
181	Venkateswara Reddy Karrevula	PHYS02201804010	Investigation of Humidity Effects on I-V Characteristics and Alpha Spectra of Commercial Non-Hermetically Sealed Silicon Pin Diodes
182	Papiya Saha	PHYS02201904010	Structure and Physical Property Correlations in Ru, Cu and Co Based Double Perovskite Oxides
IMSc, Chennai			
183	Subashri V.	PHYS10201804002	Rare Events in Cluster-Cluster Aggregation
184	Sahil	PHYS10201605002	Pre- and Post selected Measurements, and Uncertainty Relations
185	Hitesh Garg	PHYS10201805001	Bridging Induced Coil-to-globule Transition and Aggregation of Polymers
186	P. Rakesh Kumar Dora	PHYS10202004006	Fractional Quantum Hall Liquids: Their Ground States, Neutral Excitations, and Competition with Crystal Phases
IoP, Bhubaneswar			
187	Rupam Mandal	PHYS07201704008	Tailoring Resistive Switching Properties of Metal Oxide Memristors for Neuromorphic Applications
188	Subhadip Bisal	PHYS07201904006	Next-To-Leading Order Corrections to Dark Matter Direct Detection and Precision Observables
189	Siddharath Prasad Maharathy	PHYS07201804003	Collider Phenomenology of Charged Higgs in Neutrino Mass Models
190	Sandhyarani Sahoo	PHYS07201804005	Studies of Gate-Bias Controlled 2D Material-Based Devices for Photodetector Applications
191	Abhishek Roy	PHYS07201804007	Exploring Particle Physics Models: Implications for Dark Matter Phenomenology

192	Chitrak Karan	PHYS07201804010	Activating Semiflexible Filaments: Impact of Motor Protein Drive and inertia
193	Pritam Chatterjee	PHYS07201804012	Topological Superconductivity in Magnet/Superconductor Heterostructures
194	Sudipta Das	PHYS07201804013	Probing Beyond the Standard Model Scenarios in Long-Baseline and Astrophysical Neutrino Experiments
195	Arpan Sinha	PHYS07201804017	Active Nematics: Exploring Reciprocity and its Absence
IPR, Gandhinagar			
196	Janmejay Umeshbhai Buch	PHYS06201604007	Study of Edge Plasma Dynamics in Tokamak Aditya-U
197	Nitin Bairagi	PHYS06201704007	Study of MgB_2 Based Superconducting Current Feeders System for Fusion Devices
198	Ankit Dhaka	PHYS06201904002	Experimental and Molecular Dynamics Studies of Transport Phenomena in a Complex Plasma
199	Varsha Siju	PHYS06201704009	Study of Electron Dynamics in Tokamak Plasma Through Electron Cyclotron (EC) Emission Using Radiometer
200	Purvi Dave	PHYS06201704010	Surface Modification of Silicone Catheters to Mitigate Bacterial Adhesion and Biofilm Formation
201	Sagar Agrawal	PHYS06201704011	Study of Process Parameters Affecting Secondary Phase formation and Grain Size in Cu_2ZnSnS_4 Thin Film for Solar Cell Application
202	Suruj Jyoti Kalita	PHYS06201804002	Molecular Dynamics Study of Subcritical Transition to Turbulence in a 3D Yukawa Liquid
203	Kalyani Swain	PHYS06201804009	Laser Cluster interaction in Strong External Magnetic Field
204	AnjanbKumar Paul	PHYS06201804012	Vlasov-Maxwell Simulations of Whistler Mode interaction with Bulk and Beam Plasma
205	Shishir Biswas	PHYS06201804013	Turbulent Dynamo Action in a 3-Dimensional Magnetohydrodynamic Plasma
NISER, Bhubaneswar			
206	Tapas Ranjan Senapati	PHYS11201704025	Spintronics with Josephson Nano-Devices
207	Kalyan Ghosh	PHYS11201804001	Novel Synthesis of ZnTe for Optoelectronic Applications
208	Debamalya Dutta	PHYS11201904003	Electromagnetic responses in low dimensional lattice models

209	Prabhakar	PHYS11201804002	Fock Space Recursive Green's Function Technique: A Novel Method to Study Strongly Correlated Systems
210	Sujit Garain	PHYS11201804005	Quantum Sensing of Magnetic Field Using Thermal and Cold Atomic Vapor
211	Abhisek Mishra	PHYS11201804007	Spin Pumping with Quantum Materials
212	Mouli Chaudhuri	PHYS11201804008	Characterization of Low-Threshold Cryogenic Detectors and Study of Backgrounds for Rare Event Searches
213	Shaktiranjan Mohanty	PHYS11201804009	Synthetic Antiferromagnets for Spintronics
214	Sadaf Madni	PHYS11201904006	Transport Coefficients of Deconfined Nuclear Matter by Gribov Prescription
215	Subhadip Pradhan	PHYS11201904008	First-Principle Studies on Magnetic topological Semimetals and their Transports
216	Ankit Kumar Panda	PHYS11202004002	Relativistic Dissipative Causal Magnetohydrodynamics from Kinetic theory and the Effect of Electric Fields on Bulk Observables in High Energy Heavy Ion Collisions
RRCAT, Indore			
217	Yashveer Singh	PHYS03201604002	Raman Spectroscopy and Optical Trap Based Studies on Human Red Blood Cells Subjected to External Stress
218	S. K. Ramjan	PHYS03201704011	Structural, Electric and Thermo-Magnetic Properties of Rare Earth and Transition Metal Based Alloy Superconductors
219	Vivek Singh	PHYS03201804011	Studies on Cooling and Trapping of Rb Atoms on Atom Chip
220	Pradeep Kumar Gupta	PHYS03201704002	Studies on Multimode interference and Pulse Shaping in Fiber Lasers
221	Aniket Chowdhury	PHYS03201704003	Development of Novel Techniques Using Optical Tweezers for Investigating Disease and Stress Mechanisms in Human Red Blood Cells
222	Geetanjali	PHYS03201704005	Impact of Charge Carrier Localization on the Optoelectronic Properties of InAsP/InP and InGaAs/GaAs Quantum Wells and Devices

223	Ranjana Rathore	PHYS03201704006	Ultrafast Probing of Photo-induced Thermal Strain Propagation in Semiconductors Using Time Resolved X-Ray Diffraction
224	Partha Sarathi Padhi	PHYS03201704010	Studies on Al_2O_3/TiO_2 Nano-Laminates for Energy Storage Applications
225	Sourabh Sarkar	PHYS03201804001	Studies on Trapping and Manipulation of Cold Atoms Using Magnetic, Radio-Frequency and Laser Fields
226	Sonali Pradhan	PHYS03201804003	Multifunctional Nanocomposite Systems for Energy Harvesting, Sensor Applications and Exchange Bias Investigations
227	Ankur Sharma	PHYS03201804004	Structure-Property Correlation in Niobium Doped $(Na_{0.41}K_{0.09}Bi_{0.5})TiO_3$: A Lead-Free Ferroelectric Material
228	Joydipto Bhattacharya	PHYS03201804006	First-Principles Studies on Electronic, Magnetic, and Spin Transport Properties of Bulk and Heterostructures of Heusler Alloys
SINP, Kolkata			
229	Ashish Gupta	PHYS05201804007	Study of Proton induced Reactions on Er-Isotopes
230	Shefali Basak	PHYS04201904006	Study of Nuclear Structure Around A ~ 150 Mass Region
231	Rajkumar Mondal	PHYS04201904018	Study of Hot and Dense Magnetized Matter
232	Shubham Dutta	PHYS05201704011	Dark Matter Search at the CMS Experiment and Studies on Low Mass Dark Matter Detection Techniques for Underground Experiments
233	SandipHalder	PHYS05201804009	Interfacial Magnetism in Transition Metal Oxide Heterostructures
234	Sabyasachi Karmakar	PHYS05201804015	Structure-Property Correlation in Organic Functional Materials
235	Habib Ahammad Mondal	PHYS05201904010	A Study of Very High Energy Gamma Rays from Active Galactic Nuclei
236	Amanulla Karikar	PHYS05201904024	Study of Magnetocaloric Effect by Tuning the Electronic Phase in Bulk and Nanocrystalline Doped Perovskite Manganites
237	Lalit Kumar Sahoo	PHYS05201804010	Charge Particle Emitting Reaction in Nuclear Astrophysics
238	Subhadip Chowdhury	PHYS05201804012	Study of Structure and Optical Properties of Two Dimensional Hybrid Lead Perovskite Materials

239	Shubharaj Mukherjee	PHYS05201804017	Hydrological Investigation of Regional Aquifer Systems in Contrasting Climatic Regions of North West India using Isotope - Geochemical Modelling Approaches
240	Mousri Paul	PHYS05201804023	Studies on Structural and Transport Properties of Cerium Oxide Thin Film
241	Maudud Ahmed	PHYS05201804026	Defect Characterization of Certain Oxide Based Nanocrystalline Compounds using Positron Annihilation and Supportive Methods
242	Siba Prasad Acharya	PHYS05201804028	Nonlinear Waves and Chaos in Plasmas
243	Sk. Md. Adil Imam	PHYS05201904003	Deciphering the Cold Dense Matter Eos: Integrating Nuclear Theory, Experiments and Astrophysical Observations
244	Suman Das	PHYS05201904006	Toy Model of Quantum Black Holes and Correlation Functions
245	Anindita Karmakar	PHYS05201904009	Nuclear Structure Studies at High Angular Momentum
246	Koustav Pal	PHYS05201904011	Investigation of Exchange Bias and Magnetotransport in Bulk and Thin Films Materials
247	Soma Chatterjee	PHYS05201904015	Magnetic, Magnetocaloric, Electrical Transport, and Polarization Study on Various Bulk and Nanocrystalline Oxide Compounds
248	Suman Dey	PHYS05201904020	Synthesis and Characterization of Assembled Nanostructures for Surface Enhanced Raman-Scattering and Electrochemistry Applications
249	Tukai Singha	PHYS05201904022	Synthesis and Characterizations of Metal Nanostructures for Application in Direct Alcohol Fuel Cells
VECC, Kolkata			
250	Santanu Paul	PHYS04201504001	Phase Space Studies for Optimum Beam Transport and Matching During Injection and Extraction in Cyclotrons
251	Singh Vivek Kumar Rajeshwar	PHYS04201704004	Study of Beauty Hadrons using Heavy Flavour Decay Electrons with Alice Detectors at LHC
252	Kirti Atreya	PHYS04201704005	Study of Fusion Fission Dynamics of Heavy Nuclei
253	Sansaptak Basu	PHYS04201904005	Experimental Investigation of the Structure of Nuclei with Z, N~2

254	Nilanjan Chaudhuri	PHYS04201904009	Strongly Interacting Hot and Dense Matter in Background Electromagnetic Field
255	Vinay Shukla	PHYS04201904015	Studies on Coherence in Ladder System and its Extension to Atomic Beam

Integrated Ph.D.				
S. No.	**Student Name**	**Enrollment No.**	**Title of the thesis**	**Discipline**
BARC, Mumbai				
256	Ponangi Hanumath Thyagaraju	APSA01201818001	A Study of Technology Transfers from BARC	Studies on Applied System Analysis
HRI, Prayagraj				
257	Tanaya Ray	PHYS08201405007	Non-linearity as a Resource in Quantum Advantage	Physical Sciences
IMSc, Chennai				
258	Pavan Dharanipragada	PHYS10201705004	Applications of Renormalisation Group in Holography	Physical Sciences
NISER, Bhubaneswar				
259	Prottay Das	PHYS11201705001	Studying Chiral Magnetic Wave, Hadronic Rescattering and $f_1(1285)$ Production in High Energy Collisions with ALICE Detector	Physical Sciences
260	Shuvayu Roy	PHYS11201705004	Black Holes and Relativistic Fluids from the Perspective of Near-Equilibrium Dynamics	Physical Sciences

RESEARCH THESES OF HBNI's Ph.D./ Int. Ph.D. STUDENTS AT A GLANCE

APPLIED SYSTEMS ANALYSIS

1. Applied System Analysis

1.1 Bhabha Atomic Research Centre, Mumbai

1.1.1 *A quantitative assessment of the role of nuclear power reactors in a low carbon energy mix*

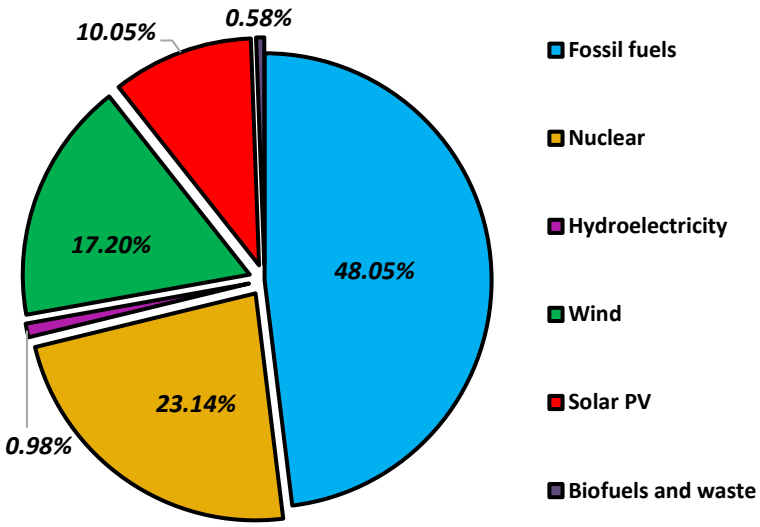

Target optimal generation portfolio for net zero India in 2070

A global low carbon emissions intensity energy transition is the need of the hour in the light of the climate crisis, that has largely been caused by anthropogenic greenhouse gas emissions. The determination of the most suitable energy transition program leading to economy-wide net zero emissions is a task that must be undertaken by each nation individually, considering its development objectives, resource availability and energy security considerations.

This thesis addresses the energy transition of India to a net zero economy by 2070 by developing mathematical frameworks for long-term energy demand estimation, demand-supply matching, and supply mix optimization. India's long term final clean energy demand is projected to be at least 24000 TWh, with about 65% energy requirement being in the form of direct electrification and rest for indirectly electrified services like hydrogen production, carbon capture etc., for industrial decarbonization.

This annual figure is scaled up to derive hourly electricity demand profiles for the entire year in 2070, using today's information from current demand patterns. A combination of low carbon generators including nuclear reactors, solar PV farms, wind farms, hydel power plants, biomass-based power plants, fossil fuel-based thermal power plants with post-combustion carbon capture are assumed to be part of the generation portfolio to meet this projected demand.

A hybrid system made up of water electrolysers and grid-scale batteries is considered as the widely deployable technological intervention needed for power demand-supply balancing and grid stability. An algorithm is proposed for optimal excess power allocation, to maximize

excess energy utilization by the electrolysers operating within their technical limits, while reducing the dependence on battery energy storage system to meet any phases of supply shortfall. This is seen to minimize the capital investment needed for the balancing infrastructure.

An optimal integrated, low carbon electricity supply portfolio with the flexible loads and dispatch technologies is designed to meet the projected demand and demand-supply balancing. This is a multi-objective optimization problem balancing conflicting needs. Under various policy preferences, it is determined that optimal supply mix for India is 2.27-11.39% solar PV, 1.56-18.89% wind power, 0.02-1.52% hydel power, 0.04-0.90% biomass-based power, 45.8-72% fossil fuels, and 22.5-24.6% nuclear power.

1.2 National Institute of Science Education and Research

1.2.1 *A behavioural profile and social-emotional reciprocity of children with autism spectrum disorder*

Autism Spectrum Disorder (ASD) is a neurodevelopmental disorder characterised by deficits in social interaction abilities; communication skills; and stereotyped and repetitive behaviour patterns. There were no available early detection instruments for parents of children with ASD, and there was no Indian tool to understand the social-emotional reciprocity of children with ASD, particularly with their parents and siblings.

After the completion of three preliminary studies, three tools were developed. First, the Nayak Autism Screening Instrument was designed with 24 2-dimensional animated videos to help parents identify ASD symptoms in children aged 3-10. The Universal Agreement methodology (S-CVI/UA) estimated the overall content validity of the NASI to be 0.40, but the Average method estimated content validity (S- CVI/Ave) to be 0.93.

Second and third, the Nayak Social-Emotional Reciprocity Questionnaire (NSERQ) (parent version) containing 23 items, and the Nayak Social-Emotional Reciprocity Questionnaire (NSERQ) sibling version containing 21 items demonstrated excellent content validity of individual items ranging from 0.89 to 1.00 and the entire questionnaire's content validity was S-CVI/ UA = 0.50, S-CVI/Ave = 0.95. To design an intervention module for children with ASD, early detection is necessary. It is also paramount to comprehend their SER with their parents and siblings. The three tools developed in this study will fulfil the purpose.

CHEMICAL SCIENCES

2. Chemical Science

2.1 Bhabha Atomic Research Centre, Mumbai

2.1.1 *The development of supramolecule based extractants and suitable diluents for the separation of radio toxic elements*

Over the last few decades various extractants such as Octyl (phenyl)-N, N-diisobutyl carbamoyl methyl phosphine Oxide (CMPO), Malonamides, Trialkyl phosphine oxides, Diisodecyl phosphoric acid and Diglycolamides (DGA), supramolecular extractant based on calix-[4]-arene, calix-[8]-arene and macro cyclic crown ether with various chelating groups are developed by different researchers for the extraction of different radiotoxic elements from the nuclear waste solution. Among all these extractants explored in the literature,

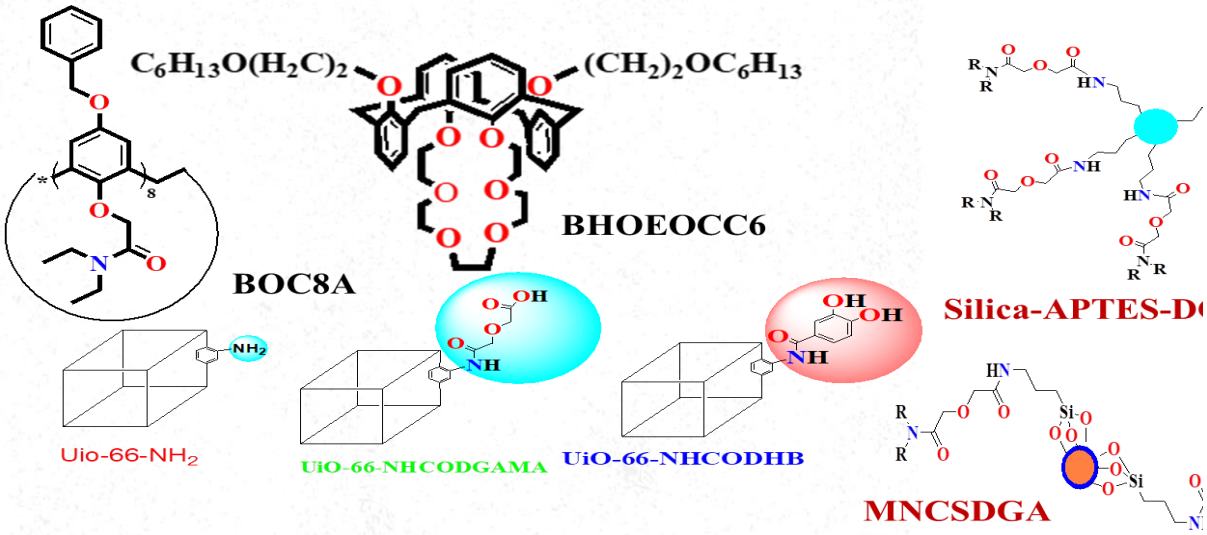

Chemical Structures of supramolecular extractants

supramolecular extractants are very much effective for the separation of radiotoxic elements. Higher extraction efficiencies and selectivity compared to simple molecular ligands are the unique features of supramolecular extractants.

Thus, being motivated by the different fascinating properties and unique sorption behaviour of supramolecular ligands, studies on "Development of Supramolecule based extractants and suitable diluents for the separation of radio toxic elements" were undertaken as a part of present dissertation work. The supramolecular extractant such as 1,3-dioctyloxycalix [4] arene-crown-6 (BOOCC6), 1,3-Bis-(hexyloxyethyl) oxycalix [4] arene-crown-6 (BHOEOCC6), Octabenzyloxyoctakis [[[(N,N-diethylamino)carbonyl)]methyl]oxy]calix-[8]-arene (BOC8A), Di-cyclohexano-18-crown-6 (DCH18C6) etc. were synthesized and explored for the separation of Cs, Sr and Tc from the acid medium resembling to nuclear high level liquid waste in solvent extraction mode.

Whereas two UiO-66-NH_2 based diglycolamic acid monoamide (DGAMA) and 1,2-dihydroxy benzene (DHB) functionalized metal organic frameworks namely UiO-66-NH-CO-DGAMA and UiO-66-NH-CO-DHB have been synthesized for sorption of U and Th from the dilute acid medium resembling to nuclear effluents originated from the front end of nuclear fuel cycle,

and diglycolamide (DGA) functionalized multi coordinated supramolecular sorbent upon silica matrix with magnetic and nonmagnetic cores namely SiO_2-APTES-DGA$(R)_2$ (R= octyl, or 2-ethylhexyl) and MNCSDGA have also been synthesized, characterized and explored for the sorption of actinides from the high acid medium resembling to high level liquid waste of nuclear industry. In addition, theoretical calculations of the ligands viz. BOC8A, BHOEOCC6 and DCH18C6 has been carried out using density functional theory (DFT) to understand the metal ligand interaction in the solvent extraction-based separation of radiotoxic element

2.1.2 *Synthesis and characterization of novel deep eutectic solvent for studying dissolution, coordination and redox chemistry of lanthanides and actinides*

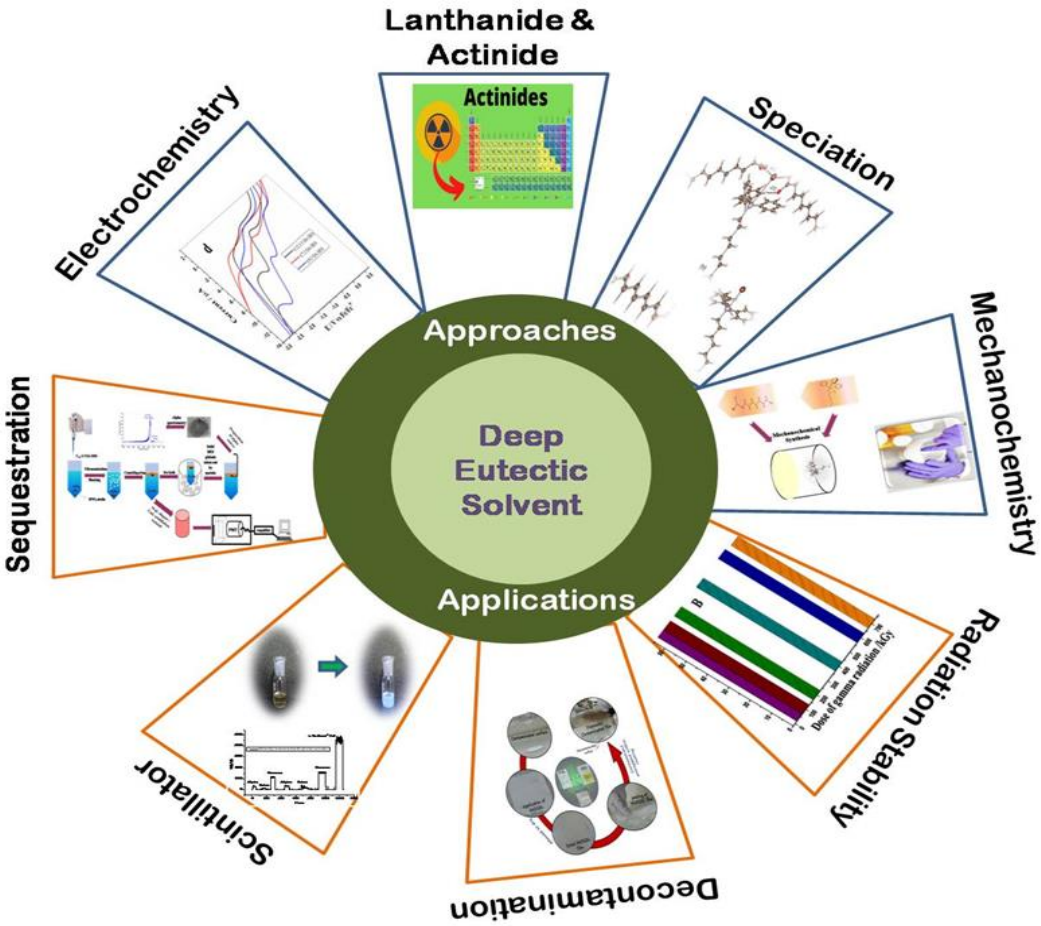

The research detailed in this Ph.D. thesis addresses the significant environmental and technical challenges associated with traditional petroleum-based energy production and the subsequent shift towards sustainable, low-carbon energy generation. Nuclear energy, utilizing fissile actinides like Uranium (U) and Plutonium (Pu), is a mature technology that currently supplies approximately 10% of the world's electricity. However, a major issue with nuclear energy is the management and reprocessing of spent nuclear fuel (SNF), which generates highly radiotoxic waste. This research explores innovative methods for SNF reprocessing to enhance sustainability and efficiency in nuclear energy. One of the key contributions of this research is the synthesis and characterization of DESs, particularly those based on alkyl triphenylphosphonium bromides combined with decanoic acid. These DESs exhibit unique properties such as bright blue photoluminescence, attributed to hydrogen bonding interactions, and have been evaluated for their potential as radioluminescent liquid scintillators. The study

underscores the thermal stability, low vapor pressure, and excellent electrochemical properties of DESs, which make them suitable for various applications in the nuclear industry. The research provides insights into the complexation, photochemistry, and redox behavior of Europium (Eu) and Uranyl ions in DESs. Advanced techniques like time-resolved photoluminescence (TRPL), cyclic voltammetry (CV), synchrotron-based extended X-ray absorption fine structure (EXAFS) spectroscopy, and density functional theory (DFT) calculations were employed. The findings reveal the presence of Eu in distinct local environments within the DES and demonstrate the quasi-reversible reduction of Eu^{3+} to Eu^{2+}. For uranyl ions, the study highlights strong interactions with DES, leading to enhanced luminescence and irreversible electron transfer processes. A significant achievement of this work is the optimization of methods for the selective extraction and quantification of Pu(IV) from complex matrices, particularly in the presence of Uranium and Americium. Among various DESs tested, a specific DES demonstrated high extraction efficiency and radiation stability, making it highly suitable for nuclear fuel reprocessing. The research also developed a single-step, effective method for Pu quantification using alpha spectrometry, which offers operational ease and minimal waste generation. The thesis introduces a novel DES-based decontamination gel, RADGEL, formulated with polyvinyl alcohol for efficient radioactive surface decontamination. RADGEL showed high decontamination efficiencies (97%-99%) across various surfaces and radionuclides, presenting a cost-effective, safe, and environmentally friendly solution for decontamination. This approach reduces secondary waste production and aligns with sustainable practices in nuclear facility operations and decommissioning. The research highlights the versatility and potential of DESs in a wide range of applications beyond nuclear fuel reprocessing, including metal processing, electrochemistry, and environmental remediation. The findings suggest that DESs can be tailored to specific needs by adjusting their components, making them a promising alternative to traditional solvents in various industrial processes. The work also points out the need for further investigation into the interactions and stability of DESs with actinides and lanthanides, particularly under radiation.

In conclusion, this PhD thesis makes significant contributions to the field of nuclear energy by proposing innovative, sustainable solutions for SNF reprocessing and radioactive decontamination. The development and application of DESs as versatile, efficient, and environmentally friendly solvents hold great promise for advancing nuclear fuel management and reducing the environmental impact of nuclear energy.

2.1.3 *Development of high energy density electrode materials for advanced lithium-based batteries*

Lithium based batteries are ubiquitous in our life, owing to their extremely high specific (volumetric/gravimetric) energy densities. Lithium sulfur batteries (LSBs) have the potential to be the next generation of lithium-based batteries, due to their high theoretical energy density, low cost, and environmental friendliness. In LSBs, the electrochemical reactions involve the reduction of sulfur to lithium polysulfides during discharge and the oxidation of polysulfides back to sulfur during charging, alongside the deposition and dissolution of lithium metal at the anode. Despite their potential, LSBs encounter significant challenges that must be overcome to achieve optimal performance. These challenges include the dissolution of polysulfides,

which results in capacity loss and poor cycling stability, as well as low coulombic efficiency, the low conductivity of reaction products, and volume expansion.

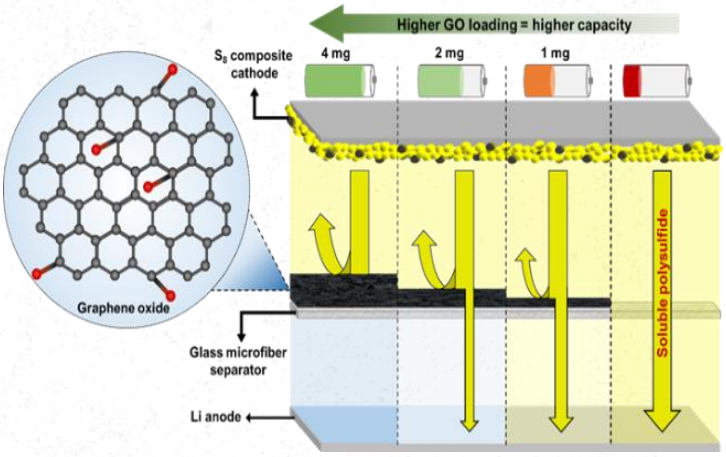

Effect of increasing separator modifier on polysulfide shuttle

This thesis discusses the effects of employing several strategies for designing composite cathode materials as well as chemical modification of separator on specific capacity, cycle life and performance at high rate of charge/discharge. A wide array of cathode hosts ranging from conducting polymer, inorganic MXene as well as carbonaceous material (viz. reduced graphene oxide, bio-derived carbon, N-doped carbon) have been evaluated as cathode hosts. Li^+ diffusivity improves considerably upon modification of separator by graphene oxide (GO). The superior performance can be explained by the excellent polysulfide adsorption by GO and its action as an upper current collector, whereby the adsorbed LiPS also participate in the electrochemical process and contribute capacity. Thus, a uniform dense coating of GO is found to be beneficial towards both cycle life, lithium diffusivity as well as initial capacity of a lithium-sulfur battery as depicted in Figure 1. N-doped carbon-based sulfur cathode with graphene oxide modified separator-based coin-cells were found to be superior to all evaluated cathodes. This cell delivered high specific capacity of offers higher discharge capacities of 1453, 1024, 866, 787, 697 mAh/g when discharged at 50, 100, 200, 300 and 500 mA/g, respectively. The key findings highlight the potential of lithium-sulfur chemistry to meet the increasing demand for energy-efficient storage solutions.

2.1.4 *Investigation of molecular interaction with advanced fluorescence correlation spectroscopy and super-resolution orientation imaging*

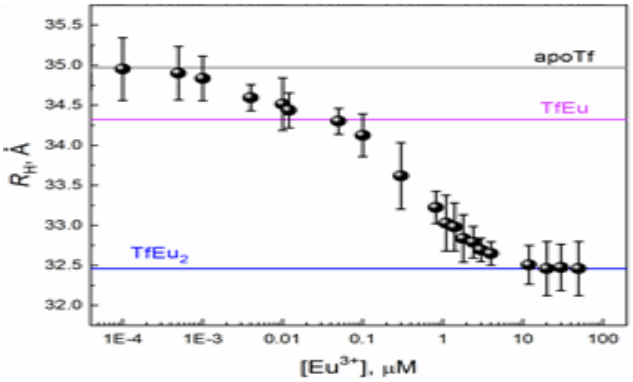

Angstorm scale change in hydrodynamic radius of Europium bound Transferrin probed using Dual-focus FCS setup

Fluorescence-based spectroscopic techniques have advanced significantly, providing crucial insights into molecular interactions, essential for predicting the structure and function of chemical and biological systems. Traditional fluorescence methods, while valuable for studying stoichiometry, kinetics, and thermodynamics, face limitations when applied to actinides and other radioactive elements due to high activity handling restrictions. This thesis addresses these challenges by developing single-molecule-sensitive methods that require minimal activity handling (<1 Bq). The interdisciplinary research focuses on creating an experimental framework and robust analytical methodologies that bridge chemistry and biology, particularly in understanding the spatio-temporal dynamics of metal ion binding to transferrin and receptor-mediated endocytosis, relevant to health concerns related to radiological materials contanimation in human body.

Europium-Transferrin binding was investigated using dual-focus fluorescence correlation spectroscopy (2f-FCS), allowing angstrom-scale monitoring of conformational changes without specific fluorescent labeling. Europium, used as a surrogate for Americium, provided insights into the sequential nature of transferrin bilobal binding. To study dynamic solute exchange and membrane partitioning, a micellar system was employed, mimicking cell membrane architecture. By integrating single-molecule-sensitive FCS with ensemble techniques like time-correlated single photon counting and steady-state spectroscopy, a unified analysis model was developed, capable of elucidating photoinduced electron transfer reactions across picosecond to second timescales.

To observe the spatial and temporal dynamics of biological processes, such as the internalization of the metal loaded transferrin-receptor complex during endocytosis, we developed a spectrally resolved single-molecule orientation localization microscopy setup. This advanced system enables super-resolution imaging beyond the diffraction limit of conventional fluorescence microscopy, while simultaneously providing detailed information on the orientation and fluorescence spectra of individual fluorophores. This approach significantly outperforms current single-particle tracking methods in probing local heterogeneity. Demonstrating its potential, we applied this technique to study sensor molecule binding on amyloid fibrils and lipid domains, revealing unprecedented details of spatio-temporal dynamics in fluorescence spectroscopy.

2.1.5 *Computational studies on fluoride and phosphate based phosphor materials for radiation dosimetry applications*

Ionizing radiations have been used in many industrial and medical applications since their discoveries more than a hundred years ago. Ionizing radiations are not visible to the naked eye, and some radiations have high penetration power against dense matters. Hence, special tools are required to detect and measure these radiations. During the last few decades enormous efforts have been dedicated to the development of suitable phosphor material for radiation dosimetry. The measurement of radiation dose should be very much accurate for the appropriate use of radiation in industrial and medical fields. Among different techniques of radiation dosimetry, Thermoluminescence (TL) and Optically Stimulated Luminescence (OSL) dosimetry have been found to be very much popular for the above applications. Till now

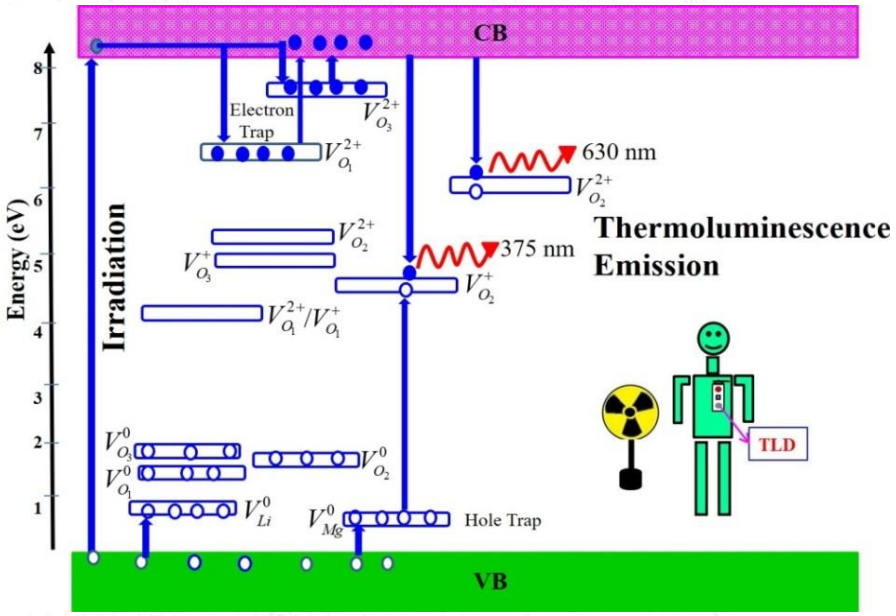

Origin of different emission behaviour of $LiMgPO_4$ due to vacancy defects

large numbers of materials have been developed for TL and OSL dosimetry. Although, a few attempts have been made to understand the role of different intrinsic defects in the undoped and doped LiF, $KMgF_3$, and $LiMgPO_4$, a systematic study of electronic structure of these undoped and doped fluorides and phosphates and effect of intrinsic defects present in them has not been attempted in the previous literatures.

Therefore, the present thesis investigates the role of defects and dopants on the optical properties of fluoride (mainly, LiF, and $KMgF_3$) and phosphate ($LiMgPO_4$) based luminescent materials. The goal of the present thesis is to develop efficient luminescent material for radiation detection and measurements. The present study revealed important role of cation lattice vacancy along with Mg and Ti towards the observed optical behavior of (Mg,Ti) doped LiF. Further, for (Mg,Cu, Ag) doped LiF, Cu contributes to the formation of recombination /luminescence centers; while Ag plays vital role in creating the hole trapping centers. For $KMgF_3$, F vacancies, aggregates of F vacancies, and mixed cluster vacancies are found to play important role towards major optical transitions. Interestingly, oxygen vacancy and their cluster towards play an important role towards major emission of $LiMgPO_4$.

2.2 Indira Gandhi Centre for Atomic Research, Kalpakkam

2.2.1 *Synthesis of bifunctional magnetic nanostructures and their applications in dye and oil removal*

The contamination of water bodies due to industrial waste discharge poses a major threat to the quality of groundwater, soil, and living organisms. Existing procedures such as skimmers and in-situ burning are no longer sufficient due to lower removal efficacy, time-consuming process, and cost factors. Magnetic nanomaterials and nanocomposites are emerging materials that offer in-situ remediation of contaminated water by separating the pollutant-sorbed nanomaterials from water bodies using an external magnet. Irrespective of large amount of work done in this

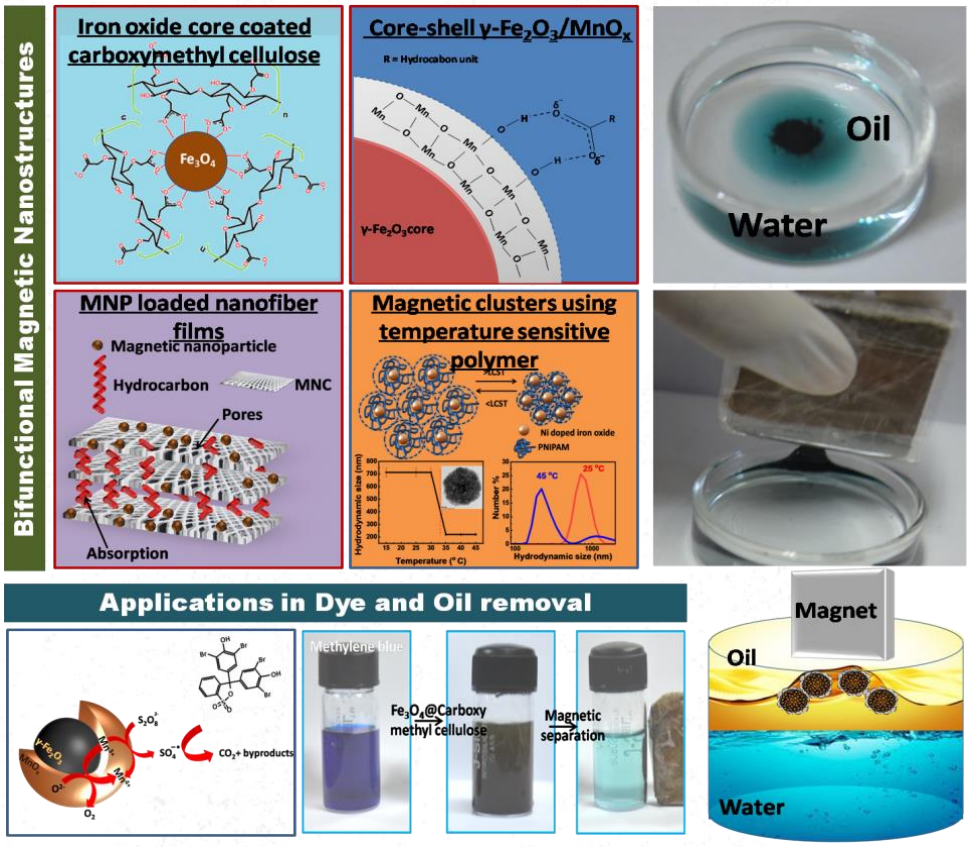

Schematic of bifunctional magnetic nanostructures for dye and oil remediation

field, still methodologies to synthesis magnetic nanoparticles with high magnetization within superparamagnetic limit, long term stability and reusability are largely unknown.

To overcome the aforementioned limitations, iron oxide core covered with a nanoshell of carboxymethyl cellulose polymer, inorganic MnO_x shell, poly (N-isopropyl acrylamide) shell were developed, using water as a solvent and at relatively low synthesis temperatures. Modification of superparamagnetic iron oxide surface with suitable layer to form core-shell bifunctional nanomaterial improved their stability against oxidation and showed high saturation magnetization allowing for controlled recovery of adsorbates from aqueous solutions. The major advantages of this approach are zero secondary pollution, good recyclability, high surface-to-volume ratio, increased pollutant removal efficiency, and cost-effective production.

2.2.2 *Investigation on the influence of polarization resistance for low-temperature operation of multi layered thin film YSZ oxygen sensors*

The thesis brings out a systemic approach toward the development of a multilayered thin film-based electrochemical YSZ oxygen sensor with the cell configuration of (RE)Pt|Cu,Cu_2O|YSZ|O_2,ITO(WE), which operates at 623 K, allowing a reduction in operating temperature by about 300 K. Factors responsible for the operating temperature of 923 K or greater in the conventional oxygen sensor of (RE)Pt|Cu,Cu_2O|YSZ|O_2,Pt(WE) was systematically analyzed and the high interface polarization resistance was identified to be the

main issue. The replacement of the conventional Pt electrode with indium tin oxide (ITO) was chosen based on its enhanced oxygen dissociative adsorption characteristics and its limited

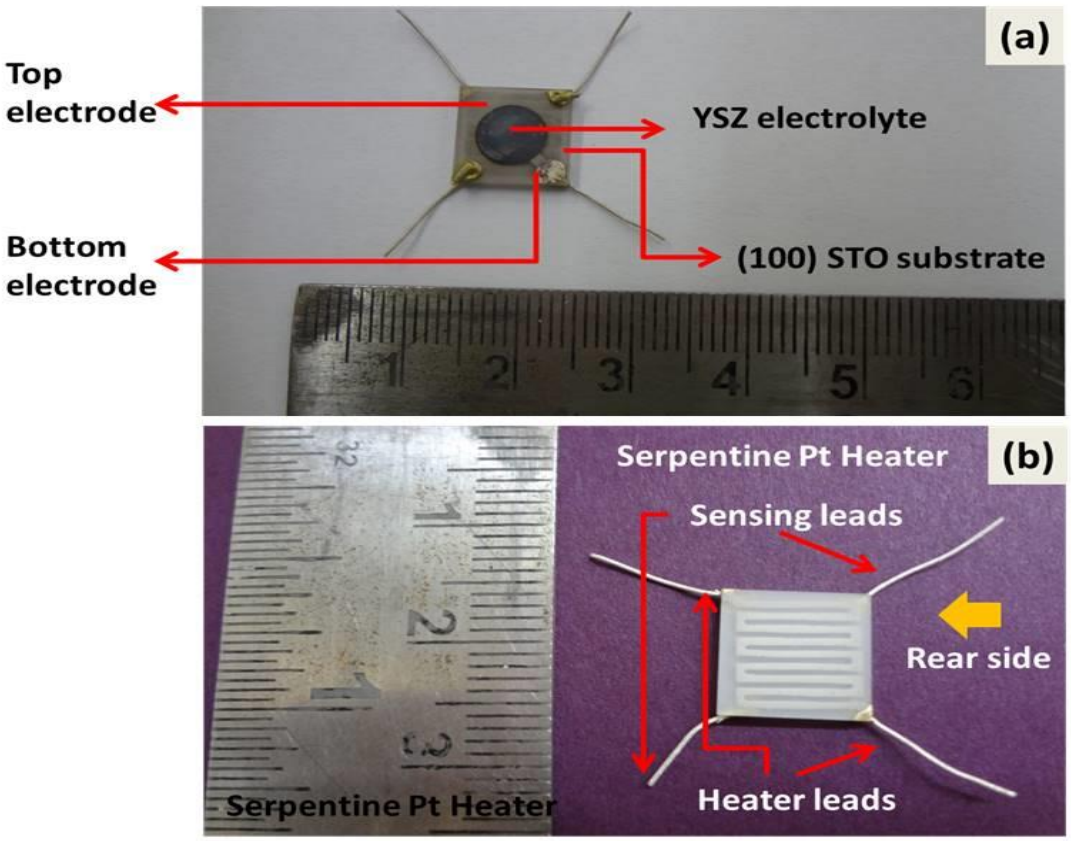

Photograph of (a) YSZ based multialyered thin film electrochemical sensor on (100) $SrTiO_3$ substrate and (b) Pt serpentine heater screen printed on the rear side

solubility in YSZ, which improved the interface. It is conceived that multilayered thin films of Pt|YSZ|Pt and ITO|YSZ|ITO are the ideal configuration to probe the effect of polarization resistance of interface of YSZ/Pt and YSZ/ITO interfaces, respectively and was realized on (100) $SrTiO_3$ (STO) substrate using the pulsed laser deposition (PLD) technique. Based on the inputs from the polarization studies, two different kinds of multilayered thin-film electrochemical oxygen sensors Pt|YSZ|Cu,Cu_2O|Pt|STO (sensor 1) and ITO|YSZ|Cu,Cu_2O|Pt|STO (sensor II) using Pt and ITO as the working electrodes were made and their performance at lower operating temperatures for sensing trace levels of oxygen in argon were evaluated. Sensors I respond to 10 to 1000 ppm of oxygen in an argon stream at 673 K, the lowest working temperature reported for YSZ-based oxygen sensors using Pt WE. However, the response was non-Nernstian, with a sensitivity of 20 mV/decade, which is against the theoretical 33.3 mV/decade. On the other hand, Sensor II with ITO WE showed a higher sensitivity of 40 mV/decade even at a lower operation temperature of 623 K for the concentration range of 10 to 826 ppm oxygen in the argon stream. The current sensor design uses a (100) STO substrate (10mm×10mm×0.5mm) with a serpentine Pt heater screen printed on the rear side and multilayered thin films grown sequentially on the top side of the substrate. Finally, PtO detected during the optimization of Pt deposition, which is not amenable to conventional synthetic routes, is stabilized as a thin film using PLD.

2.2.3 *Probing and maneuvering the third phase formation in diglycolamide/n-dedecane systems*

The diglycolamides, TODGA and TEHDGA, have been extensively studied for trivalent actinide separation from nitric acid solution and HLLW. However, these ligands have some limitations of third phase formation. To overcome this limitation, it is necessary to understand the root cause of third phase formation at fundamental levels. Therefore, in the present work, it was proposed to investigate the extraction behavior of nitric acid and Nd(III) in a solution of TEHDGA/n-DD and TODGA/n-DD and probe the extracted organic phase by dynamic light scattering and FTIR spectroscopic techniques before and after third phase formation.

Several authors proposed the addition of phase modifiers such as tri-n-butyl phosphate (TBP), N,N-dioctylhexanamide (DHOA), long chain alcohols, to the solvent phase for preventing the third phase formation during solvent extraction. However, these phase modifiers also pose some limitations such as they facilitate the co-extraction of unwanted metal ions from HLLW and generate secondary organic waste. In addition, the phase modifiers proposed contain phosphoryl and amide derivatives, structurally different from diglycolamides, even though the DGA class of modifiers is indeed desirable. In this context, it was proposed to employ N,N-dioctyl hydroxy acetamide (DOHyA), which was one of the degradation product of TODGA, as well as the higher homologue of TODGA namely N,N,N',N' tetradodecyldiglycolamide (TDdDGA) as phase modifiers in the present work and explore the possibility of using these phase modifiers for trivalent actinide separation. Therefore, the extraction behaviour of nitric acid and Nd(III) was studied in binary solution composed of 0.1 M TODGA + 0.2 M DOHyA/n-dodecane and 0.1 TODGA + 0.1 M TDdDGA/n-dodecane. The aggregation and third phase formation behaviour of the nitric acid and Nd(III) extracted organic phase was probed using dynamic light scattering and ATR-FTIR spectroscopic techniques.

In addition to the employment of phase modifiers to the solvent phase, researchers have proposed the longer alkyl chain derivatives of DGA for preventing the third phase formation. Therefore, the structurally modified ligand containing dodecyl group on one side and octyl group on the other side of diglycolamide namely the N,N-didodecyl-N',N'- dioctyl diglycolamide (D3DODGA), was synthesized and the modifier-free solution containing 0.2 M D3DODGA/n-DD was studied for the extraction of trivalent actinides and lanthanides from nitric acid solution, in the present work. The extracted phase was probed by dynamic light scattering and ATR-FTIR spectroscopic techniques to understand the aggregation and co-ordination behavior of trivalent ion in the extracted phase.

The study extensively explored the extraction and aggregation behavior of different diglycolamide (DGA) systems in n-dodecane to manage third-phase formation during the separation of trivalent f-elements from nitric acid. Key findings highlighted the role of structurally similar phase modfiers such as DOHyA and TDdDGA for TODGA in improving the extraction limits of nitric acid and Nd(III) without any third phase formation. In addition, D3DODGA, structurally modified DGA in n-dodecane emerged as a superior candidate for high-level nuclear waste processing due to its enhanced extraction capacity without organic phase splitting. These findings pave the way for optimizing solvent systems for efficient and stable recovery of lanthanides and actinides.

2.2.4 *Studies on adsorption of ruthenium on carbon based nano materials*

The thesis focuses on the development of an alternative method for its application in bioassay especially adsorption method to streamline and simplifying the radiochemical procedures, with particular focus on the feasibility of nano-materials owing to their efficiency and cost-effectiveness. This study evaluates the performance of three promising nano adsorbents such as Multi Walled Carbon Nanotubes (MWCNTs), Tri-n-butyl phosphate functionalized Multi Walled Carbon Nanotubes (MWCNTs-COO-TBP) and Graphene Oxide (GO) for adsorption of Ru (III) from aqueous solutions. The work is highly relevant in the context of nuclear energy sustainability, especially adoption of three-stage nuclear power program in India, and the challenges associated with managing Bioassay. The thesis consists of six well-organized chapters detailing about introduction to experimental methods containing synthesis and characterization, with various analytical techniques followed by adsorption studies with the evaluation of thermodynamics, kinetics and isotherm. The thesis also investigates the thermal and radiation stability of these materials.

Finally, it summarizes the major outcomes and future scope, highlighting the avenues for further research in optimizing adsorption efficiency and kinetics through modification of nanomaterials, exploring novel hybrid materials and advanced characterization techniques to enhance the understanding and performance and exploring the scalability of the adsorption processes for investigating the potential of these nanomaterials in real-world bioassay scenarios.

Key findings include:

- Adsorption was pH dependent and followed Pseudo second order kinetics and Langmuir isotherm unfolding homogenous and monolayer adsorption.
- Adsorption capacity was increased from MWCNTs (105.187 $mg.g^{-1}$) to MWCNTs-COO-TBP (141.23 $mg.g^{-1}$) due to the introduction of TBP on Multi Walled Carbon Nanotube skeleton.
- Free energy change was high at higher temperature resulting spontaneity, favourable and faster adsorption.
- Quantification of defects by Raman study revealed that, -COO-TBP acts as a p-type dopant to MWCNTs during functionalization and its reduction in MWCNTs-COO-TBP was observed due to Ru(III) adsorption.
- Compressive strain was negligibly released during adsorption of Ru(III) on MWCNTs-COO-TBP due to reorganization of their constituent atoms.
- Adsorption of Ru(III) varied inversely with ionic strength of NaCl and $MgCl_2$.
- Desorption of Ru(III) was maximum at 8M HNO_3.
- The presence of Ru(III) was confirmed by on EDS and XPS analysis and its oxidation states by XPES analysis.
- MWCNTs was stable upto 800 ºC and radiation stability > 1000 kGy. MWCNTs-COO-TBP was stable upto 220 ºC and radiation stability < 100 kGy. Graphene Oxide was stable upto 210 ºC and radiation stability < 100 kGy.

In conclusion, the potential application of these materials were explored for the first time for adsorption of Ru(III) from aqueous solution. This study would be helpful in understanding the feasibility and suitability of adsorption method in bioassay in shortening and simplifying the radiochemical procedure.

2.3 National Institute of Science Education and Research (NISER), Bhubaneswar

2.3.1 *Carbon supported metal composites and heteroatom doped carbons for electrochemical energy conversion and sodium ion battery*

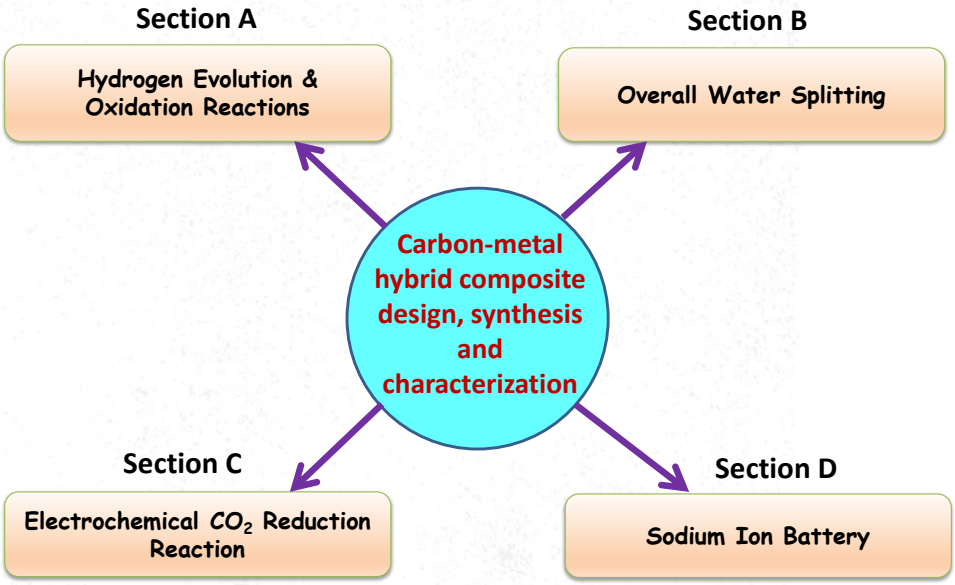

The thesis focuses on developing of carbon-metal and heteroatom-doped carbons for Hydrogen evolution and oxidation reaction (HER/HOR); Overall water splitting; Electrochemical CO_2 reduction reaction, and Sodium ion battery anodes. Depending on the application and work structure, the thesis can be divided into four sections.

Section-A shows the interface engineering of PdO to improve its catalytic activity for both the alkaline and acidic HER & HOR. In this regard, three catalyst PdO-RuO_2/C, IrO_2-PdO/C, and Pt-PdO/C were prepared and their performance were tested for the reactions in a systematic way. We found that incorporation of RuO_2 in PdO systems increases the alkaline HER/HOR activity dramatically compared to other two catalysts; while acid HER of Pt-PdO/C dominates others. To know the behavior of the catalysts during the HER/HOR reactions in base, we study the mechanism of these reactions on the catalytic sites and based on the experimental finding, we concluded that the reactions go through the bi-functional mechanism, where both Hydrogen binding energy and oxophilicity plays equal role to enhance the HER/HOR activity.

Section-B consists of catalyst design strategy for the overall water splitting in the alkaline as well as all pH solutions. Two catalyst, CoOx/CNx and IrO2-RuO2/C were produced for overall water splitting. We found the during OER process CoOOH forms, which is the key active species for the improved OER; while for HER, after 1000^{th} cycle, Co/CoO_x species forms. This interface is responsible for high HER activity. But, the catalytic activity of this catalyst is only limited to the base media. So, we tried to synthesize a catalyst, which will be active and stable in broad pH range. In this regard, we prepared IrO_2-RuO_2/C catalyst for overall water splitting

in broad pH range. Experimental results shows that the heterojunction between the IrO_2 and RuO_2 is responsible for the high activity of the catalyst. The catalyst shows good overall water splitting as well as stability in all the pH medium. In **Section-C**, we try to improve the selectivity of the electrochemical CO_2 reduction reaction by catalyst designing. In this regard, we prepared four catalysts; Sn/SnO_2-CN_x; Cu-SnO_x/rGO; Bi_2O_3-CN_x to increase HCOOH selectivity; while insitu MOF derived Cu-Cu_2O/C was found to increase the ethylene and methanol production. It was found that Bi_2O_3-CN_x is more selective for HCOOH production compared to Sn/SnO_2-CN_x, and Cu-SnO_x/rGO catalyst; while insitu formed Cu-Cu_2O/C catalyst was selectively producing CH_4OH and C_2H_4 in a certain potential. Further, DFT calculations were also carried out to support the catalytic mechanism and results. **Section-D** talks about hard carbon design strategy to improve the sodium ion storage performance. In this regard, we prepared S,N-co-doped-hard carbon (SNHC-X) and Si-doped hard carbon (Si@HC-X). The doping of heteroatom into the hard carbon skeleton increases the interlayer distance, thereby, increases the plateau capacity. We also prepared full cell by complying the anodes with sodium vanadium phosphate and achieved a remarkable capacity. The mechanism of Na^+ storage was also studied by electrochemical measurements and ex-situ XRD and Raman study. We also synthesized MoS_2/C composites for sodium ion battery anode. We successfully incorporated that morphology has a role in the Na^+ storage. Further, to improve the cyclic stability of the cell electrolyte additive was used. We also concluded the role of succinic anhydride as electrolyte additive to improve the cyclic stability. The succinic anhydride reacts easily with electrode material during sodiation-desodiation compared to solvents and electrolytes and forms Na_2CO_3 rich SEI, which increases the conductivity as well as thermal stability. The electrolyte decomposition was also hindered in presence of succinic anhydride. Further, Full cell performance supports its practical application.

2.3.2 *Pd, Ru, Mg – complexes for CO_2 utilisation, cross-coupling/transfer-hydrogenation reactions: base-mediated synthesis of isothiazole*

The chemical conversion of carbon dioxide (CO_2) into useful organic compounds has received considerable attention as it represents an abundant, inexpensive, and nontoxic C1 source. Coupling reactions of CO_2 with epoxides/aziridines to produce cyclic carbonates/oxazolidinones as valuable chemicals under mild conditions is an important and attractive method for utilising carbon dioxide (Figure 1).

An important aspect of efficient catalysis is combining multiple (at least two) mechanistically distinct reactions (tandem reactions) in one-pot. This process offers several advantages in terms of atom economy, number of steps involved, consumption of energy, and reduction of chemical waste. Incorporating multiple metal centres into a single molecular framework offers several advantages in terms of improved or new properties and activity as compared to their mono- and dimetallic analogues. This system brings the active centres closer, thereby exhibiting synergistic or cooperative interaction and increasing catalytic activity (Figure 2).

Isothiazoles are an important family of five-membered heterocycles that received growing interest owing to their biomedical, agricultural and industrial activities. Wide applications of isothiazoles stimulated researchers to identify and develop different synthetic pathways to make isothiazoles. Although considerable progress has been made, the development of simple

and efficient protocols for the synthesis of substituted isothiazoles is always in demand (Figure 3).

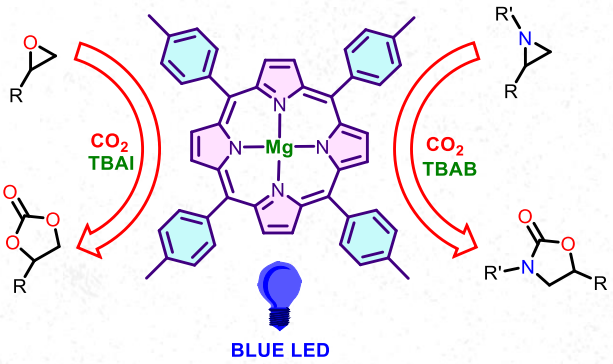

Fig.1: CO_2 utilization reactions by Mg-Porphyrin

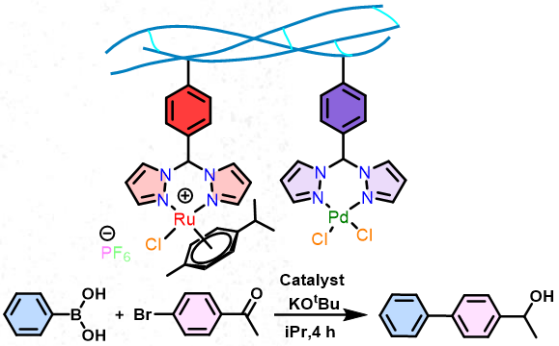

Fig.2: Polymer based catalyst P2@RuPd was used for tandem cross-coupling and transfer hydrogenation reactions

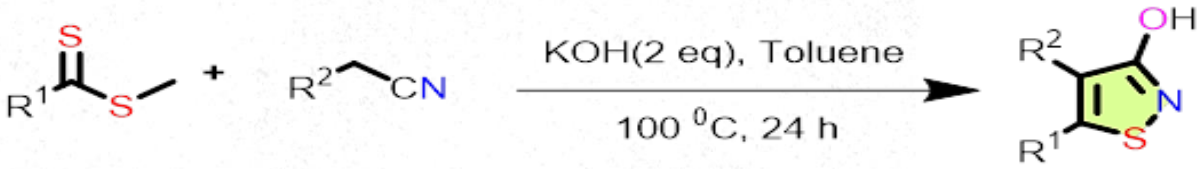

Fig.3: Synthesis of Isothiazole

2.3.3 *Metal - free approaches towards C-N and C-O bond formation*

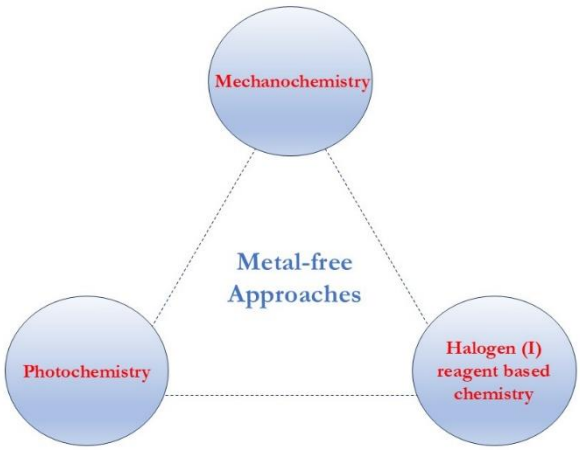

Various metal free approaches towards heterocyclic compound synthesis

Eco-friendly synthetic methodologies are becoming increasingly popular in response to pressing environmental hazards and financial constraints faced by chemists. As a result, transition metal-free protocols with significant potential for selective transformations are being embraced. Among these, solvent-free mechanochemistry, photo-redox catalysis, and reactions using mild reagents at room temperature are the most notable. In this context, the primary focus of this thesis is to present transition metal-free and operationally simple protocols for

constructing various heterocyclic scaffolds through C-N and C-O bond formation. To demonstrate mechanochemistry as an effective alternative to traditional methods, a wide range of 1,2-disubstituted benzimidazoles and quinazolin-4(3*H*)-one derivatives were synthesized using solvent-free ball milling process. Further a mild reagent N-Iodosuccinimide was employed for intramolecular C-N coupling to deliver benzimidazole-fused phenanthridines scaffolds at room temperature stirring for 22 hours. Mechanistic study revealed a radical pathway for this transformation. Subsequently, we proposed a room temperature activation of EDA complex to facilitate brominative cyclization of o-styrylbenzamide. Here, in presence of CH3CN, 4-bromo-isochromanone O-methyl oxime, whereas in CH3OH solvent exclusively 4-bromo-isochromanone, were yielded. Next, we demonstrated visible light promoted regioselective synthesis of quinazolinone-fused phenanthridines employing a metal free photocatalyst e.g., Mes-Acr-MeClO$_4$. Detailed control experiments were performed to validate the proposed mechanism.

2.3.4 *Ultrafast and single molecule studies of photo-physical process in quantum – confined materials*

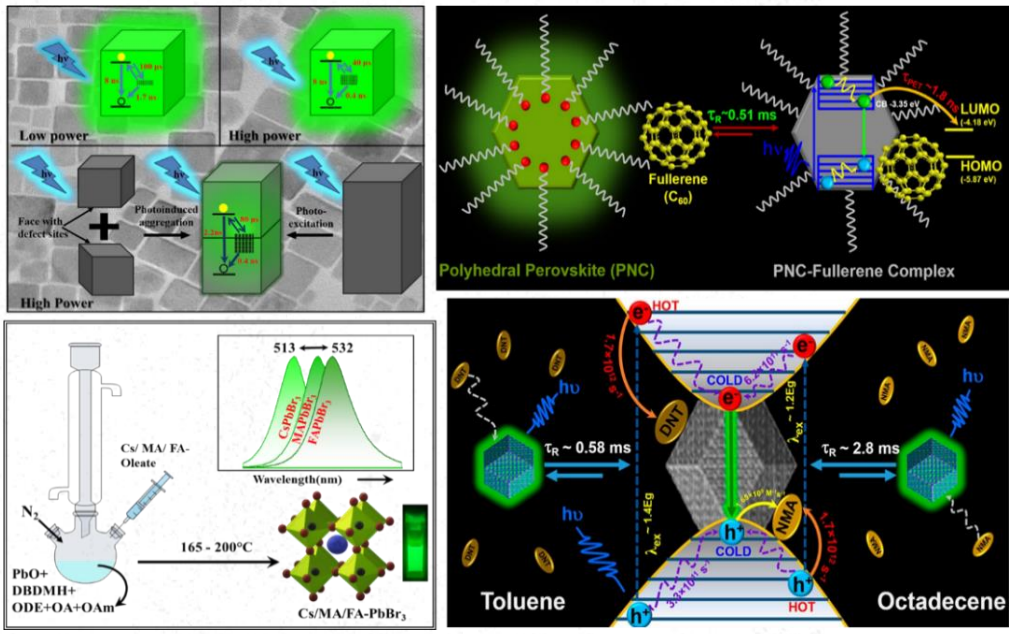

Perovskite nanocrystals (PNCs), renowned for their exceptional optical and electronic properties, hold great promise for next-generation optoelectronic devices, such as solar cells and light-emitting diodes. However, their performance is still limited by challenges like intermittency in their emission (Blinking) and carrier dynamics under different conditions, unexplored photophysical properties, etc. Addressing these challenges, Chapter 3 uses a single-molecule-based Fluorescence Lifetime Correlation Spectroscopy (FLCS) technique to investigate the role of sample heterogeneity on blinking and carrier diffusion dynamics. This study delves into the presence of multiple emissive states with varying lifetimes and their contributions to blinking kinetics.

Chapter 4 examines all three green-emitting colloidal NCs using DBDMH as a bromide source, achieving high photoluminescence quantum yield (PLQY) and stability without additional

post-synthesis modifications or doping. Chapter 5 explores facet-engineered, 12-faceted d-PNCs in efficiently harvesting photogenerated carriers through photoinduced electron transfer (PET), using fullerene as an electron acceptor. The chapter also applies Tachiya's stochastic model to accurately determine the timescale of PET.

The final working chapter highlights the use of 12-faceted d-PNCs in hot carrier solar cells, showcasing their reduced hot carrier cooling rates relative to traditional six-faceted cubic NCs, which enhances hot carrier harvesting. It introduces model systems using these 12-faceted NCs to enable efficient extraction of both hot electrons and hot holes. This research aims to advance our understanding of PNCs, thereby optimizing their photovoltaic properties for next-generation device applications.

2.4 Saha Institute of Nuclear Physics

2.4.1 *Designing electrocatalysts for sustainable future: Applications toward electrolyzers and fuel cells*

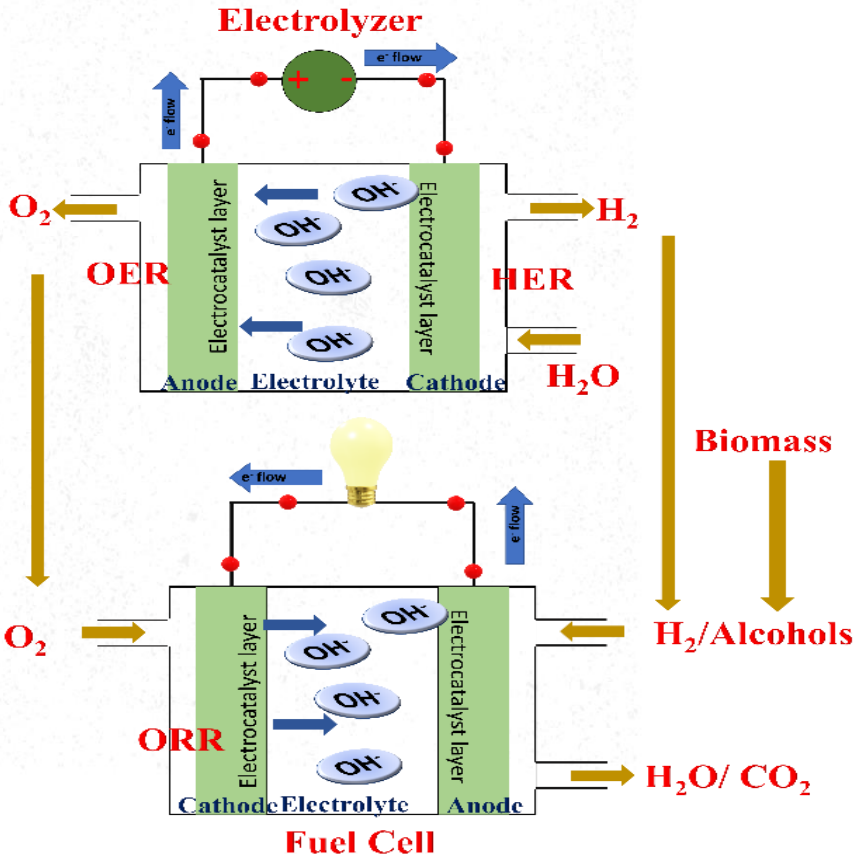

Fuel cells and electrolyzers will be one of the key components for the transition towards renewable power sources and a sustainable environment. Briefly, in a fuel cell, fuel (e.g., alcohol or hydrogen) is oxidized in anode chamber and oxygen gets reduced in the cathode chamber (known as Oxygen Reduction Reaction (ORR)). For a water electrolyzer, hydrogen is produced in the cathode (known as Hydrogen evolution reaction (HER)) and in anode, oxygen is produced (known as Oxygen Evolution reaction (OER)). These electrochemical reactions involved in both fuel cells and electrolyzers are kinetically sluggish processes and thereby need the help of catalysts to increase the rate of reactions. Currently, the state-of-the-

art electrocatalysts in these regards are noble metal based (Pt, Ru, Ir based materials), which are scarcely available, making them highly costly. This disadvantage will undoubtedly halt those systems' continued progress. This forces us to develop electrocatalysts which are 1) cost-effective, 2) highly active and stable during operating conditions and 3) devoid of Pt, Ru and Ir- which is one of the main goals of this thesis. Additionally, we tried to correlate the surface structure, morphology of the newly developed electrocatalysts and the local environment of its active sites with their electrochemical performances. The first work outlines the electrocatalyst's progressive developing step, with each subsequent step getting better performance. The best electrocatalyst (made of Au and Ag) which has a porous structure and large number of defects, differs the pathway of alcohol oxidation from the Pt/C (State-of-the art electrocatalyst) as evident from electrochemical studies. Direct Alcohol Fuel Cells operate at ~80 ^{o}C. For that reason, we also checked temperature dependent activity of the electrocatalyst for alcohol oxidation and ORR. The results showed the possibility of structural changes during the reactions. All these findings lead to the conclusion that further development of the elctrocatalyst is still needed. In the 2nd work, more focus was given to ORR. By further developing the previous fabrication process, we developed an electrocatalyst with a multilayered appearance where a Au layer remains sandwiched between two Ag layers, creating a multilayered core-shell spherical nanoparticles. The modified fabrication technique leads to reduction of Au usage in the electrocatalyst with its enhanced performance towards ORR. It turned out that presence of Au in the structure is crucial to enhance the overall performance of the electrocatalysts and the reason behind this has been discussed in the thesis. For the third work, efforts were made to enhance the performance of NiFe based structure for OER in water electrolyzers. Typically, NiFe based materials (efficient OER electrocatalysts) suffer from rapid degradation because of Fe dissolution. By introducing Cu and P in the NiFe structure, leading to surface modification and electronic property modulation, we can see the enhanced stability and activity of the elctrocatalyst. It turned out local structural reorganization has an impact on the performance of the newly developed electrocatalysts.

ENGINEERING SCIENCES

3. Engineering Sciences

3.1 Bhabha Atomic Research Centre, Mumbai

3.1.1 *Experimental and computational studies on hydrodynamics and mass transfer in liquid-liquid pulsatile flow in column contactors*

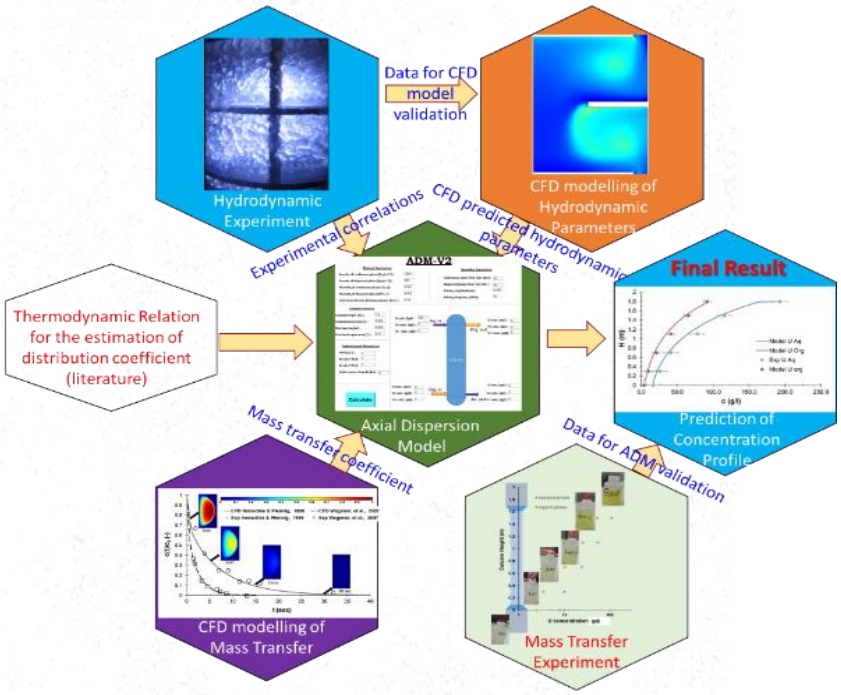

Graphical abstract depicting combination of experimental and CFD analysis leads to design of pulsed disc and doughnut column

This thesis delves into the world of pulsed contactor design, specifically focusing on Pulsed Disc and Doughnut Column (PDDC) and Annular Pulsed Disc and Doughnut Column (APDDC) utilized in solvent extraction processes, a crucial step in nuclear fuel reprocessing. The core objective of the research is to gain a fundamental understanding of how liquids behave within these pulsed columns when two immiscible liquids flow together in a pulsating manner.

To achieve this understanding, a two-pronged approach: experimentation and computer simulations is employed. Experiments involving single-phase and liquid-liquid two-phase flow were conducted in various sized PDDC and APDDC. These experiments helped measure factors like dispersed phase holdup, axial dispersion, and Sauter mean drop diameter.

On the other hand, computer simulations called Computational Fluid Dynamics (CFD) were used to create virtual models of the flow within the contactor. By comparing these simulations to the experimental results under various conditions, CFD models are validated. This paves the way for reliable predictions of flow behaviour in different contactor designs and operating conditions.

Furthermore, the research delved into the realm of mass transfer. Mass transfer in pulsed column is investigated using uranium extraction and stripping. A model is developed to predict the rate of mass transfer based on CFD simulations of single droplets. Additionally, a separate

axial dispersion model is developed to predict mass transfer and axial concentration profile within the contactor.

In essence, this thesis provides a comprehensive set of tools and knowledge to optimize the design and operation of pulsed columns.

3.1.2 *Thermo-mechanical processing of AISI 304L to achieve an ultrafine grained microstructure and its correlation with mechanical properties*

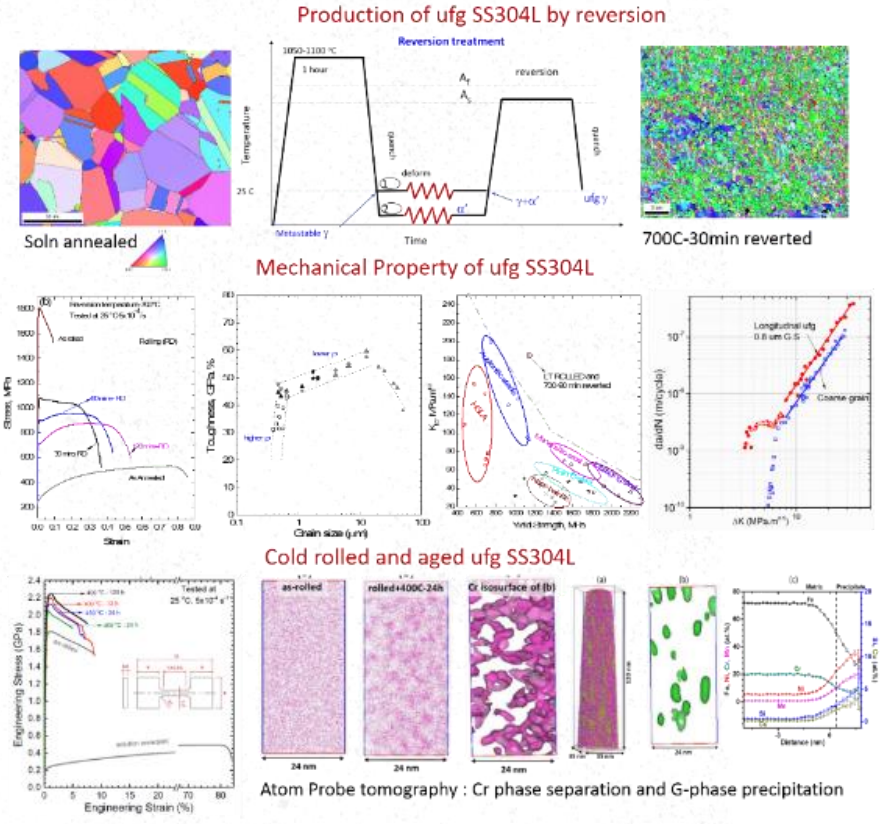

SIMRT process of producing ufg SS304L and corresponding mechanical property of ufg SS304L such as tensile behaviour, fracture and fatigue crack growth and mechanical properties and atom probe tomography maps of cold rolled and warm temperature aged SS304L

Austenitic stainless steels are extensively used as structural materials in the nuclear, automobile, marine and food processing industries due to their superior corrosion resistance, weldability and moderate mechanical properties. Of the various chromium-nickel austenitic stainless steels, AISI 304 is one of the most widely used. However, it has moderate strength that lies in the range of 300 to 500 MPa. Grain refinement in AISI 304 to ultrafine and nanocrystalline levels is a potential method to achieve high strength along with favorable biocompatibility and exceptional radiation tolerance. Grain refinement in these steels has been achieved by severe plastic deformation such as severe mechanical attrition treatment, recrystallization following cold/warm working, and strain induced martensite reversion treatment (SIMRT). This is a simple technique that has the potential for the production of large-scale components of metastable austenitic stainless steels.

Here it is shown potential SIMRT method to produce bulk ufg SS304l. The mechanical testing revealed that ufg SS304L offers significantly enhanced yield strength along with improved resistance to crack initiation in high-cycle fatigue tests. The optimum grain size for SS304L to obtain highest toughness is ~12 um. However, the UFG SS304L showed lower fracture toughness and fatigue crack growth resistance compared to its coarse-grained counterpart, although its fracture toughness remained superior to steels with comparable yield strengths. A novel thermo-mechanical process was also developed, enabling the production of ultra-high-strength SS304L (~2.2 GPa) through warm thermal treatment. The increase in strength was attributed to Cr- phase separation and the formation of G-phase precipitates.

3.1.3 *Identification of contaminant sources in groundwater using simulation optimization models with uncertainty analysis*

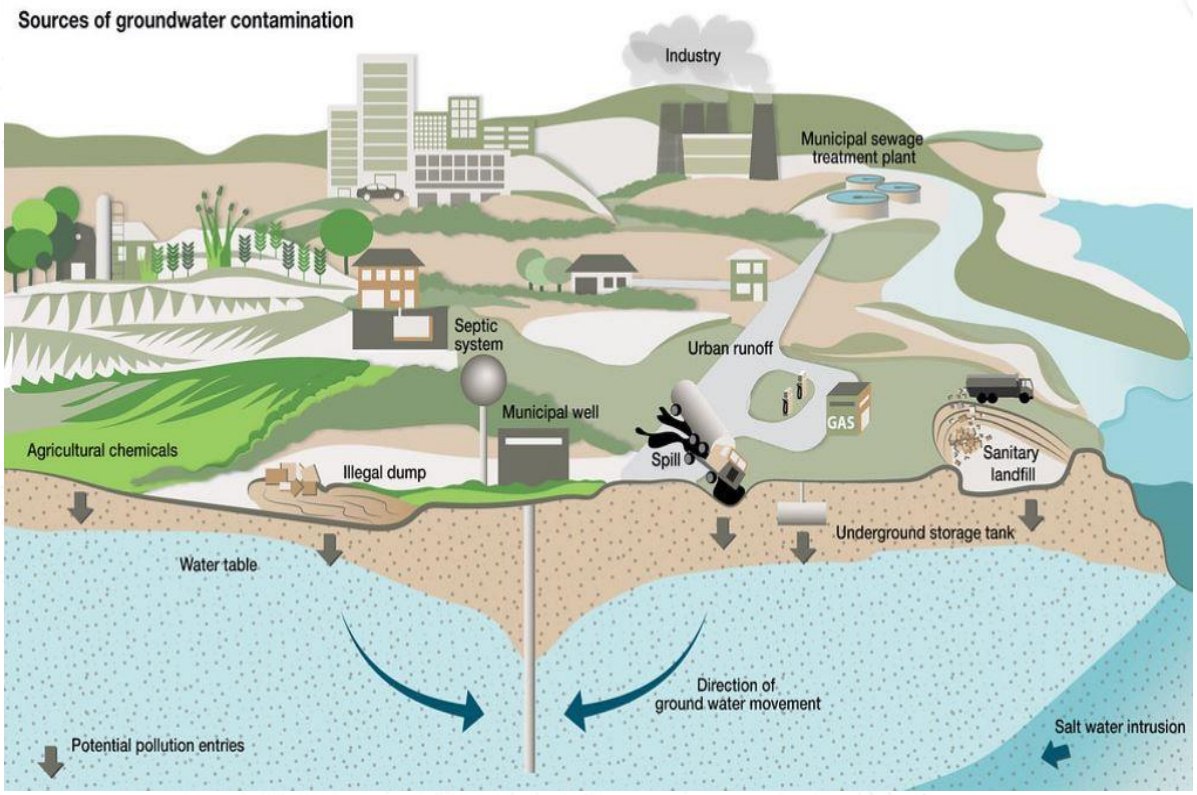

Sources of groundwater contamination [Image source: Zaporozec and Miller (2000)]

Any industrial or nuclear facilities have several storage components or tanks, pipes, disposal facilities etc. from which inadvertent release of radioactive or other contaminants is possible. Due to multiple possible sources, it will be difficult to predict the exact source or facility responsible for any leakages of radioactivity or other contaminants. It is necessary to develop a computational tool to identify the leakage quantitatively to stop further leakage and also help in any remediation. In this study, a simulation optimization model is developed for identification of groundwater contaminant sources. Simulation optimization model consists of two steps namely, simulation and optimization. The simulation step involves groundwater flow and contaminant transport model development in which the unknown state variables of the

system (head and concentration) are predicted by solving the groundwater flow equation and advection-dispersion-reaction equation (ADRE), respectively. A meshless method, known as Local radial point interpolation method (LRPIM) is used as a simulation model to couple the flow and transport in the domain. The groundwater head and contaminant concentration were obtained as an output from the simulation model. The simulation model is linked with the three different optimization techniques namely, particle swarm optimization (PSO), grey wolf optimization (GWO) and teaching-learning based optimization (TLBO) to form the simulation optimization models such as LRPIM-PSO SO model, LRPIM-GWO SO model and LRPIM-TLBO SO model. The simulation optimization model minimizes the. deviation between the predicted and observed concentrations to find the unknown source characteristics (source location and release history). The applicability of the developed simulation optimization (source identification) model is demonstrated with hypothetical and real aquifer to identify the groundwater contaminant sources. The model was also applied for estimating the flow and transport parameters.

LRPIM-PSO SO model is found to be optimal in accuracy and computational efficiency for 2D hypothetical case study involving injection type contaminant source. The results are observed to remain stable in the observation wells even after altering the nodal arrangement. Uncertainty analysis is carried out with measurement error in observed data, missing of data from record, uncertainty in the parameters used in model. It is found that the percentage error obtained is less than 20%. The error is found to be more when the error incorporated in the observed data is 20 percent or when the number of observation wells is less or when the number of unknown sources is high.

3.1.4 *Multiscale processing of seismic ambient noise with application to imaging earth's interior*

1. In this work, to eliminate the presence of unwanted transient signals from the seismic records, a technique is proposed where duration of the transients is detected first and then the transients are removed using multiscale soft thresholding technique without altering the ambient noise characteristic.

2. Time-frequency domain normalization technique is also proposed to eliminate the effect of unwanted transient signals and obtain diffusive ambient noise.

3. To obtain the reliable estimate of dispersion curves, it is required to retrieve weak surface waves present in the empirical Green's function. A technique based on continuous wavelet transform using complex Morlet filters is proposed to estimate dispersion curves. The wavelet filters have tendency to coincide with the local frequency of the signals and therefore efficiently captures the oscillations present in the signal compared to Gaussian band pass filters.

4. Higher resolution dispersion curves are estimated using the proposed method than the conventional method. This would eventually lead to more accurate ambient noise tomography of the earth, upon inverting the estimated dispersion curves. In addition, reduced number of filters in the proposed method makes it computationally efficient.

3.1.5 *Pulse power application in cell biology and cancer treatment*

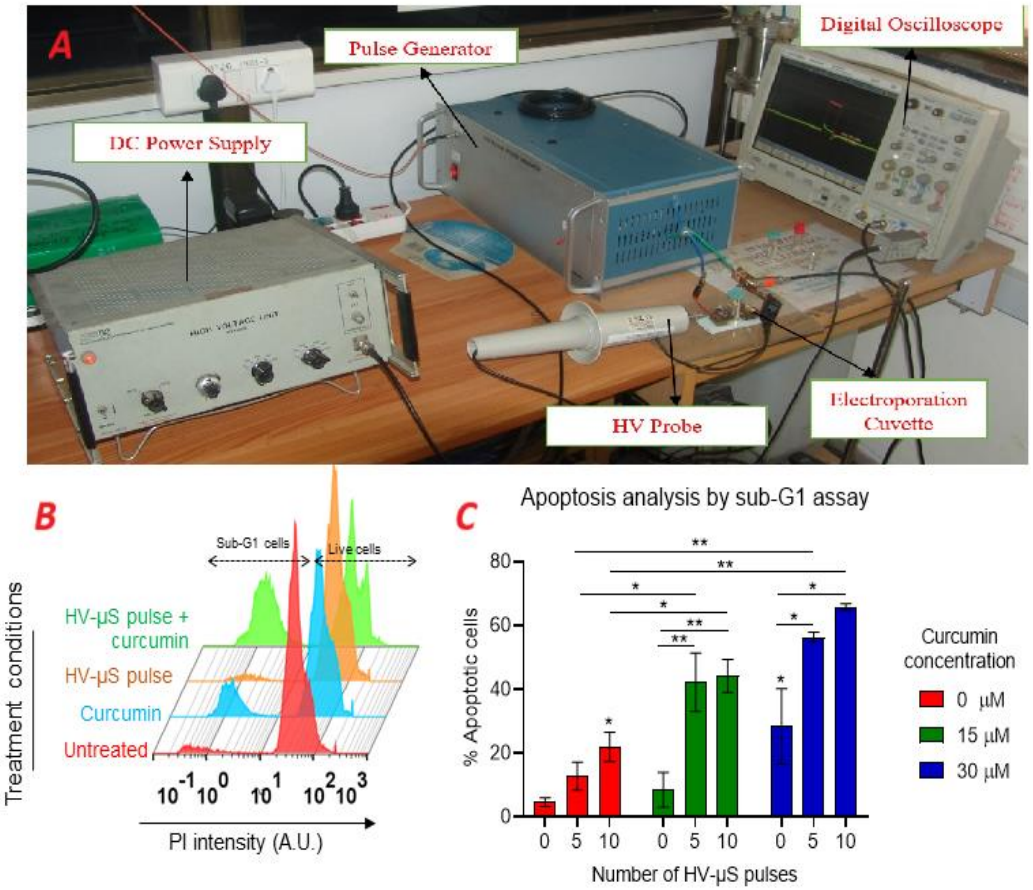

(A) Pulsed Electric Field exposure set-up (in vitro experiment) (B) Flow-cytometric result of pulse exposure (C) Percentage of apoptotic cells vs No. of pulse graph

Pulsed Electric Field (PEF) treatment for tumors and cancer is a targeted, non-thermal, and drug-free method. In this technique, cancer cells are exposed to short but intense electrical pulses, which cause irreversible permeabilization or disruption of cell membranes and internal organelles. This damage prevents the cells from recovering, ultimately leading to their death. An electric field with a duration ranging from microseconds to milliseconds, and strength of a few hundred volts per centimeter, can cause reversible changes in cell membranes. The reversible effect of a pulsed electric field, known as 'Electroporation'. This process temporarily disrupts the cell membrane, allowing it to return to its normal state once the field is removed. Electroporation is utilized to introduce external substances, such as chemicals, genes, drugs, or DNA, into the cell's cytoplasm.

Here, the impact of exposing cells to electrical pulses at varying electric field intensities—1.0 kV/cm, 1.5 kV/cm, and 2.0 kV/cm—with a pulse duration of 50 µs and a repetition rate of 1 Hz was explored. Immediate cell mortality, viability after a 24-hour interval, and isolated cell growth were evaluated. Trypan blue staining, the MTT assay, and the clonogenic assay were utilized for these assessments, respectively. It was found that exposure to 2.0 kV/cm pulses, lasting 50 µs and delivering approximately 4 J of energy, had a profoundly detrimental effect on cell integrity, leading to necrotic cell death. In contrast, a low-energy 1.0 kV/cm electric field, also lasting 50 µs, had minimal influence on cell viability. Notably, the application of a

1.5 kV/cm electric field for 50 μs significantly reduced cell viability, resulting in lower initial cell mortality but substantially increased cell death 24 hours post-exposure. The simultaneous application of electrical pulses and curcumin exhibited a synergistic effect on cell viability, attributed to electroporation. The use of a 50 μs, 1.5 kV/cm pulsed electric field was found to enhance curcumin absorption, indicating its synergy with HV-μsPEF for inducing apoptosis. Additionally, the electric field increased ROS levels and decreased mitochondrial membrane potential (MMP), while their combined application further amplified ROS production and MMP loss. This heightened ROS and mitochondrial depolarization triggered programmed cell death.

3.1.6 *Time-frequency domain machine and deep learning approaches for automated detection of sleep stages using EEG recordings*

Accurate and reliable classification of sleep stages is challenging. Sleep expert uses polysomnographic records for sleep scoring. Traditionally, an expert classifies sleep signals by visual inspection. This process is tedious and requires a significant amount of time and experience. The sleep stage scoring is prone to fatigue errors due to its monotonous and laborious nature. Also, the classification may be impacted by intra- and inter-rater reliability. As a result, there is a lot of diversity in the classification of sleep stages, affecting the accuracy of the procedure. This thesis aims to develop new and more accurate techniques to classify sleep stages automatically using EEG signals.

Firstly, a random forest classifier is used to classify sleep stages using features from EEG subbands. The 30 s epochs of single-channel EEG (Fpz-Cz or Pz-Oz) are divided into 8 EEG subbands. Ninety-six features, i.e., twelve features per band, are extracted from these subbands. Different features are extracted from EEG subbands that give information about the sleep state. Ensemble-based classifier random forest is trained using this labelled feature dataset for automatic sleep stage classification.

Secondly, sleep stages are classified using CWT images of single-channel EEG signal epochs. The wavelet transform can simultaneously provide the time and frequency information, giving a complete time-frequency representation of the signal. Each CWT image represents 30 s epochs of single-channel EEG. Then, convolution neural network model (CNN) is used to classify these CWT images of 30 s epochs into their sleep stages. The transfer learning technique and fine-tuned SqueezeNet model are used for classification. The same procedure is repeated for a 150 s EEG epoch. The 150 s epoch is helpful for cases where epochs consist of sleep stage transition boundaries.

Finally, the raw single-channel EEG, their short-time Fourier transform (STFT) and stationary wavelet transform (SWT) are considered for sleep stage classification. Different CNN models (1D-CNN, STFT-CNN and SWT-CNN) are trained to classify sleep stages. The results of sleep stage scoring employing a raw EEG signal epoch and their short-time Fourier transform and stationary wavelet transform are compared using a CNN classifier. The advantage of this method is that the preprocessing steps e.g., time-frequency decomposition and features extraction steps, are integrated seamlessly with the classifier stage.

This thesis investigates the performance comparison of deep networks trained on time-frequency representation with models trained on features extracted from time-series data. Evaluation results show that these methods achieved near state-of-the-art accuracy even using single-channel EEG signals. The automatic classification and analysis of sleep characteristics and stages will help sleep experts and clinical doctors work more efficiently in diagnosing sleep disorders.

3.1.7 *Study, design, and experimental verification of plasma opening switch for high current applications*

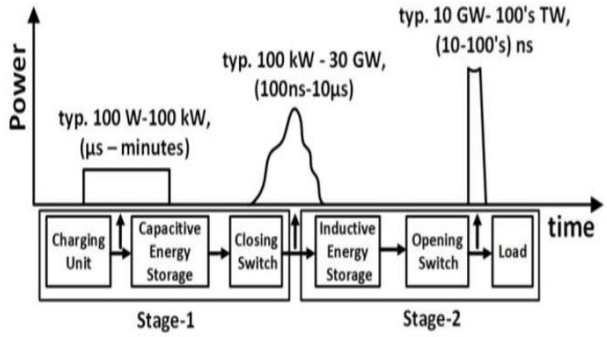

Fig-1: Pulsed power stages with respect to time and power

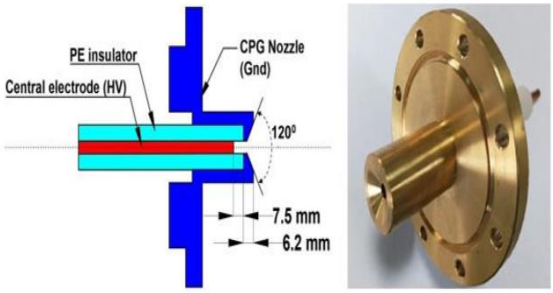

Fig-2: Coaxial Cable Plasma Gun

The primary energy storage capacitors are used as a primary or basic component of pulse power source and alone cannot provide extremely high values of voltages and powers. To further amplify them, one requires power conditioning circuits. These power conditioning devices are intermediate between primary energy storage and load. This intermediate stage is charged for longer durations (in microseconds to minutes), i.e., it stores energy in low powers for longer durations than its discharge times in the order of picoseconds to milliseconds thereby enhancing the power. Figure 1 shows the stages involved in developing an intense pulse power scheme using an opening switch with power conditioning. In this thesis, a plasma opening switch (POS) based pulsed power generator is designed and developed.

Generation of intense pulse power using pulse forming lines and Tesla transformer-based plasma opening switch systems increase the complexity in the design of individual systems and required to generate a nanosecond pulse before applying to the POS, and a compact capacitor bank-based POS system can be designed with microsecond range pulse. This thesis aims to design and develop the plasma opening switch and experimentally verify the opening action with a generator as a compact capacitor bank.

The following studies have been carried out to achieve the intense pulse power at the load:

1. The microsecond pulsed power generator designed is a capacitor bank using synchronization of field distortion spark gap switches, which are synchronized within 10 ns with a fast trigger generator with 3.1 ns as trigger jitter.

2. The non-invasive sensors such as V-dot, Rogowski coil, and B-dot for high voltage and high current measurements are designed and implemented at different locations in the experimental

setup. A magnetic field sensor based on the Faraday rotation principle is designed and developed for magnetic field measurement.

3. A coaxial cable plasma gun based on surface flashover of polyethylene insulator is designed to generate the plasma for POS experiments. The cable gun is characterized by the triple Langmuir probe, and Faraday cup diagnostics are used to measure plasma parameters and plasma divergence.

4. An inductive energy storage system with a plasma opening switch is designed based on the time domain simulations. The POS is operated in hydrogen and carbon plasma regimes, which was verified experimentally with a microsecond pulsed power generator as a capacitor bank

3.2 Indira Gandhi Centre for Atomic Research

3.2.1 *Analysis for performance optimization of a fast reactor fuel vault ventilation system*

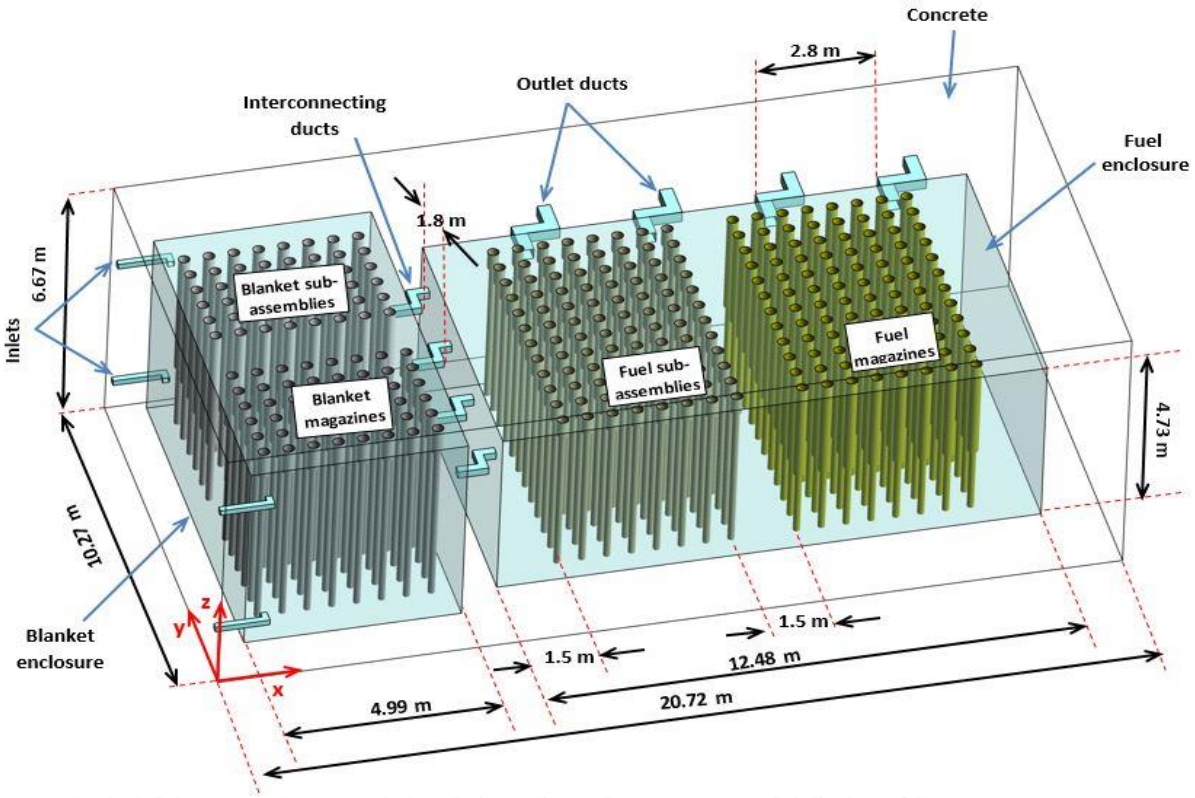

Schematic of a fuel storage vault

This research explores the critical domain of nuclear fuel storage within power plants, focusing on the design of an optimized cooling system for an upcoming Indian nuclear facility. The goal is to ensure the safety and efficiency of the fuel storage system before deployment. Rather than relying on costly and hazardous physical experiments, the study leverages computer simulations to assess and enhance a pre-designed cooling system for a fresh fuel storage facility. A Computational Fluid Dynamics (CFD) model is developed, validated against independent data, and employed to evaluate the system's performance.

A key finding of this research is the significance of duct positioning in maintaining the safe temperature of the nuclear fuel storage vault. Introducing a supply jet above the heat source

improves air mixing, ensuring uniform temperature distribution and preventing localized heating. This leads to a more stable and controlled environment, vital for safeguarding the structural integrity of the vault. Additionally, the study identifies that increasing the aspect ratio of interconnecting ducts results in reduced air exchange rates and lower heat removal efficiency. Optimizing duct geometry, such as smoothing edges, significantly reduces flow losses, thereby increasing air velocity and improving heat transfer efficiency. The research further suggests that multiple small air supply nozzles outperform a single large duct, enhancing air penetration into the fuel storage area and promoting better heat removal.

The study also explores the thermal performance of different duct shapes and nozzle configurations. Square ducts, when paired with square nozzles, provide effective heat removal, with the incorporation of diffusers at the nozzle tips further improving air dispersion and preventing localized heating. The research also investigates the cooling system's performance under failure scenarios. Without backup equipment, the system can operate for up to 100 seconds without risking contamination of the air in the facility, as natural convection becomes the primary mechanism for air circulation.

In the event of equipment failure, prompt activation of backup systems within 100 seconds ensures stability. The upper inlet position plays a critical role in containing aerosol-containing air, ensuring that the vault remains safe.

A significant component of this study is the optimization of a large thermosyphon with external fins to enhance heat transfer through the nuclear fuel storage vault. Experiments on thermosyphons with water and ethanol as working fluids reveal that vertical thermosyphons with a 60% filling ratio operate with minimal resistance and effectively cool the vault. These optimized thermosyphons are integrated into the vault ceiling, and their thermal conductivity is used in CFD simulations to predict performance. The results show that adding external fins significantly increases heat transfer, aiding in air circulation and stabilizing fuel temperatures at approximately 332 K.

In conclusion, this research makes a vital contribution to the safety, efficiency, and reliability of nuclear fuel storage. It advances the design of cooling systems for nuclear facilities and supports the national energy security program by ensuring safe and efficient fuel storage solutions.

3.2.2 *Numerical investigations on the performance of coupled natural circulation loops with application to nuclear reactor safety*

The research presented in the thesis titled "Numerical Investigations on the Performance of Coupled Natural Circulation Loops with Application to Nuclear Reactor Safety" focuses on detailed numerical studies of coupled natural circulation loops (C-NCL) and their application to passive heat removal systems (PHRS) in nuclear reactor designs.

These passive systems play a critical role in reactor core cooling during accident scenarios, particularly under station blackout (SBO) conditions. They are also important for the safety and reliability of advanced reactors, such as small modular reactors (SMRs) and Gen IV. However, the coupling configurations, operating conditions, etc. are reactor-dependent, and hence their dynamics.

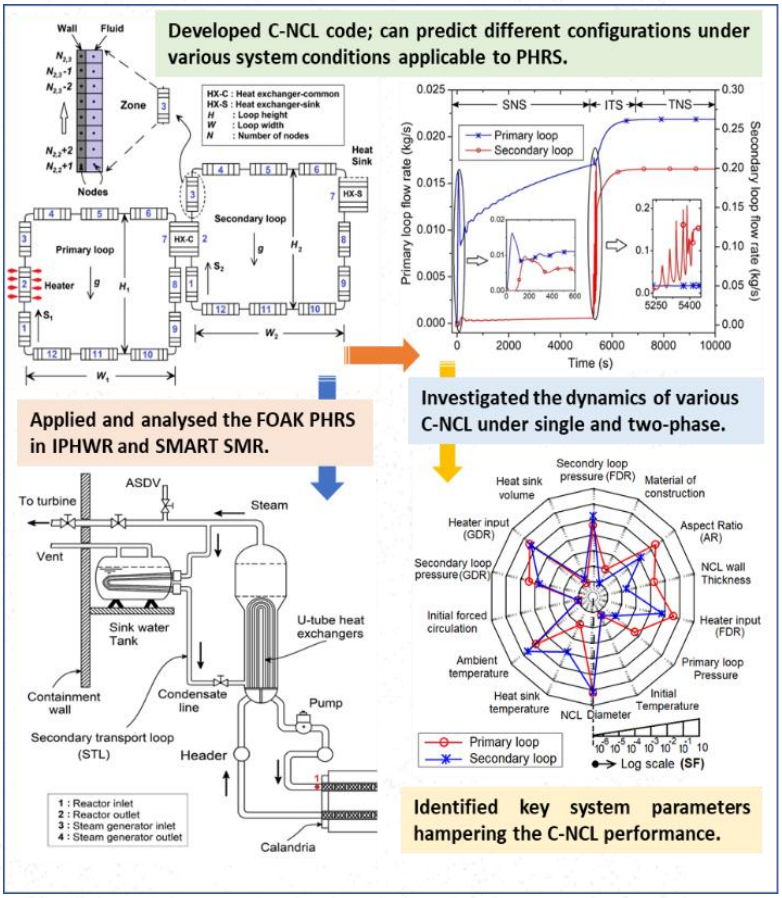

C-NCL code and application to various PHRS

In this thesis, a C-NCL numerical code is developed and validated with the capability to evaluate PHRS performance in various nuclear reactor designs. It includes features for coupling configurations, fluid conduction, ambient influence, and simulations under single-phase (SP), two-phase (TP), and superheated and property formulations instead of Boussinesq approximation. Using the code, the transients of vertical and horizontal C-NCL under SP and TP conditions are investigated. Their complex coupled dynamics are predicted and explained. The effect of geometrical and operating parameters is quantified and key ones are identified through sensitivity analysis. The influence of parameters is found different for SP and TP coupled loops. Coupled transients are found to sluggish and longer grace time than NCLs. In C-NCL, if one loop is unstable, the other also becomes unstable even with stable configuration. Further, the coupling and heater-cooler orientations showed strong effect on C-NCL.

The code has been applied to investigate the performance of First Of A Kind (FOAK) PHRS of an Indian pressurized heavy water reactor (IPHWR). The analyses demonstrated the adequacy of PHRS to remove decay heat by establishing natural circulation. The effects of various parameters are studied, quantified, and the optimum values identified. The code is further applied to study the transients of PHRS with application to SMRs. The transients under SP, TP and superheated conditions are captured. The impact of accident induced conditions on PHRS performance is investigated. Fire, seismic deformations, ambient and sink conditions are found to be influencing the PHRS. The outcomes of this thesis address the key gap on C-NCLs in the open literature. Additionally, these studies can form the basis for evaluating the performance of various C-NCL-based PHRS concepts in both current and advanced reactor designs.

3.2.3 *Organic electrochemical transistor-based biosensing of salt stress in plants*

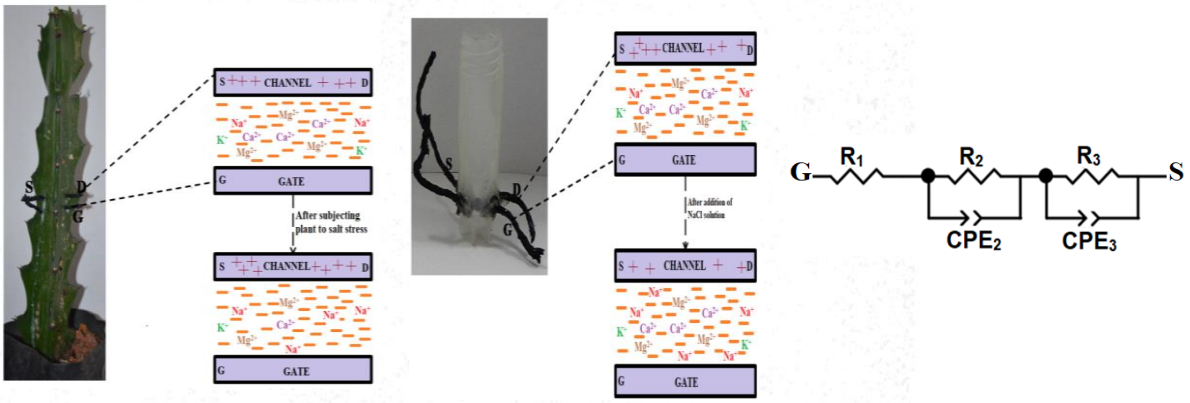

In-vivo and in-vitro OECT-based biosensing of salt stress in plants

OECT-based biosensor devices fabricated from three different conducting polymers, PEDOT: PSS, PANI and PPy have been demonstrated for in-vivo and in-vitro monitoring of salt stress in plants. Plant sap flowing through xylem and phloem in a living plant was utilized as electrolyte for the transistor-based device in the case of in-vivo monitoring while plant sap extracted in a vial was utilized as electrolyte in the case of in-vitro monitoring. Elemental analysis of plant sap extracted from cactus plant was done by INAA technique, a sensitive analytical technique for the elements, sodium and potassium. Analysis of elements, calcium and magnesium was done by CCD based ICP-OES. Thread functionalized with PEDOT: PSS with and without plant sap on its surface was characterized by E-SEM.

Electrochemical Impedance Spectroscopy studies for the biosensor device were carried out in order to understand variation in its channel current as control voltage was varied, to understand sap/thread interface and to derive equivalent electrical circuit for the device. Impedance studies were carried out across gate and source terminals and also across source and drain terminals and under both in-vivo and in-vitro salt stress conditions. EIS studies carried out for the device under both in-vivo and in-vitro salt stress conditions helped in understanding response of plant to salt stress and to verify the in-vivo and in-vitro salt stress monitoring mechanisms claimed in DC studies of the biosensor device. All the impedance studies have been carried out by varying frequency from 1 Hz to 106 Hz. Modulation in channel current observed in the OECT device with changes in ionic concentration in plant sap proved to be an efficient tool to monitor salt stress in plants, establishing this technology as a crop phenotyping tool for plant breeding and precision agriculture. Also, an electronics module for on-field monitoring of salt stress in plants has been designed, fabricated and deployed.

3.3 Institute for Plasma Research

3.3.1 *Experimental and simulation studies of effective thermal conductivity of compressed and uncompressed pebble beds for fusion blankets*

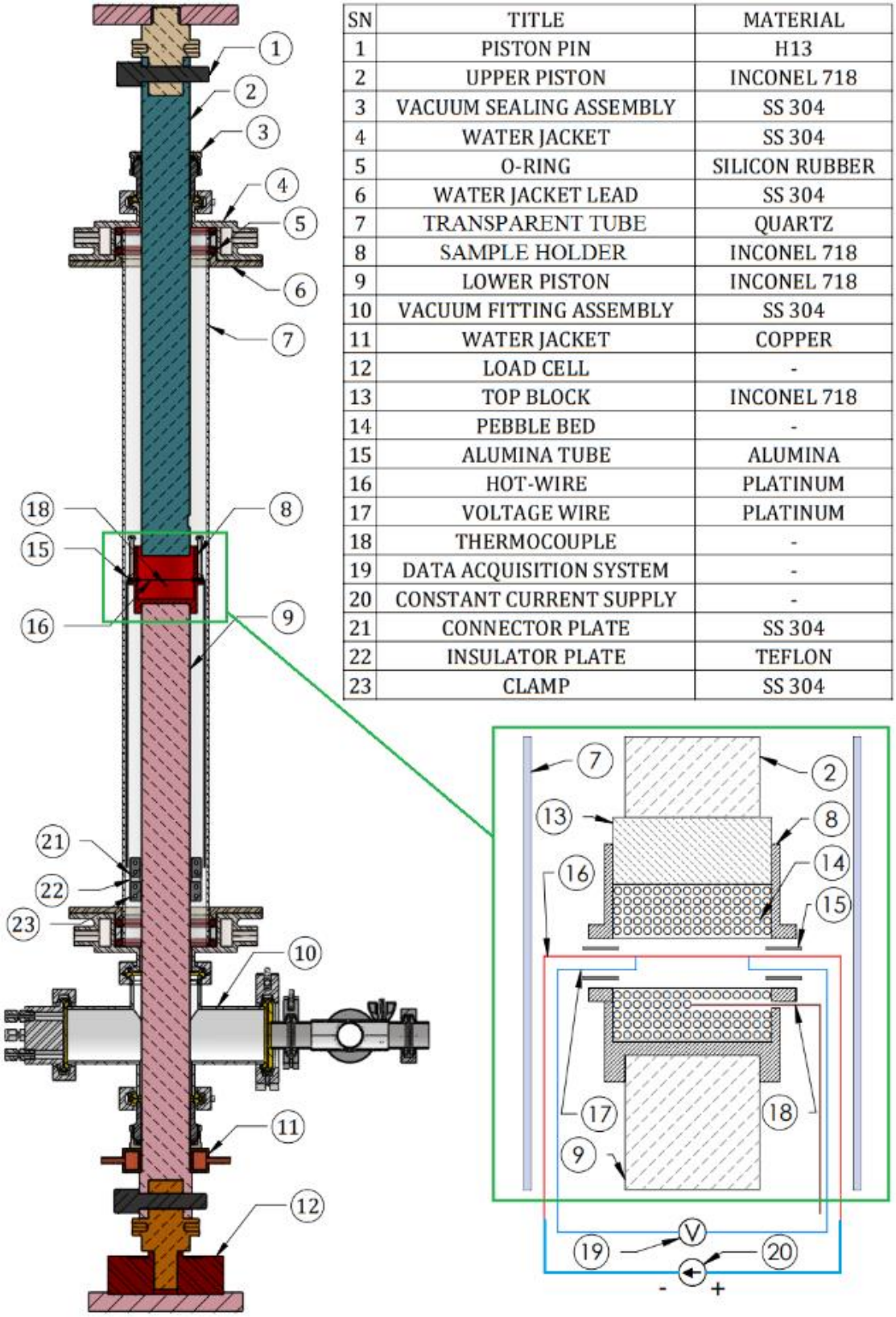

SN	TITLE	MATERIAL
1	PISTON PIN	H13
2	UPPER PISTON	INCONEL 718
3	VACUUM SEALING ASSEMBLY	SS 304
4	WATER JACKET	SS 304
5	O-RING	SILICON RUBBER
6	WATER JACKET LEAD	SS 304
7	TRANSPARENT TUBE	QUARTZ
8	SAMPLE HOLDER	INCONEL 718
9	LOWER PISTON	INCONEL 718
10	VACUUM FITTING ASSEMBLY	SS 304
11	WATER JACKET	COPPER
12	LOAD CELL	-
13	TOP BLOCK	INCONEL 718
14	PEBBLE BED	-
15	ALUMINA TUBE	ALUMINA
16	HOT-WIRE	PLATINUM
17	VOLTAGE WIRE	PLATINUM
18	THERMOCOUPLE	-
19	DATA ACQUISITION SYSTEM	-
20	CONSTANT CURRENT SUPPLY	-
21	CONNECTOR PLATE	SS 304
22	INSULATOR PLATE	TEFLON
23	CLAMP	SS 304

Developed thermo-mechanical test setup

This thesis discusses the development of a thermo-mechanical test setup for ceramic pebble beds. The developed setup works on the principle of the hot-wire method to measure the effective thermal conductivity of pebble beds as a function of temperature, filling gas pressure, and mechanical compression stress. The setup is optimized to minimize the errors of the hot-wire method. The setup provides a novel design that enables the use of the 4-wire method (modified hot-wire configuration) for compressed beds' effective thermal conductivity measurement. The present hot-wire assembly provides accurate amount of supplied heat ($Q=V\times I$) inside the sample material. The setup uses continuous hot wire, which prevents "cold ends" inside the measurement region, eliminating the axial heat-flow error. An insulator assembly is designed which enables the use of bare platinum wires, which reduces the diameter of the hot wire, reducing the heat capacity error in the measurement. The connections between the platinum wires and the extension wires are outside the heated zone, preventing error in measurement due to the Seebeck effect. The measured effective thermal conductivity of 1±0.15 mm Li2TiO3-He bed increases with temperature (56%, room temperature – 800°C), compressive stress (37%, 0 – 6 MPa), and helium gas pressure (7%, 1 – 4 bar). The accuracy of the present configuration of setup is obtained ±1.5% using ASTM D5334.

Discrete Element Method simulations have been used to study the packing behavior of mono-sized, binary-sized, and poly-dispersed spherical and ellipsoidal-shaped pebbles studied in different vibration conditions. These beds are used in thermal Finite Element Method simulations to obtain their effective thermal conductivities. To avoid point contact between pebbles and ensure successful meshing, two approaches were employed: (i) shrinking (ii) enlarging the diameters of contacting pebbles using Python programs. The simulation results are benchmarked using experimental data of similar.

The present work provides the setup for accurate measurement of effective thermal conductivity of pebble beds as a function of temperature (up to 1000°C), mechanical load (up to 50 kN), and filling gas pressure (up to 4 bar (3 bar gauge)). It also provides experimental data of the effective thermal conductivity of Li2TiO3-He bed complemented by the larger simulation data set. The setup can also be used to study the stress-strain behavior of pebble beds and the measurement of their coefficient of thermal expansion (CTE) by using an LVDT attachment.

3.3.2 *FPGA based real time density feedback control system for ADITYA-U Tokamak*

Control of plasma parameters is not only necessary but also essential to improve plasma discharge parameters in any tokamak. To control the plasma parameters, a closed-loop feedback control system is required. The present work involves the development of a real time density feedback control system (RTDFC) implemented in FPGA to achieve the desired electron density in ADITYA-U Tokamak.

The essential components required to control the electron density during the plasma discharge are the real-time density measurement system, a fast logic unit to decide the required action, and feedback action unit that can act to increase or decrease the plasma density. The real time density measurement is performed by a 100 GHz heterodyne interferrometer with CORDIC

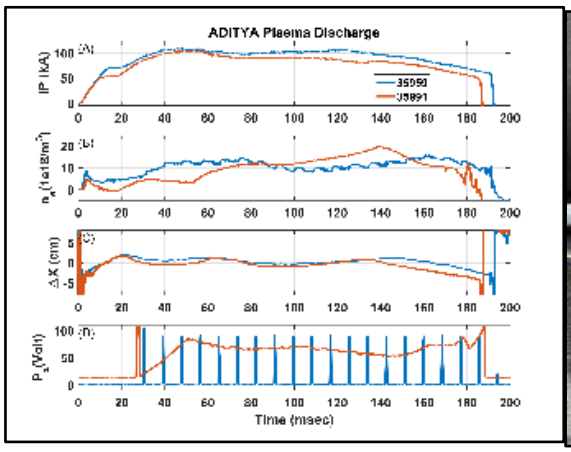

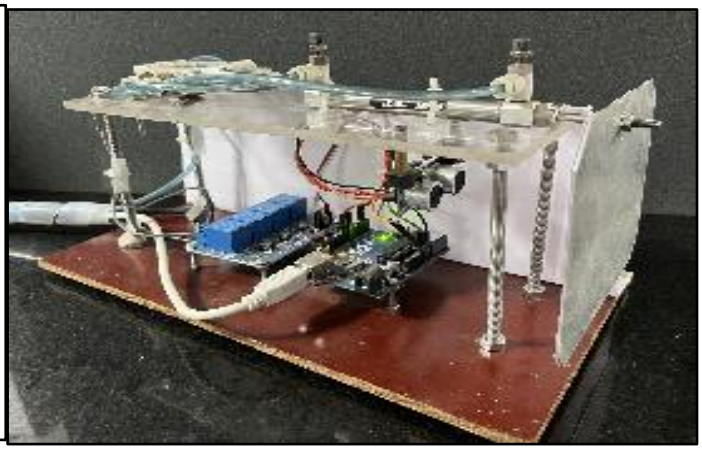

Neutral pressure is measured using LabVIEW-based data acquisition and control system during the plasma discharge.

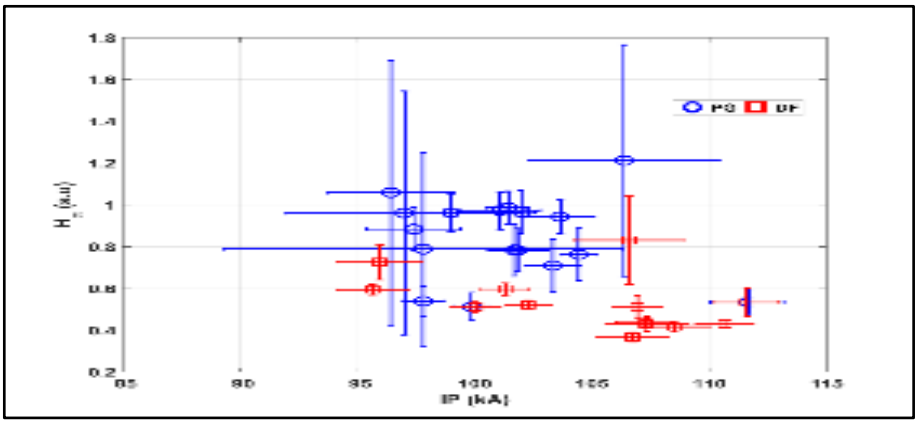

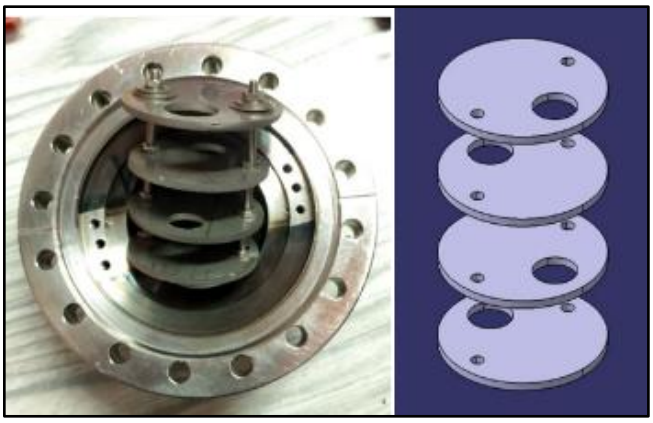

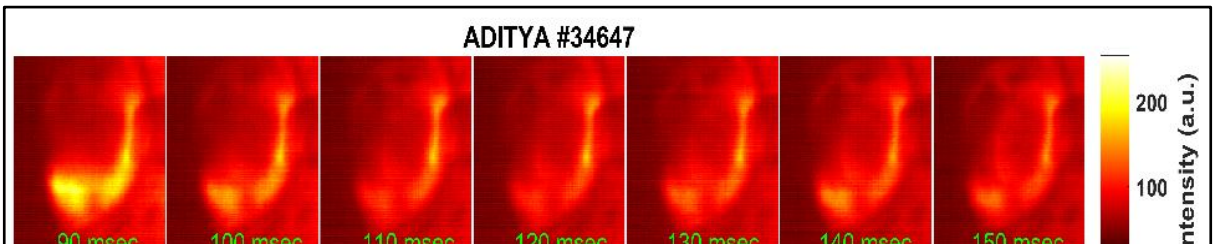

algorithm for fast estimation of phase and subsequently density. To achieve fast logical decision making, an FPGA based real time density feedback control system has been developed and implemented in ADITYA-U. The density feedback action is performed using piezo valves and their control units. The system is extensively calibrated to achieve the optimum amount of gas feed. In order to measure the pressure inside the VV during plasma discharges, a pressure measurement system based on ASDEX gauge is developed and commissioned in ADITYA-U.

To protect the gauge head from high-energy neutrals during the discharge, a baffle was designed to thermalize them within the discharge interval.

The thesis also focuses on the improvements done to the plasma discharges due to the real time density feedback. The quantitative analysis of the plasma parameters with the density feedback is performed and compared with the discharges where the RTDFC is not in use. The plasma discharges with density feedback gas injection show that the plasma current and density are achieved with less gas injection compared to normal discharges without RTDFC. This optimal use of gas injection results in less wall loading of the gas and thus results in decrease in the intensity of the hydrogen alpha (Hα) emission. The evolution of plasma parameters such as density and plasma current is also more smooth as compared to the normal pre-programmed gas feedback used before the incorporation of RTDFC. Density feedback also reduces Hα radiation, indicating reduction in wall recycling and hence improvement in plasma confinement time.

3.4 Raja Ramanna Centre for Advanced Technology

3.4.1 *Investigation on laser directed energy deposition based multi-material additive manufacturing of copper and stainless-steel*

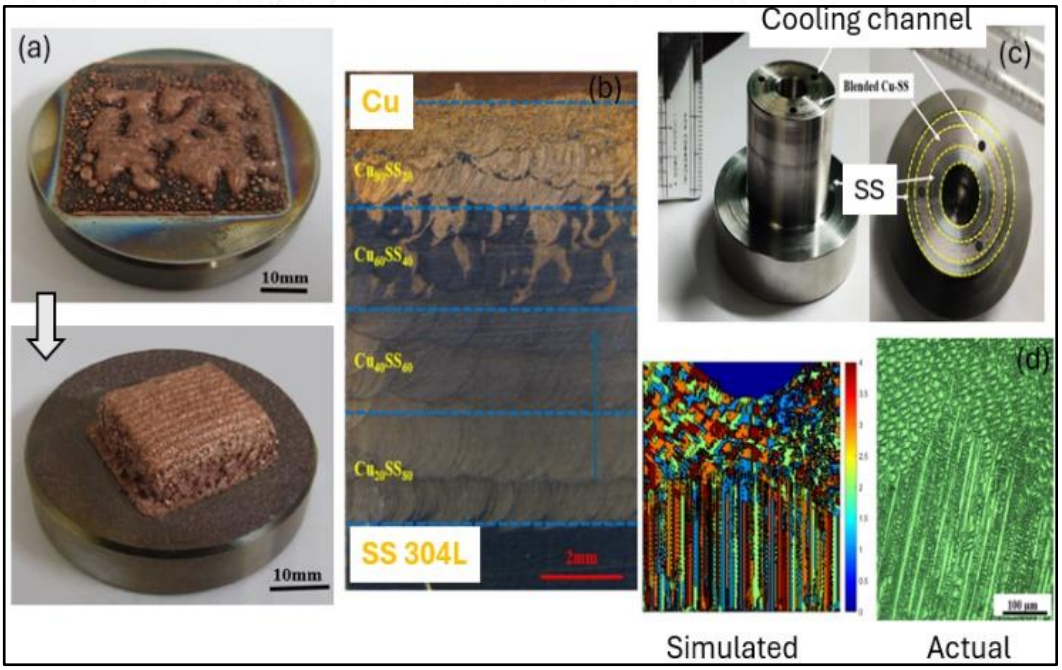

LDEC (a) cu (b)FGM (c) multi-material injection mold (d) hybrid phase filed modelling

Laser Directed Energy Deposition (LDED)-based Additive Manufacturing (AM) has emerged as a promising technique for fabricating dense, complex-shaped multi-material components, offering high build rates and advanced material properties. This research focuses on the challenges and potential of LDED for Copper (Cu)-Stainless Steel 304L (SS) multi-material components, which are critical for industries such as tooling, aerospace, cryogenics, and energy. Cu-SS components offer enhanced thermal and electrical conductivity, corrosion resistance, and mechanical robustness. However, the significant differences in thermo-physical properties, including the thermal expansion coefficient and solubility between Cu and SS, present considerable challenges during LDED, leading to issues like micro-cracks and porosity at the Cu-SS interface.

The study investigates the LDED processing of pure Cu, Cu-SS blends, and Functionally Graded (FG) Cu-SS materials. The work begins by exploring the optimal process parameters for LDED of pure Cu (figure1(a), revealing the impact of Laser Energy per unit Powder feed (LEPF) on build quality. Various deposition strategies, such as constant, decreasing, and increasing LEPF, are examined, with the increasing LEPF strategy yielding defect-free deposits and enhanced mechanical properties compared to conventionally built Cu. Further investigation into the LDED of Cu-SS FG materials (FGM) identifies key challenges in crack formation and porosity. Three approaches to FGM fabrication (figure 1(b))—are explored, by as varying porcoess parameters and inter-layer delay to mitigate defects. Additionally, a multi-material injection mould prototype (figure 1(c)) is built using the identified parameters for the Cu50SS50 composition. Numerical modelling reveals that multi-material leads to a faster cooling rate (~17-23%) compared to that of a conventionally built SS mould. A data-driven and Phase Field Model (PFM)-based approach is developed to predict microstructural evolution during LDED, offering a closer match to experimental results than conventional models (figure 1(d)).

This research makes significant strides in optimizing LDED for Cu-SS multi-material fabrication, addressing processing challenges, microstructural understanding, and expanding the applicability of LDED in industrial applications involving dissimilar materials. The findings contribute to the broader goal of advancing additive manufacturing techniques to produce Cu-SS multi-material component.

LIFE SCIENCES

4.1 Bhabha Atomic Research Centre

4.1.1 *Molecular physiology of metal tolerance and transport in Chryseobacterium sp. strain PMSZPI isolated from a uranium ore deposit*

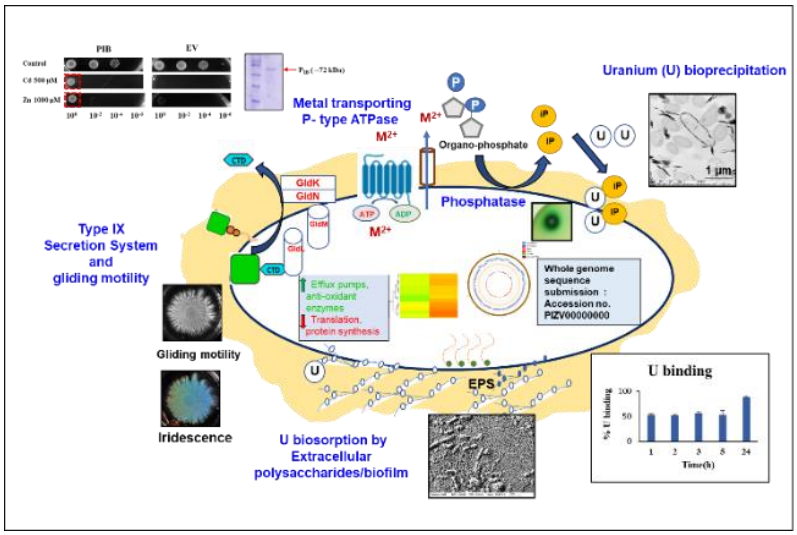

Cellular and molecular mechanisms underlying uranium/ heavy metal tolerance in Chryseobacterium sp. PMSZPI

Anthropogenic activities result in widespread environmental contamination with heavy metals and radionuclides. This poses significant ecological and public health risks. Certain metals such as silver, cadmium, lead, mercury, and uranium are non-essential and exhibit toxicity at elevated concentrations to the organisms residing in metal enriched environments. Microorganisms have evolved diverse resistance mechanisms to mitigate metal toxicity which include extracellular and intracellular sequestration, development of permeability barriers, enzymatic detoxification, and active transport mediated by efflux pumps. Studies of microorganisms inhabiting extreme environments such as industrial sites, deep-sea hydrothermal vents, and mine tailings have aided in our current understanding of the microbial metal resistance. In this thesis, an attempt has been made to understand the mechanistic aspects of remarkable tolerance exhibited by *Chryseobacterium* sp. PMSZPI isolated from sub-surface soil of uranium ore deposit to uranium and other heavy metals. An integrated molecular, biochemical and physiological approach was employed to investigate the fundamental mechanisms underlying metal transport and tolerance in *Chryseobacterium* sp. PMSZPI. Genome sequencing of the *Chryseobacterium* sp. PMSZPI strain followed by comparative genomics with other closely related strains revealed a unique set of genes in PMSZPI encoding for transporters, phosphatases, T9SS secreted proteins and biofilm that are likely to be of adaptive significance. Additionally, PMSZPI showed resistance to a wide array of antibiotics and tolerance to 1.5 kGy of gamma radiation in line with in-silico predictions. This study also revealed the functional Type IX secretory system and gliding motility in PMSZPI, wherein periodicity within the spreading colonies led to the phenomenon of iridescence. The transcriptomic response to U indicated the upregulation of antioxidant responses and downregulation of energy- intensive processes, highlighting the adaptive strategies employed by *Chryseobacterium* sp. PMSZPI to survive in U-induced oxidative stress conditions. Exposure to heavy metals and U also led to the transcriptional induction of metal-translocating

P_{IB}-type ATPase, which was identified and characterized as a Zn(II)/Cd(II)/Pb(II) P_{IB-2}-ATPase based on the substrate specificities. The ATP hydrolysis activity and metal tolerance function of P_{IB-2}-ATPase were confirmed through in-vitro and in-vivo assays, highlighting its importance in metal efflux in PMSZPI. The other probable key mechanisms underlying its U tolerance were efficient uranium binding (~90% of 100 µM U) and phosphatase mediated U bioprecipitation (~93–94% of 1 mM U at pH 5, 7 and 9) abilities. This study also demonstrated the effective uranium (U) removal by biomineralization with free and immobilized *Chryseobacterium* sp. PMSZPI biomass, that precipitated U as stable uranyl phosphate mineral under both batch and continuous flow through conditions. The long-term stability of lyophilized and immobilized cells for uranium removal suggested the promising potential of this strain for bioremediation of uranium-contaminated environments.

The understanding of the cellular and molecular mechanisms gained herein could potentially be employed for designing potential bioremediation strategies for U and other heavy metals.

4.1.2 *Development of diagnostic and prognostic algorithms for neuroendocrine tumors from RNA-sequencing profiles of peripheral blood cells*

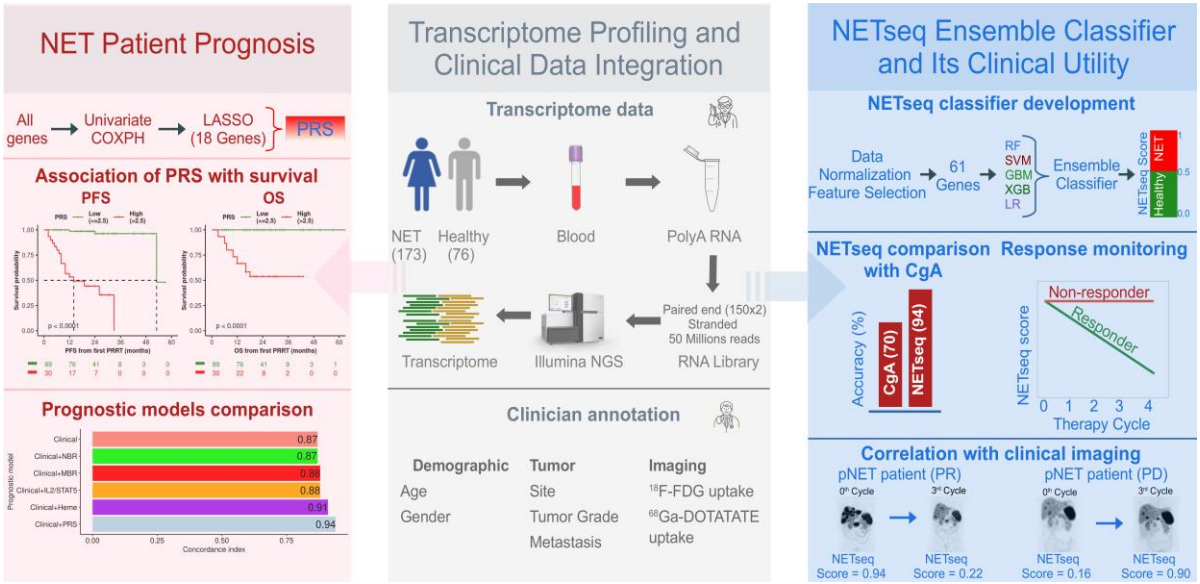

Schematic showing the development and utility of diagnostic and prognostic algorithms for NET patients

Neuroendocrine tumors (NETs) are heterogeneous neoplasms often diagnosed late due to the lack of sensitive, specific biomarkers, particularly in India. This study used RNA-Seq of peripheral blood cells as a liquid biopsy to develop multi-gene classifiers for NET diagnosis, treatment monitoring, and prognosis prediction via machine learning. Peripheral blood transcriptome profiles were generated using the PolyA enriched RNA, on Illumina platform in paired end with 50 million target reads (n = 249). The NETseq ensemble classifier, built using RNA-Seq data from an age- and gender-matched cohort (n = 97) with five machine learning algorithms, achieved 100% training accuracy in training cohort. In independent validation

cohort (n = 109) model achieved 93% sensitivity, and 91.4% specificity, and AUROC of 95.4%, outperforming serum CgA. NETseq scores correlated with RECIST-1.1 responses and 68Ga-DOTATATE PET/CT findings, showing treatment monitoring potential. Several prognostic models were evaluated, including one based on clinical parameters alone, and others integrating immune cell ratios (such as NLR and MLR), novel inflammation indices (NBR and MBR), and systemic cancer hallmarks including heme metabolism and IL2/STAT5 signaling with clinical parameters. A prognostic risk score (PRS) model, derived from an 18-gene signature measurable in peripheral blood, demonstrated the strongest predictive performance and offers a robust tool for prognosis prediction in NET patients undergoing PRRT. In conclusion, this study highlights peripheral blood RNA-Seq and machine learning for NET diagnosis, treatment response monitoring, and prognosis advancing precision medicine in NET management with direct clinical utility of NETseq ensemble classifier and PRS with further validations.

4.1.3 *Studies on development of radioimmunotherapy agents and understanding their mechanism of action*

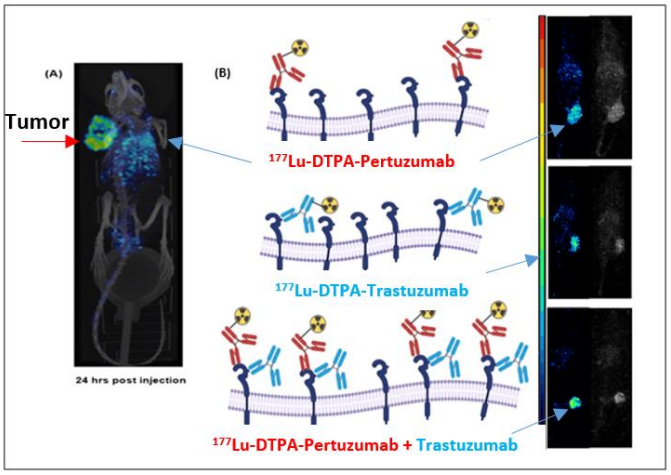

Tumor uptake and retention of ^{177}Lu-DTPA-Pertuzumab in HER2 overexpressing SKOV-3 tumor. The radioformulation revealed binding synergism in presence of cold Trastuzumab both in-vitro & in vivo

Solid cancers, such as breast and ovarian cancers characterized by the overexpression of the HER2 receptor, pose significant clinical challenges with poor prognostic outcomes. Breast cancer, in particular, represents a leading cause of cancer-related deaths globally, with 15-20% of cases exhibiting HER2 overexpression. HER2-targeted therapies, such as Trastuzumab and Pertuzumab, have revolutionized treatment paradigms. Radioimmunotherapy (RIT) employs radiolabeled monoclonal antibodies or their fragments to deliver targeted radiation therapy to cancer cells expressing specific antigens, such as HER2. Pertuzumab, although less studied compared to Trastuzumab, has shown promising results in molecular imaging using PET and SPECT radiotracers.

The current investigation has demonstrated optimization of the radiolabeling protocol for ^{177}Lu-DTPA-Pertuzumab, complemented by characterization and extensive biological evaluation conducted across multiple batches to confirm the effectiveness of the

radioformulation in targeting HER2-positive cancers. The data generated were submitted to DAE-RPC for approval of clinical application. Additionally, the study emphasizes the challenges posed by large molecular weight radioimmunotherapeutic agents and proposes addressing these limitations by exploring the potential of $F(ab')_2$ fragments of Pertuzumab as theranostic agent. The study also explored the molecular mechanisms responsible for the clinical synergy and improved survival benefits achieved with the Trastuzumab and Pertuzumab in combination by experimental analyses to assess the interaction of radiolabeled antibodies in the presence and absence of a second unlabeled antibody with HER2. The radioimmunoconjugates preserve the existing binding synergism between Pertuzumab and Trastuzumab to HER2 receptors in both *in-vitro* and *in-vivo* testing conditions.

Understanding radiobiological responses such as radiation-induced biologic bystander effects (RIBBEs), are crucial for optimizing therapeutic doses to achieve the desired response while minimizing side effects. The study has investigated the in-vitro radiation-induced biologic bystander effects mediated by radiolabeled Trastuzumab with three therapeutic radioisotopes ^{90}Y, ^{177}Lu, and ^{125}I, each with different type of emission i.e., β^-, β^-/γ and auger electron respectively. The results demonstrated notable bystander toxicity across all three radioimmunoformulations under *in-vitro* conditions.

4.1.4 *CRISPR based analysis of essential genes in Mycobacteria*

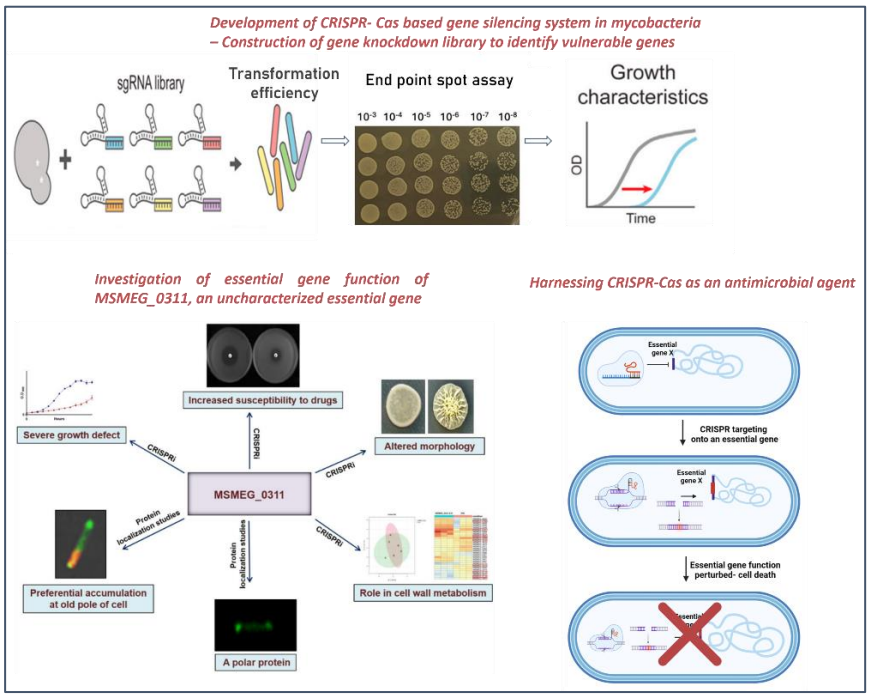

Schematic showing the CRISPR based analysis of essential genes in mycobacteria

Mycobacterium species are famous for their uniquely resilient cell walls, which make them highly resistant to antibiotics and genetically intractable. Understanding the biology of Mycobacterium species has proven vital for developing effective treatments against infections like tuberculosis. The research involved the application of two different CRISPR-associated proteins: the well-documented Cas9 and the novel Cas12 protein. Using Cas12-based knockdown system, approximately 50 gene knockdown strains were generated and

phenotypically characterised. The screen identified a conserved gene cluster containing putative cell wall metabolism genes that were previously uncharacterised. This discovery prompted a focused investigation of one of the essential genes, MSMEG_0311, to gain a deeper understanding of its function. Extensive research revealed that MSMEG_0311 plays a crucial role in cell morphology and permeability. It was determined to be a polar protein that influences the presence of trehalose-conjugated mycolic acid on the outermost layer of the mycobacterium cell. This finding adds to the understanding of the complex cell wall structure of mycobacteria. In addition to the functional characterization of MSMEG_0311, the thesis also explored the potential of CRISPR-Cas systems as an antimicrobial tool against mycobacteria. The research demonstrated that mycobacteria are unable to repair the double-strand breaks induced by the Cas9 protein from *S. pyogenes*. This inability to repair the breaks signifies the potential of CRISPR-Cas systems in developing novel antimicrobial strategies against mycobacterial infections. Overall, the thesis provides significant insights into the application of CRISPR interference in mycobacteria, the functional role of the MSMEG_0311 gene, and the potential of CRISPR-Cas systems as an antimicrobial tool. The findings contribute to the broader understanding of mycobacterial genetics and offer promising avenues for future research in combating mycobacterial diseases.

4.1.5 *Physiological and molecular insights into radiation induced salt tolerant mutant of sugarcane*

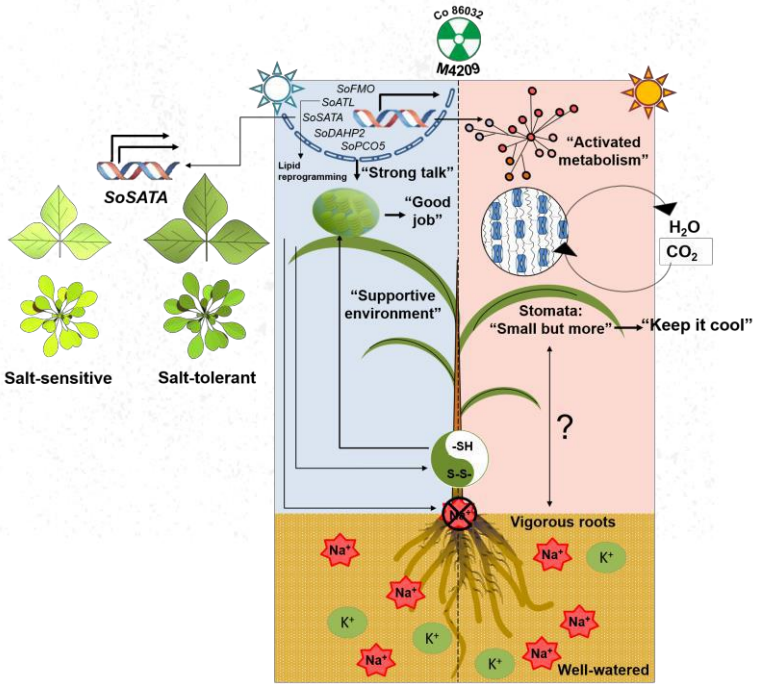

Proposed model for the physio- molecular adaptions mediating inducible salt tolerance in M4209

Sugarcane is a major food and biofuel crop of global socio-economic relevance. Soil salinization in sugarcane-cultivating regions causes 25-30% reduction in cane and sugar yield. Bridging this gap requires development of robust and sustainable approaches for

improving salt tolerance in sugarcane. However, due to the long life-cycle and genome complexity of sugarcane, its salt-adaptive mechanisms remain poorly understood. To address these lacunae, we characterized M4209, a promising salt-tolerant sugarcane mutant derived from an elite salt-sensitive variety Co 86032, via the radiation induced *in vitro* mutagenesis (RiMu) approach.

Compared with Co 86032, M4209 exhibited 30% higher yield under saline field conditions, without significant yield penalties under control field conditions. A joint transcriptomics and physio- biochemical investigation of this 'inducible salt tolerance' trait revealed that the relatively improved plant growth, ionic balance, redox homeostasis, and photosynthetic efficiency observed in salt-stressed M4209 plants was due to the active transcriptional reprogramming of genes involved in photosynthesis, metabolic processes, stress-responsive pathways, and transmembrane transport, suggesting a nucleus-chloroplast communication. Comparative evaluation under combined heat and salt stress (HS-stress) revealed that M4209 plants exhibited better retention of the heat-induced enhancement in photo- assimilation. The improved transpirational cooling and gas exchange observed in M4209 under high temperatures was attributable to its novel Open-Small-Dense (OSD) stomatal phenotype, consequent of the transcriptional shift in the '*SoEPF9-SoEPF2'* regulatory module. Concurrent with better ionic balance, source strength and sucrose loading, the dually improved photosynthetic rate and stomatal response resulted in better plant growth and vigor under HS-stress conditions. Finally, the overexpression of *SoSATA* (SALT ACTIVATED TRANSCRIPTION ACTIVATOR), a key salt-responsive gene isolated from M4209, improved plant growth and biomass in Arabidopsis and soybean under NaCl stress conditions, suggesting *SoSATA* to be a positive regulator of salt tolerance. Taken together, our study demonstrated the potential of RiMu in addressing the dual objective of advancing fundamental understanding of salt- and HS-stress tolerance mechanisms in sugarcane and potentially augmenting crop-improvement programs.

4.2 The Institute of Mathematical Sciences

4.2.1 *Machine learning and predicting clinical outcomes*

This thesis has explored the intersection of machine learning and its applications in predicting clinical outcomes. The integration of machine learning models into the healthcare domain offers a paradigm shift in the way we approach patient care, treatment planning, and medical decision-making. We have reviewed how machine learning models can leverage diverse healthcare data sources, ranging from electronic health records to medical imaging, to predict a spectrum of clinical outcomes. These outcomes include disease diagnosis, prognosis, patient readmission rates, and adverse events prediction. We have demonstrated examples in our work. However, while machine learning shows immense promise, several challenges need to be effectively addressed. These encompass issues related to data quality, model interpretability, ethical considerations, and seamless integration of these models into the clinical workflow. Collaboration between healthcare professionals, data scientists, and policymakers is crucial to ensure that these predictive models are both reliable and actionable. In this thesis we have described two projects in detail, and a few others briefly. In first project we used the Gompertz model to describe the growth of fetal biometric ultrasound measurements and used it to build

a predictive model for birth weight. While in other, we described a clustering algorithm for heterogeneous data and used it to develop an algorithm for synthetic data generation. Lastly, we described our work on predicting SIRS in ICU settings using levels of circulating endothelial progenitor cells, predicting gestational age using maternal blood transcriptomics; and radiogenomic brain tumor classification. The thesis thus covers both method development and applications. While there is decades-long research in methods, and increasing interest in biomedical applications, the international interest in this interface is exploding in recent years and we expect significant future developments in AI/ML methods and their applications to biomedicine, to which we hope to contribute.

4.2.2 *Computational data-driven investigation of chemical exposome and its links to human and ecosystem health*

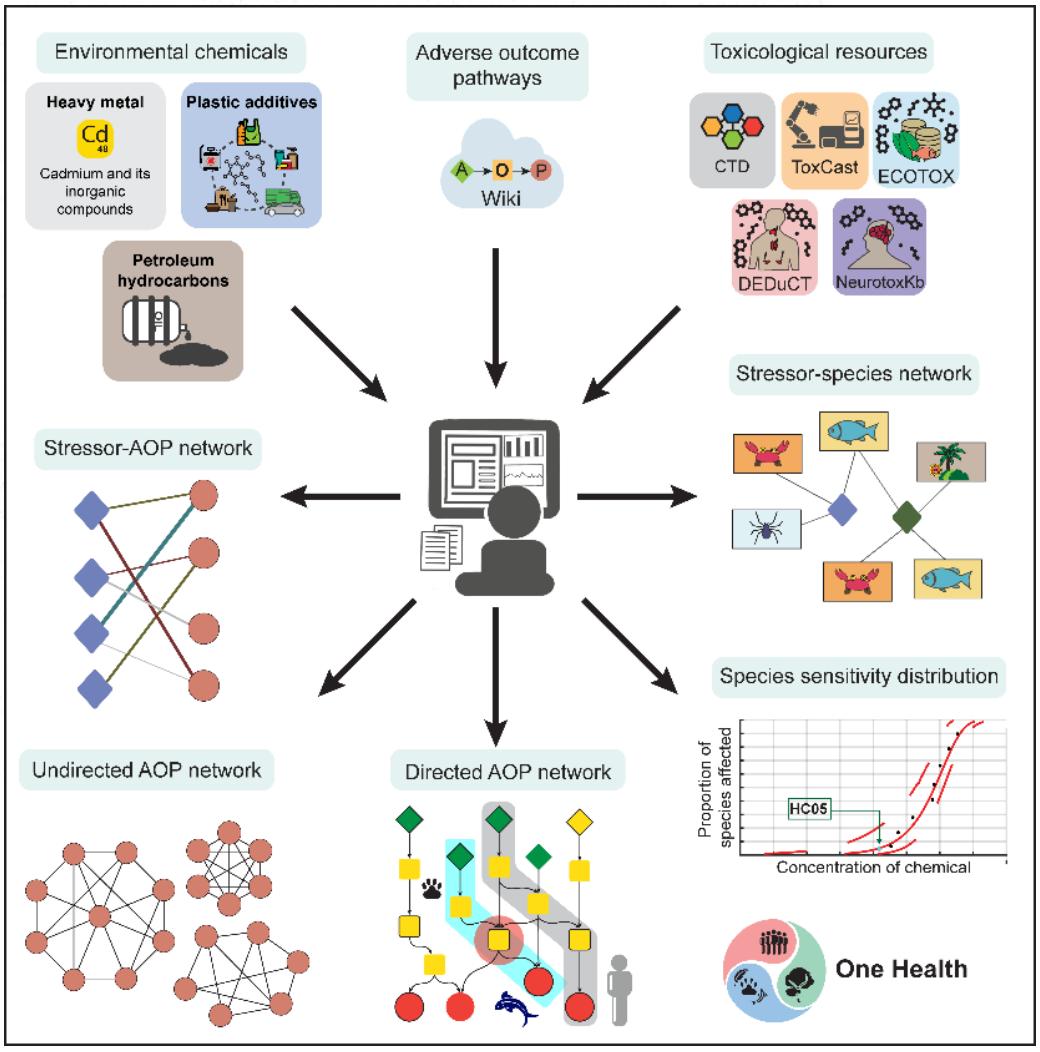

Schematic summary of the investigations of the chemical-induced toxicities in human and ecosystem using network-based and integrative toxicological data-centric approaches

The concept of chemical exposome encompasses a broad range of chemicals including consumer products, industrial pollutants and pesticides, that affect humans and ecosystem. Computational approaches offer an efficient and cost-effective alternative to traditional animal-based toxicity testing, thus enabling a comprehensive characterization of the ever-expanding space of chemical exposome.

This thesis computationally investigates the structure-activity landscape of environmental chemicals binding to two endocrine receptors, namely the androgen receptor (AR) and the thyroid stimulating hormone receptor (TSHR), revealing the presence of activity cliffs, where structurally similar chemicals exhibit large differences in their activity. These activity cliffs are classified into several structural categories. Additionally, investigation of mechanism of action (MOA) annotations for the TSHR binding chemicals reveals MOA cliffs, where structurally similar chemicals have different mechanisms of action. Furthermore, this thesis leverages the adverse outcome pathway (AOP) framework to investigate chemical-induced health effects associated with heavy metal cadmium, plastic additives, and petroleum hydrocarbons (PHs). In each case, biological endpoints data from several toxicological resources aided in the construction of different types of AOP network.

The constructed AOP network reveals key biological events and toxicity pathways, providing insights into chemical-induced adverse health effects in both humans and ecological species. The stressor-species networks for PHs highlight the diverse species or species groups most affected by PH exposure. The species sensitivity distribution of the PHs helps in deriving the hazard concentration of the chemical that is not harmful to a large proportion of species in aquatic environment.

In sum, this thesis systematically examines diverse environmental chemical spaces and their health impacts on humans and ecosystem, presenting a holistic view of the chemical exposome and its implications from a One Health perspective.

4.3 National Institute of Science, Education and Research

4.3.1 *Regulation of cell-mediated immune (CMI) responses associated with immunosuppression*

Immunosuppression is characterized by the abated effector responses associated with immune cells, accompanied by the modulation of the cellular events important to mount an effective immune response, followed by the reduced ability to recognize and/or counter foreign antigens. Several diseases, including cancer, are observed to progress through alleviating immune responses, causing systemic immunosuppression. The tumor microenvironment plays an important role in cancer progression and metastasis by employing an immunosuppressive network suppressing anti-tumor immune responses. B16F10, a murine transplantable melanoma cell line, has been reported to hinder T cell function, in vivo and in vitro. Similarly, various medications, including drugs used in transplantation, and several modulators function through the inhibition of effector immune responses associated with antigen-presenting cells (APC), lymphocytes, and other accessory immune cells. Transient receptor potential vanilloid 1 (TRPV1) and transient receptor potential ankyrin 1 (TRPA1) are polymodal, non-selective cation channels present in different cell types and are reported to regulate effector responses associated

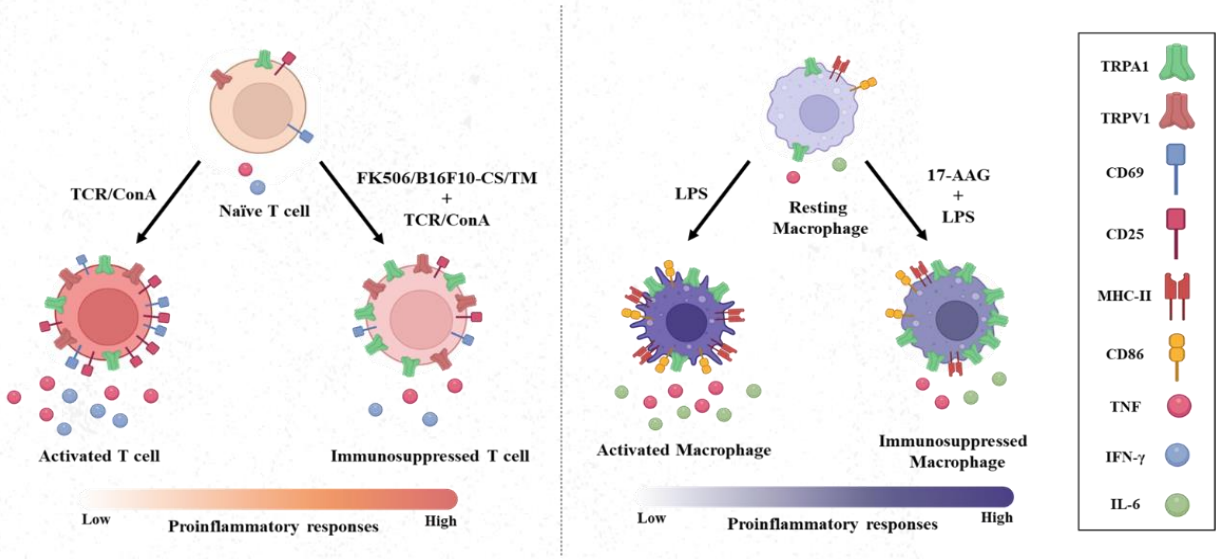

Figure: Functional association of TRPV1 and TRPA1 towards regulating cell-mediated immune responses during experimental immunosuppression.

with various immune cells, including macrophages, dendritic cells, and T cells. However, the information towards the possible involvement of these channels in immunosuppression associated with T cells and macrophages remains scanty. In this study, first, we have explored the possible role of TRPV1 in FK506- and B16F10-CS-mediated immunosuppression of T cells. It was observed that induction of TRPV1 expression occurs during experimental immunosuppression and TRPV1 plays an important role in regulating immunosuppression-mediated Ca2+ influx. Next, we have investigated the possible role of TRPA1 in 17-AAG-induced Hsp90 inhibition-mediated suppression of pro-inflammatory responses associated with macrophages. It has been found that TRPA1 induction ensues during Hsp90 inhibition-mediated suppression of macrophages, and it plays an anti-inflammatory role in regulating pro-inflammatory responses. Next, we have studied the possible association of TRPV1 and TRPA1 channels in Telmisartan (TM) (an anti-hypertension drug)-mediated immunosuppression of T cells. It was found that both TRPV1 and TRPA1 expressions were elevated in TM-driven immunosuppression of T cells, in vitro. TRPV1 activation during TM-mediated immunoregulation overrides TRPA1 activation-mediated suppression of T cells by upregulating T cell activation and effector cytokine productions, in vitro. This study may have implications for understanding the functional regulation of cell-mediated immune (CMI) responses associated with immunosuppression in altered physiological conditions toward devising better strategies for future therapeutics.

4.3.2 *Understanding hypoxic gastric cancer microenvironment*

CEACAM6 is a GPI-anchored immunoglobulin-like cell surface glycoprotein. Its extracellular domains include an N-terminal variable Ig domain and two C2-type Ig domains, enabling homotypic and heterotypic interactions. CEACAM6 regulates tissue architecture, signal transduction, and extracellular matrix dynamics by modulating fibronectin-integrin binding, influencing cell adhesion, proliferation, and immune responses. Overexpressed in epithelial

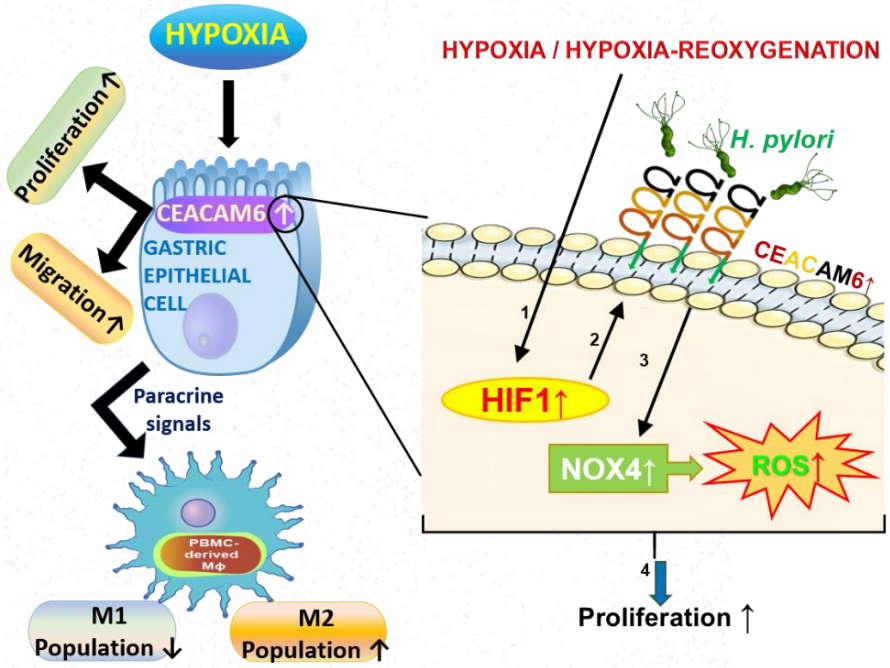

The HIF1-CEACAM6-NOX4 axis in hypoxia and hypoxia-reoxygenation promotes ROS generation and cell proliferation. Paracrine signals from hypoxia-regulated CEACAM6 cells promote gastric cancer aggressiveness and train macrophages towards a pro-tumorigenic M2 phenotype

carcinomas, it disrupts anoikis, promotes mesenchymal traits such as, F-actin stress fibers and enhances cancer cell survival, invasiveness, metastasis, and drug resistance. In gastric cancer, CEACAM6 correlates with advanced tumor stage, TNM classification, and lymph node metastasis. Hypoxia, which is prevalent in epithelial tumors stabilises HIF1, driving hypoxia-responsive gene expression. Hypoxia also recruits macrophages, initially M1-like, which polarize to M2-like under hypoxia, fostering immunosuppression, angiogenesis, and aggressive tumor growth. Although deferoxamine-mediated chemically-induced hypoxia upregulates CEACAM6 in colon cancer, existing research has not examined the effect of hypoxia-mediated CEACAM6 modulation on disease progression in a hypoxic gastric tumor microenvironment.

Here, it is shown that hypoxia upregulates cellular CEACAM6 through the action of HIF1, which leads to enhanced migration and proliferation of gastric epithelial cell (GEC)s and heightened reactive oxygen species (ROS) production. ROS production is mediated by overexpression of NOX4 enzyme. Hypoxia and hypoxia-reoxygenation facilitates enhanced binding of *Helicobacter pylori* to GECs through CEACAM6. HopQ-CEACAM6 interaction aids increased CagA entry into the cell which leads to a fusiform transformation in GECs leading to enhanced hummingbird phenotype appearance. Similarly, immunofluorescence probing confirmed elevated levels of HIF1α, CEACAM6 and NOX4 in gastritis and metastatic cancer tissue samples. Also, CEACAM6 cell secretome influences macrophage polarisation through paracrine signalling. Hypoxia-treated CEACAM6 cell extracts downregulate M1 marker and ROS generation in peripheral blood mononuclear cell-derived macrophages while upregulating Arginase1, a functional marker associated with the pro-tumorigenic M2 phenotype. Correspondingly, metastatic biopsy tissue specimens also show higher Arginase1

+ve M2 macrophage infiltration and a reduced number of iNOS +ve M1 macrophages when compared to paired control tissue. In summary, this thesis establishes the importance of CEACAM6 in oncogenic transformations in the hypoxic gastric cancer milieu and presents it as an interesting molecule with potential as a therapeutic drug target.

4.3.3 *Unlocking the therapeutic potential of EEF1A2 in breast cancer: Unravelling molecular mechanisms, crosstalk, and small molecule inhibitors for effective treatment strategies*

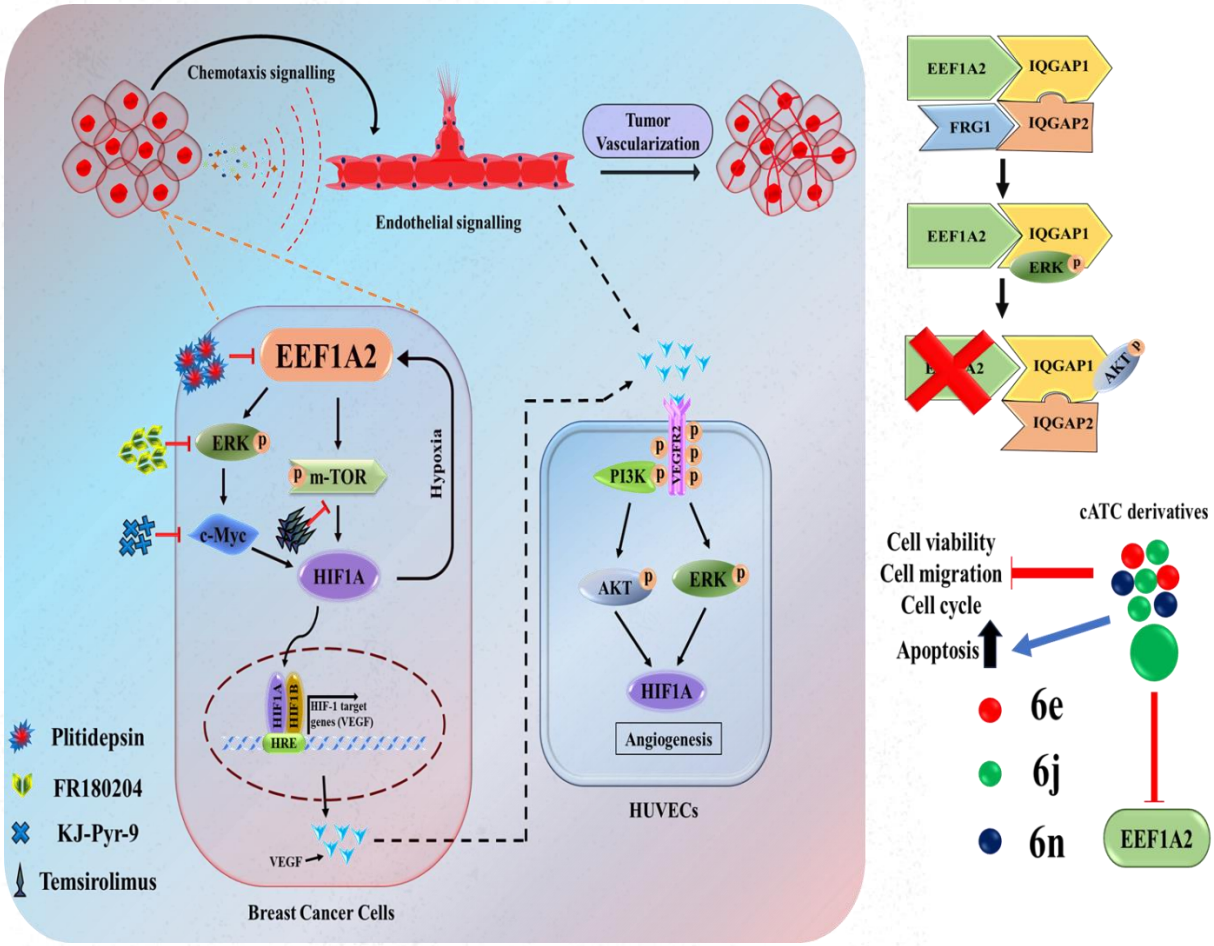

Overall summary of EEF1A2 as a proangiogenic marker. The feedback loop between EEF1A2 and HIF1A. EEF1A2 is a modulator of IQGAP1, which triggers the activation of ERK. cATC derivative 6j inhibits EEF1A2 expression in cancer cells

Breast cancer is the second most commonly diagnosed cancer and 4th leading cause of death worldwide. It is a heterogeneous disease encompassing diverse molecular subtypes and associated with distinct clinical outcomes. However, despite notable progress in diagnosis and therapeutic interventions, the prognosis for individuals with advanced-stage breast cancer remains desolate. Chemotherapeutic treatment primarily targets central oncogenic or angiogenic signaling pathways. Therefore, treatment failure in breast cancer patients has been observed due to the bi-directional cross-talk between other pathways like ER and HER2. The involvement of scaffolding proteins also led to the activation of alternative escape survival pathways like ER and ERK1/2 signaling, eventually resulting in treatment resistance. Hence, it is crucial to identify target molecules that regulate multiple hallmarks of cancer and act as

upstream regulators of various oncogenic signaling pathways. This approach could pave the way for more effective therapies with a reduced possibility of resistance development.

In this context, a potential candidate is Eukaryotic elongation factor 1 alpha 2 (EEF1A2), one of the two isoforms of EEF1A. It is a translation elongation factor protein expressed in specialized tissues. This thesis deciphered the in-depth role of EEF1A2 in regulating tumor angiogenesis. Initially, we have validated the EEF1A2-mediated angiogenesis. Upon inhibiting EEF1A2 with its known inhibitor, Plitidepsin, we observed a decrease in an EEF1A2-mediated tubulogenesis, confirming its angiogenic potential. This thesis explores the role of Eukaryotic elongation factor 1 alpha 2 (EEF1A2) in breast cancer, with a focus on tumor angiogenesis and its potential as a therapeutic target. EEF1A2, a translation elongation factor, is primarily expressed in specific tissues and implicated in cancer progression. Here, we confirm EEF1A2's role in promoting angiogenesis and explore the underlying mechanisms.

Using Plitidepsin, an inhibitor of EEF1A2, we observed a reduction in tubulogenesis, highlighting EEF1A2's angiogenic potential. Mechanistically, EEF1A2 upregulates VEGF in breast cancer cells, which subsequently activates VEGFR2 in endothelial cells, triggering PI3K-AKT and ERK signaling pathways. Further analysis revealed that EEF1A2 transcriptionally regulates HIF1A via the ERK-Myc and mTOR pathways in MDA-MB-231 and MCF7 cell lines, respectively. HIF1A, in turn, upregulates VEGF, enhancing angiogenesis. Notably, EEF1A2 also influences VEGF translation in a cell-line-specific manner, increasing it in MDA-MB-231 cells but not in MCF7 cells. We also identified EEF1A2 as a hypoxia-regulated gene, with its levels increasing under hypoxia in a HIF1A-dependent manner. A novel feedback loop between EEF1A2 and HIF1A was discovered, potentially contributing to drug resistance. Patient sample analyses confirmed that higher EEF1A2 levels correlate with increased microvessel density, irrespective of breast cancer subtype. EEF1A2 also acts as a modulator of signaling crosstalk. Mass spectrometry data revealed interactions between EEF1A2, the tumor suppressor FRG1, and scaffolding proteins IQGAP1 and IQGAP2. Our co-immunoprecipitation assays confirmed the direct interactions between these proteins, showing that EEF1A2 depletion enhances IQGAP1-IQGAP2 interactions, activating AKT signaling. Re-expression of EEF1A2 restored ERK binding to IQGAP1 and reactivated ERK signaling, positioning EEF1A2 as a regulator of ERK-AKT signaling balance.

In the context of drug resistance, we screened small molecules targeting EEF1A2. Tropolone derivatives, particularly cATC (6e, 6j, 6n), were found to reduce cancer cell viability, inhibit migration, and promote apoptosis by upregulating P53 and P38 signaling. These derivatives also inhibited EMT markers and increased E-cadherin expression, indicating their potential to suppress metastasis. Notably, 6j reduced both EEF1A2 and HIF1A levels, validating its anti-cancer efficacy in vitro and in vivo.

In conclusion, EEF1A2 plays a critical role in breast cancer angiogenesis and drug resistance by modulating VEGF and HIF1A expression and influencing ERK-AKT signaling pathways. Our findings highlight EEF1A2 as a promising therapeutic target, and the identified cATC derivatives, particularly 6j, offer potential as effective anti-cancer agents. These insights could pave the way for developing novel treatments for breast cancer, regardless of molecular subtype.

4.4 Raja Ramanna Centre for Advanced Technology, Indore

4.4.1 *Molecular characterization of bacterial insecticidal proteins*

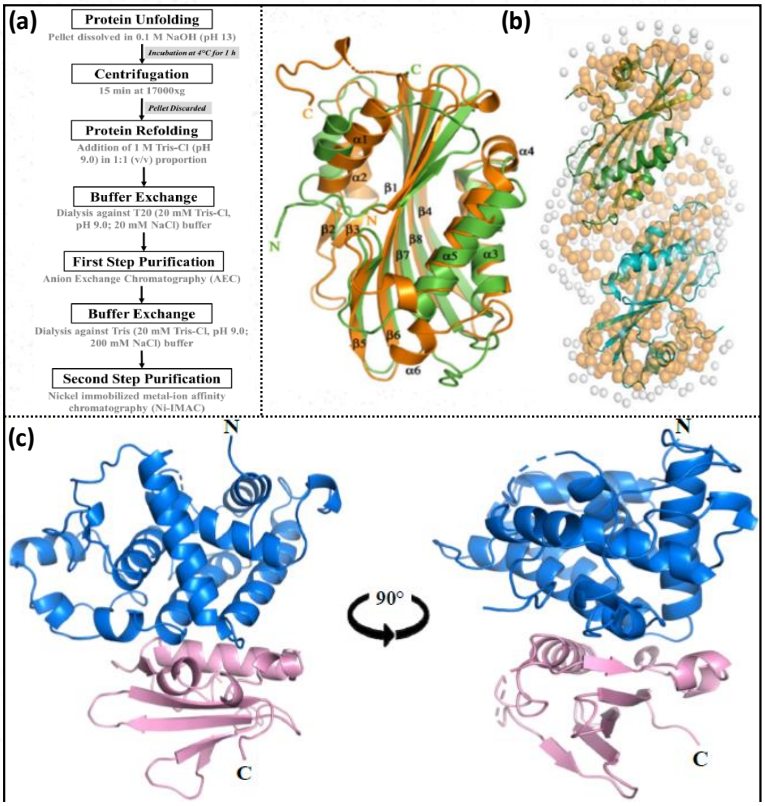

(a) Schematic representation illustrating the novel in-vitro refolding method used for recombinant Cry11Aa purification. (b) Structural superimposition of P20 model (Green) with Cyt1Aa [Left] and Dummy chain model from experimental SAXS data (spheres) superimposed with dimeric P20 model (ribbon) [Right]. (c) The structure of Txp40 is composed of two domains. The N-terminal domain is colored in blue, while the C-terminal domain is shown in pink

Insect pests pose a major threat to agriculture, livestock, and public health. This research addresses the pressing need for eco-friendly biopesticides, focusing on *Bacillus thuringiensis (Bt)* and *Xenorhabdus nematophila* as sources of effective insecticidal proteins. These studies aim to overcome insect resistance and enhance the efficacy of biopesticides. In this study, genes encoding six key insecticidal proteins and accessory proteins were identified in local isolate *Bt* subspecies *israelensis* (ISPC-12) and deposited in the NCBI GenBank. Codon-optimized Txp40 gene from *X. nematophila* was synthesized for recombinant studies. Cry11Aa, P20, and Txp40 were purified using chromatographic and/or refolding methods. A novel protocol for Cry11Aa purification was designed and optimized. Bioassays demonstrated insecticidal activities of the purified proteins, with lethal concentrations determined for target insects. Advanced techniques such as size-exclusion chromatography (SEC), dynamic light scattering (DLS), and circular dichroism (CD) spectroscopy elucidated the oligomeric state and secondary structure of the proteins, respectively. Stability assessments via variable temperature measurements (VTM) and thermal denaturation provided insights into the robustness of these proteins. Txp40's 3D structure was resolved at 2.08 Å, unveiling a unique two-domain toxin with a novel "Indus" domain. P20 was modeled and identified as a non-toxic member of the

cytolytic toxin family through in-silico studies and SAXS analysis. Txp40 was identified as a prokaryotic toxin-antitoxin (TA) system, offering avenues for future research. Proteolysis studies and molecular dynamics simulations shed light on Cry11Aa activation and structural features essential for its insecticidal function**.** Overall, this work significantly advances our understanding of insecticidal proteins and proposes novel strategies to mitigate resistance. It lays a foundation for the development of next-generation biopesticides with enhanced efficacy and stability.

4.5 Saha Institute of Nuclear Physics, Kolkata

4.5.1 *Remodelling of extracellular matrix by chromatin regulator UBR7 in triple-negative breast cancer: Insight into chemoresistance*

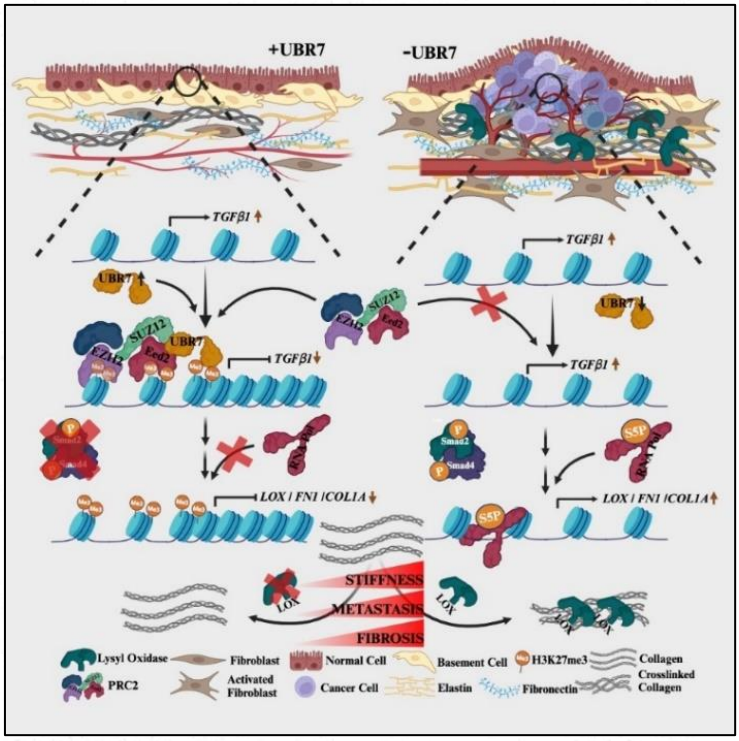

UBR7 in concert with EZH2 inhibits TGF-β signalling pathway, thereby impacts on ECM remodelling by reducing ECM stiffness and metastasis in triple-negative breast cancer

Breast cancer continues to pose a formidable challenge as the second leading cause of cancer-related mortality among women, demanding the pressing need for effective interventions. Remodelling of extracellular matrix causes breast cancer malignancy. Understanding the mechanisms by which tumor cells reshape the ECM is pivotal in identifying targets for therapy. Increasing evidence underscores a correlation between epigenetic modifications and the progression of breast cancer. Notably, the decrease in the facultative heterochromatin mark H3K27me3 can be correlated with large tumor volumes. Additionally, a propensity for reduced H3K27me3 enrichment is observed in estrogen-negative subtypes and cases with positive lymph nodes. A multi-omic profiling study has shown the depletion of H3K27me3 and enrichment of H3K27ac signals in super-enhancers of oncogenes in TNBC, leading to their hyper-activation. These reversible transitions between epigenetic states eventually support tumors in developing resistance to escape therapeutic pressure. Thus, the regulation of epigenetic transitions on various oncogenic pathway genes, including a dynamic switch between H3K27me3 and H3K27ac needs further investigation.

In the present study, we investigate the role of UBR7 in counteracting ECM stiffness and fibrosis in TNBC by targeting the TGF-β/SMAD axis. UBR7 is instrumental in recruiting the canonical polycomb repressor complex PRC2 thereby augmenting the H3K27me3 mark at the promoter leading to the suppression of *TGFB1* and its downstream target genes of the ECM pathway, specifically in TNBC. Besides regulating the transcription mechanistically, UBR7 is intricately involved in the deposition and modifications of ECM. In this context, we further reveal that UBR7 is a key determinant of LOX activity and total collagen content from tumorspheres, in vivo mice model and TNBC patient tissues. Thus, our study provides an insight into the role of UBR7 in epigenetic regulation of chromatin architecture which has significant implications in effectively curbing matrix stiffness to reinstate an anti-metastatic phenotype. In this perspective, we highlight the significant potential role of UBR7 to alleviate the challenges of chemo-resistance, offering promising prospects for therapeutic efficacy.

4.5.2 *Reprogramming of epigenetic landscape of chromatin by E3 ubiquitin ligase in oncogenesis and infection*

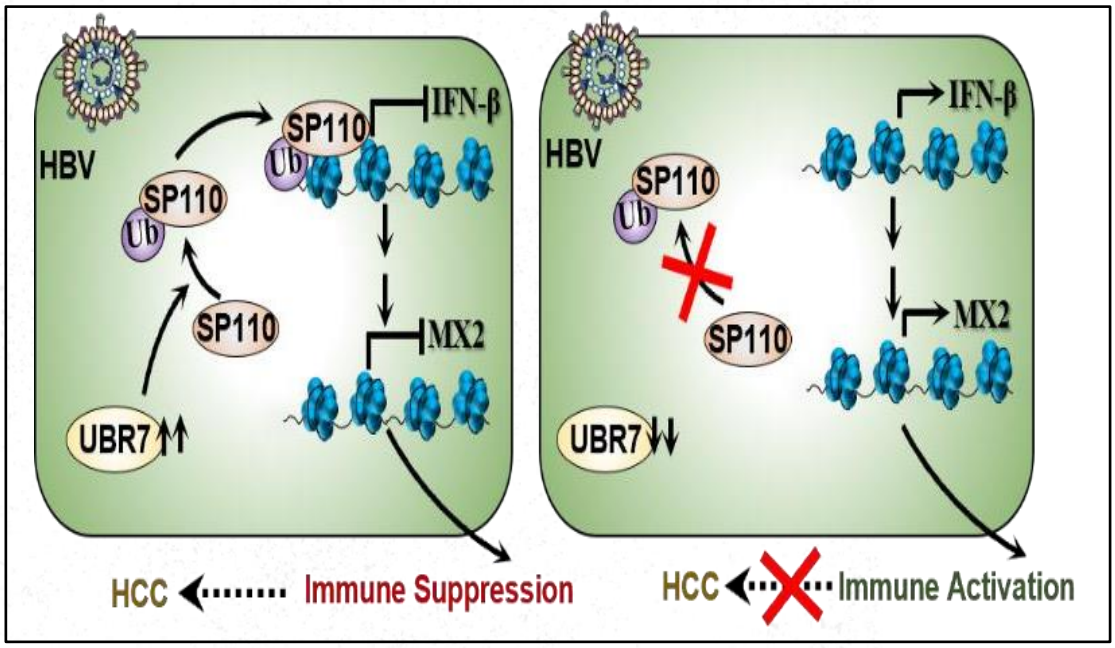

UBR7 Ubiquitinates and stabilizes Sp110 which Promotes transcriptional suppression of Type1 IFNβ response genes in HBV

Our study reveals the pivotal and multifaceted role of UBR7, part of the UBR box-containing protein family (UBR1 to UBR7), which is involved in the N-end rule pathway. This pathway suggests that the lifespan and degradation of a protein are influenced by its N-terminal residue. UBR7, specifically, has garnered interest due to its unique E3 ubiquitin ligase activity facilitated by its PHD finger, which is characterized by a distinctive non-canonical Cys4-His2-Cys2 motif. This differentiates UBR7 from other proteins containing PHD and RING finger domains, marking it as a novel and significant player in cancer research, especially in chromatin regulation and tumor suppression.

We demonstrate that UBR7 interacts with the epigenetic mark H3K27me3 via its UBR Box

domain, a feature unique to UBR7 among the UBR protein family. This interaction contributes to transcriptional suppression and highlights UBR7's role in regulating gene expression. Additionally, UBR7 associates with the Polycomb Repressive Complex 2 (PRC2), which is crucial for depositing the H3K27me3 mark—a repressive histone modification. Our experiments revealed that loss of UBR7 results in a significant reduction in H3K27me3 levels, indicating UBR7's critical role in sustaining PRC2 function and maintaining chromatin in a repressive state.

In the context of triple-negative breast cancer (TNBC), we found that UBR7 plays a tumor suppressor role by repressing the expression of VEGFA, a key factor involved in angiogenesis. This repression is mediated through the UBR Box domain, with specific residues (Y59, Y80, F89) identified as essential for UBR7's ability to suppress VEGFA. Mutations in these residues (Y59A, Y80AA, F89A) disrupt UBR7's function, leading to dysregulation of VEGFA expression and highlighting the significance of UBR7's UBR Box domain in tumor suppression. Beyond its role in chromatin regulation and cancer, we identified Sp110, a member of the speckled family of proteins, as a critical substrate of UBR7's E3 ubiquitin ligase activity. Sp110, typically found in promyelocytic leukemia nuclear bodies (PML-NBs), is SUMOylated under normal conditions. During HBV infection, however, Sp110 undergoes deSUMOylation and exits the PML body, making it susceptible to ubiquitination by UBR7. Our study demonstrates that UBR7 ubiquitinates Sp110 at key residues within its SAND domain, leading to the downregulation of genes involved in the type I interferon (IFN) response pathway. Here it is shown that when UBR7 is present, it ubiquitinates Sp110, which in turn suppresses the interferon-β (IFN-β) response, allowing the virus to evade the host immune system.

This newly identified role of UBR7 in non-histone protein ubiquitination, particularly its regulation of Sp110 during HBV infection, sheds light on how UBR7 contributes to viral persistence. By suppressing the IFN-β response, UBR7 aids HBV in evading immune detection and supports the development of hepatocellular carcinoma (HCC). These findings offer important insights into UBR7's dual function in both cancer and viral pathogenesis, with potential therapeutic implications for targeting UBR7.

4.5.3 *Architectural roles of IHF and Tfam in genome organization: A single-molecule spectroscopic approach to study Holliday Junction Dynamics and mitochondrial DNA bending*

Integration Host Factor (IHF) in *Escherichia coli* is a nucleoid-associated protein crucial for DNA packaging, viral integration, and recombination. IHF binds double-stranded DNA with a 13-bp consensus sequence, inducing a 160° bend. While Wild-type IHF (WtIHF) primarily facilitates foreign DNA integration, its engineered variant, Single-chain IHF (ScIHF), is tailored for biotechnological applications. This study investigates their interactions with Holliday junctions (HJs), key intermediates in DNA repair and recombination. Microscale thermophoresis revealed strong affinity of both variants for HJs containing H' and H1 sequences. Circular dichroism and single-molecule FRET experiments demonstrated IHF-induced stabilization of the open conformation of HJs, enhancing their dynamicity. These findings highlight IHF's role in modulating HJ conformation, emphasizing its potential in understanding DNA repair and engineering applications.

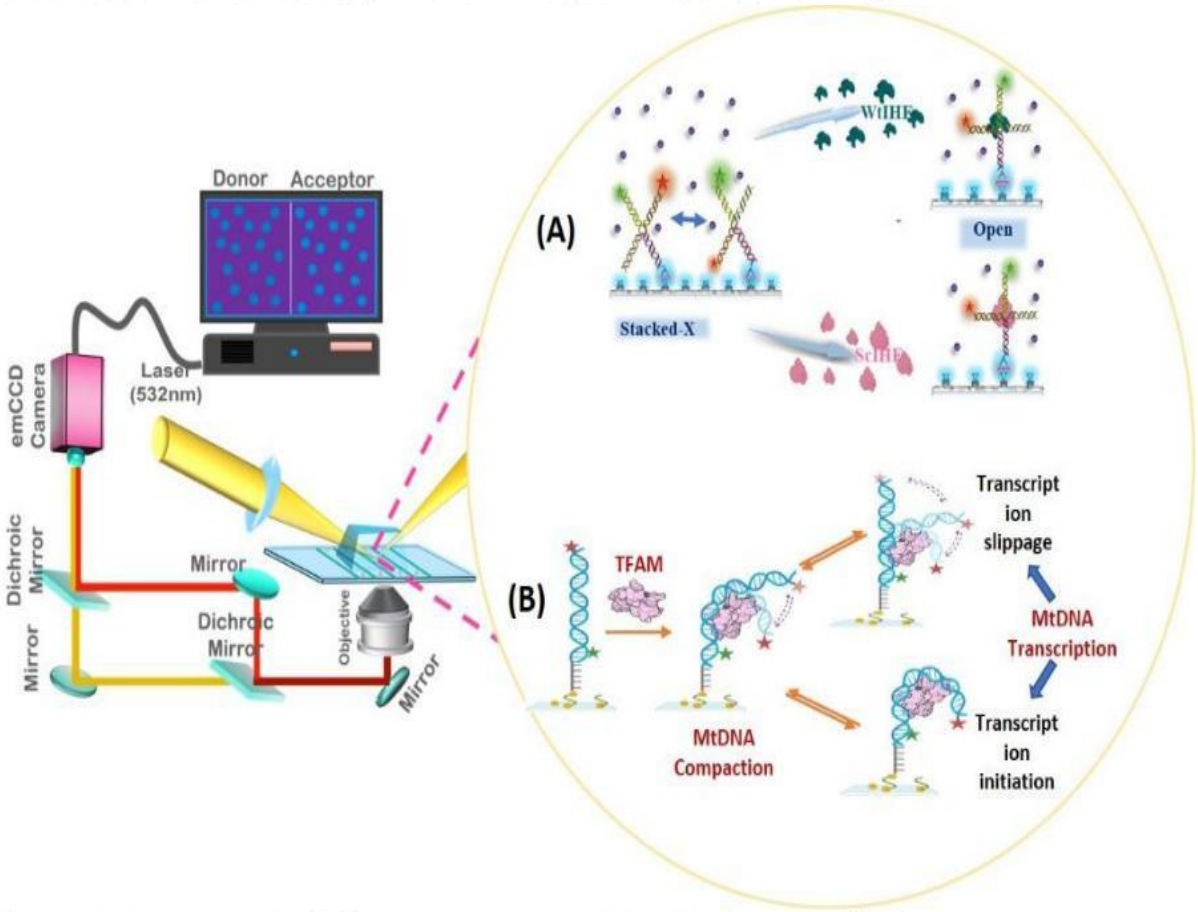

(A) Upon binding, IHF stabilizes the junction in the open conformation and shifts the population distribution to that state, thereby possibly facilitating the process of branch migration. (B) TFAM-mediated dual role in DNA dynamics brings about mitochondrial genome compaction and transcriptional regulation via distinct bending states

Similar to IHF's role in bending bacterial DNA, Mitochondrial transcription factor A (TFAM) induces significant DNA bending and compaction in mitochondria, which is critical for packaging the circular mitochondrial DNA into nucleoids. TFAM plays a dual role in transcription regulation and genome compaction through DNA bending.

We examined TFAM's binding to specific promoter sequences (LSP, HSP) and non-specific (NS) DNA using circular dichroism and single-molecule FRET. LSP DNA exhibited low FRET efficiency in its linear form but transitioned to a fully bent state upon TFAM binding, with occasional partial bending, supporting its role in transcription initiation. In contrast, HSP binding revealed transitions between linear and partially bent states, indicating TFAM does not fully stabilize bending, and suggesting limited facilitation of transcription initiation. With NS DNA, TFAM stabilized the fully bent conformation while maintaining flexibility, enabling transitions to partial bending. These findings demonstrate TFAM's sequence-dependent modulation of DNA structure, balancing transcription regulation and genome packaging.

4.6 Tata Memorial Centre, Mumbai

4.6.1 *Structural and functional characterization of different domains of BRCA1 and its interacting proteins*

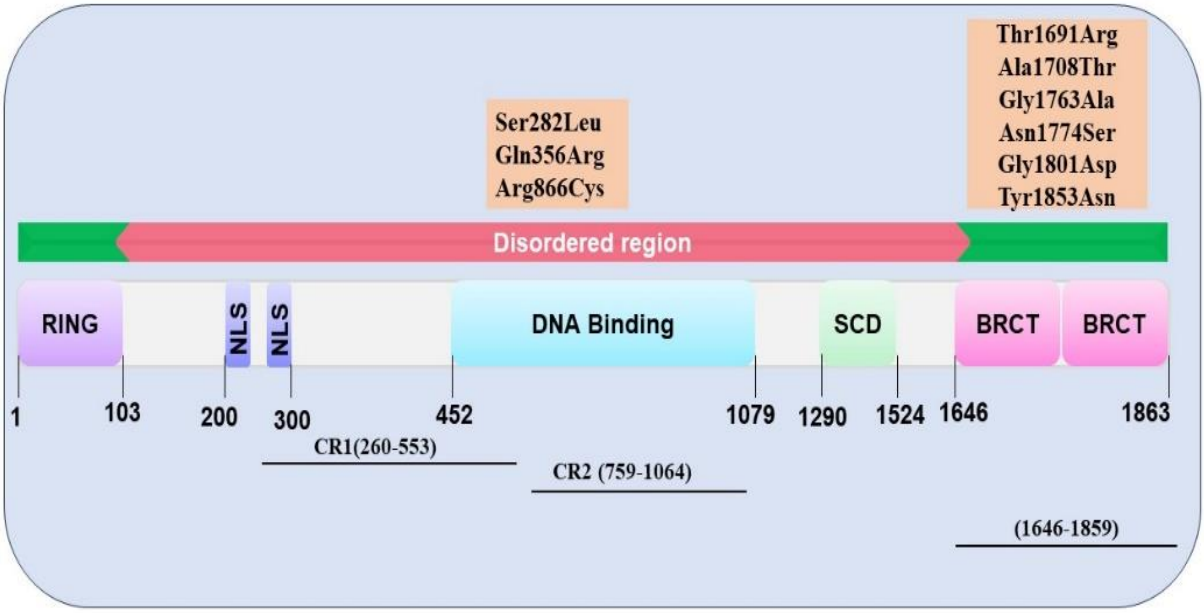

Domain organization of BRCA1 and the mutations studied present in the different functional domains of BRCA1

This study investigated the structural and functional properties of BRCA1 protein and reported variants, specifically focusing on intrinsically disordered regions (IDPRs). The research highlighted the importance of IDPs in cellular function and how mutations altered the folding pattern and protein-protein interactions. The salient key findings are:

BRCA1 Wild-type and Ser282Leu variant:

- Wild-type protein exhibits a partially disordered structure.
- Ser282Leu variant shows increased flexibility and potential amyloidogenic tendencies.
- This variant might contribute to breast cancer predisposition

BRCA1 Wild-type and Gln356Arg variant:

- Variant displays a propensity to form amyloid-like fibrils.
- Case-control study suggests a potential role in breast cancer, particularly in homozygous states.
- Understanding its functional effects is crucial for elucidating its impact on disease.

BRCA1 Wild-type and Arg866Cys variant:

- Located in the essential DNA binding region (EDBR).
- Variant exhibits altered folding patterns and reduced DNA binding affinity.
- This potentially hinders its role in DNA repair mechanisms.

BRCA1 BRCT repeats and phosphopeptide binding:

- Certain mutations alter the binding efficiency of phosphopeptides.
- This highlights the functional consequences of mutations even beyond canonical binding sites.

Overall, this research provides valuable insights into how BRCA1 mutations influence protein structure, and function, and potentially contribute to breast cancer pathogenicity. Understanding these mechanisms paves the way for future development of targeted therapies for BRCA1-related diseases.

4.6.2 *Discovering the molecular mechanisms governing cellular senescence in glioblastoma*

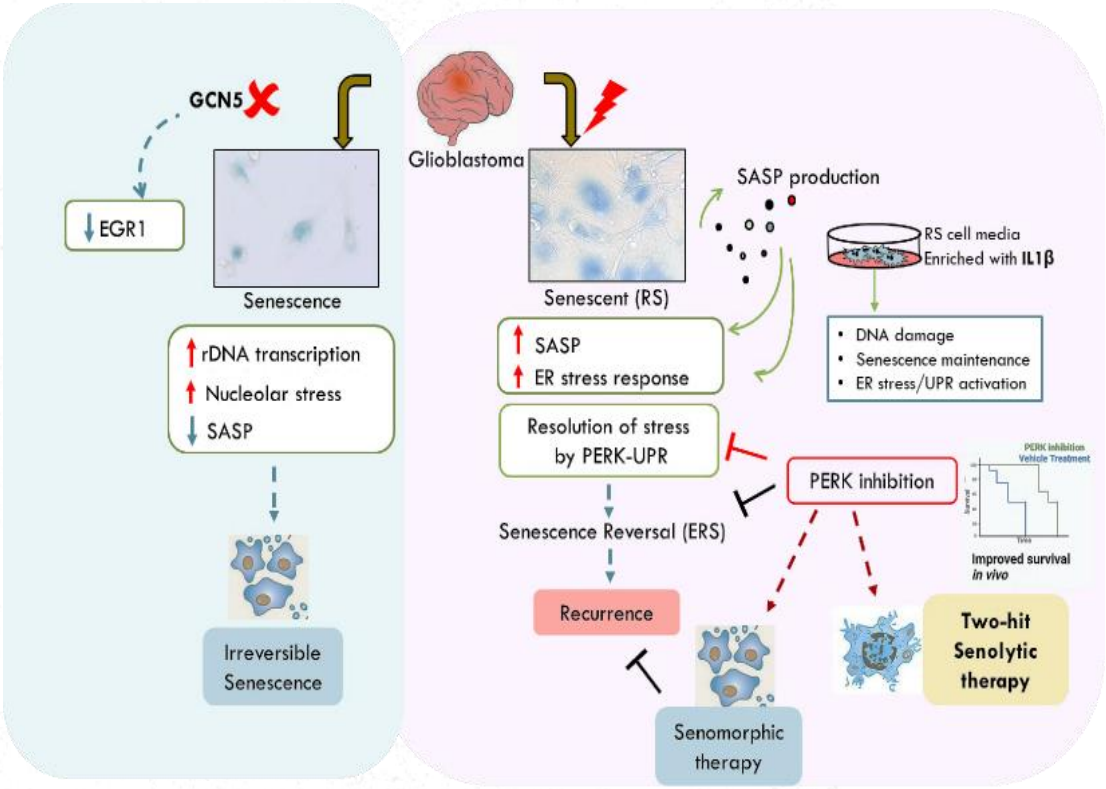

Mechanisms of cellular senescence induction as a senotherapy approach for glioblastoma

Glioblastoma is a fatal disease with 5-year overall survival of 5%. Its treatment is an arduous task due to its location, heterogeneity, resistance to therapy and high frequency of recurrence. To understand the mechanism behind this recurrence, we established an *in vitro* and *in vivo* radiation therapy resistance model where we observed that, irradiation leads to Therapy Induced Senescence (TIS) in glioblastoma cell lines and treatment naïve patient-derived primary cultures. Unfortunately, this TIS in glioblastoma is reversible and the Residual Senescent (RS) cells revert back to proliferation, causing recurrence. Using RNA sequencing of 40 GBM samples collected post radiation *in vitro*, we observed a significant co-expression

of Senescence phenotype with SASP (Senescence associated secretary phenotype) and ER stress/UPR signaling pathways. Following with biochemical assays, *ex vivo* cell survival, proliferation, apoptosis assays, immunoblotting, qRT-PCR, and chromatin immunoprecipitation, here, we identify that TIS reversal is dependent on the activation of Unfolded Protein Response (UPR) pathway as a consequence of inflated ER stress. Mechanistically, transcription factor CHOP non-canonically binds to the promoters of anti-apoptosis and senescence associated genes, likely steering the senescent cells towards survival rather than apoptosis. PERK-ATF4-CHOP activated UPR acts as a switch for reversal of TIS in GBM residual senescent cells and its Inhibition in combination with radiation leads to senomorphic therapy devoid of SASP thereby eliminating their unwelcome pro-inflammatory consequences. Remarkably, perturbation of PERK in the vulnerable senescent phase shows a selective senolytic action in culture as well *in vivo*, preventing recurrence and improving survival. Here, we provide evidence for a novel senolytic drug, PERK inhibitor GSK2606414 with the ability to cross blood brain barrier as an exceptional senotherapeutic option for combating residual disease. Independently,

we have observed that sole genetic depletion of a histone acetyltransferase GCN5 leads to an irreversible senescence phenotype in glioblastoma devoid of SASP response. RNA sequencing and transcriptome analysis of GCN5 proficient and deficient cells revealed a global protein coding gene downregulation, non-coding RNA upregulation, increased rDNA transcription inside nucleoli, larger but fewer nucleoli per cell signifying nucleolar stress. In this study, we identify GCN5 as novel upstream regulator of nucleolar stress, non-coding RNA synthesis and senescence in GBM. The irreversible nature of this senescence and lack of deleterious SASP response makes it an excellent monotherapeutic candidate for senescence therapy in primary glioblastoma.

4.6.3 *Investigating role of MAPK-ERK & PIK3CA-AKT signalling on autophagic flux in Ovarian Cancer Stem Cells*

This thesis uncovers a novel molecular mechanism controlling platinum sensitivity in ovarian cancer stem cells through autophagy regulation. The research establishes that ovarian cancer stem cells maintain high basal autophagy regulated by a balance between ERK (promoting) and AKT (suppressing) signaling pathways. When autophagy exceeds a critical threshold, it triggers selective degradation of the stemness factor ID1, liberating the transcription factor TCF12 to activate SLC31A1 expression—the major cisplatin influx transporter.

This autophagy-ID1-TCF12-SLC31A1 axis functions as a molecular switch transforming chemo-resistant cancer stem cells into chemo-sensitive cells. Additionally, the thesis reveals distinct autophagy patterns across ovarian cancer subtypes, with clear cell carcinoma exhibiting uniquely elevated p62 expression. These findings provide a mechanistic foundation for therapeutic strategies targeting autophagy to overcome platinum resistance and improve patient outcomes.

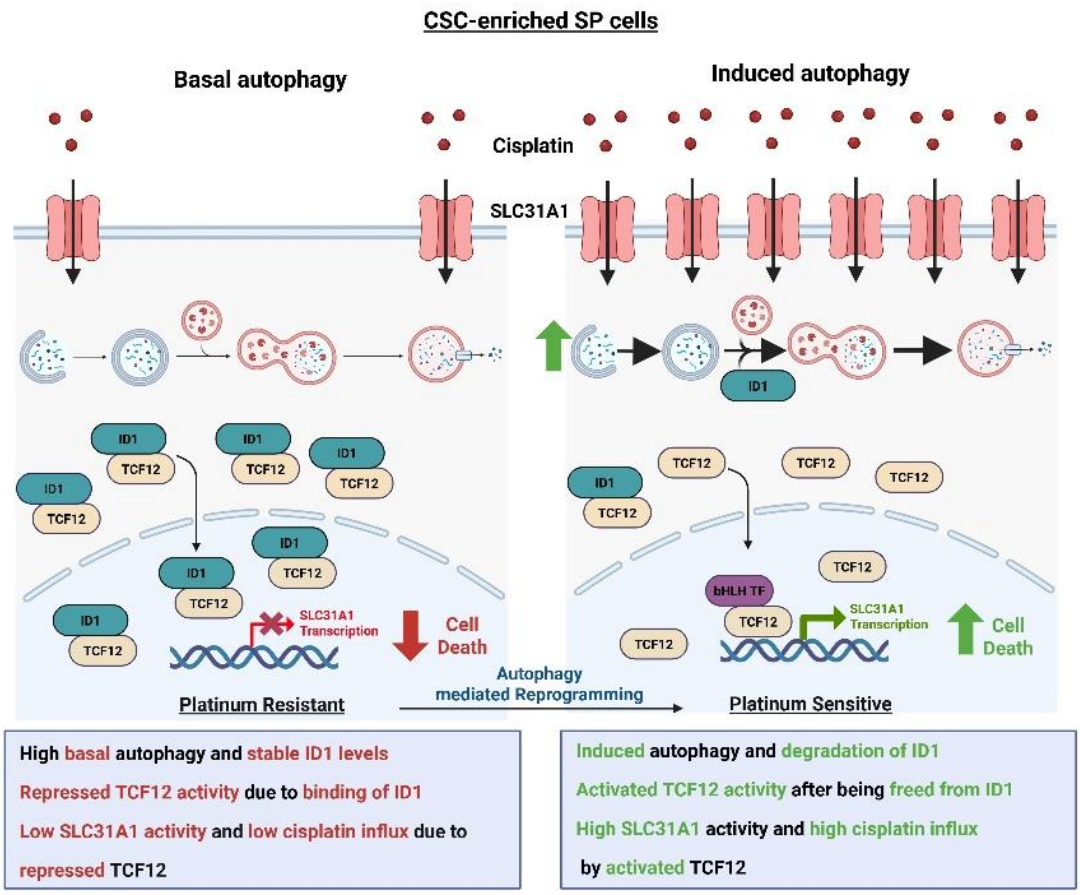

Autophagy regulation of platinum sensitivity in ovarian cancer stem cells. This figure shows how autophagy levels control platinum sensitivity in cancer stem cells. Left panel: Under basal autophagy, high ID1 levels sequester TCF12, preventing SLC31A1 cisplatin transporter expression and resulting in platinum resistance. Right panel: Induced autophagy degrades ID1, releasing TCF12 to activate SLC31A1 transcription, enhancing cisplatin uptake and cellular sensitivity to platinum therapy. This autophagy-ID1-TCF12-SLC31A1 axis represents a molecular switch converting resistant cancer stem cells to a chemo-sensitive state

4.6.4 Understanding the role of Wnt signaling in epidermal homeostasis and stem cell regulation

Epidermis is endowed with a remarkable capacity to self-renew due to the presence of the stem cells (SCs) in various appendages such as hair follicles (HFs), sebaceous glands (SGs) and interfollicular epidermis (IFE). The HF, which contains multi-potent SCs, is an excellent model to study mechanisms regulating adult SCs quiescence and activation. Disabled 2 (Dab2), an adaptor protein, is up regulated in the hair follicle stem cells (HFSCs); however, its role in any tissue stem cells has not been studied. In the present study, we have reported that Dab2 conditional knockout (Dab2-cKO) mice exhibit a delay in the HF cycle due to perturbed activation of HFSCs. Further, Dab2-cKO mice shows a reduction in the number of HFSCs and reduced colony forming ability of HFSCs. Dab2-cKO mice shows extended quiescence of HFSCs concomitant with an increased expression of Nfatc1. Dab2-cKO mice shows a decreased expression of anti-aging genes

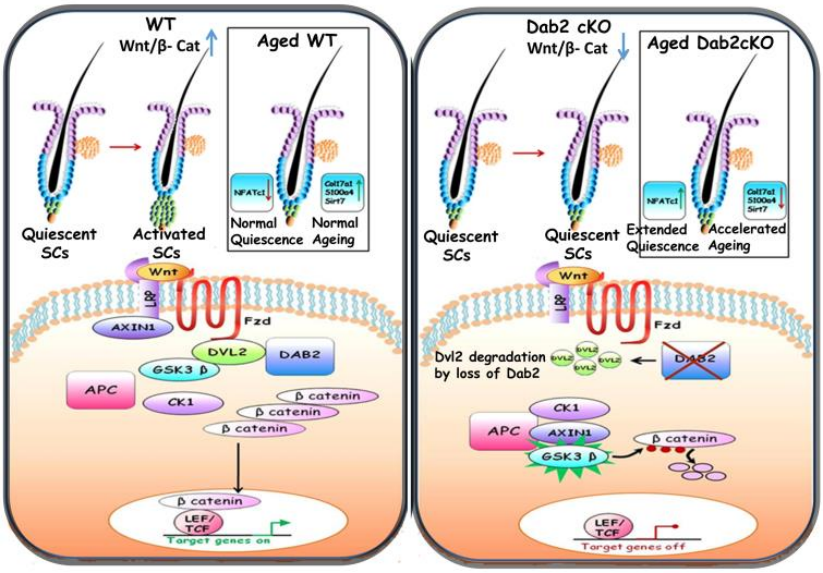

Schematic diagram showing the role of Dab2 in Wnt signaling mediated regulation of HFSCs

such as Col17a1, decorin, Sirt2 and Sirt7. Aged Dab2-cKO mice do not show full hair coat recovery thereby suggesting an accelerated aging process. Moreover, Dab2 loss also results in delayed papilloma initiation and reduced papilloma burden in chemical induced skin carcinogenesis model.

The detailed analysis of the molecular mechanisms involved in Dab2 mediated regulation of HFSCs reveals that loss of Dab2 results in the reduced expression of Dvl2, the upstream mediator of Wnt signaling. The present study proposes a model in which Dab2 plays an important role in the activation of canonical Wnt signaling. In the presence of Dab2, Dvl2 is stabilized, providing a platform for the formation of the Wnt signalosomes, which include scaffolding proteins (Axin1) and kinases (GSK3β and CK1γ). Loss of Dab2 results in the degradation of Dvl2. As a result, the destruction complex is no longer recruited to the receptor which leads to the stabilization of the destruction complex in the cytoplasm followed by degradation of β-Catenin and inactivation of the canonical Wnt signaling. In addition, Dab2 may also regulate the destruction complex directly to control the activation of Wnt signaling in HFSCs (Figure 1). Overall, we unveil for the first time, the role of Dab2 that regulate activation and self-renewal of HFSCs.

MATHEMATICAL SCIENCES

5. Mathematical Sciences

5.1 Harish-Chandra Research Institute

5.1.1 *Invariants of moduli spaces and (Semi-) Tannakian categories of twisted quiver bundles*

This thesis addresses two important areas of algebraic geometry: the computation of invariants for moduli spaces and the study of (semi-) Tannakian subcategories of the category of quiver representations.

In the first part of the thesis, the author focuses on the moduli space of holomorphic $L\lambda$-connections over compact Riemann surfaces of genus $g \geq 3$, where $\lambda \in \mathbb{C}$ and L is a holomorphic Lie algebroid of rank 1. The thesis computes the Picard group of the moduli space of these $L\lambda$-connections, achieving this by constructing an explicit smooth compactification of the moduli space for stable vector bundles, where the complement forms a smooth divisor. In the special case where $\lambda=1$, the work focuses on the Lie algebroid de Rham moduli space of L-connections, and the thesis computes the corresponding Chow group.

The second part of the thesis shifts focus to the study of representations of loop quivers and the associated Tannakian category structures. The author investigates twisted representations of loop quivers with two distinct tensor structures: Kronecker tensor and Simpson tensor. By examining the rigidity properties of these categories, the thesis provides examples of both (semi-) Tannakian subcategories within the category of loop quiver representations. A key contribution is the introduction of the concept of essentially finite loop quiver bundles, which are studied in the context of Tannakian category structures. These structures are applied to the study of equivariant bundles and Hitchin pairs.

Finally, the thesis studies the category of representations of flat loop quiver diagrams with permissible relations, particularly focusing on the Kronecker tensor structure. One of the main results is the realization that Γ-linearizations of vector bundles, as well as Γ-equivariant objects on a scheme with a finite group action, can be viewed as representations of loop quiver diagrams with localized relations, providing a new approach to the neutral Tannakian category structures on certain equivariant vector bundles. Furthermore, this thesis introduces the concept of H-nflat twisted loop quiver bundles and establishes the Tannakian category structures of these objects.

5.1.2 *Some problems in quadratic forms over number fields and related topics*

This thesis deals with problems on quadratic forms over number fields and some other problems associating algebraic numbers with certain combinatorial objects.

First, we have tried to find a lower bound of a positive integer ‘m’ such that all algebraic integers divisible by ‘m’ of a complex number field K can be written as sums of five integral squares.

In the second problem, for any given positive integer ‘m’ we have constructed certain totally positive algebraic integers ‘a’ of a real bi-quadratic field K and have obtained some necessary conditions for which ‘ma’ cannot be represented as sum of integral squares. We have showed this for integers lie in quadratic subfields of K and for integers which are in K but not in any quadratic subfield of K. We have provided examples in tabular form for each case to

corroborate the results.

In the third part, we have established some relation between class group and universal quadratic forms for totally real number fields of degree four. In order to find some examples, we have also obtained a relation between the norm of fundamental units and the parity of the class number of quadratic subfields of a real bi-quadratic field.

Finally, in the last part, for some specific type of matrix A of order n and for any positive integer k we have found a general lower bound for the sum of 2^k-th power of eigenvalues of A, which depends on n as well as some other variables. And in particular, we have obtained that the sums of squares of eigenvalues of A is atmost 5n-6. As a strong outcome of this result we have showed that the smallest limit point of absolute trace-2 measure of eigenvalues of all such matrices is 6. We have also obtained a lower bound of smallest limit point of absolute trace 2^k measure of A for any positive integer k > 1 and for the same set of matrices. Furthermore, we have exhibited that the famous results of Smyth on density of absolute trace measure and absolute trace-2 measure of totally positive integers are also true for the set of symmetric integer connected positive definite matrices.

5.2 Institute of Mathematical Sciences

5.2.1 *Demazure crystal structure for flagged skew tableaux and flagged reverse plane partitions*

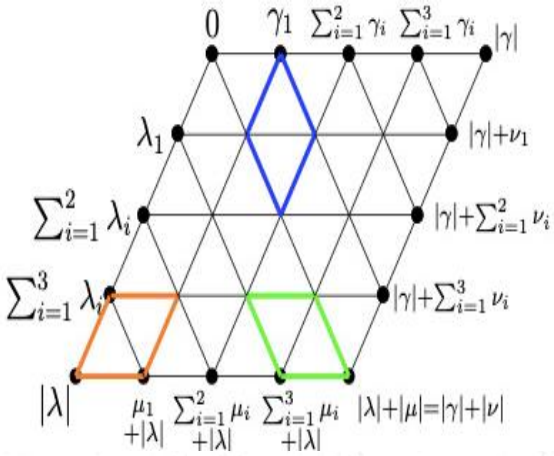

The boundary labels of skew hives in $SHive_{\mathbb{Z}}(\lambda,\mu,\gamma,\nu)$ with three kinds of small rhombi (highlighted in three different colors)

This thesis is divided into two parts. The first part includes the Demazure crystal structure for flagged reverse plane partitions and flagged skew semi-standard tableaux. The second part addresses the saturation theorem of the flagged skew Littlewood-Richardson coefficients.

Demazure crystals (which are indexed by partitions and permutations) are certain subsets of the set of all semi-standard tableaux whose shapes are of that partition. In this thesis, every connected component of the crystal graph of the set of all flagged reverse plane partitions is shown to be a Demazure crystal (upto isomorphism). As an important corollary, it provides an explicit decomposition of the flagged dual stable Grothendieck polynomial into a non-negative

integral linear combination of key polynomials. The Demazure crystal structure for flagged reverse plane partitions extends the Demazure crystal structure for flagged skew semi-standard tableaux. The earlier result lifts the key-positivity result of the flagged skew Schur polynomial, proved by Reiner and Shimozono, from character level to crystals.

The multiplicities of irreducible representations in the tensor products of irreducible polynomial representations of general linear groups are known as Littlewood-Richardson coefficients. The saturation property for the Littlewood-Richardson coefficients was established by Knutson and Tao. The flagged skew Littlewood-Richardson coefficient $c^{\nu}_{\lambda,\mu/\gamma}(\Phi)$ is the multiplicity of the Schur polynomial $s_{\nu}(x_1, x_2, \dots, x_n)$ in the Schur expansion of $T_{w_0}(\mathbf{x}^{\lambda} s_{\mu/\gamma}(X_{\Phi}))$. These coefficients will reduce to the usual Littlewood-Richardson coefficients $c^{\nu}_{\lambda,\mu}$ if $\Phi = (n, n, \dots, n)$ and γ is empty partition. In this thesis, we prove the saturation property for the flagged skew Littlewood-Richardson coefficients namely if $c^{k\nu}_{k\lambda,k\mu/k\gamma}(\Phi) > 0$ for some $k \geq 1$ then $c^{\nu}_{\lambda,\mu/\gamma}(\Phi) > 0$. We give a tableau model to compute the flagged skew Littlewood-Richardson coefficients using the Demazure crystal structure for flagged skew semi-standard tableaux. We then produce a hive model for these coefficients to conclude the saturation property.

5.2.2 *On multi-parameter CCR flows*

An E_0-semigroup is a semigroup of normal, unital *-endomorphisms of $B(\mathcal{H})$, where $\mathcal{H}$ is an infinite-dimensional separable Hilbert space. Though initially considered only in the one-parameter context, multiparameter E_0-semigroups have recently been studied and provide for an interesting area of research. The goal of this thesis is to further explore multiparameter CCR flows, which are a class of E_0-semigroups, and to produce prime multiparameter CCR flows with non-trivial index.

In the first part of this thesis, we provide the preliminaries required to understand the subject. We also define the index of a spatial E_0-semigroup over a closed, convex cone in $\mathbb{R}^d$, extending the definition of Arveson's index from the one-parameter theory. We prove that the index of a CCR flow is equal to the index of the associated isometric representation. We also provide a necessary and sufficient condition for when such a CCR flow will be of type I.

In the second part of this thesis, we study E_0-semigroups indexed by Lie semigroups. We show that the CCR functor is injective when considered in the context of Lie semigroups, thereby extending results from the one-parameter theory and also the case where the semigroup considered is a closed, convex cone in $\mathbb{R}^d$. Next, we analyse a class of CCR flows that was previously considered over closed, convex cones by Arjunan, Srinivasan and Sundar. We show that, in the non-commutative case, the results obtained in the commutative case hold but partially. We also construct the first examples of prime CCR flows over closed convex cones that have index one.

In the last part of our thesis, we induce isometric representations from discrete semigroups to continuous semigroups and use this to construct uncountably many examples of prime multiparameter CCR flows with any given index.

5.2.3 Poissonian pair correlation in higher dimensions

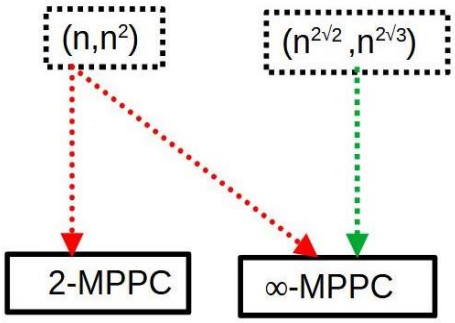

In this thesis, we study local statistics pair correlation for higher dimensional sequences of the unit cube. Our results produce many sequences which have Poissonian pair correlation for sup-norm (∞-PPC), as well as Poissonian pair correlation for 2-norm (2-PPC). We study one more local statistics, minimal gap and investigate its bounds for higher dimensional sequences of the unit cube.

The pair correlation function detects the distribution of spacings of points in the unit cube at distances of order of the mean spacing. In this thesis, we consider sequences of the form $(\{an\alpha\}) \subseteq [0,1)d$. We study the following: (1) INTEGER SEQUENCE. where (an) is a sequence of Nd such that each of its component is increasing. In this case, we introduce a new type of GCD sum, "generalised GCD sum" and, with the help of its upper bound we show that $(\{an\alpha\})$ has ∞-PPC (2-PPC for d=2) for almost all $\alpha \in Rd$, if the joint additive energy of (an) satisfies $\ll N3-\delta$ for some $\delta>0$. (2) REAL SEQUENCE. where (an) is a sequence of $Rd>0$ such that each component is well spaced, i.e. for some $c>0$, $a(i)n+1-a(i)n>c$ for all i and n. Using the moment estimate of the Riemann zeta function we show that $(\{an\alpha\})$ has ∞-PPC for almost all $\alpha \in Rd$ if the "real" joint additive energy satisfies a certain upper bound.

We show the variance of the pair correlation function is "small", then by applying Chebyschev inequallity and the first Borel-Cantelli lemma, our results follow. As an application of them we show that $(\{n\alpha 1\},\{n2\alpha 2\})$ has ∞-PPC as well as 2-PPC for almost all $(\alpha 1,\alpha 2) \in R2$ and for non-integer real numbers $\theta 1,\theta 2>2$, $(\{n\theta 1\alpha 1\},\{n\theta 2\alpha 2\})$ has ∞-PPC for almost all $(\alpha 1,\alpha 2) \in R2$.

We study the bounds of minimal gaps for higher dimensional sequences of $[0,1)d \cong Rd/Zd$ under the norm induced by the sup-norm of Rd. We consider higher dimensional sequence $(\{an\alpha\})$ and the linear forms $(\{an\cdot\alpha\})$ (which is a one-dimensional sequence), where all components of $(an) \subseteq Nd$ are increasing sequences. The method uses the first Borel-Cantelli lemma, metric theory of Diophantine approximation and the variance estimate to conclude upper and lower bounds. Furthermore, we study the van der Corput sequence and show that the minimal gap satisfies $\asymp 1/N$.

5.3 National Institute of Science Education and Research

5.3.1 *Weighted inequalities for multilinear operators in dunkl setting*

In the field of harmonic analysis, fundamental operators such as maximal function operators, singular integral operators, Fourier multiplier operators, and fractional integral operators and their multilinear extensions play a crucial role in studying various function spaces. These operators are also essential in the realms of partial differential equations, complex analysis, and quantum mechanics. A key aspect of harmonic analysis involves studying the weighted boundedness of these operators. In recent times, there has been significant focus on exploring the multilinear operators in harmonic analysis.

Dunkl operators provide a framework for developing a theory parallel to classical Fourier analysis, associated with root systems and reflection groups. However, there has been limited investigation into multilinear operators and weighted inequalities within this framework. This thesis aims to address this gap by exploring the weighted boundedness of these operators within the Dunkl framework.

The thesis begins by examining multilinear Dunkl-Calderón-Zygmund operators that involve both the 'Dunkl metric' and the usual metric in their definition. The main contribution lies in providing one- and two-weight estimates for these multilinear Calderón-Zygmund type singular integral operators, as well as for maximal operators associated with truncated singular integral operators, extending the corresponding results from the classical setting to the Dunkl setting.

Subsequently, new Littlewood-Paley type theorems are proved in the Dunkl setting and are used to establish the Coifman-Meyer type bilinear multiplier theorem related to the Dunkl transform. It is illustrated that these multiplier operators serve as examples of multilinear Dunkl-Calderón-Zygmund operators, and one and two-weighted estimates are obtained for the bilinear Dunkl-multiplier operators.

Finally, weighted inequalities are extended for different types of operators, namely multilinear Dunkl fractional integral operators and multilinear fractional maximal operators, which further extends the corresponding results from the classical framework to the Dunkl framework.

5.3.2 *Graph Neural Networks: Privacy and Applications*

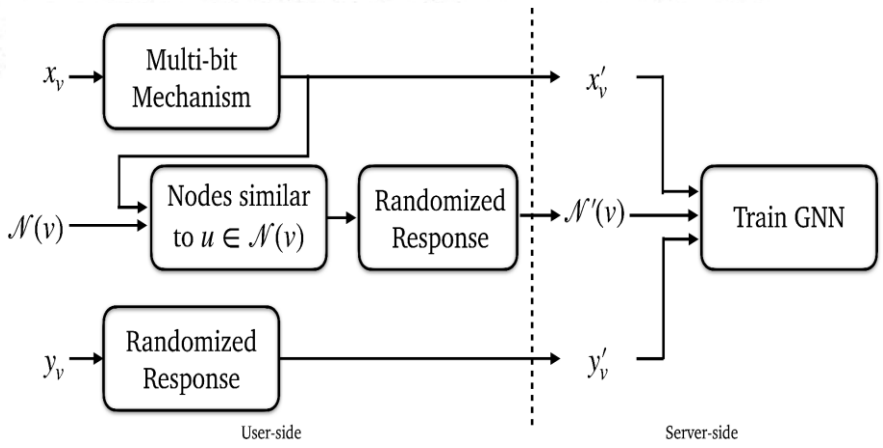

This thesis delves into the application and privacy aspects of Graph Neural Networks (GNNs) in solving real-world problems through graph-structured data analysis. GNNs are essential for

tasks such as node classification, link prediction, and graph classification, which are crucial in domains like personalized recommendations, fraud detection, and bioinformatics. The research focuses on two specific application areas: energy analysis in Building Information Modelling (BIM) and indoor localization. By employing various GNN techniques, the study demonstrates superior performance compared to state-of-the-art methods in these domains.

However, analyzing graph data with GNNs poses significant privacy risks, potentially disclosing sensitive information. To address these concerns, the thesis proposes a privacy-preserving approach that protects the privacy of local graph structures while allowing for meaningful analysis. The key contributions include the development of advanced GNN techniques tailored for energy analysis in BIM and indoor localization, achieving better results. The introduction of methods like EP-GNN, LSPGNN, and GraphPrivatizer ensures the structural privacy of graph nodes. Additionally, the implementation of a local privacy setting with centralized training involves sharing a locally perturbed neighborhood structure of the graph for GNN training. The feature, structure, and label information of nodes is perturbed, adhering to ϵ-Local Differential Privacy (LDP), with ϵ representing the privacy budget for feature, label, and structure perturbation. The research provides theoretical privacy guarantees and validates the effectiveness of the proposed methods through empirical analysis on real-world datasets. This work contributes to developing GNNs that perform effectively while preserving the privacy of sensitive information, addressing a critical need in modern data analysis.

MEDICAL AND HEALTH SCIENCES

6. Medical and Health Sciences

6.1 Tata Memorial Centre (Tata Memorial Hospital)

6.1.1 *Characterization of therapeutically relevant alterations in Human thyroid cancers*

The present thesis work describes the first landscape of molecular profile and pathogen profile in papillary thyroid cancer and anaplastic thyroid cancer of the Indian population. Pathogens have been largely ill-explored in thyroid cancer globally. This study is the first effort globally to describe the potential pathogens associated with papillary and anaplastic thyroid cancer. Whole exome and transcriptome sequencing found the significant pathogens associated with thyroid cancer. Our study represents the microbes, such as Ralstonia, Pseudomonas and Corynebacterium etc., in papillary and anaplastic thyroid cancer, which are present in the normal microflora of the thyroid. Further, we found a higher abundance of *Cutibacterium acnes* in both papillary and anaplastic thyroid cancers. We have shown that a higher abundance of Cutibcterium acnes is associated with the immunosuppressive phenomenon in papillary and anaplastic thyroid cancers in Indian patients. This study provides new insights into pathogens and their potential mechanism associated with thyroid cancer and opens the opportunity of application of highly specific antibiotic treatment in patients.

Whole exome sequencing of papillary thyroid cancer and anaplastic thyroid cancer describes the first landscape of somatic molecular profile in Indian patients. In anaplastic thyroid cancer, the whole exome sequencing analysis revealed the recurrent mutations in *TP53*, *BRAF*, *KRAS*, *NRAS*, *HRAS*, *PIK3CA*, etc., hallmark genes of anaplastic thyroid cancer. Anaplastic thyroid cancer is molecularly characterized by TP53 mutations and known to be significant driver mutations. Besides the hallmark mutations, we found significant recurrent mutations in THRA (~11%) gene, thyroid hormone receptor α, in a subset of anaplastic thyroid cancer in Indian patients. THRA gene is one of the thyroid lineage-specific differentiation genes. In a subset of anaplastic thyroid cancer patients, we found THRA mutations co-occur majorly with TP53 and other hallmark genes. THRA mutations signify its potential role in lineage-specific plasticity in anaplastic thyroid cancer. The molecular profile of anaplastic thyroid cancer compared to papillary thyroid cancer is much more distinct, wherein anaplastic thyroid cancer uniquely represents TP53 mutations. We found PKD1, whose mutations are enriched in a subset of anaplastic thyroid cancer compared to papillary thyroid cancer, which may suggest its potential role in transformation.

Similarly, the first landscape of molecular alterations of papillary thyroid cancer in Indian patients reveals hallmark mutations in BRAF and RAS driver genes along with many cancer related genes. We found a subset of significant number of patients that do not show alterations in hallmark genes, and we termed these patients as iBR–independent of BRAF and RAS. The iBR subset of patients showed relatively higher recurrence than patients with BRAF and RAS mutations.

Further, we have shown that the iBR subset of patients has demonstrated poor recurrence-free survival. Thus, we showed that the iBR group of patients who may show a higher recurrence rate and may respond poorly to the standard treatment line and results in poor outcome in clinics may require other treatment strategies. Additionally, we found recurrent and pathogenic

germline mutations in the DUOX2 gene. DUOX2 is an essential gene in thyroid metabolism and plays a critical role in T3 and T4 hormone synthesis. DUOX2 genes are frequently mutated in patients with congenital hypothyroidism or thyroid dyshormonogenesis. Abnormalities in the DUOX2 gene are well characterized to cause thyroid dyshormonogenesis and lead to hypothyroidism in children and adults. We have shown the association of germline mutations in the DUOX2 gene with papillary thyroid cancer, which is largely unknown worldwide. Therefore, we proposed that germline mutations in the DUOX2 gene might be present at the early onset of disease and may be involved in tumorigenesis in papillary thyroid cancer. We showed that DUOX2 germline mutations are associated with poor outcomes and metastasis. Hence, DUOX2 germline mutations can be adopted as a biomarker to be associated with advanced papillary thyroid cancer and predicted for poor long-term outcomes in clinics. Overall, this thesis work provides insights into distinct molecular features of papillary and anaplastic thyroid cancer in Indian patients.

Significance: The present work provides first comprehensive landscape of molecular alterations in Indian thyroid cancers (papillary thyroid and anaplastic thyroid cancer) which provides insights for targeted therapy implementation and patient management in clinics. The DUOX2 germline mutations can be established as germline biomarker for papillary thyroid cancer. The molecular subtype, independent of BRAF – RAS (iBR) could help predict recurrence in papillary thyroid cancer and patient treatment management. This study provides new insights into pathogens and their potential mechanism associated with thyroid cancer and opens the opportunity of application of highly specific antibiotic treatment in thyroid cancer patients.

PHYSICAL SCIENCES

7. Physical Sciences

7.1 Bhabha Atomic Research Centre

7.1.1 *Electrostatic complexation of charged nanoparticle-polyelectrolyte and their evaporation-induced assembly*

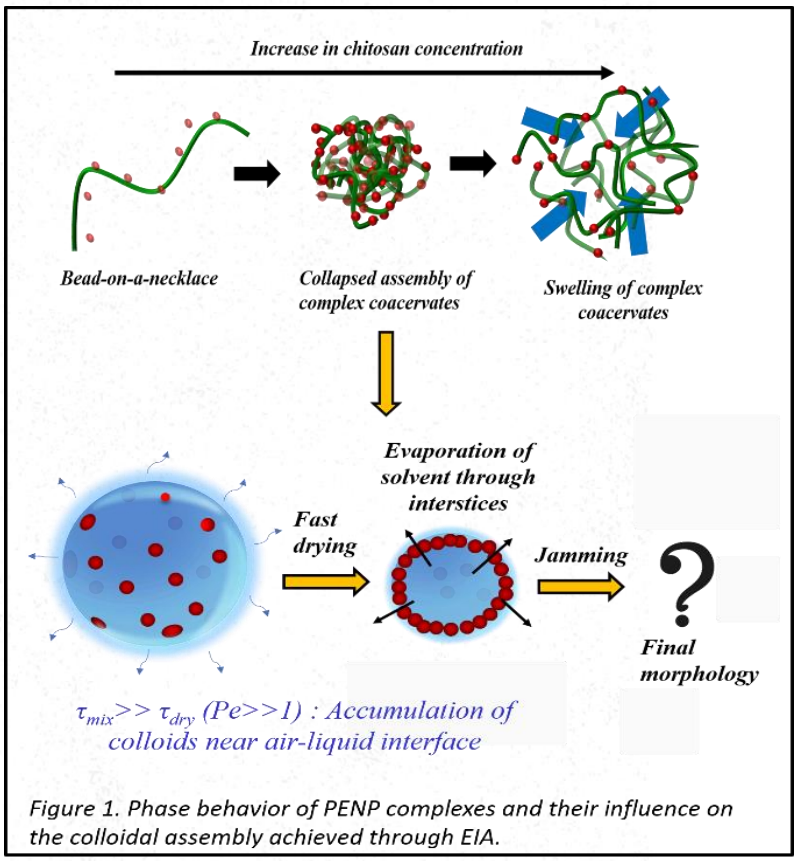

Figure 1. Phase behavior of PENP complexes and their influence on the colloidal assembly achieved through EIA.

Phase behavior of PENP complexes complexes and their influence on the colloidal assembly achieved through EIA

Self-assembly, a fundamental process in nature, occurs across microscopic and macroscopic scales. Efficiently organizing building blocks into functional nanostructures is highly envisioned in present era. Evaporation-Induced Assembly (EIA), a prime example of directed self-assembly, harnesses capillary forces to organize colloidal particles. While single-component colloidal systems, governed by DLVO theory, have been extensively studied, the EIA of multicomponent systems presents additional complexities due to the interplay of DLVO and non-DLVO forces during drying. This thesis addresses these challenges by investigating the phase behavior and EIA of multicomponent systems composed of nanoparticles (NPs) and polyelectrolytes (PEs). The study reveals that polyelectrolyte-nanoparticle (PENP) complexes undergo distinct phase transitions in response to variations in NP size, NP concentration, PE concentration, chain length, and ionic strength. For silica nanoparticles and PEI (polyethylenimine), a re-entrant phase behavior is observed due to the electro-sorption of PEI onto silica NPs.

EIA of silica-PEI dispersions resulting in silica-PEI microgranules exhibiting non-monotonic jamming behavior and interaction-dependent colloidal glass formation. Interestingly, larger silica NPs (27 nm) exhibit morphological non-monotonicity in microgranules, unlike smaller

NPs (10 nm, 16nm). A detailed spatial analysis of microgranules reveals a transition from ordered arrangements at outer region to random jamming in the inner region of the microgranules. This "rush hour behavior," driven by self-pinning of colloids at the liquid-air interface during drying, enables packing fractions (ϕ_s~0.7) exceeding random close packing (ϕ_rcp ~0.64). Slowing the drying kinetics enhances degree of localized ordering, highlighting the dynamic interplay of assembly forces. Furthermore, silica-chitosan systems exhibit a transition from bead-on-necklace structures to dense coacervates (ϕ_sc~0.62) at high PE concentrations, followed by complex swelling.

These structural transitions govern NP packing and microgranules morphologies, ranging from doughnut-like shapes to multi-invaginated spheres. This work emphasizes the pivotal role of tunable phase behavior in guiding colloidal assembly and highlights the potential of PENP-based materials for advanced applications. Notably, NP-PE microgranules demonstrate excellent performance in CO_2 capture, achieving high sorption capacities (~2 mmol/g) and stability over multiple cycles, underscoring their promise for scalable, cost-effective carbon capture technologies. In summary, this thesis elucidates the fascinating the complex phase behavior of PENP complexes and their subsequent colloidal assembly and establishes the relation between the two. Further revealing how the tunable colloidal assembly governs and optimizes CO_2 sorption capacity, thereby advancing their potential for real-world applications.

7.1.2 *Investigations on thin film electrode-based lithium-ion battery*

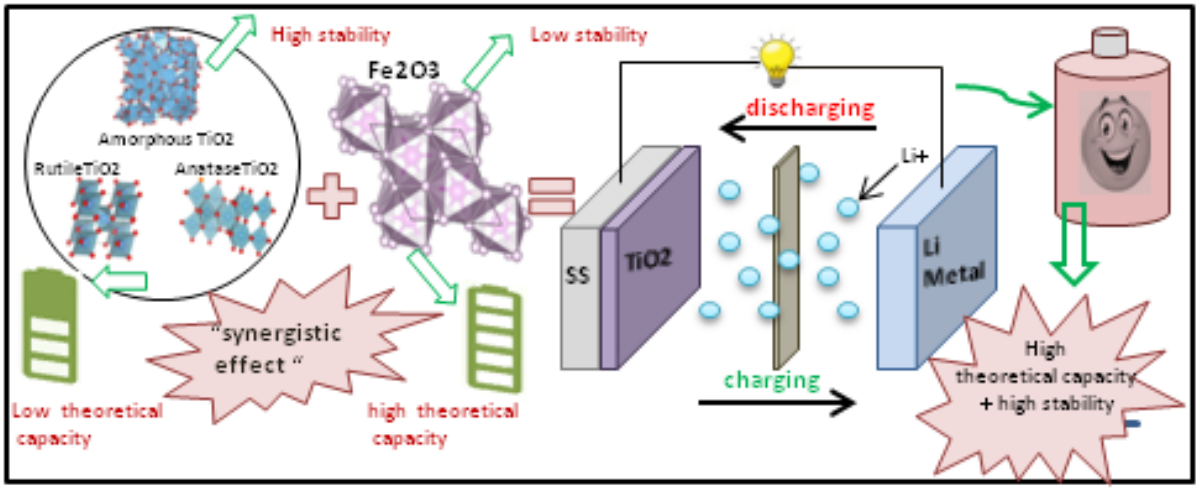

Thin film Lithium-ion batteries (TFLIBs) are progressively gaining interest for application in the field of micro devices. Thin film electrodes are the heart of TFLIBs as they carry various advantages of controlled mass loading, increased ionic and electronic conductivity and higher energy and power density. In the present thesis, many efforts have been given to improve the performance of LIBs with TiO_2 thin film anode for better cycling stability and increased energy density. It has been observed that that LIBs with rutile phases of TiO_2 thin film anodes prepared by a relatively simple, highly reproducible, easily scalable, and commercially used magnetron sputtering technique yielded very high specific capacity values which are better or comparable to that reported in the literature so far which could otherwise be obtained by much more cost intensive or complicated techniques like Atomic Layer Deposition (ALD) or multi-step chemical routes.

Structural and morphological investigations of the samples by various techniques show that a synergy between the deposited TiO_2 film and the Fe_2O_3 layers present on the stainless steel (SS) substrate along with an increase in porosity in the films during the charge–discharge cycling has given rise to the highest capacity of the rutile TiO_2 thin film cells which increases gradually with cycling. To further improve the electrochemical performance of TiO_2 at high current rates, transition metal doped TiO_2 films were prepared and it has been shown that 10% Fe doped rutile TiO_2 thin films have yielded the highest specific capacity at high current rate due to higher porosity and highest diffusion coefficient. To further enhance the performance, the TiO_2/ZnO thin film bi-layer and multilayer electrodes have been deposited. Batteries with multilayer electrodes SSML1 (ZnO:TiO_2 in the ratio 1:1) deposited on SS and SSGML2 (ZnO:TiO_2 in the ratio 5:1) deposited on Au coated SS substrates have shown the highest specific capacities both at low current rate and high current rate. At the end, thin film solid electrolyte of Lithium phosphorus oxynitride (LiPON) was deposited and its compatibility with the TiO_2 thin film anode was explored. With the further development of a compatible thin film-based cathode, the present thesis work can be extended in future for the development of all solid-state full cell lithium-ion micro-battery for applications in various modern micro devices like MEMS.

7.1.3 *Development of doped NASICON-type glass ceramics systems as solid state electrolyte for lithium ion battery*

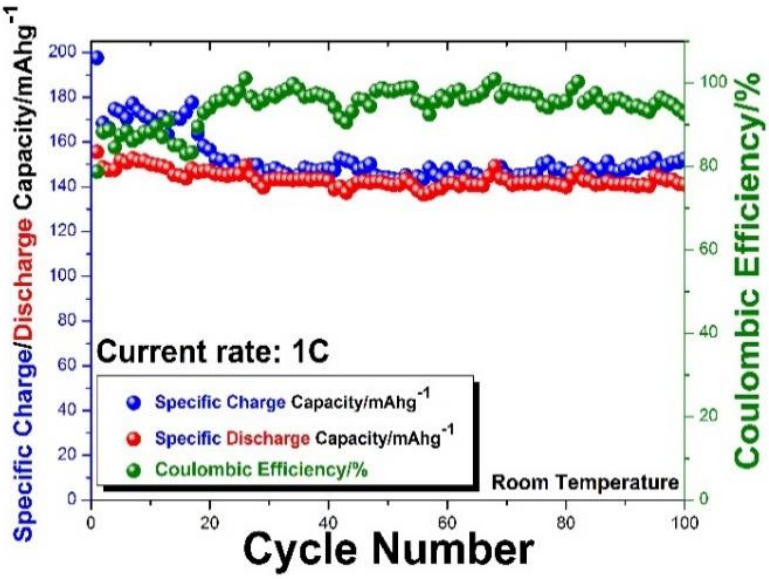

Specific charge/discharge capacities and coulombic efficiency versus cycle number

The doctoral thesis titled "Development of Doped NASICON-Type Glass-Ceramics Systems as Solid-State Electrolyte for Lithium-Ion Battery" presents a comprehensive study on the design, synthesis, and characterization of doped NASICON-type glass-ceramics for application as solid-state electrolytes (SSEs) in lithium-ion batteries (LIBs). Aiming to overcome safety and performance limitations of liquid electrolytes—such as flammability, poor thermal stability, and dendrite formation—the research identifies NASICON-type structures as promising candidates due to their high room-temperature ionic conductivity and chemical

stability. Using Density Functional Theory (DFT), the author screened dopants and found Al^{3+} substitution in $LiGe_2(PO_4)_3$ (forming LAGP) to be optimal for enhancing lithium-ion mobility.

Two compositional systems, LAGPS (Al_2O_3 and SiO_2-based) and LAGPM (Al_2O_3 and MoO_3-based), were developed via melt-quenching and optimized through thermal treatments. These systems demonstrated successful NASICON-phase formation as verified by XRD and neutron diffraction. An average ionic conductivity of $(4.93\pm0.04)\times10^{-4}Scm^{-1}$ was achieved, as measured by Electrochemical Impedance Spectroscopy (EIS). Initial coin cells revealed high interfacial resistance; hence, Composite Solid Electrolytes (CSEs) were formulated by blending glass-ceramics with polymers to improve flexibility and electrode-electrolyte contact.

The resulting solid-state cells, especially those incorporating CSEs, exhibited high discharge capacities ((143.484±0.706) $mAhg^{-1}$ at 1C over 100 cycles) with good cycling stability, thus validating the viability of doped NASICON-type glass-ceramics in next-generation all-solid-state batteries (see Figure 1). This thesis lays a robust foundation for scalable, safe, and high-performance SSE development in advanced energy storage technologies.

7.1.4 *Neutrino mass ordering, Earth tomography and Lorentz invariance violation study in ICAL@INO, Long Baseline and Reactor Experiments*

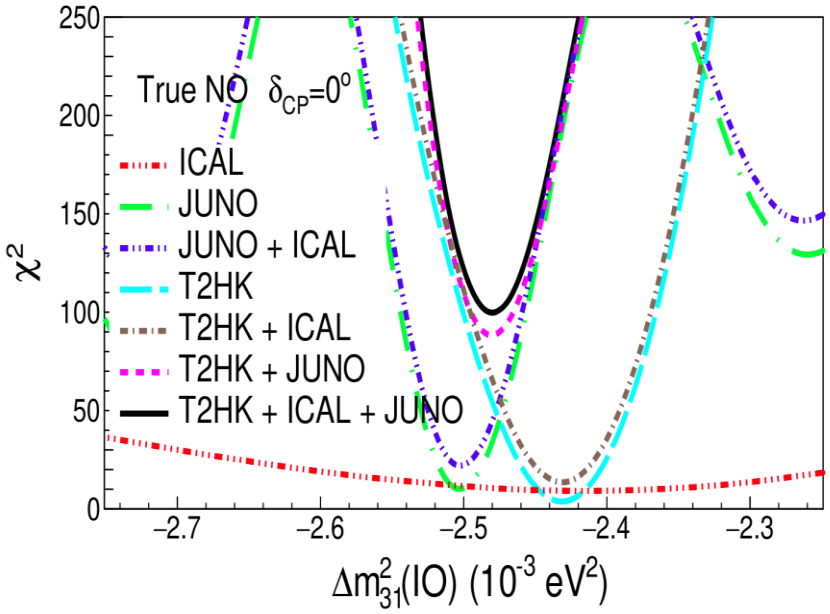

Mass ordering sensitivity as a function of Δm 231 (test) for δ CP = 0 corresponding to T2HK

Neutrinos are among the most mysterious particles in the Standard Model, and understanding their properties requires multiple large-scale detectors. In my thesis, I explore the role of neutrinos in probing physics beyond the Standard Model (BSM), with a particular focus on improving our understanding of neutrino mass ordering (MO). I investigated the potential of combining data from different experiments—ICAL, JUNO, and T2HK—to enhance sensitivity to the MO. By leveraging the synergy between these experiments, the combined analysis achieves more than 10σ sensitivity to mass ordering under favorable conditions and maintains a robust sensitivity above 5σ even in the most pessimistic scenarios. The impact of this synergy is clearly demonstrated in the accompanying figure, which illustrates the improvement in MO sensitivity through this multi-experiment approach.

The ICAL detector is uniquely sensitive to changes in Earth's internal matter density, thanks to its capability to detect atmospheric neutrinos coming from all directions. As neutrinos traverse different layers of the Earth, they carry information about the varying densities they encounter. In our work, we simulated this behavior to study ICAL's sensitivity to these density variations. Our results show that ICAL can achieve sensitivity to Earth's internal structure comparable to that of other large-scale neutrino detectors such as PINGU and ORCA. This highlights ICAL's potential not only for particle physics but also for geophysical studies.

Neutrinos interact with Earth's matter potential as they propagate, which modifies their effective mixing angles and masses. Similarly, potential effects from physics beyond the Standard Model (BSM)—such as non-standard interactions or LIV—can alter neutrino oscillation patterns, leaving imprints on the mixing parameters and mass splittings. In our study, we explore ICAL's sensitivity to such BSM-induced effects. ICAL demonstrates strong sensitivity to both CPT-even and CPT-odd parameters, reaching a performance level comparable to that of DUNE. Furthermore, combining ICAL and DUNE data significantly enhances the overall sensitivity to several key BSM parameters, providing the most stringent constraints in some regions of parameter space.

7.2 Harish-Chandra Research Institute

7.2.1 *Unitary/non-unitary correspondence, and defects in 2d CFTs*

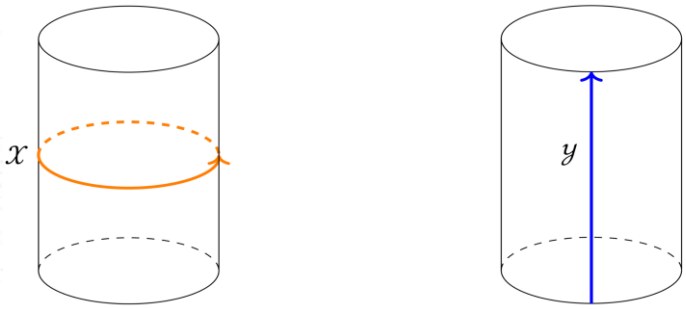

In the radial quantisation picture of the 2-Dimensional CFT: the operator X (orange) inserted along a "spatial" slice. the defct line Y (blue) running along the "Edclidean time" axis

Quantum field theories (QFTs) with an additional conformal symmetry are rarer than ordinary QFTs with only Poincare symmetry. Nevertheless, conformal field theories (CFTs) are ubiquitous and play a crucial role in various physical contexts. For instance, they describe physical systems at criticality, serve as the worldsheet theories of strings, and provide the holographic duals of anti-de Sitter (AdS) spacetimes. Among CFTs, 2-dimensional (2D) CFTs hold a special significance due to its infinite-dimensional symmetry algebra - the Virasoro algebra. In this thesis, we employ holomorphic modular bootstrap techniques to explore correspondences and dualities among 2D CFTs.

The highest-weight representations of the affine su(2) current algebra CFTs at the Kac-Wakimoto admissible fractional levels. We use the known modular properties of the highest-weight representations to construct the *even sector*. We relate the characters of the even sector to known unitary CFTs by a procedure we call *unitarisation*. We show that this can only be

achieved when the fractional levels are either the boundary admissible levels or the isolated level -5/4. Although each character in the even sector is well-defined at positive half-integer levels, the unitarised theory does not possess positive semi-definite Verlinde fusion rules. At every other admissible fractional level, we find that the even sector has at least one special inadmissible character called the *quasi-character*.

Next, we construct the even sector for the chiral algebras corresponding to the *Deligne-Cvitanovic* sequence of Lie algebras at negative rational levels, which saturate the unitarity bounds on 4D rank 1 SCFTs. Again, we unitarise the 2D non-unitary CFT with an admissible fractional level, corresponding to a unitary 4D SCFT, to a unitary CFT. In particular, we use the unitarisation map to propose a construction for the elusive 4D rank 1 SCFT with a broken G2 global flavour symmetry. We also write the 1/2 BPS line defect partition functions in the proposed G2 SCFT.

Finally, we explicitly construct and classify topological duality defects for the 2D Niemeier Lattice CFTs (NL CFTs) with affine so(2n) current algebra factors at level 1. These CFTs occur with the central charge c=24. We extend the group of symmetries of the NL CFTs, with an additional non-invertible duality defect, to the Tambara-Yamagami fusion category. We provide the duality defect partition function for each of these NL CFTs.

7.2.2 *Nonequilibrium dynamics of photo-pumped correlated insulators*

Strongly correlated systems, when driven out of equilibrium by external stimuli such as laser pulses, exhibit rich transient dynamics before reaching thermal equilibrium. While energy injection eventually raises the system's temperature, the equilibration pathway is highly nontrivial and depends sensitively on interaction strength. In metals, thermalization is relatively fast and enhanced by stronger interactions. However, in correlated insulators with strong interactions and commensurate filling, equilibration is significantly slower and can be accompanied by transient transitions to metallic states. These systems frequently display a separation of timescales—rapid relaxation in the electronics sector contrasted by the slow evolution of order parameters such as magnetic or charge order. In certain regimes, these order parameters settle at an effective temperature different from that of the electrons, giving rise to long-lived quasi-steady states. Such phenomena have been observed experimentally and pose major challenges for theoretical modeling, as traditional equilibrium techniques fail to capture the far-from-equilibrium dynamics. Existing computational approaches, including exact diagonalization and cluster-based methods, are either limited by system size or fail to account for non-local correlations and domain dynamics. To overcome these limitations, we develop a hybrid method that combines time-dependent mean-field dynamics with non-equilibrium Langevin dynamics, allowing us to model both fast electronic processes and slower domain evolution over extended spatiotemporal scales. This approach captures key features such as the slow recovery of broken symmetry phases and the emergence of new, sometimes hidden, orders following a photoexcitation. By analyzing energy flow and order parameter evolution in both charge-ordered and Mott insulating systems, we show that this method reproduces experimental trends and provides insight into the non-equilibrium phase behavior at a fraction of the computational cost. The framework is broadly applicable and opens up new avenues for

exploring nonequilibrium dynamics in a range of strongly correlated materials, including superconductors and systems with spin or orbital order.

7.2.3 *Some phenomenological studies of a neutrinophilic U(1) model*

This thesis investigates a minimal yet phenomenologically rich extension of the Standard Model (SM), based on an additional Abelian gauge symmetry U(1), which does not directly couple to any of the SM fermions. The motivation for this study stems from two unresolved phenomena that the SM fails to explain, such as the origin of neutrino masses, the nature of dark matter (DM). The proposed model introduces a new gauge boson (Z'), three vector-like SM gauge neutral fermions, a singlet scalar, and an additional SU(2) scalar doublet. All these new particles are charged under the U(1) symmetry, while SM fields remain neutral.

In this framework, SM neutrino masses are generated through an inverse seesaw mechanism involving interactions with new vector-like fermions. The new Z' boson can interact with the SM particles via kinetic mixing with the SM hypercharge boson and through Z–Z' mass mixing. We find that such a light Z' boson, with mass in the 200–500 GeV range, is still consistent with present experimental bounds. We observed that multilepton final states such as 4ℓ + missing energy and 3ℓ + 2 jets + missing energy can serve as clean discovery channels at the LHC.

Further study considers the scenario where the Z' boson is lighter than the SM gauge bosons and the kinetic mixing is extremely small, rendering it difficult to produce directly at colliders. In such cases, an exotic decay of the SM Higgs boson, namely $h \rightarrow Z'Z'$, becomes an important probe, made possible by mixing between the SM Higgs and the singlet scalar. Additionally, one-loop processes involving hidden-sector fermions can give rise to lepton flavor-violating decays of Z', offering another potential signature of the Z'.

In scenarios where Z' couples very weakly to SM particles, its production is viable only through the decay of heavier particles charged under the U(1) symmetry. The thesis explores such cascade processes involving the new scalar states from the second Higgs doublet. These include decays like $H^+ \rightarrow W^+Z'$, $h_2 \rightarrow VV$ (where V = W, Z, Z'), and $A_2 \rightarrow h_1Z'$. These channels can lead to clean multilepton signals such as 4ℓ + X, which offer great potential for its detection at the LHC.

Dark matter aspects of the model are also thoroughly studied. The lightest heavy neutrino in the model, due to its small Yukawa couplings, can have a lifetime longer than the age of the universe and serve as a viable DM candidate. Depending on the parameter space, the DM can fall into either the Weakly Interacting Massive Particle (WIMP) regime or the Feebly Interacting Massive Particle (FIMP) regime. In the WIMP scenario, relic density is achieved via Z' and singlet scalar portal annihilations. In the FIMP case, the DM is produced via the freeze-in mechanism, with the Z' and the singlet scalar-playing crucial roles in DM production.

Finally, the thesis explores the situation where the Z' boson is very heavy and couples more strongly to the hidden sector than to the SM particles. In this case, it predominantly decays to charge-neutral long-lived particles or DM, making it invisible to standard collider searches. The production cross-section for such a Z' at the LHC is negligible. To address this, a novel detection strategy is proposed where Z' is produced in association with a high-energy photon at a future muon collider ($\mu^+\mu^- \rightarrow \gamma Z'$). The resulting mono-photon signature, with missing

energy from the invisible Z' decay, provides a potentially discoverable signature even when the Z' is completely hidden from direct observation.

Overall, this thesis offers a unified framework to simultaneously explain two outstanding problems in modern particle physics, neutrino masses, dark matter, while remaining compatible with all current experimental bounds. Additionally, the thesis provides collider-accessible signatures of neutrinophilic U(1) extension at both current and future collider experiments.

7.3 Indira Gandhi Centre for Atomic Research

7.3.1 *The impact of ion irradiation on the texture, grain boundary characteristics, void swelling behavior and surface morphology of nanocrystalline Ni*

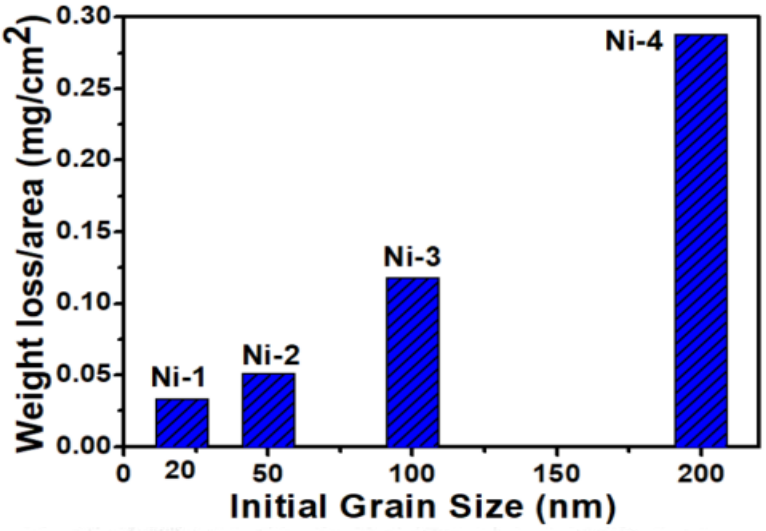

Weight loss measurements as a function of grain size

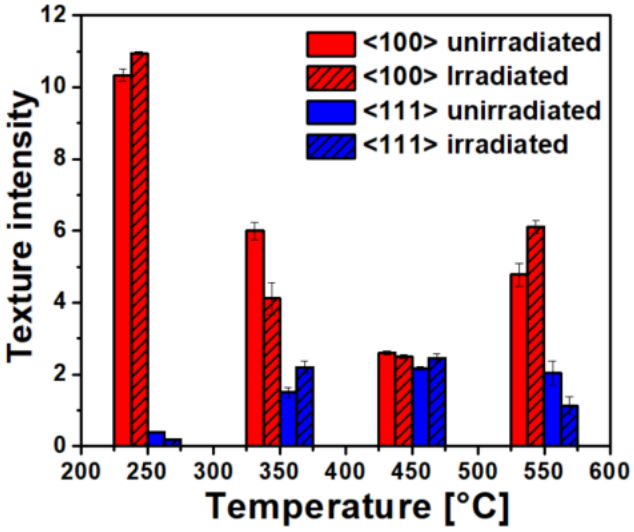

Texture evolution under irradiation and temperatures

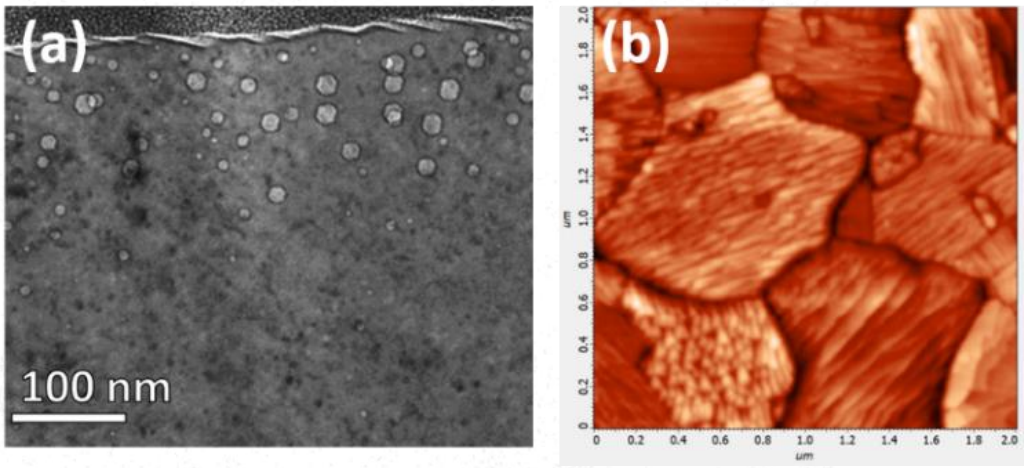

(a) Voids are in close proximity to the surface (b) void-induced facets at 450℃

The primary concern in developing molten-salt reactors (MSRs) is the corrosion of structural components. A promising solution is electrodepositing structural materials with Ni coating to create a barrier against Cr diffusion, enhancing corrosion resistance. For irradiation resistance, materials with a high density of grain boundaries (GBs) are needed, as GBs absorb radiation-induced defects. Thus, nanocrystalline Ni (NC-Ni) is used to prevent corrosion and irradiation-induced defects. The effects of irradiation on texture, GB properties, and surface roughening in NC-Ni are crucial since they influence corrosion. The present thesis focused on electrodeposited NC-Ni coatings with varying grain sizes (20 nm-Ni-1, 50 nm-Ni-2, 100 nm-Ni-3, 200 nm-Ni-4) created using pulsed electrodeposition. The goal was to assess the corrosion behavior and irradiation response of these coatings.

NC-Ni samples were annealed at 650℃ to simulate MSR conditions, and electron backscattered diffraction (EBSD) revealed a strong <100>//ED texture and Σ3 twin boundaries in all samples, with Ni-1 and Ni-2 showing desirable Σ3 twin boundaries for corrosion resistance. The influence of grain size on corrosion behavior in a FLiNaK environment was examined for the first time. Corrosion tests in FLiNaK at 650℃ for 24 hours indicated that a lower grain size (Ni-1) significantly improved corrosion resistance, revealing a nuanced correlation with texture, twin boundary fraction and GB length per area. During corrosion, a novel observation of facet formation on the surface of NC occurred, attributed to impurities in the salt, altering surface anisotropy.

Grain growth in Ni-1, Ni-2, and Ni-3 samples was monitored during annealing up to 550℃, showing onset at progressively higher temperatures, with Ni-1 and Ni-2 exhibiting superior corrosion resistance. The irradiation stability of Ni-1 and Ni-2 was assessed at 550℃, revealing that the attributes required for corrosion resistance were preserved under irradiation up to 18.5 dpa. Additionally, the evolution of texture during irradiation and temperature was studied in Ni-1 and the study unveiled that irradiation enhances thermally activated textures within the 350℃ to 550℃ temperature range, challenging existing concepts of ion channeling. At 250℃, ion mixing caused the growth of <100> orientations due to differential damage resulting from ion channeling.

Depth-dependent void swelling behavior was studied in Ni-1 during ion irradiations at 350℃ to 550℃. Various void distributions around GBs are noticed, influenced by the instability of NC grains and high internal sinks. Furthermore, various types of facets are formed as a

consequence of voids formed near surfaces, the variations depend on grain orientations. These findings are valuable insights for the design of nanocrystalline coatings for corrosion prevention and control in MSR.

7.3.2 *Transition metal oxides decorated vertical graphene nanosheets for supercapacitor applications*

Supercapacitors offer high power density, rapid charge-discharge, and long cycle life but suffers from low energy density than batteries. This thesis develops binder-free hybrid electrodes by integrating nickel oxide (NiO) and cobalt oxide (Co_3O_4) with vertically aligned graphene nanosheets (VGNs). The synergy of VGNs' high surface area, good electrical conductivity with redox properties of TMOs', alongside tailored microstructure, morphology, and stoichiometry, addresses shortcoming and enhances performance.

1) Binder-Free NiO/VGN Hybrid Electrodes: NiO was deposited on VGN templates using pulsed laser deposition, with different microstructures and morphologies, such as nano-particles nano-crystals, and film-like structures by varying process parameters. Fig. 1 illustrates the significant influence of microstructure and morphology variations on the electrochemical active surface area (ECSA). These morphological changes also strongly

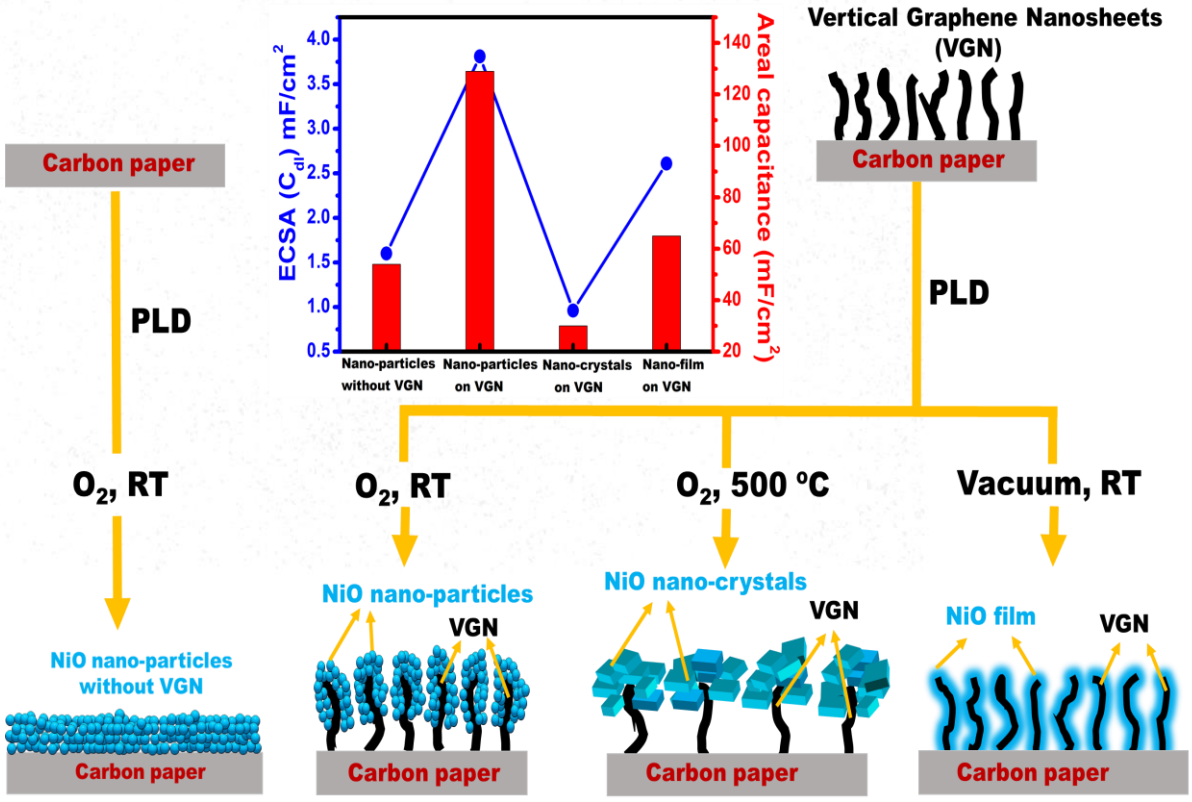

Variation of areal capacitance values and ECSA with microstructure & morphology of NiO/VGNs hybrid electrode

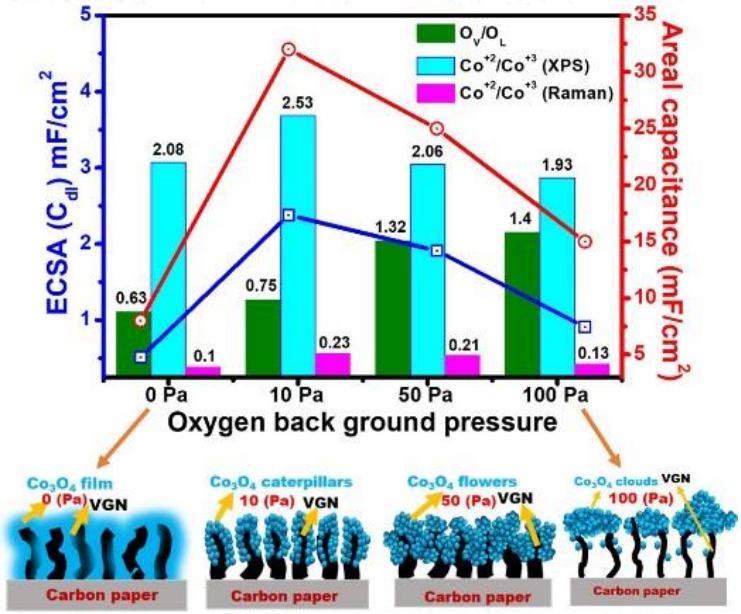

Graph of correlation between ECSA, areal capacitance, O_V/O_L, and Co^{+2}/Co^{+3} for Co_3O_4/VGNs hybrid electrode

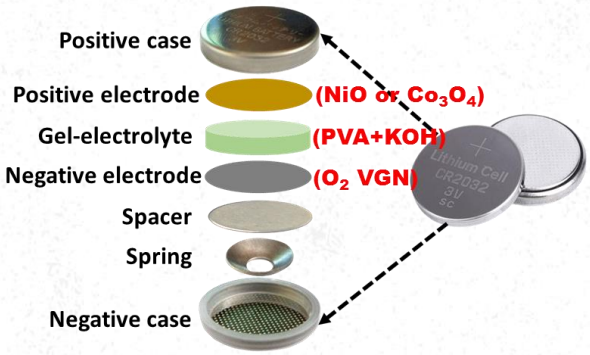

Schematic diagram of asymmetric coin-cell device(s)

impacted diffusion resistance, with both factors collectively influencing the areal capacitance and cyclic stability. Among the tested configurations, the NiO electrode with a nano-particulate microstructure demonstrated the highest areal capacitance of 129 mF/cm² (2200 F/g, 85 % of the theoretical capacitance) and good cyclic stability (82 % after 2000 cycles). This remarkable performance is attributed to the smaller NiO particle size (5–10 nm), which enhances the surface-to-volume ratio. Additionally, the VGN template contributes a high surface area, with uniform, conformal growth that minimized particle aggregation, creating densely packed structures. This effectively boosted the electrode's capacitance by approximately 2.5 times.

2) Binder-Free Co_3O_4/VGN Hybrid Electrodes: Co_3O_4 was deposited on VGNs templates at varying oxygen (O_2) background pressures using pulsed laser deposition, resulting in diverse microstructures and morphologies, including films, caterpillars, flowers, and cloud-like formations. As shown in Fig. 2, these different morphologies significantly influenced the ECSA, oxygen vacancies, and the Co^{2+}/Co^{3+} ratio. Additionally, diffusion resistance was greatly affected by these morphological variations. All these parameters collectively impacted the areal capacitance and cyclic stability. Among all configurations, the sample with a caterpillar-like microstructure exhibited the highest areal capacitance of 32 mF/cm² (1900 F/g, the highest reported value) and excellent cyclic stability, retaining 87 % of its capacitance after

3000 cycles. This superior performance is attributed to the high surface area provided by the VGNs template and the uniform, conformal growth that minimized particle aggregation, creating densely packed caterpillar-like structures. Additionally, the Nanoscale particle size (5–10 nm) improved the surface-to-volume ratio, while the optimized Co^{2+}/Co^{3+} ratio further enhanced electrochemical performance.

3) Fabrication of the Asymmetric devices: Two asymmetric coin cells were fabricated using NiO/VGN and **Co**$_3O_4$/VGN hybrid cathodes, O_2 VGN anodes, and a PVA+KOH gel electrolyte. Schematic diagram of asymmetric coin-cell device(s) shown in Fig.3. The NiO/VGN device showed C_s = 2 mF/cm², E = 0.4 μWh/cm², P = 102 μW/cm², and the Co_3O_4/VGN device achieved C_s = 4 mF/cm², E = 1.8 μWh/cm², P = 218.8 μW/cm². Both devices exhibited ~92 % capacitance upto 3000–5000 cycles and powered an LED.

7.4 The Institute of Mathematical Sciences

7.4.1 *Fractional Quantum Hall liquids: Their Ground States, Neutral excitations, and competition with crystal phases*

Just as water can exist in distinct phases—solid, liquid, and gas—depending on external parameters like temperature and pressure, a many-electron system in a material can exhibit a variety of quantum phases depending on factors such as temperature, electron density, magnetic field, or spatial dimensionality. The central focus of this thesis is to investigate the distinct phases of electrons confined to a two-dimensional plane under a strong perpendicular magnetic field at very low temperatures. In this regime, the most celebrated phases are the fractional quantum Hall (FQH) states, which exhibit several remarkable properties. These include quantized Hall conductance, long-range entanglement without any local order, gapped

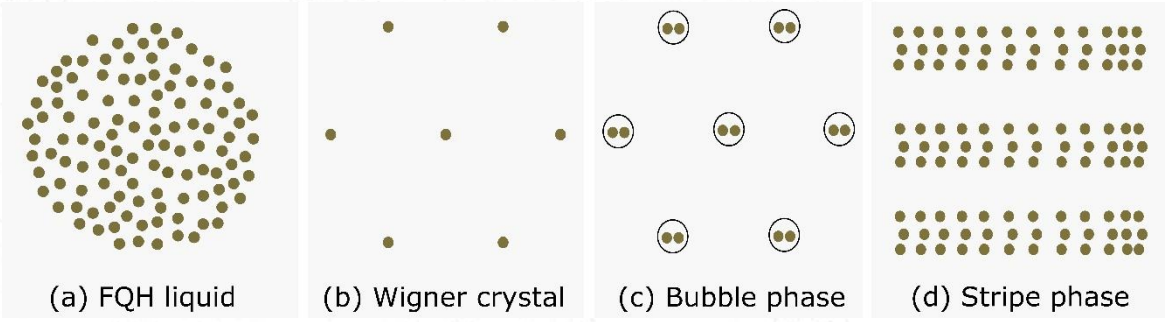

Different phases of two-dimensional electrons in a perpendicular magnetic field

bulk excitations, elementary excitations that carry a fraction of the electron charge, and gapless edge modes. In experiments, many FQH states have been observed, each exhibiting distinct properties.

In this thesis, we provide a microscopic understanding of the recently observed FQH state at 4/13, highlighting its elementary charged excitations and gapless edge modes. In addition to charged excitations, neutral excitations also require finite energy to be created and play a crucial role in determining the stability of an FQH state. These neutral excitations can be described using two different approaches: the composite fermion exciton (CFE) wave function and the Girvin-MacDonald-Platzman (GMP) ansatz. Although CFEs typically provide a more

accurate description of neutral excitations, we demonstrate that in the long-wavelength limit, the CFE and GMP modes become nearly identical for a class of FQH states known as the primary Jain states. Apart from FQH states, other possible phases of a two-dimensional electron gas under a perpendicular magnetic field include the Wigner crystal, bubble, and stripe phases. These phases can compete with FQH states as the electron density is varied at a fixed magnetic field, or vice versa. In this thesis, we investigate such competition in graphene-based systems, particularly in bilayer and trilayer graphene heterostructures.

7.4.2 *Fractional quantum hall liquids: Their ground states, neutral excitations, and competition with crystal phases*

Cloudbursts occur due to rapid coagulation of water droplets. Alzheimer's disease is characterized by the coagulation of amyloid-β proteins, forming plaques in the brain. The dominant physical process in both events is aggregation, an irreversible, non-equilibrium process wherein particles coalesce on contact to form larger particles. Although rare, such events significantly impact quality of life.

Past studies on aggregation have focused mainly on the study of typical mass distributions, described by a deterministic rate equation for the number of clusters of mass m in time t known as the Smoluchowski equation. Given two masses, the collision rate is in general dependent on the colliding masses, through a function known as collision kernel. The Smoluchowski equation can be solved exactly only for three kernels - constant, sum and product. Using the

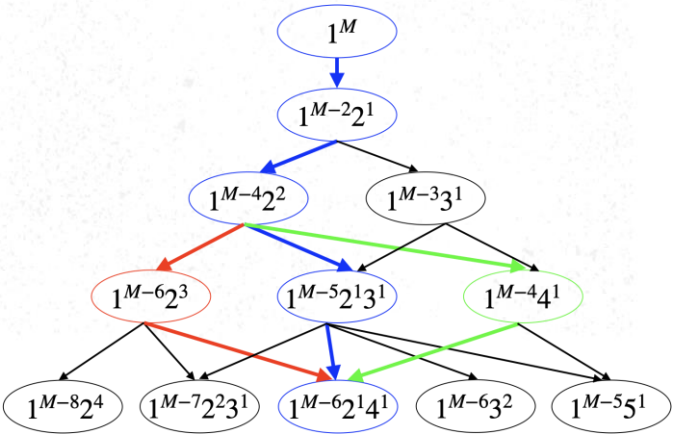

All possible configurations and trajectories for 4 collisions. The configurations after each collision are shown inside the bubbles. For the trajectory shown in blue, the red and green lines denote possible alternate paths that alter only the 4th configuration.

framework of large deviation theory, we develop an analytical formalism to compute the probability of N clusters remaining at time t, given that there were M clusters initially, for arbitrary kernels. In the limit of infinite total mass, we find that a large deviation scaling exists

for arbitrary kernels. Moreover, we obtain the explicit large deviation functions and optimal trajectories for the constant, sum and product kernels, and verify them with Monte-Carlo results.

Mean mass distribution for the product kernel exhibits a phase transition known as gelation, in which a giant cluster of the order of total mass of the system forms and begins to consume the smaller clusters. We observe the signature of gelation in the second derivative of the large deviation function, which shows a discontinuity at a critical fraction of remaining clusters. The analytical formalism is used to calculate the large deviation function and optimal trajectories for k-nary coalescence, wherein k particles coalesce into l particles ($k>l$) at a constant rate. Results are benchmarked with the exact answer.

The numerical study of rare events requires sophisticated techniques, because it is computationally expensive to sample rare trajectories through direct sampling. We develop a biased algorithm which modifies trajectories through local moves, and waiting times between collisions using importance sampling. The algorithm obtains the probabilities of rare events for arbitrary collision kernels, and is rigorously proved to be ergodic. It is benchmarked with the exact answer for constant kernel aggregation. Probabilities as low as 10^{-40} are obtained, and the large deviation scaling which was obtained in our analytical results is verified.

7.5 Institute of Physics

7.5.1 *Exploring particle physics models: Implications for dark matter phenomenology*

The thesis addresses some of the limitations of the Standard Model (SM) of particle physics, such as the hierarchy problem, the existence of non-zero neutrino masses, baryon asymmetry, and the puzzle of dark matter. While the SM has successfully explained a wide range of experimental observations, it leaves some questions unanswered. This thesis explores novel Beyond the Standard Model (BSM) models, focusing specifically on dark matter (DM) and its signatures in terrestrial experiments and astrophysical observations. The work also bridges the gap between mechanisms for dark matter production and the generation of neutrino masses.

First, we explore the Dynamical Scotogenic Model. This model extends the original Scotogenic framework by incorporating the spontaneous breaking of global $B-L$ symmetry, which produces light neutrino masses and introduces a potential DM candidate. The model differs from its predecessor by offering additional DM annihilation channels. These new annihilation channels, including those involving the majoron, allow for a consistent DM relic abundance over a wide range of parameters, making the model more viable compared to its predecessor.

The research also investigates the production of scalar DM through freeze-in mechanisms in a gauged $B-L$ model. In this scenario, DM is produced through the decay and annihilation of the Standard Model and $B-L$ Higgs bosons. By considering different statistical distributions and accounting for thermal mass corrections, the study highlights the crucial role of electroweak symmetry breaking in enhancing DM relic density. These insights have broader implications and can be applied to other models, providing new avenues for understanding scalar interactions and their role in dark matter production. Furthemore, we also investigated the interplay between the freeze-in and super-WIMP mechanism of DM production in an extended gauged $B - L$ model. We consider the secluded dark sector comprising two dark sector particles. In this framework, the lightest Z2-odd particle is the DM candidate, having a

feeble interaction with all other SM and BSM states. The next-to-lightest Z2-odd particle in the dark sector with large interaction strength with the SM and BSM states.

Finally, the thesis explores the phenomenology of the Singlet Triplet Fermionic Model, which offers two potential DM candidates while simultaneously explaining neutrino masses and oscillation parameters. The research examines different production mechanisms, including thermal production and late-time decay of particles, to account for the observed DM relic density. The study also looks ahead to potential discoveries, discussing the detection prospects of triplet fermions and scalars at the Large Hadron Collider (LHC) and the possibility of probing long-lived particles at future detectors like MATHUSLA. This work provides essential insights for ongoing and future experimental searches for dark matter.

7.5.2 *Next-to-leading order corrections to dark matter direct detection and precision observables*

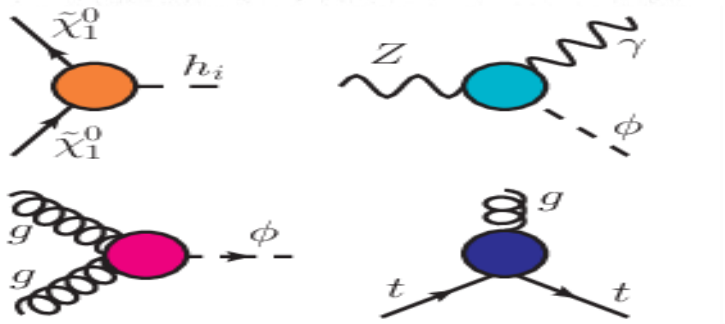

Schematic diagrams for DM-Higgs vertex corrections (top left), Z→ φγ (top right), gg→φ (bottom left), and chromomagnetic dipole moment of the top quark (bottom right)

This thesis explores theoretically motivated extensions of the Standard Model (SM) in both supersymmetric and non-supersymmetric contexts. New physics is probed through direct signatures—such as light BSM Higgs production via gluon fusion, rare Z decays, and dark matter (DM) detection—and indirect effects, like deviations in precision observables (e.g., the muon g−2, chromomagnetic moment of top quark, and the Higgs decay $h_{SM} \rightarrow Z\gamma$). A key focus is the role of radiative corrections at one- and two-loop levels, where BSM contributions significantly affect observable predictions. The main highlights of the thesis are:

(a) The lightest neutralino is a neutral, weakly interacting particle and a strong DM candidate in the R-parity conserving MSSM, often arising as a Bino, Wino, Higgsino or a mix of these. The Bino, defined by the parameter M_1, lacks direct gauge boson couplings and thus requires a Higgsino admixture to interact with Higgs bosons and produce detectable signals in direct detection experiments. This study calculates next-to-leading order (NLO) corrections to the DM-Higgs vertices (top left of Fig. 1), focusing on mostly Bino- and Wino like DM. By evaluating all the one-loop MSSM contributions and associated counterterms, the impact on spin-independent (SI) DM-nucleon scattering cross-sections is assessed. We found that the NLO corrections to the cross-section can be up to 20% for Bino-like DM and can exceed 100% for Wino-like DM. Also, for Wino-like DM, we identified the blind spot in direct detection at both LO and NLO.

(b) We have studied the rare Z boson decays into a photon and either a CP-even or CP-odd scalar (top right of Fig. 1), focusing on the NMSSM framework to identify parameter regions that maximize the branching ratio. It highlights that the decays $Z \rightarrow H_1\gamma$, $A_1\gamma$ serve as valuable complementary probes with $h_{SM} \rightarrow Z\gamma$ decays, and presents benchmark points consistent with deviations observed by ATLAS and CMS.

(c) At leading order, a scalar that is mostly an SM singlet is produced primarily through gluon fusion via its mixing with the $SU(2)_L$ scalar doublet, since the singlet component itself does not contribute directly to production. For such a scalar with mass below that of the SM-like Higgs, the dominant NLO corrections to the production cross-section can be up to 7% compared to the LO value (bottom left of Fig. 1).

(d) We have presented analytical expressions for the anomalous chromomagnetic moment of a quark at both one-loop and two-loop levels (bottom right of Fig. 1) using model-independent parameterizations, with an off-shell external gluon. We applied these results to various two-Higgs-doublet models, evaluating the contributions to chromomagnetic moment of top quark at different gluon momentum transfers ($q^2 = \pm M_Z^2$ and 0). The findings show that one-loop contributions are $O(10^{-3})$, while two-loop contributions are $O(10^{-4})$ and interfere destructively with the one-loop contributions.

7.5.3 *Tailoring resistive switching properties of metal oxide memristors for neuromorphic applications*

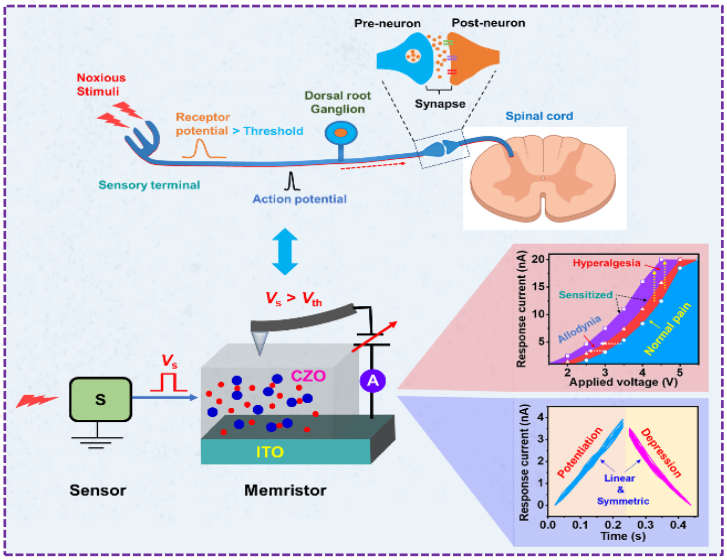

The proposed artificial nociceptor capable of "on-receptor computing" consisting of a CZO memristor at nanoscale using cAFM

Mimicking biological brain-like functionalities in memristor is the most sought-after attribute leading to the recent development of neuromorphic devices for advanced computing applications. The intrinsic defects in the form of oxygen vacancy (O_V) or metal ions vacancy play a decisive role to decide the resistive switching (RS) property and artificial synaptic functionalities of an oxide-based memristor. This thesis investigates the resistive switching behaviour of various binary metal oxide-based memristors through defects engineering approaches, employing conducting atomic force microscopy (cAFM) and conventional bulk

measurement techniques to explore their potential applications in neuromorphic devices. The main highlights of this thesis are:

(a) The Cu-doped ZnO (CZO) memristors exhibit stable, forming-free, bipolar RS characteristics with improved ON/OFF ratios, higher endurance, and excellent uniformity. The observed superior performance is attributed to the formation and stability of conducting filaments influenced by copper-oxygen vacancies (Cu-O_V complexes). The devices demonstrate bio-synaptic functions and nociceptive behavior, which is crucial for on-receptor computing applications.

(b) The sputter-grown WO_{3-x} memristors exhibits excellent memristive and bio-synaptic behaviours when they are grown as nano-columnar structure by employing glancing angle-deposition (GLAD) technique as compared to their uniform thin film counterparts. The improved electrical behavior is found to be arising from a more controlled O_V migration through the nano-columns due to their higher concentration inside the nano-columns.

(c) The CuO_x memristors demonstrate variable RS behaviours depending on the crystalline phase, which is affected by growth angle variations; while lower growth angles often result in unstable Cu filament formation, glancing angle growth yields devices with stable bipolar RS and enhanced bio-synaptic functions due to effective Schottky barrier modulation.

(d) The studies on bilayer memristors (WO_{3-x}/CuO_x and WO_{3-x}/CZO) reveal significant performance enhancements regarding stability, ON/OFF ratios, and retention when compared to single-layer devices. Impedance spectroscopy insights indicate that in the WO_{3-x}/CZO configuration, CZO effectively acts as a virtual electrode during switching.

7.6 Institute for Plasma Research

7.6.1 *Study of edge plasma dynamics in tokamak Aditya-U*

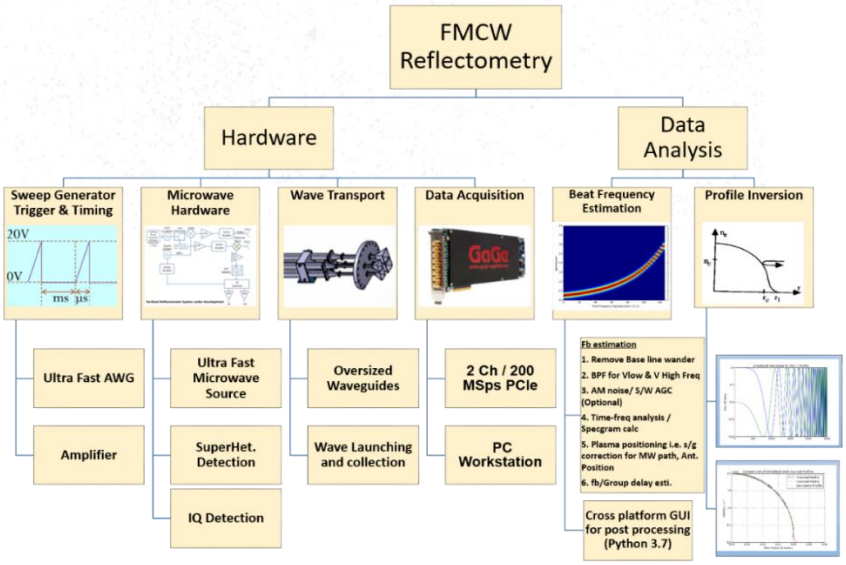

Frequency Modulated Continous Wave Reflectometry system developed for Aditya-U tokamak

One of the critical physics challenges is the understanding of the edge plasma dynamics in tokamaks. Edge plasma dynamics is the interplay of magnetic field, velocities parallel perpendicular and parallel to the magnetic field and the non-linear dynamics between local electron densities and electrostatic plasma potential. Confinement of plasma in the core depends significantly on the edge dynamics as fuelling, external heating and exhaust occur only through the edge. A prime example is the observation of the H-mode when external heating crosses a certain threshold. To enable us to measure the transition to the H-mode a reflectometer diagnostic was developed which is requires a state-of-the-art microwave detection system, an advanced digital signal processing algorithm in addition to complex electronics for driving and acquiring the data. The complete system was developed and deployed on the indigenous Aditya-U tokamak. To understand the measurement results a Pseudo-Spectral code was developed which enable numerical experiments using simple models of turbulence. These simulations show that for the density profile measured from the FMCW reflectometry an inverse cascade of turbulent eddies is seen. It is also found that the plasma potential decays as k-3.5 which matches with other published work and also with experiments.

7.6.2 *Turbulent dynamo action in a 3-dimensional magneto hydrodynamic plasma*

This Thesis addresses several of the important issues including turbulence and magnetic field generation in various astrophysical systems. To this end, highly efficient parallel numerical solver GMHD3D is developed to address these complex problems. In this Thesis work, I have initially examined the turbulent characteristics of different flows in both two and three dimensions. The influence of fluid helicity on kinematic dynamo action has been studied utilizing these flow fields. Using direct numerical simulation, I demonstrate that by controlled injection of fluid helicity, a systematic route emerges that connects “non-dynamo” to “dynamo” regime. However, for a nonlinear dynamo or self-consistent dynamo model, the nonlinear effects start to change the flow (once the magnetic field is large enough) to stop further growth in magnetic field energy, i.e, the flow and magnetic field “back react” on each other leading to nonlinear saturation. The influence of helical and non-helical drive in such a nonlinear or self-consistent dynamo model is shown to have some crucial dynamics. Evidence of small-scale dynamo activity is found for both helical and non-helical drives. The spectrum analysis shows that the kinetic energy evolution adheres to Kolmogorov’s $k^{-5/3}$ law, while the magnetic energy evolution follows Kazantsev’s $k^{3/2}$ scaling. These scalings are observed to be valid for a range of magnetic Prandtl numbers (P_m). Statistical analysis is found to support our numerical finds. We have also investigated the shear dynamo action using a kinematic dynamo model. Specifically, we find that in the absence of shear flows, the considered non-helical flow is unable to induce exponential amplification of magnetic energy. Interestingly, when the flow shear is introduced, it is found that the small scale non-helical base flow produces magnetic energy that grows exponentially with time.

7.6.3 *Study of process parameters affecting secondary phase formation and grain size in Cu_2ZnSnS_4 thin film for solar cell application*

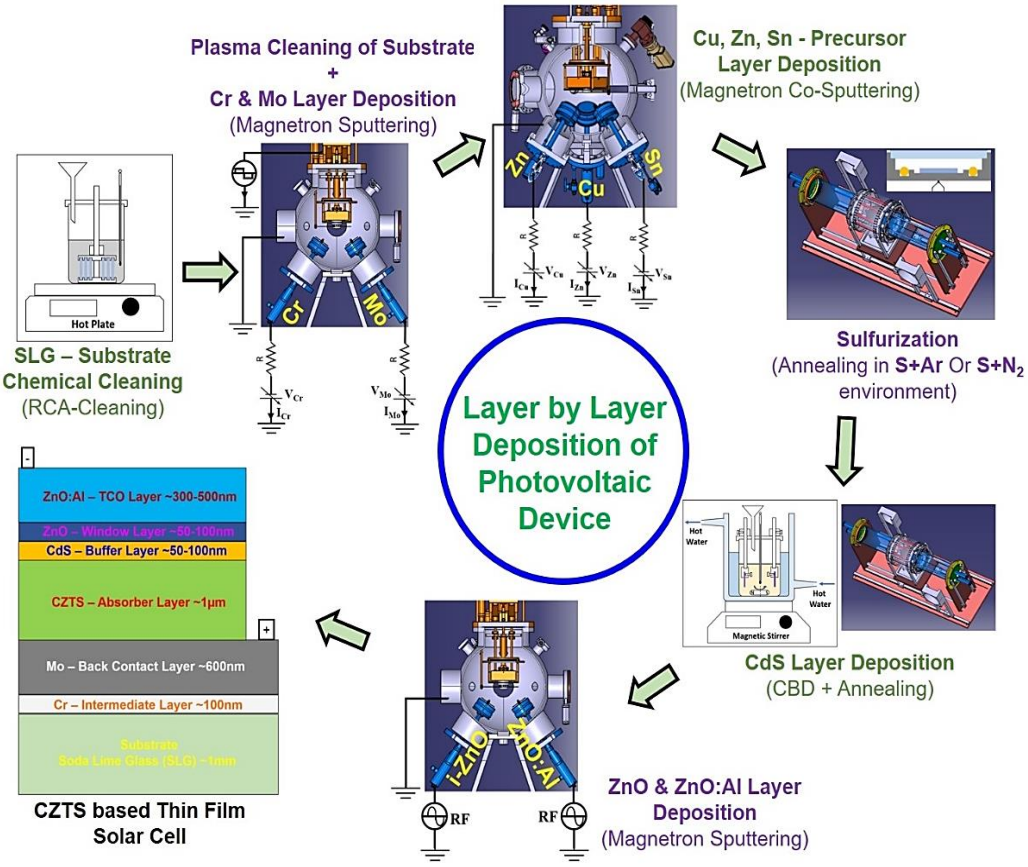

Schematic of layer-by-layer deposition process for the preparation of solar cell (PV) device

The present thesis is motivated by the need for understanding the factors affecting solar cell efficiency especially those related to CZTS (Cu_2ZnSnS_4) absorber material based thin-film solar cells (TFSCs). The preparation of the CZTS layer in the present work involves a two-step process, starting with magnetron co-sputtering of Cu, Zn, and Sn (thin film precursor) followed by sulfurization (*i.e.*, annealing in S + N_2/Ar environment). The issue of formation of secondary phases, such as ZnS, SnS, SnS_2, CuS, Cu_2S, Cu_2SnS_3, Cu_3SnS_4, etc., which affect the absorber layer's electrical and optical properties and hence the efficiency of solar cell devices, is addressed. Understanding the formation mechanism of these secondary phases during the growth of CZTS thin film, including its grain growth, is crucial for creating high-efficiency solar cells. The thesis explores the influence of various process parameters on CZTS layer properties, secondary phase formation, and grain size, demonstrating their impact on device efficiency through the fabrication of a multilayer solar cell device (SLG/Cr/Mo/CZTS/CdS/i-ZnO/ZnO:Al as shown in Figure 1) and simulation studies. XANES spectroscopy is extensively employed in the current work to estimate the secondary phases in CZTS layer because of the limitations of commonly used XRD and Raman spectroscopy methods for a tangible, decisive analysis. Following points highlight the key findings of the thesis:

1. Although all the process parameters like sulfurization pressure, heating rate, etc., affect the secondary phase formation, the elemental composition of the precursor is observed to be the most dominant factor affecting the secondary phase formation and hence the efficiency of device.
2. The secondary phases having a bandgap close to the CZTS (like CTS) are found to be more efficiency-deteriorating compared to the secondary phases with a much higher bandgap than the CZTS (like ZnS), which is one of the novel findings of the thesis.
3. Another unique finding of the thesis is the effect of ambient gas (N_2/Ar) of the sulfurization process on the grain size of the absorber layer and hence, on the efficiency of the device.

7.7 National Institute of Science Education and Research, Bhubaneswar

7.7.1 *Spin pumping with quantum materials*

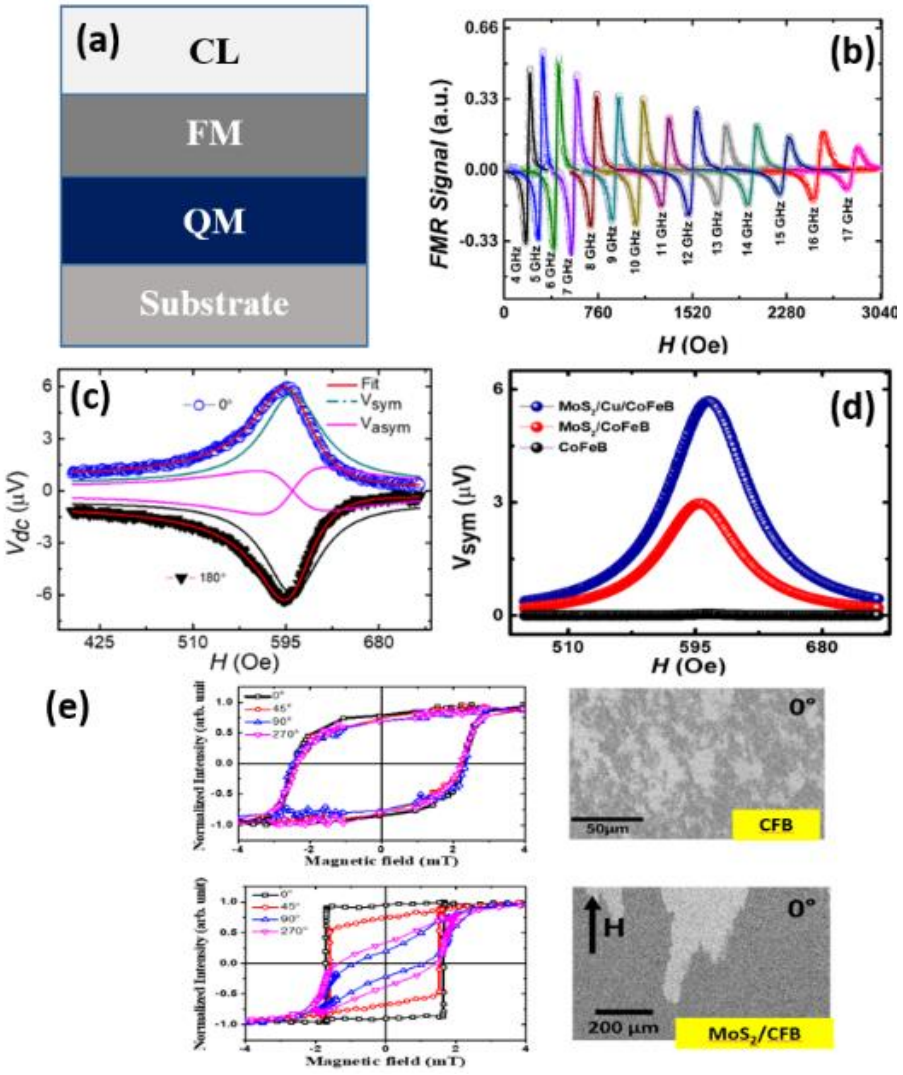

(a) Schematic of the FM/QM heterostructure capped with a capping layer (CL). (b) Frequency dependent ferromagnetic resonance spectra (c) Reversal of voltage signal in spin pumping (d) Enhanced spin pumping due to insertion layer (e) Modified anisotropy due to the presence of QM

Quantum materials (QM), such as transition metal dichalcogenides (TMDs), topological insulators (TIs), and altermagnets (AMs), offer a promising alternative to heavy metals in spin-orbit torque (SOT)-based magnetic random-access memory (M-RAM). Traditional SOT devices rely on high spin-orbit coupling (SOC) metals like platinum, which, while efficient, introduce challenges related to material scarcity and energy dissipation. Quantum materials, on the other hand, can provide comparable or even superior spin-to-charge conversion while introducing additional functionalities such as interface-driven anisotropy and long spin diffusion lengths. By leveraging their unique electronic and spin properties, these materials could enhance energy efficiency and scalability in next-generation M-RAM devices.

In this thesis, we focused on using MoS_2 as a transition metal dichalcogenide (TMD), Bi_2Se_3 as a topological insulator (TI), and RuO_2 as an altermagnet (AM) to explore their viability as replacements for conventional heavy metals in SOT-based applications. Using spin pumping, a non-invasive technique for studying spin dynamics, we assessed their efficiency. TMDs are typically synthesized as monolayers or in few-layer forms using mechanical exfoliation or chemical vapor deposition.

However, these techniques often limit film continuity and scalability. To address this, we successfully prepared large-area, continuous thin films of MoS_2 using magnetron sputtering, enabling broader functional exploration. Our spin pumping experiments, where spins were injected from the ferromagnet (FM) CoFeB (CFB) into the MoS_2 layer, revealed a high inverse spin Hall effect (ISHE) voltage signal and a spin Hall angle. Additionally, MoS_2 exhibited a spin diffusion length of 7.83 nm and induced anisotropy in the otherwise isotropic CoFeB layer, likely due to orbital hybridization at the interface.

To further enhance spin-to-charge conversion efficiency, we introduced a copper (Cu) spacer layer between MoS_2 and CoFeB. Cu, known for its long spin diffusion length, significantly improved the spin Hall angle of MoS_2 from 0.02 to 0.30. Similarly, we explored Bi_2Se_3-based heterostructures with Co_2FeAl (CFA), a highly spin-polarized Heusler alloy. Bi_2Se_3/Co2FeAl films demonstrated efficient spin pumping with a spin diffusion length of 5.6 nm and a spin Hall angle of 0.048. Interestingly, the Bi_2Se_3 underlayer induced additional anisotropy in CFA, with an optimal thickness of 4 nm beyond which anisotropy declined due to surface state coupling effects.

The introduction of a Cu spacer layer further improved spin-to-charge conversion, yielding a 1.7-fold increase in spin pumping voltage and spin Hall angle. Finally, we investigated RuO_2, an emerging altermagnetic material, grown with a (110)-oriented structure on an MgO substrate. Our findings revealed a small spin memory loss (15%) and high interfacial spin transparency (90%), highlighting its potential for energy-efficient spintronic applications. These results collectively underscore the promise of quantum materials in replacing heavy metals for next-generation SOT-based M-RAM, offering enhanced spin transport properties, tunable anisotropy, and improved scalability for future spintronic devices.

7.7.2 *Studying chiral magnetic wave, hadronic rescattering and f1(1285) production in high energy collisions with ALICE detector*

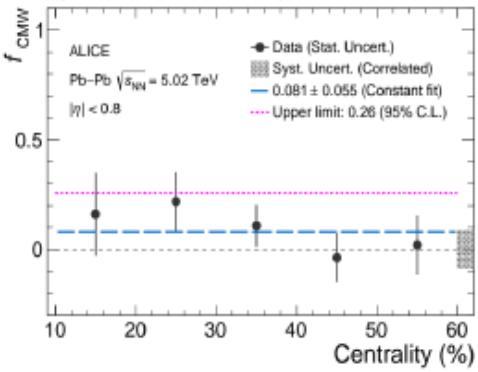

Centrality dependence of the extracted CMW fraction. The upper limit with 95% confidence level is shown by the magenta dotted lines

Quantum Chromodynamics (QCD) predicts that at very high temperatures or densities, quarks and gluons become deconfined, forming a quark-gluon plasma (QGP). This state can be created in ultra relativistic heavy-ion collisions, generating intense magnetic fields (~1015 Tesla) from the relativistically moving spectator protons. These fields allow the exploration of novel QCD phenomena, such as chiral symmetry restoration and parity violation. QCD interactions between quarks and gluonic fields can cause transitions between different topological states of the QCD vacuum, leading to a local chiral imbalance. In a strong magnetic field, this results in a phenomena known as Chiral Magnetic Wave (CMW), which induces an electric quadrupole moment, affecting the eliptical flow v2. This effect can be obscured by background effects, primarily Local Charge Conservation (LCC), which can be investigated by measuring v3. We present measurements of v2 and v3 in Pb-Pb collisions at 5.02 TeV. The slopes of the normalized difference in v2 (r2Norm) and v3 (r3Norm) for positively and negatively charged particles are determined as a function of their eventwise normalized number difference. Our results show that r2Norm and r3Norm are consistent within uncertainties. A blast wave parameterization including LCC accounts for the magnitude of r2Norm, indicating significant background contribution. Additionally, we establish an upper limit of 26% for the fraction of the CMW signal at the 95% confidence level.

Furthermore, the study of hadronic resonance production provides insights into the late-stage evolution of heavy-ion collisions. The short lifetime of the K*resonance (~4 fm/c) makes it a useful probe for examining the hadronic phase properties, as its yield is affected by interactions between its decay products and the surrounding medium. We studied for the first time K*+/- production at mid-rapidity for various centralities in Pb-Pb collisions at 5.02 TeV. Recent high multiplicity pp collisions show similarities to heavy-ion collisions, prompting us to also study K*0 production as a function of charged particle multiplicity in pp collisions at 5.02 TeV. Our comparative analysis explores system size dependency across different collision systems. The K*/K yield ratio is found to decrease with increasing charged particle multiplicity due to re-scattering effects of K* decay daughters in the hadronic phase. Finally, we studied for the first time in ALICE an inclusive measurement of the production cross-section of the exotic candidate, f1(1285) meson at mid-rapidity in pp collisions at 13 TeV. We provide measurements of its pT spectra, integrated yield, and <pT>. Comparing its yield with other

charged particles and calculations from canonical thermal model offered insights into its quark composition.

7.7.3 *Relativistic dissipative causal magnetohydrodynamics from kinetic theory and the effect of electric fields on bulk observables in high-energy heavy- ion collisions*

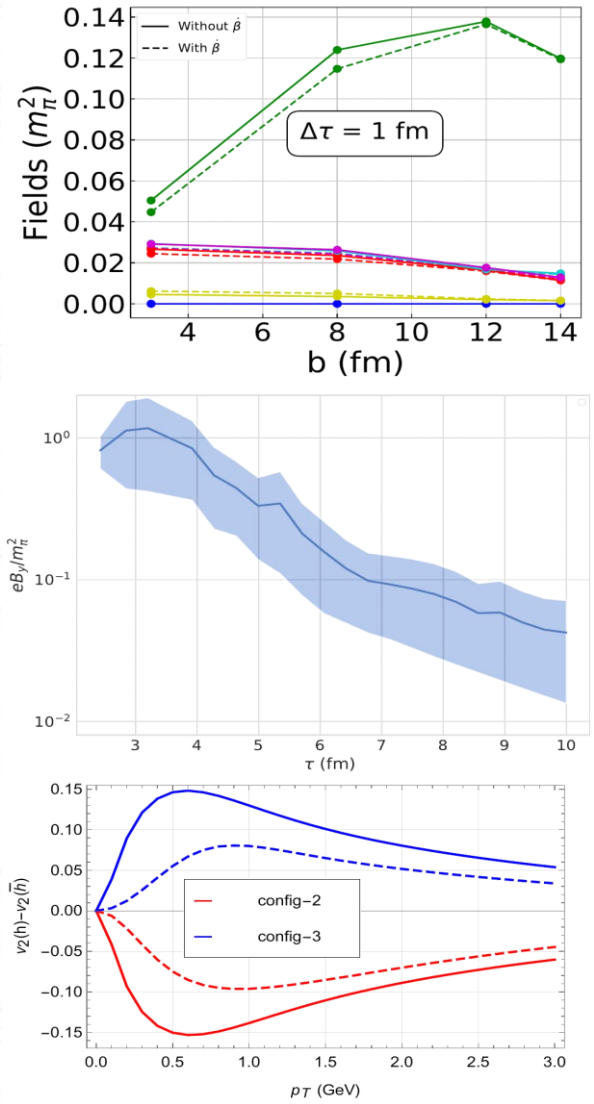

(Upper) EM field with impact parameter, (middle) eB_y with time (participant charges) and (lower)Δ v2 with pT for pions (solid), protons (dashed)

In high-energy heavy-ion collisions, two relativistic heavy nuclei undergo Lorentz contraction and collide, forming a Quark Gluon Plasma (QGP), a deconfined state of quarks and gluons. Initially, the QGP exists in a highly non-equilibrium state from which it rapidly evolves towards equilibrium where it can be described well assuming it as a fluid, after which it expands and cools. This fluidic expansion and cooling process is successfully described by relativistic viscous hydrodynamics. As it cools and expands, the QGP transitions into hadrons through hadronization, with these hadrons continuing to interact until they cease collisions and stream freely into detectors. Alongside the QGP, an intense transient magnetic field is generated by spectators—nucleons that are not directly involved in the collision. Theoretical models predict that the magnitude of this magnetic field can reach as high as 10^{14}-10^{15} Tesla in non-central

collisions at RHIC and LHC energies, opening the door to the study of various novel phenomena such as the CME, CSE, and CMW. Since the QGP consists of charged particles, it exhibits finite conductivity and responds to external electromagnetic fields, thus altering these fields themselves. Hence, studying such interactions between the fluid and EM fields becomes crucial, and relativistic magnetohydrodynamics (RMHD) offers a comprehensive framework for such analysis.

As the medium is affected the transport properties, which govern the QGP's non-equilibrium behavior, are largely likely to be influenced by external electromagnetic fields. In this work, by solving RMHD equations, the effects of these fields on transport coefficients, particularly shear, bulk, and diffusion, are examined. The results show that electromagnetic fields introduce anisotropy in the transport coefficients at the leading order. However, we also developed causal second-order RMHD evolution equations using RTA as the collision kernel. Apart from spectator charges, the study here also focuses on electromagnetic fields generated by charged participants, exploring their spatio-temporal evolution. Unlike the fields generated by spectators, those from participants first increase and then decrease over time. A comparison suggests that fields from participants dominate at later stages, highlighting their importance in the overall dynamics of the medium at a later stage. At lower center-of-mass energies such as at FAIR energies, nuclear stopping becomes prominent as is predicted in experiments, where the decelerating nucleons start accumulating in the mid-rapidity region. This deceleration would certainly impact the EM fields, particularly at low energies. Thus, by incorporating an energy-dependent stopping power into a Monte-Carlo Glauber model, the effects of baryon stopping on the electromagnetic fields are seen at lower energies. Here a sizable difference is seen at more central and lower collision energies while studying the EM fields against impact-parameter and centre of mass energies. Finally, the effect of electric fields on bulk observables, such as particle spectra and flow harmonics, is investigated using a blast wave model. Here flow harmonics are studied by taking various electric field configurations on the transverse plane of the freeze-out surface. A key observation is the behaviour of with pT for protons and pions, which increases with transverse momentum and saturates around 3 GeV. Moreover in case of directed fields (predicted to be present in case of asymmetric collisions like p+ Au, d+ Au etc), the mirror symmetry of charged particle multiplicity is broken in the azimuthal plane. This gives rise to additional parity odd terms in the fourier expansion.

7.8 Raja Ramanna Centre for Advanced Technology

7.8.1 *Studies on Al_2O_3/TiO_2 nano-laminates for energy storage applications*

Considering the growing demand for new high-k and low dielectric loss (*tanδ*) materials, in this thesis work, a pulsed laser deposition (PLD) and thermal atomic layer deposition (ALD) technique are optimised to fabricate $Al_2O_3/TiO_2/Al_2O_3$ nanolaminate (ATA NL) based device-grade metal-insulator-metal capacitors (MIMCAPs). A detailed interfacial characterization of the as-grown NLs are carried out to correlate the structural and dielectric properties. The interface-confined carrier relaxation and sublayer conductivity contrast-induced Maxwell-Wagner (M-W) relaxation mechanism was engineered by precisely tailoring the individual sublayer thickness (t_s). The leakage current density and cut-off frequency of NLs are tailored by adding appropriate top-bottom Al2O3 capping layer thickness across electrode/NL interfaces. The relative response of oxygen vacancy-generated carriers in Titania sublayers is

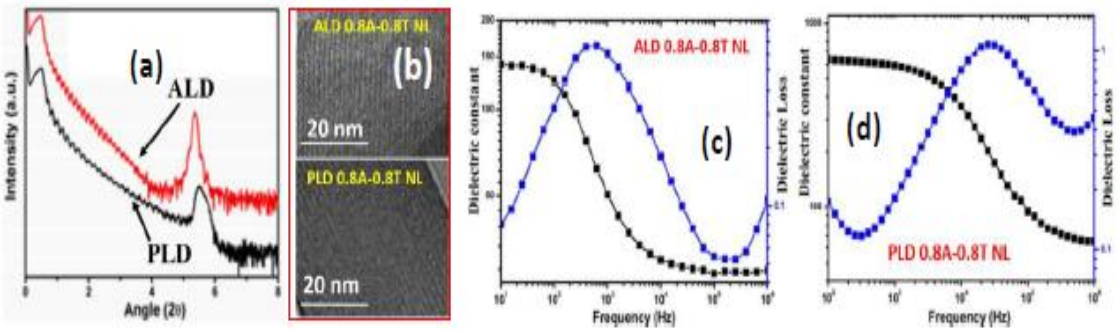

(a) XRR profiles and (b) Cross-sectional TEM image of ALD and PLD ATA NL with 0.8 nm sublayer thickness (0.8A/0.8T NL). Frequency dispersed dielectric constant and dielectric loss spectra for (c) 0.8A-0.8T NL, (d) PLD 0.8A-0.8T NL

assigned responsible for both charge storage and leakage. The frequency dependent small polar hopping and quantum tunnelling transport mechanism in NLs were confirmed from the temperature dependent AC conductivity and current-voltage measurements, respectively, which is further validated using resonant photoelectron spectroscopy measurements. While comparing the ALD and PLD grown ATA NLs of similar t_s, the PLD NLs demonstrated higher-k values, although exhibiting slightly higher interface interdiffusion, as shown in figure below. The optimised PLD NL with TiO2 and Al_2O_3 sublayer thickness combination of ~1 and 0.6 nm, respectively, sandwiched between ~ 3 nm Al2O3 barrier layers and top-bottom Pt electrode demonstrated an improved capacitance density (~ 37.5 fF/μm^2) and corresponding volumetric energy storage density (~ 4.6 J/cm^3), which is comparable to the state-of-the-art capacitive devices. Furthermore, this optimised capacitor displayed a high cut-off frequency (~ 1 MHz), low dielectric loss (~ 0.016), small quadratic voltage coefficient of capacitance (−121 ppm/V^2), linear coefficient (−116 ppm/V), together with a temperature coefficient of 80 ppm/°C, and reduced leakage current density (~ 6.08 x 10^{-8} A/cm^2 at 1V). These values are very close to reaching all the requirements set by international technology road-map of semiconductors (ITRS) for capacitors, which renders this NL as a promising candidate for next generation energy storage applications.

7.8.2 *Investigation of ultrafast structural dynamics in solids using time-resolved X-ray diffraction*

Understanding of various ultrafast phenomena such as phase transition, coupling of different subsystems (e.g., electron and phonon, etc.), sound propagation, carrier diffusion, and heat transport and their timescale requires monitoring of ultrafast structural dynamics. Also, a constant demand to increase the computational power of semiconductor chips either by miniaturization or by increasing their clock speed results in high heat density (>10^6 W/m^2), which requires understanding of the response and heat dissipation characteristics of semiconductor materials for next-generation electronic device applications. The thesis work focuses on the thermal strain propagation (which in turn gives the information of heat dissipation) in group IV and group III-V semiconductors and nonlocal probing of amplitude mode dynamics in novel $EuTe_4$ in its charge density wave (CDW) phase after photoexcitation using the time-resolved X-ray diffraction (TXRD, an

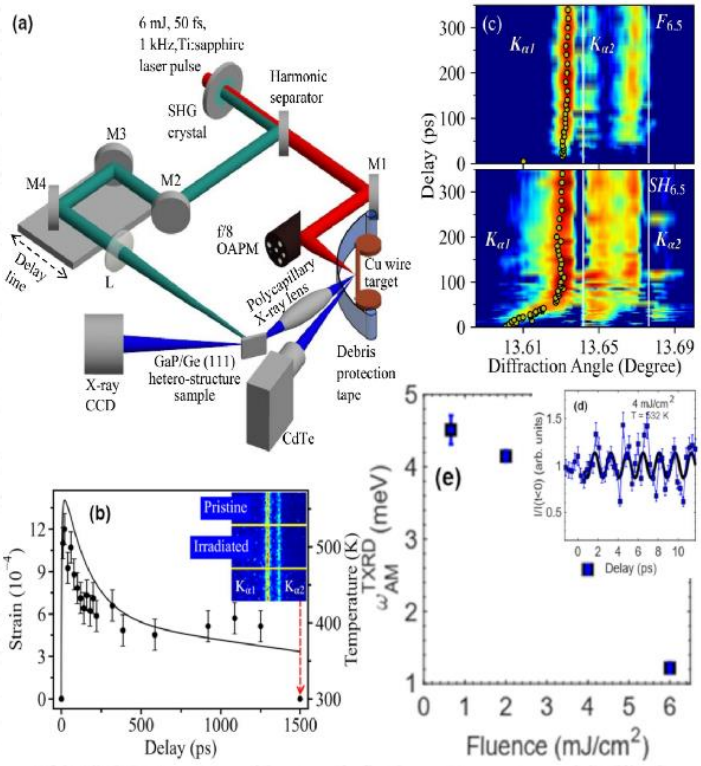

(a) TXRD setup, (b) Thermal strain evolution in InSb (111) crystal. (c) Effect of excitation wavelengths in Ge (111) and observation of DP effect for SH pump (d) oscillation of CDW peak's intensity (AM) after excitation and (e) its variation with fluence

optical pump-X-ray probe) technique (setup is shown in Fig. 1(a)). Here, the ultra-short (fs) Cu Kα X-ray probe is generated by the interaction of ~50 fs, 1kHz Ti:sapphire laser pulses with a Cu wire target. A Laue diffraction pattern is recorded for the first time using such a source by increasing its spectral range. At first, the thermal strain evolution in InSb (111) ample was studied, which shows lattice expansion (recovers at ~1.5 ns delay) after photoexcitation due to crystal heating (Fig. 1(b)). Next, the effect of different (viz., [100] and [111]) directions and excitation wavelengths (viz., 800 nm (F) and 400 nm (SH), Fig.1(c)) on strain generation and propagation in Ge crystal was investigated. Similar strain propagation velocity is observed in both directions, which increases with an increase in excitation fluence. Due to the high energy of excited electrons for SH excitation, these electrons get trapped in higher conduction band valleys, which in turn gives rise to long-lasting (~100 ps) deformation potential (DP)-induced strain (earlier, it was reported for <1ps). Subsequently, the heat transport in GaP/Ge(111) hetero-structure was studied, which indicates the trapping of heat in the GaP epilayer due to impedance mismatch at the GaP/Ge interface. Finally, the TXRD study (in transmission geometry) of a novel $EuTe_4$ sample in its CDW phase is performed. The elastic and inelastic X-ray scattering measurements were performed to identify its CDW peaks and phonon frequencies. TXRD study of $EuTe_4$ shows that the CDW peak's intensity oscillates with time (Fig. 1(d)), revealing nonlocal amplitude mode (AM) dynamics. The oscillation frequency matches with the AM frequency (ω^{AM}), which decreases with laser excitation fluence owing to a rise in the sample temperature (Fig. 1(e)). The nonlocal behavior of the AM is from

propagating phonon-polariton, observed for the first time in any CDW compound due to the polar nature of the AM.

7.8.3 *First-principles studies on electronic, magnetic, and spin transport properties of bulk and heterostructures of heusler alloys*

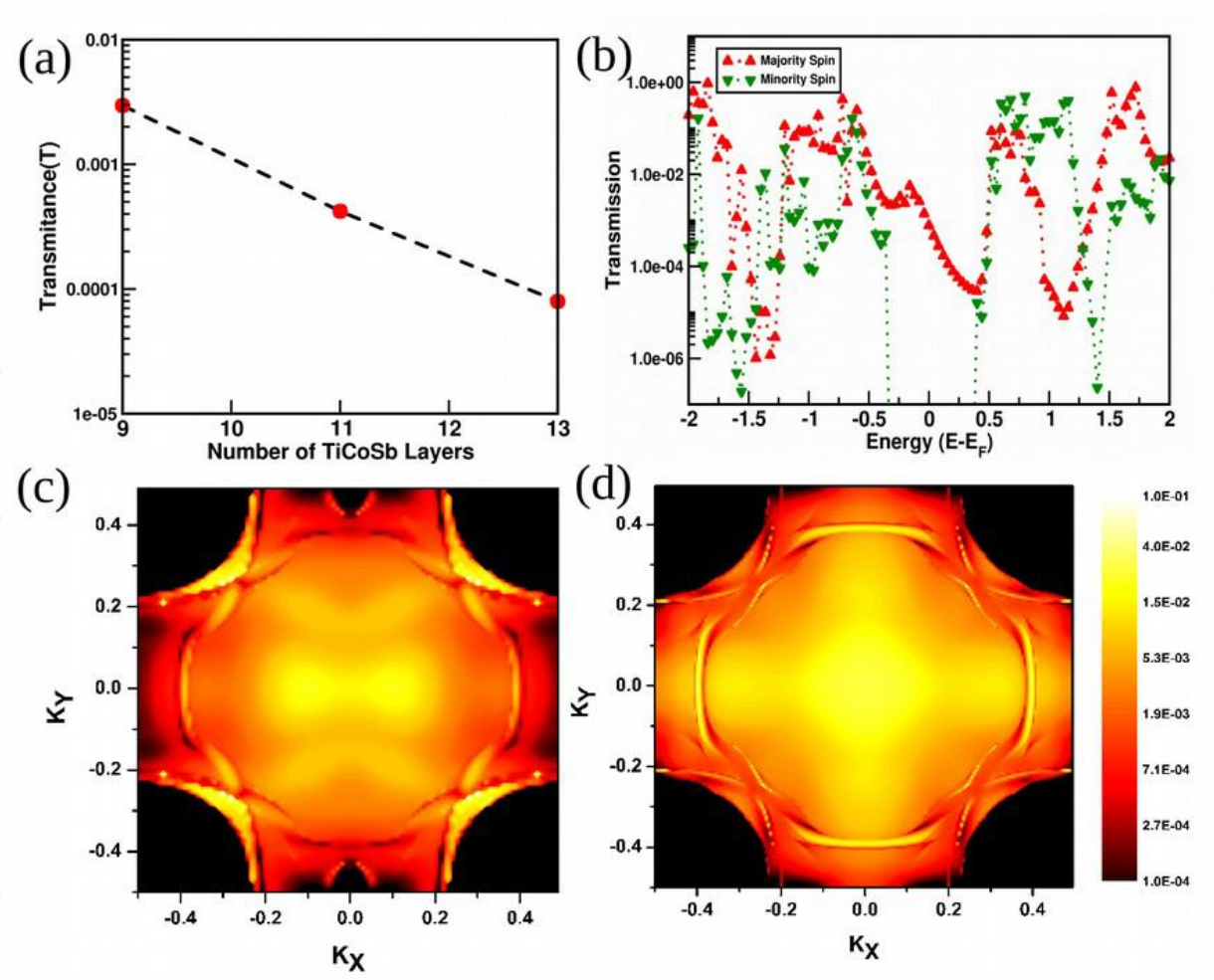

Transmission properties of Co2MnSb/TiCoSb heterojunction; Transmission as function of (a) Barrier layer thickness; (b) Incident electron energy; K|| (c) Mn-Sb, (d) Mn-Mn interface The

Heusler alloys have shown superior performance for various applications. Spintronics is one such field. Magnetic tunneling junctions (MTJs) form the cornerstone of many cutting-edge spintronic devices, crucial for applications in random access memory, spin transfer torque devices, and next-generation neuromorphic computing. These devices, comprising two ferromagnetic (FM) electrodes separated by a non-magnetic insulator or semiconductor spacer, have been at the forefront of recent research. The tunneling magnetoresistance (TMR) of MTJs is highly sensitive to the relative spin orientations of the electrodes (parallel (P) or anti-parallel (AP)), enabling the electric readout of magnetically stored information. The TMR ratio, a key performance metric, is defined as the difference in conductance between the two magnetic orientations, normalized by the smaller conductance value.

In this thesis, we work on predicting new Heusler alloys with interesting and desirable electronic and magnetic properties. Our work resolves the long-standing controversy of the structure of the martensite phase of well-known Heusler alloy, Ni_2MnGa. We explore the magnetic properties of transition metal adlayers on the surfaces of Heusler alloys. Our work

showcases interesting aspect of two-dimensional magnetism. Most important work of this thesis deals with the demonstration of the potential of designing an all-Heusler alloy-based MTJ using semiconductor TiCoSb and HfIrSb alloys as spacer materials. Our investigation reveals that the half-metallic (HM) properties of the Mn–Sb/Co interface are robust, even in the presence of various disorders and defects. The spin-dependent transport behavior indicates that these properties are highly sensitive to the heterojunction interfaces and the thickness of the spacer material. In these insulating materials, the smallest complex band decay coefficient is associated with Δ_1(s, p_z, d_z^2 orbital) symmetry, enabling desirable symmetry-based spin-filtering properties at the Γ point in the 2D Brillouin zone. We further calculate the resistance area (RA) product for all heterojunctions, which is crucial for the development of highly sensitive magnetic sensors. Our findings show that other commonly used spacer layers yield an RA product several orders of magnitude higher compared to the Heusler alloys TiCoSb and HfIrSb. With their chemical compatibility leading to minimal interface buckling and an ultra-low RA product, TiCoSb and HfIrSb may turn out to be promising materials for MTJs with Co_2MnSb electrodes, particularly in overcoming variability and current-injection challenges.

7.8.4 *Studies on cooling and trapping of Rb atoms on atom chip*

In the thesis, we have described the in-house development of an atom chip setup for cooling and trapping of Rb atoms. Further, experiments with cold atoms on atom chip have been discussed in detail. The atom chip has been designed and developed indigenously. The atom chip has been initially used for the realization of a magneto-optical trap (MOT) to generate cold atoms. Fig. 1 shows the schematic of the vacuum system for the atom chip experimental setup. The effect of quadrupole field distribution due to copper U-wire and bias fields was investigated on loading of cold ^{87}Rb atoms in the U-MOT. The loading of cold atoms in an ultra high vacuum (UHV) environment was investigated in detail. A new methodology was developed to estimate the UHV pressure in the chamber from MOT loading data. The background non-rubidium UHV pressure as low as 1.1 x 10^{-10} Torr was estimated.

We have employed Stern-Gerlach technique to separate and detect atoms in different Zeeman hyperfine states (m_F) in the cold atom cloud. Fig. 2 (a) shows the CCD image of population of atom cloud in m_F states. Utilizing this SG technique, the efficiency of optical pumping process was quantified. Nearly 92 % of the cold ^{87}Rb atoms were optically pumped to the trappable Zeeman hyperfine state ($F = 2$, $m_F = +2$) as shown in Fig. 2 (b). These optically pumped cold ^{87}Rb atoms were finally trapped in a micro-trap due to gold z-wire on the atom chip as shown in Fig. 3. After the trap was formed, possible processes affecting the lifetime of atoms in the trap were investigated.

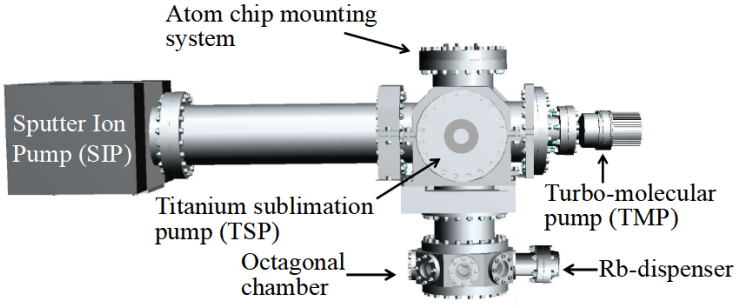

Schematic of the UHV system for atom chip experimental setup

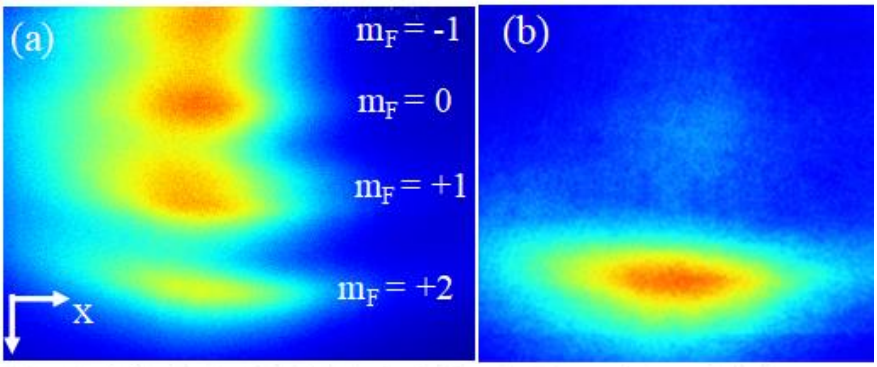

The CCD images of atom cloud under Stern- Gerlach force showing the distribution of population of ^{87}Rb atoms in different m_F state: (a) without optical pumping, and (b) with optical pumping pulse of duration ~ 500 µs

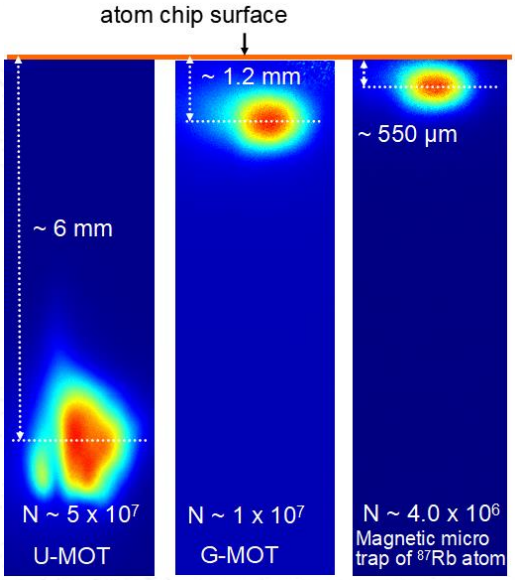

CCD images of cold ^{87}Rb atoms in U-MOT, G-MOT and magnetic micro-trap

7.9 Saha Institute of Nuclear Physics

7.9.1 *Investigation of exchange bias and magnetotransport in bulk and thin films materials*

Recent advancements in science and technology have significantly increased the demand for materials exhibiting giant exchange bias (EB) and magnetoresistance, which are essential for applications in spin valves, high-density magnetic storage, and sensors.

Magneto-transport studies have uncovered the presence of a super spin zone gap in certain incommensurate antiferromagnets, where an applied magnetic field induces a notable jump in magnetoresistance. The present research focuses on understanding the effects of defects, disorder, distortion, and structure on EB and magnetotransport properties by preparing and characterizing various systems.

Oxygen-deficient $SrFe_{0.5}Co_{0.5}O_{3-\delta}$ was synthesized to investigate the impact of oxygen vacancies on EB. The introduction of vacancies mimics the effects of ion doping, resulting in enhanced EB due to interactions between ions of different charges. Additionally, non-magnetic Ir doping in $SrFe_{0.5}Co_{0.5}O_{3-\delta}$ further increased EB by reducing the size of magnetic clusters, achieving an EB of 1.86 T. To attain higher EB values, Sr_2CoRuO_6 was studied, revealing a giant EB of 2.36 T attributed to small ferromagnetic clusters pinned within an antiferromagnetic matrix and strong exchange coupling between Co and Ru.

The effects of size and thickness of ferromagnetic layers on EB were explored using a Gd/MnPt thin-film structure, where the thickness of the Gd layer was varied. This study highlighted the anisotropy dependence of EB and its relationship to the ferromagnetic layer's thickness. Further investigations into Sr_2FeIrO_6 and Sr_2CoIrO_6, both antiferromagnetic compounds, revealed EB effects not explained by conventional theories. Strong spin-orbit coupling and the Dzyaloshinskii-Moriya interaction were identified as potential mechanisms driving EB in these systems.

Hexagonal structures have recently gained attention for their potential in quantum materials. By introducing interacting ions into specific Wyckoff positions, substantial EB can be induced. Additionally, Monte Carlo simulations combined with experimental studies provided insights into the micromagnetic structure of complex systems, elucidating how cluster size, length, and next-nearest-neighbor interactions influence magnetization and EB.

Finally, the magnetic and transport properties of intermetallic materials $DyFe_2Al_{10}$ and $GdFe_2Al_{10}$ were explored. These materials exhibit a superzone gap caused by the non-trivial arrangement of antiferromagnetically ordered moments, resulting in giant magnetoresistance. $DyFe_2Al_{10}$ showed a 23% magnetoresistance at 6 K, increasing to 33% in $GdFe_2Al_{10}$ at 14 K. These findings underscore the significance of such materials in fundamental research and their potential applications in spintronic devices.

7.9.2 *Toy model of quantum black holes and correlation functions*

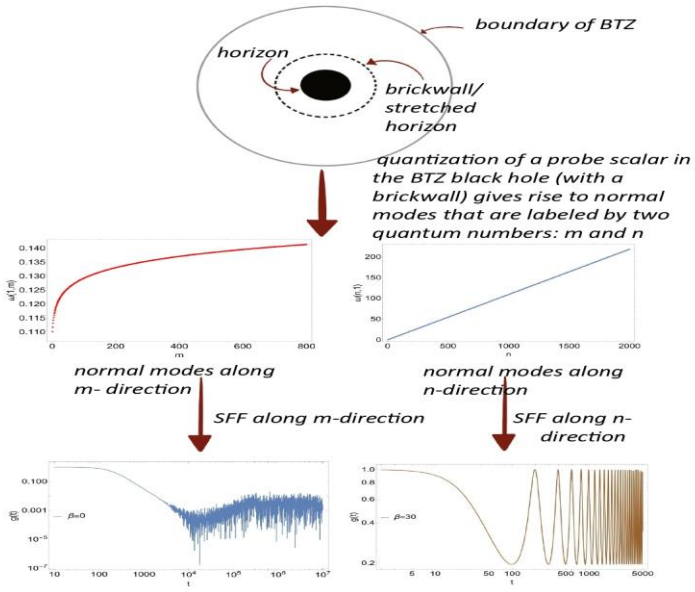

Schematic of the model and results

Black holes are thought to be chaotic. This idea is supported by the AdS/CFT correspondence, where black holes correspond to strongly interacting field theories on compact spaces, which are expected to exhibit chaos. However, proving this explicitly is challenging, both from the bulk perspective, and from the boundary field theory side. A simpler approach might be to explore signs of chaos in the probe sector. Out-of-time-ordered correlators (OTOCs) in black hole backgrounds reveal a positive Lyapunov exponent, indicating early-time chaos, but early-time chaos does not always imply chaos at late times. Thus, a key question is how to detect late-time chaos in the probe sector. Measures like the Spectral Form Factor (SFF) and Level Spacing Distribution (LSD) depend on the spectrum but straightforward quantization of a probe field in a black hole background yields quasinormal modes that lead to a vanishing SFF at late times due to the infalling boundary condition at the horizon.

String theory offers examples of fuzzballs / microstate geometries, which, unlike black holes, have no horizon but still resemble them from afar. Quantizing a probe scalar in these geometries could hint at chaos, but most known fuzzballs correspond to extremal black holes at zero temperature, where chaos is less relevant. This thesis proposes a toy model for "synthetic" fuzzballs by introducing a brick wall outside the horizon. Quantizing a scalar field in this setup produces real-valued normal modes that display a dip-ramp-plateau (DRP) structure in the SFF—a sign of RMT chaos—though the LSD is not of the Wigner-Dyson (WD) type. By generalizing the boundary conditions, the WD LSD can be achieved, which could model more realistic fuzzballs with fluctuations. These chaotic features are also observed in rotating BTZ black holes and persist unless the system is at extremality, where they vanish, and the spectrum becomes linear, consistent with microstate geometries. The thesis also demonstrates that certain deterministic sequences can mimic the DRP structure, with the logarithmic sequence showing a linear ramp. Finally, the thesis shows that as the stretched horizon nears the event horizon, the boundary Green's function increasingly resembles a thermal Green's function, assigning a temperature to the horizonless state that matches the Hawking temperature.

7.9.3 *Magnetic, magnetocaloric, electrical transport, and polarization study on various bulk and nanocrystalline oxide compounds*

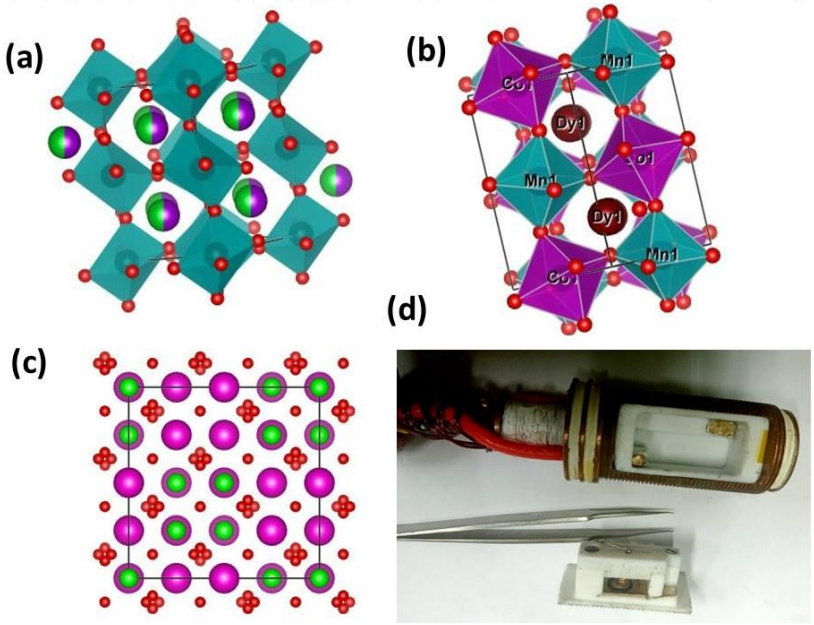

(a) Crystal structure of perovskite oxide, (b) Crystal structure of double-perovskite oxide, (c) Crystal structure of pyrochlore oxide, (d) fabrication of sample holder for electric polarization measurement of bulk sample at cryogenic temperature

In the thesis, research work is carried out on rare-earth and transition metal-based polycrystalline as well as nanocrystalline oxide materials having general formula $R_xB_yO_z$ (where R is rare-earth ions, B is transition metal ions and x, y, z are numbers). Here, a variety of oxides materials are discussed from the variety of structures, chemical nature of elements, and bonding characters, such as, RBO_3 types perovskite oxides (with orthorhombic structure in Fig. (a)), $R_2B_2O_6$ types double perovskite oxides (with monoclinic structure in Fig. (b)), and $R_2B_2O_7$ types pyrochlore oxides (with cubic structure in Fig. (c)). From crystal structure point of view, all studied oxide compounds are the member of Ruddlesden-Popper (RP) series with general formula $A_{n+1}B_nO_{3n+1}$ for $n \rightarrow \infty$. All these compounds have taken major research endeavours in the field of solid-state physics and material science due to the presence of strong relationship between structural, physical and electrical properties. In this thesis work, we will highlight the structural, magnetic, magnetocaloric, magneto-transport, and electrical polarization properties of rare-earth-based oxide systems. In perovskite system, the emergence of colossal magnetoresistance due to the melting of charge-ordered state is elaborately explained. Moreover, the emergence of charge ordered state due to lattice distortion and hence emergence of colossal magnetoresistance is also discussed in another perovskite system. Moreover, double perovskite systems are investigated for their multiferroic behaviour and pyrochlore systems are studied due to their geometric frustration. In addition, fabrication of a sample holder for polarization measurement of the bulk samples under 6kV (maximum limit 10 kV) external voltage at cryogenic temperature (bottom part is shown in Fig (d)) is produced during Ph.D tenure.

7.9.4 *Synthesis and characterizations of metal nanostructures for application in direct alcohol fuel cells*

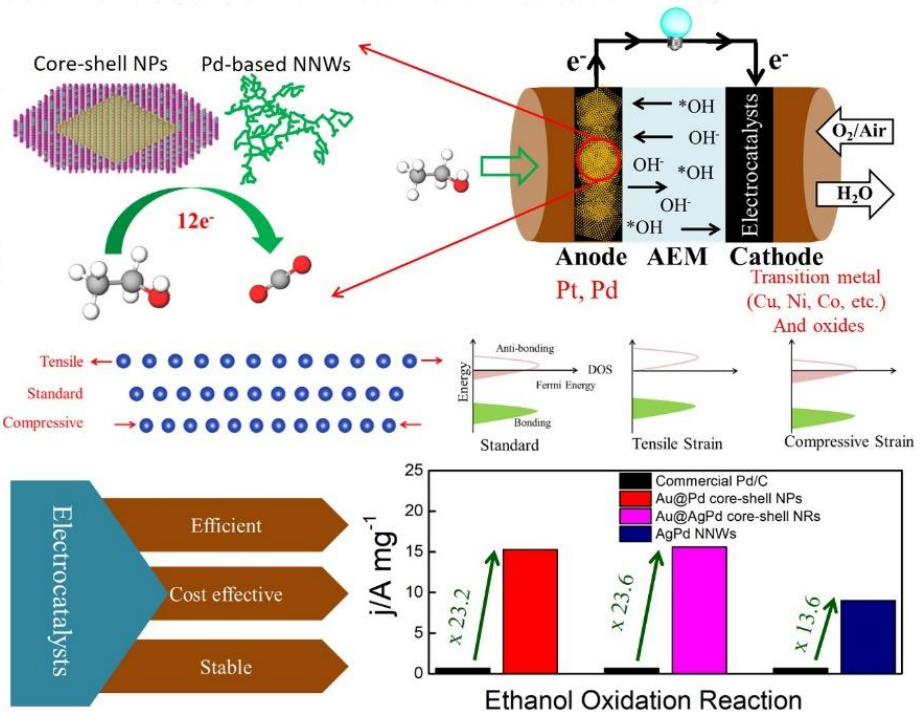

Effect of strain and higher surface-to-volume ratio to boost sluggish alcohol oxidation reaction at the anode of a DAFC

The increasing energy crisis and environmental concerns have intensified the search for efficient, biorenewable energy solutions like Direct Alcohol Fuel Cells (DAFCs). While DAFCs offer high energy density and convenient fuel storage, their commercialization is hindered by the sluggish alcohol oxidation reaction (AOR) at the anode. To address this, we developed Pd-based nanostructures electrocatalysts with enhanced catalytic activity through strain engineering as shown in the Figure. We first designed pentatwinned Au@Pd core-shell nanoparticles (NPs), where the Pd shell was epitaxially grown on pentatwinned Au nanobipyramids. The presence of twin boundaries and lattice mismatch induced tensile strain in the Pd shell, which shifted the Pd d-band center upward, improving AOR kinetics. These Au@Pd NPs demonstrated outstanding electrocatalytic activity towards ethanol oxidation reaction, with mass and specific activities 23.26 and 10 times higher than commercial Pd/C, surpassing most Pd-based electrocatalysts reported in the literature. Building on this, we synthesized Au@AgPd core-shell nanorods (NRs) using a controlled galvanic replacement reaction (GRR). The epitaxial growth of Pd led to Ag diffusion, forming an AgPd alloy that further enhanced catalytic performance. TEM, HRTEM, and XRD confirmed the conformal growth of Pd on the Au@Ag core-shell nanorods, while DFT calculations revealed that tensile strain improved adsorption behavior and reaction kinetics. These Au@AgPd NRs achieved mass activities up to 23 times higher than Pd/C for ethylene glycol, ethanol, and glycerol oxidation reactions. Additionally, we explored strain modulation through alloying, synthesizing AgPd and CuPd nanowire networks (NNWs). AgPd NNWs, under tensile strain, exhibited 13.6 times higher activity for ethanol oxidation reaction than Pd/C, while CuPd NNWs, under compressive strain, showed reduced performance, confirming the role of strain in tuning AOR kinetics.Overall, our work highlights tensile strain engineering and nanostructuring as effective strategies for designing high-performance Pd-based catalysts for next generation DAFCs.

7.9.5 *Study of structure and optical properties of two-dimensional hybrid lead perovskite materials*

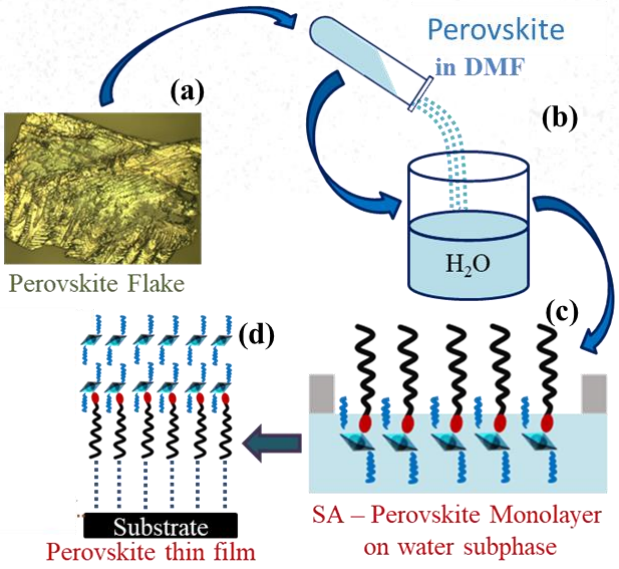

Hybrid perovskite flake (a) is in DMF solution which is mixed with water (b) and spread on water surface (c). Schematic of transfer films (d) contain multilayer structure

Hybrid perovskite is widely used in optoelectronic materials and has a variety of technological applications. The materials science community has recently given this class of materials a lot of attention because of their tunable band gap properties, which are crucial for contemporary optoelectronic applications. Preparation of a molecularly thin perovskite layer is a good opportunity, as a result, one can get exciting optical properties. The availability of halide ions is limited, which makes some restrictions. But there is an unexplored region called Pseudohalides. This is an alternative of halide ion and has great structural stability as well as bandgap variety.

Here in this thesis, two Ruddlesden-Popper phase perovskite flakes, denoted as (BA)2PbBr4 and (BA)2PbCl4, have been synthesized, and using these perovskites mentioned above, another thin film of formate (pseudohalides) perovskite has also been produced on the water surface. The formation of monolayers is revealed using in situ synchrotron x-ray scattering experiments. Both of the two halide perovskites have promising optical properties. Br-containing perovskite displays lasing action without a cavity having blue light emission. On the other hand, Cl-containing perovskites show white light emission. We have developed a technique to prepare a large-scale perovskite preparation on the water surface. The transferred monolayer on Si substrate has good crystallinity and can be used as wide bandgap materials in different technological applications. To comprehend the structure of these perovskites, in-situ XRR, GID, and XRF have been carried out at PETRA-III, while ex-situ XRD, GIWAX, and XRR have been carried out at the Indian beamline at the Photon Factory, Japan. These perovskite monolayers are transferred onto solid substrates, and AFM, TEM, and EDX experiments are carried out. Raman experiments have been performed on these samples to understand the different vibration frequencies of the chemical components of the hybrid perovskite materials. We have also conducted temperature-dependent photoluminescence experiments to understand the optical properties of these perovskite materials.

7.9.6 *Nonlinear waves and chaos in plasmas*

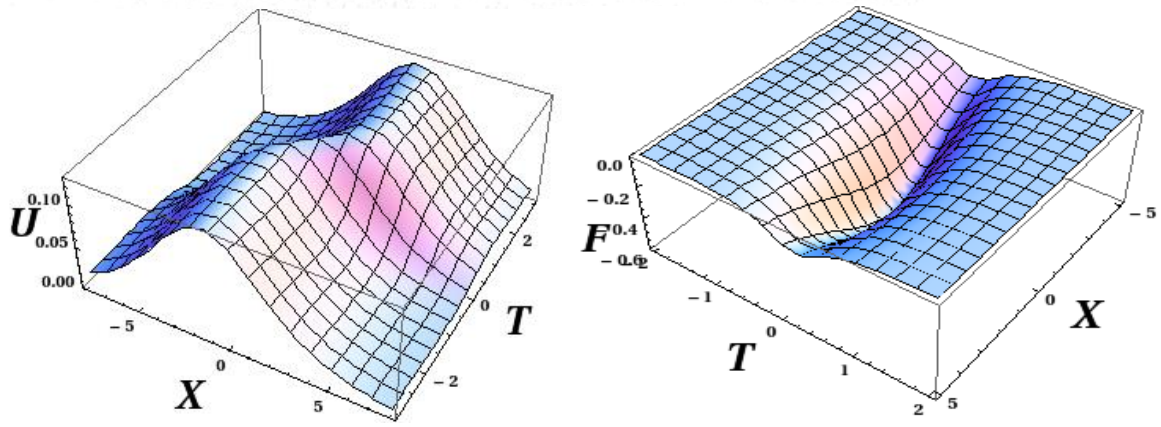

Exact accelerated soliton solution U and forcing function F representing charged space debris objects where the bending nature on X-T plane characterizes the accelerating behavior

The primary objective of this thesis is to investigate characteristic dynamical features of different nonlinear waves in certain plasma systems of intense current research interest. Initially, some interesting exotic solitary wave solutions of forced Korteweg-de Vries equation as well as forced Kadomtsev-Petviashvili equation pertaining to ion acoustic waves and dust-ion acoustic waves in addition to magnetosonic waves have been derived which are excited by orbital charged space debris objects in ionospheric plasma. In particular, these include exact and approximate accelerated solitary wave solutions of forced KdV equation besides one exact accelerated soliton solution for ion acoustic waves, exact accelerated as well as novel curved solitary wave solutions of forced KPII equation for dust-ion acoustic waves; also, exact as well as approximate accelerated lump wave solutions of forced KPI equation and accelerated as well as curved solitary wave solutions of forced KPII equation for magnetosonic waves. These exotic solutions are pinned in nature, i.e. they move with the same velocity as charged space debris objects in ionosphere whose orbital motions are characterized by the nature of forcing functions.

Apart from these debris-induced nonlinear wave excitations, we have also theoretically investigated the experimentally observed phenomenon of excitation of high frequency electrostatic drift waves using a novel nonlinear equation derived from a plasma fluid model for the first time. The theoretical excitations of these high frequency electrostatic drift waves have been explored in detail resulting in a novel dispersion relation for these drift waves. In addition to these nonlinear waves excited in different plasma systems, we have also explored chaotic evolution of nonlinear magnetic fields in flowing magnetohydrodynamic (MHD) plasmas using a set of coupled nonlinear equations of second order originally derived by Lee and Parks [Geophysical Research Letters 19, 7, 637-640, (1992)] without considering external forcing term. This yields a quasi-periodic route to chaos upon variations of the electron-to-ion mass ratio which has been further investigated by employing different nonlinear time series analysis techniques such as phase space, fast Fourier transform, Hurst exponent, correlation dimension etc. Some traces of self-organized criticality (SOC) have also been witnessed in quasi-periodic oscillations of nonlinear magnetic fields as well.

7.10 Variable energy Cyclotron Centre

7.10.1 *Fusion-fission dynamics study of heavy nuclei*

This thesis explores fusion-fission dynamics at excitation energies significantly above the Coulomb barrier, an area largely under-explored in nuclear physics. The primary goal was to assess whether theoretical models developed for near-barrier conditions can accurately predict fission behavior at higher energies, particularly in the context of quasi-fission and fast fission processes.

Two experiments were conducted at the VECC cyclotron facility in India, targeting energy regions with limited prior data. The first experiment focused on fission-fragment mass distributions from reactions like, across excitation energies of 70-110 MeV. The results revealed minimal quasi-fission contributions, challenging existing theoretical predictions and suggesting the need for model refinements. The second experiment, using the VECC K-130

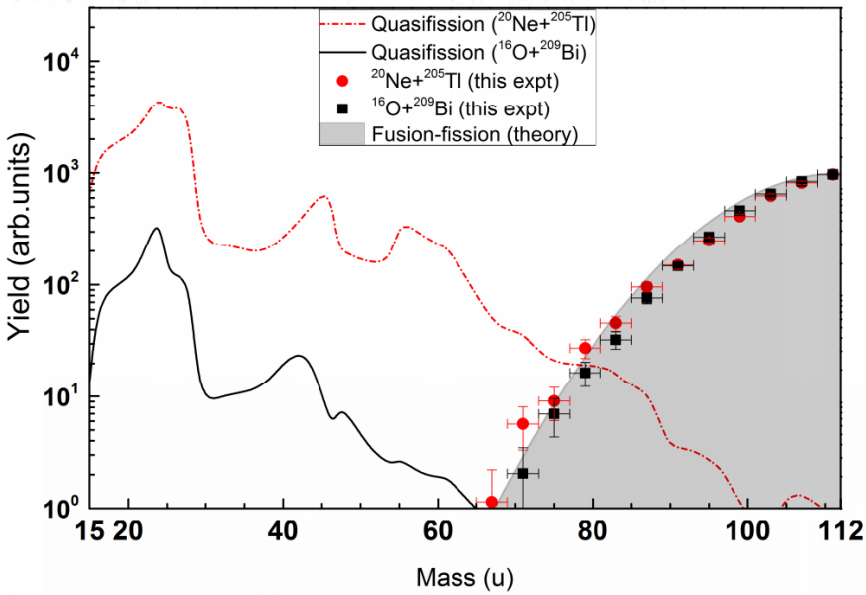

Calculated mass distributions up to the symmetric mass (A_{CN} /2 ≈ 112) at the excitation energy ≈ 83 MeV. The normalised fusion-fission yield (produced in both reactions) is shown by the shaded area and have been compared with the experimental data. The quasifission yields for ^{20}Ne + ^{205}Tl and ^{16}O + ^{209}Bi reactions are shown by dashed (red) and solid (black) lines, respectively

cyclotron, examined reactions like and others, focusing on mass distributions and fast fission dynamics at high excitation energies. The findings showed symmetric, Gaussian mass distributions with increasing variance at higher energies, aligning with statistical model predictions but diverging from semi-empirical calculations. Notably, fast fission events with mass asymmetry of 0.22 were observed, providing new insights into fast fission dynamics. These experiments contribute crucial data to the understanding of fission at high excitation energies, offering benchmark results for refining theoretical models. This work advances the field of nuclear physics, laying the groundwork for future studies of fusion-fission dynamics in previously unexplored energy regions.

7.10.2 *Strongly interacting hot and dense matter in background magnetic field*

Modern physics categorizes particle interactions into four distinct groups: gravitation, electromagnetic, weak, and strong forces. Among these interactions, the Standard Model of particle physics provides a comprehensive framework for describing electromagnetic, weak, and strong interactions, excluding gravitation. Within the Standard Model, Quantum Chromodynamics (QCD) provides a framework for studying the strong interactions between quarks and gluons. The non-Abelian nature of QCD leads to phenomena like asymptotic freedom and confinement, where quarks interact weakly at high momentum transfer (small distances) and become confined within hadrons at lower momentum transfer (larger distances). Exploring QCD under extreme conditions of high temperature and baryon chemical potential offers a valuable opportunity to understand the dynamics of the theory. Under such circumstances, the system is expected to exhibit characteristics akin to a weakly interacting system comprised of quarks and gluons, called quark-gluon plasma (QGP). Such a state can

exist in the early universe and neutron star cores. Additionally, in non-central heavy ion collisions, very strong magnetic fields of the order ~ 1018 Gauss or larger might be generated. Since the strength of these magnetic fields is equivalent to the typical QCD energy scale ($eB \sim \Lambda^2_{QCD}$), various microscopic and bulk properties could be significantly modified.

This thesis is dedicated to the study of the thermodynamic properties of strongly interacting hot and dense matter in presence of background magnetic field (eB) considering finite values of the anomalous magnetic moment (AMM) of the quarks. One of the key findings of this investigation is that the presence of AMM leads to inverse magnetic catalysis (IMC) of the transition temperature from chiral symmetry broken to the restored phase. In contrast the transition temperature increases in absence of AMM, indicating magnetic catalysis (MC). Mass, spectral function and dispersion relations are obtained in the scalar and pseudoscalar channels as well as in the vector and axial vector channels. Moreover, considering finite values of AMM of the quarks, dilepton production from hot, dense and magnetized quark matter is studied. The analytic structure of the spectral function in the complex energy plane has been analyzed in detail revealing a nontrivial Landau cut contribution due to finite magnetic field effects, leading to a significant enhancement in the low invariant mass region of the differential production rate. The general structure of the self-energy at one loop order of a massive fermion is obtained in a magnetized medium considering the finite values of AMM. It is found that the self-energy of a thermo-magnetically modified massive fermion contains five nontrivial structure factors. It is found that presence of AMM modifies the magnetic mass and lifts the degeneracy of doubly degenerate first excited states.

Discipline and CI/ OCC wise details of the students who have been awarded DM, MCh and MD degree during August 01, 2024- July 31, 2025

DM (TMC, Mumbai)

S. No.	Name	Enrolment No.	Specialisation
1	Addagalla Sree Siva Kumar Raja	HLTH09202110061	Medical Oncology
2	Aditya Dhanawat	HLTH09202110007	Medical Oncology
3	Akhil Mahajan	HLTH09202110004	Gestroenterology
4	Amrutha N.	HLTH09202010021	Pediatric Oncology
5	Aneeta J.	HLTH09202110005	Pediatric Oncology
6	Annesha Chakraborti	HLTH09202110049	Pediatric Oncology
7	Anusree Majumder	HLTH09202110020	Onco-Pathology
8	Arvind Vaidyanathan	HLTH09202110010	Medical Oncology
9	Ashok Singhal	HLTH09202110011	Medical Oncology
10	Athira Surendran	HLTH09202110012	Medical Oncology
11	Bhame Suraj Dilip	HLTH09202110002	Interventional Radiology
12	Debdeep Samaddar	HLTH09202110017	Medical Oncology
13	Dharmpal	HLTH09202110013	Medical Oncology
14	Khedkar Rutvij	HLTH09202110021	Onco-Pathology
15	Mili Aggarwal	HLTH09202110048	Pediatric Oncology
16	Noorzia Sultana Syed	HLTH09202110018	Medical Oncology
17	Patel Dhwaniben Jasvantbhai	HLTH09202110014	Medical Oncology
18	Rahul Puri	HLTH09202110003	Gestroenterology
19	Rajput Abhisheksingh	HLTH09202110001	Citical Care Medicine
20	Reshmi J.	HLTH09202110019	Onco-Pathology
21	Ritam Joarder	HLTH09202110015	Medical Oncology
22	Rumeli Roy	HLTH09202110016	Medical Oncology
23	Sandeep Gedela	HLTH09202110047	Medical Oncology
24	Shah Anokhi Anilkumar	HLTH09202110008	Medical Oncology
25	Shah Keyurkumar Bhupendrakumar	HLTH09202110051	Citical Care Medicine
26	Srigadha Vivekkumar	HLTH09202110046	Medical Oncology

MCh (TMC Mumbai)

S. No.	Name	Enrolment No.	Specialisation
1	Abhishek Ganguly	HLTH09202110057	Surgical Oncology
2	Aditya Singh	HLTH09202110058	Surgical Oncology
3	Akshay Kumar Dhaiya	HLTH09202110056	Surgical Oncology
4	Amroskar Shahin	HLTH09202110039	Surgical Oncology
5	Antony Raj James S.	HLTH09202110060	Head & Neck Oncology
6	Anup Srinivas	HLTH09202110059	Head & Neck Oncology
7	Geet Midha	HLTH09202110036	Surgical Oncology
8	Jasmine G.	HLTH09202110037	Surgical Oncology
9	Kanmani M.	HLTH09202110050	Gyneacological Oncology
10	Katyayani Kumari	HLTH09202110033	Surgical Oncology

11	Latika Kansal	HLTH09202110044	Head & Neck Oncology
12	Mandavgane Mayank	HLTH09202110023	Plastic Surgery
13	Meghana V.	HLTH09202010048	Surgical Oncology
14	Meghna Reddy Gumi Reddy	HLTH09202110052	Plastic Surgery
15	N. Bijeta Devi	HLTH09202110022	Gyneacological Oncology
16	Navneet Kaur	HLTH09202110053	Plastic Surgery
17	Patel Dhruv	HLTH09202110040	Surgical Oncology
18	Patil Pooja Ashok	HLTH09202110034	Surgical Oncology
19	Patnala Prem Kamal	HLTH09202110055	Surgical Oncology
20	Peta Pavan	HLTH09202110041	Surgical Oncology
21	Rukmini M.	HLTH09202110045	Head & Neck Oncology
22	Shruti Darak	HLTH09202110024	Plastic Surgery
23	Snigdha Kamini	HLTH09202110030	Surgical Oncology
24	Sree Ganesh	HLTH09202110038	Surgical Oncology
25	Sreekanth T.	HLTH09202110042	Surgical Oncology
26	Sudha Dhiyanesh R.	HLTH09202110054	Surgical Oncology
27	Vadisetti Satya Niharika	HLTH09202110027	Surgical Oncology
28	Vasa Dhaval	HLTH09202110026	Surgical Oncology
29	Vinayaka	HLTH09202110028	Surgical Oncology
30	Y. Aditya V. S. Sai Ram	HLTH09202110032	Surgical Oncology
31	Yelamanchi Raghav	HLTH09202110025	Surgical Oncology

MD (BARC, Mumbai)			
S. No.	**Name**	**Enrolment No.**	**Specialisation**
1	Amal Paul	HLTH01202109005	Nuclear Medicine
2	Austin Saju Mangan	HLTH01202109002	Nuclear Medicine
3	Jadhav Vishwajeet Baburao	HLTH01202109004	Nuclear Medicine
4	Patil Kavita Ashok	HLTH01202109006	Nuclear Medicine
5	Rangat Rameshbhai Bagasariya	HLTH01202109003	Nuclear Medicine
6	Roopal Agrawal	HLTH01202109001	Nuclear Medicine

MD (TMC, Mumbai)			
S. No.	**Name**	**Enrolment No.**	**Specialisation**
1	Adapa Sai Spandhan	HLTH09202109038	Microbiology
2	Adhau Ashwini Ramdas	HLTH09202109014	Radio-Oncology
3	Aditya Mittal	HLTH09202109004	Radio-Oncology
4	Adole Prachi Wasudeo	HLTH09202109015	Radio-Oncology
5	Ajila A.	HLTH09202109039	Medicine Palliative
6	Anagha Ingle	HLTH09202109031	Radio-Diagnosis
7	Archana C. C.	HLTH09202109044	Immuno-Hematology & Blood Transfusion
8	Bari Mansi Madhukar	HLTH09202109028	Radio-Diagnosis

9	Bhandarwar Krishanshu Rajanna	HLTH09202109011	Radio-Oncology
10	Bilala Disha Aashish	HLTH09202109072	Pathology
11	Bodagala Salamma	HLTH09202109043	Immuno-Hematology & Blood Transfusion
12	Deeksha A.	HLTH09202109016	Radio-Diagnosis
13	Deshmukh Arnav Sanjay	HLTH09202109024	Radio-Diagnosis
14	Devika R.	HLTH09202109045	Anaesthesiology
15	Dhele Rudrani Pradeep	HLTH09202109029	Radio-Diagnosis
16	Doshi Jenil Jinesh	HLTH09202109009	Radio-Oncology
17	Gemson George	HLTH09202109035	Nuclear Medicine
18	Gulati Simran Mahendra	HLTH09202109010	Radio-Oncology
19	Hange Akshay Namdeo	HLTH09202109078	Pathology
20	Harshini Victor	HLTH09202109022	Radio-Diagnosis
21	Jose V. Siju	HLTH09202109019	Radio-Diagnosis
22	Kamble Shruti Siddharth	HLTH09202109041	Medicine Palliative
23	Kedar Anurag Rajendra	HLTH09202109061	Anaesthesiology
24	Krishnaveni Krishnakumar	HLTH09202109076	Pathology
25	Kshire Poorval Manoj	HLTH09202109074	Pathology
26	Kumbhare Mugdha Rajeev	HLTH09202109063	Anaesthesiology
27	Lohiya Urvashi Kanhaiya	HLTH09202109062	Anaesthesiology
28	Madhurima Sen	HLTH09202109047	Anaesthesiology
29	Maduri Sivateja	HLTH09202109053	Anaesthesiology
30	Mahambre Siddhi Shreyas	HLTH09202109033	Nuclear Medicine
31	Maitri Manish Shah	HLTH09202109071	Pathology
32	Mansi Dipak Atal	HLTH09202109075	Pathology
33	Masal Harshvardhan Annasaheb	HLTH09202109089	Anaesthesiology
34	Maske Rahul Bhaskar	HLTH09202109036	Nuclear Medicine
35	Monika Narain	HLTH09202109048	Anaesthesiology
36	Mude Parag Prakashrao	HLTH09202109013	Radio-Oncology
37	Musheera Aziz	HLTH09202109073	Pathology
38	Ngasepam Memtombi Devi	HLTH09202109001	Radio-Oncology
39	Nidhi Kulkarni	HLTH09202109049	Anaesthesiology
40	Nithin Krishnan	HLTH09202109018	Radio-Diagnosis
41	Nyayadhish Madhura Avdhut	HLTH09202109027	Radio-Diagnosis
42	P. Sravya	HLTH09202109054	Anaesthesiology
43	Pankhudi Pathak	HLTH09202109020	Radio-Diagnosis
44	Patel Vinisha Harshad	HLTH09202109064	Anaesthesiology
45	Patwardhan Eesha Milind	HLTH09202109059	Anaesthesiology
46	Pranjal Rai	HLTH09202109026	Radio-Diagnosis
47	Radhika Jayan	HLTH09202109069	Pathology
48	Rakhshanda Mashhood Mohd Shafique	HLTH09202109088	Anaesthesiology

49	Ram Aniruth R.	HLTH09202109087	Anaesthesiology
50	Raunak Singh	HLTH09202109080	Radio-Oncology
51	Rishika Rikumar Mody	HLTH09202109008	Radio-Oncology
52	Sabarathinam M.	HLTH09202109091	Pathology
53	Sachin G. S.	HLTH09202109055	Anaesthesiology
54	Sarath M. S.	HLTH09202109005	Radio-Oncology
56	Sarwade Komal Prakash	HLTH09202109084	Immuno-Hematology & Blood Transfusion
57	Satamwar Yogesh Sanjayrao	HLTH09202109037	Nuclear Medicine
58	Satao Mugdha Ashok	HLTH09202109065	Anaesthesiology
59	Saurabh Nandkumar Bhangare	HLTH09202109032	Radio-Diagnosis
60	Shabnam Bano Mohammed Shabbir	HLTH09202109012	Radio-Oncology
61	Shah Isha Jatin	HLTH09202109040	Medicine Palliative
62	Shejule Ankita Kalyan	HLTH09202109030	Radio-Diagnosis
63	Shreya Dhingra	HLTH09202109002	Radio-Oncology
64	Shubham D. Krishan	HLTH09202109046	Anaesthesiology
65	Shweta Khatri	HLTH09202109082	Nuclear Medicine
66	Sinha Amala Sankar Uday Sankar	HLTH09202109056	Anaesthesiology
67	Solanke Swetal Sudhakar	HLTH09202109060	Anaesthesiology
68	Sukriti Patra	HLTH09202109034	Nuclear Medicine
69	Sumona Kundu	HLTH09202109051	Anaesthesiology
70	Swapnil Kumar Singh	HLTH09202109057	Anaesthesiology
71	Swetha M. Nair	HLTH09202109021	Radio-Diagnosis
72	Tanay Sharma	HLTH09202109070	Pathology
73	Tharani M.	HLTH09202109086	Anaesthesiology
74	Unnati Chouksey	HLTH09202109025	Radio-Diagnosis
75	Uppor Subramanya Adiga	HLTH09202109006	Radio-Oncology
76	Vaibhavi Gopal Desikan	HLTH09202109050	Anaesthesiology
77	Vaishali Madhariya	HLTH09202109017	Radio-Diagnosis
78	Vaishnavi Pahwa	HLTH09202109003	Radio-Oncology
79	Varun T. M.	HLTH09202109083	Medicine Palliative
80	Vaze Siddharaaj Shashishekhar	HLTH09202109058	Anaesthesiology
81	Vipul Tripathi	HLTH09202109052	Anaesthesiology
82	Waghmare Ashwini Siddharth	HLTH09202109079	Pathology

Discipline and CI/ OCC wise details of the students who have been awarded M.Tech. degree during August 01, 2024-July 31, 2025

BARC, Mumbai			
S. No.	**Student Name**	**Enrollment No.**	**Title of the thesis**
1	Uppara Pradeep Kumar	ENGG01201901014	Design and Development of Instrumentation and Technique for In-Situ Response Time Estimation for Thermocouples
2	Sreeju H.	ENGG01201901037	Thermal Hydraulic Analysis of Vitrified Waste Product Storage Vault
3	Govind Sharma	ENGG01201901041	Development of Resistance Welding of non-Conventional Shaped Thin Tubes with End Plugs and its Validation: Numerical Simulation and Experiments
4	Mohan Chandra Tiwari	ENGG01202101007	Study, Development and Performance Analysis of Isolated Two Winding Bouncer Scheme for Droop Correction in Hard Switched Modulator
5	Achal Kumar	ENGG01202101019	Development of Clock Synchronization Framework for VME Controller Card
6	Ayush Gupta	ENGG01202101021	Study, Design, and Development of Machine Learning Based Technique for Spam Detection and Analyze its Capability, Limitations, and Suitability in RRCAT Environment
7	Devireddy Naveen Kumar Reddy	ENGG01202201004	Design Optimization of Radiation Source Localization (RSL) System Through Radiation Interaction Simulations using Geant4
8	Ganshyam	ENGG01202201012	Study and Design of Control Scheme for Addition and Control of Moisture Content in Dry Gas Stream for AmO_2 - UO_2 Pellet Stabilization.
9	Rahul Raj	ENGG01202201017	Development of AI Model for Reactivity Estimation Under Stochastic Noise
10	Abhisek Nayak	ENGG01202201028	Study of NoSQL Databases and Development of Data Logging and Visualization Application for Fast Data Acquisition (FDAQ) System of Indus - 2
11	Patil Shubham Rajesh	ENGG01202201047	Study of UO_2-Al Alloy Dispersion Fuel using Finite Element Based Thermal Modelling

12	Chavda Jay Mahendrabhai	ENGG01202201049	Study on Inter-Subchannel Flow Mixing Behavior of Coolant in SMR ROD Bundles
13	Mohit Gupta	ENGG01202201052	Development of Model for Containment Clean Up and Heat Removal
14	Smrity Prakash	ENGG01202201053	Studies on Recovery of Uranium from Simulated HLLW using DHOA in n-dodecane Solvent and CALmsu Contactor
15	Devendra Adhikari	ENGG01202201067	Nonlinear Seismic Analysis of Reinforced Concrete Structure with and without Infill Walls using Simplified Macro-Models
16	Akhand Pratap Singh	ENGG01202201068	Seismic Behaviour of Buildings and Building Foundations Located on Hill Slopes
17	Milansingh Dalipsingh Dhamu	ENGG01202201080	Study of Effect of Welding Parameters on the Mechanical Properties and Oxidation Behaviour of Zr-4 to Zr-2.5Nb Weld
18	Laddha Shlok Kirti	ENGG01202201081	A Study on the Mechanical Stress Relieving in Laser Welded Tubes
19	Bakre Nisarg Prakash	ENGG01202201082	Mathematical Modelling of Coast Down Characteristics of a Canned Motor Pump
20	Jaiswar Shubham Virendra Ranu	ENGG01202201084	Study on Thermo-Physical Properties of Different Fuel Alloys/Compounds as Dispersion in Aluminum Matrix
21	Sabbavarapu Sai Ganesh	ENGG01202201091	Investigating the Effect of Inclusions on Fatigue Behaviour of Cr-Mo-V Pressure Vessel Steel
22	Hitlar	ENGG01202201092	Development of Carbon Fibre Reinforced Boron Carbide Composites
23	Prabhjot Kaur Bhatia	ENGG01202201096	Motion Mapping Between Kinematically Dissimilar Master and Slave Manipulator Arms
24	Bodhisattwa Banik	ENGG01202201105	Friction Stir Processing of Laser-Clad Copper on Commercially Pure Titanium (Grade 2)
25	Albin Mathew	ENGG01202201106	Oxidation Studies of Zr-2.5Nb Alloy in Superheated Steam Relevant to Accidental Condition Under Static Oxidation Testing

26	Saurav Bhattacharya	ENGG01202201107	Experimentation and Modeling of HIx Purification of Iodine Sulphur Thermo-Chemical Process for the Production of Hydrogen
27	Saumyajeet Mukherjee	ENGG01202201108	Dynamic Simulation of Combined Electrolysis and Catalytic Exchange (CECE) Process
28	Dhairyadhar Abhimanyu Bhelave	ENGG01202201110	Computational Modelling and Simulation of Desublimation of PG in Cooled Storage Cylinders
29	Palli Chaitanya Sai Sri Krishna	ENGG01202201116	Studies on Effect of Green Microstructure on Densification of RBSiC Composite
30	Abhijeet Dadarya	ENGG01202201117	Fabrication of U_3Si_2 Pellets by Powder Metallurgy Route and its Characterization
31	Kommula Satwik	ENGG01202201118	Study of the Nanoscale Phase Separation Behaviour in the Fe-Cr-Co System and its Correlation with the Micro Hardness and Magnetic Properties
32	Lokendra Singh	ENGG01202201127	Monte Carlo Simulation of Energy Response of Special Purpose Neutron Survey Meter and its Validation
33	Devashish Gautam	ENGG01202201130	Survival Analysis for Electrical System of a Nuclear Facility
34	Sanjay Kumar	ENGG01202201132	Life Estimation of Light Emitting Diode under Radiation Environment in Nuclear Facility
35	Shreyansh Bharadwaj	ENGG01202201133	Design Optimization of Multi Stage Coil Gun Through Numerical Simulation
36	Suru Gayatri	ENGG01202201135	AI Based Protection System to Enhance Power System Reliability, Security and Efficiency
37	Pritam Panigrahi	ENGG01202201142	Study, Design and Analysis of AI-Based Network Intrusion Detection System (NIDS)
38	Namrata Singh	ENGG01202201143	Real Time Estimation of Rotor Position and Speed Control of Switched Reluctance Motor Using Sensorless Measurement Techniques
39	Shubham Kawde	ENGG01202201144	Development of Image Processing Algorithm for Automated Detection

			and Classification of Defects in Weld Joint of PFBR Fuel Pin
40	Subham Pal	ENGG01202201145	User Internet Browsing Behaviour Analytics
41	Dheeraj Kumar	ENGG1A202201014	Design and Development of Remotely Operated Battery Powered 150kV Pulsed Power Supply
42	Immella Eswara Manikanta	ENGG1A202201016	Parametric Analysis, Design, Modelling and Simulation of a High Voltage DC Power Source with Optimum Performance Parameters for EBW Machine in Zircaloy Fabrication Process
43	Saunak Mondal	ENGG01202101005	Development of Algorithms Used for the Protection of Alternator of Emergency Diesel Generator (EDG) in NPP and Their Hardware Implementation
44	Tasleem Siddiki	ENGG01202201018	Design and Development of Control System for Mecanum and Tracked Wheels Mobile Vehicle for Remote Inspection
45	Dhivahar Chezhian	ENGG01202201059	Use of Small Punch Test Technique for Evaluating the Ductile to Brittle Transition Temperature of Irradiated Fe-3.5 wt. % Ni Steel
46	Kathirvelan R.	ENGG01202201064	Studies on Microstructure and Mechanical Properties of Tungsten Inert Gas Welded Alloy 740H
47	Aakash Rajesh	ENGG01202201079	Microstructure Characterisation and Low Cycle Fatigue Behaviour of Ti-4Al-2V Alloy
48	Sumer Singh Choudhary	ENGG01202201085	Heat Transfer Studies for Development and Optimization of a Molten Salt Heat Exchanger
49	Sanyam Singhai	ENGG01202201087	Experimental Studies and Analysis of the Transients in Natural Circulation Based Parallel Channel System
50	Patel Pratikkumar Kanaiyalal	ENGG01202201088	Design of an Electrically Heated Fuel Bundle Simulator for Supercritical Water Nuclear Reactor Studies
51	Vaibhav Vashishth	ENGG01202201094	Numerical Simulation of Cooling of RSW Glass Slabs Under Different Conditions

52	Manan Gulati	ENGG01202201099	Design and Analysis of LN_2 based Refrigeration System for Special Articles with Provision for Dehumidification
53	Agni Shekhar	ENGG01202201114	Development of Process Scheme for Sr-90 Recovery from High Level Waste and Preparation of Sr-90 Heat Source
54	Deepak Patel	ENGG01202201115	Development of Signal Analysis Methodology for Improved Assessment of Subassembly Protrusion by Under Sodium Ultrasonic Imaging in PFBR
55	Himanshu Melkani	ENGG01202201123	Performance based Seismic Design of Steel Structure
56	Ankush Ghosh	ENGG01202201134	Analysis, Design and Development of Fast Ramp, Bipolar Current Controlled Scanning Magnet Power Supply
57	Kartik Arvind Gajera	ENGG01202201137	Design and Development of Fast Actuation System for Safety Interlocks of 10 MeV,15 kW LINAC
58	Anand Kumar	ENGG01202201141	Development of Fast Beam Parameter Measurement and Beam Loss Detection System for LINAC
59	Annu Nain	ENGG1A202201023	Numerical Modelling and Optimization of $H_2{}^{18}O$ Production Plant Based on Water Distillation Process
BARCTS (AMD), Hyderabad			
60	Rounak Datta Roy	ENGG1G202201001	Litho-Structural and Sedimentological Studies of Uraniferous Phosphatic Sediments of Jhamarkotra Formation in Kirauli Area, Udaipur and Rajsamand Districts, Rajasthan with Special Emphasis on Control of Uranium Mineralization.
61	Raghvendra Shukla	ENGG1G202201002	Characterisation of Hydrothermal Alteration Zones in the Deformed Horizons of the Shahabad Limestone and Basement Granite with its Implications on the Uranium Mineralisation in Kanchankayi
62	Smrutiranjan Sahoo	ENGG1G202201003	Litho-Tectonic and Geochemical Characterization of Lithounits in the

			Vicinity of Tan Shear Zone from Uran-Barbhata- Barimundra- Barbahari Area, GPM & Korba District, Chhattisgarh: Inference on Genesis of Uranium Mineralization
63	Abhishek Chaurasiya	ENGG1G202201004	Geochemical Characterisation of Aegirine/Riebeckite Bearing Granite and Rhyolite and their Potentialities for REE-Nb-Zr Mineralisation in Gugrot Area, Siwana Ring Complex, Barmer District Rajasthan
64	Bulu Chandra Mahanta	ENGG1G202201005	Study on Provenance and Paleodepositional Setting of Manikaran Quartzite Vis-a-Vis Genesis of Uranium Mineralisation in Bradha Sangchan Tract, Kullu District, Himachal Pradesh
65	Abhishek Kumar Yadav	ENGG1G202201006	Sedimentological and Geochemical Study of Basal Siliciclastics of Dhanjori Basin and their U-AU Potential Along Phuljhari-Haludbani Tract, East Singhbhum District, Jharkhand
66	Bitihotri Rit	ENGG1G202201007	Structural and Petro Mineralogical Studies of Granite Related Uranium Mineralisation in the Southern Margin of Cuddapah Basin at Rachakuntapalle Area, YSR District, Andhra Pradesh
67	Ajay Haridas	ENGG1G202201008	A Geochemical Study to Understand the Hydrothermal System Responsible for U-REE Mineralization in Bagjata and Pathargora Areas, East Singhbhum District, Jharkhand
68	Arindam Gope	ENGG1G202201009	Facies Architecture and Depositional Environment of Uranium-Bearing Sediments of Kaimur Group of Vindhyan Basin Along Maharampura-Rajgarh Sector, Gwalior and Shivpuri District, Madhya Pradesh
69	Mukunda Madhab Borah	ENGG1G202201010	Study on the Occurences of Uraniuma and REE Phases in Abilities of Ghasipura -Rayan Ka Bas Area, Sikar District, Rajasthan: An Integrated Approach Through Geological,

			Mineralogical and Geochemical Studies
70	Ashish Mahanta	ENGG1G202201011	Study of Control of Uranium Mineralisation Based on Petrography and Geochemistry of Mineralised Granite from Chundi and its Adjoining Area, Garhwa District, Jharkhand
71	Vivek Kumar Yadav	ENGG1G202201012	Structural, Petro-Mineralogical and Geochemical Studies of Mylonite/Cataclasite Zone with Special Emphasis on Uranium Mineralization in B.R. Palle-Katimayakuntamadhavaram Area, Annamayya District, Andhra Pradesh
72	Sandip Choudhuri	ENGG1G202201013	Constraints on Uranium Mineralization in Migmatitic Terrain of Chhotanagpur Granite Gneiss Complex (CGGC) at Kudar Area, Sonbhadra District, Uttar Pradesh: A Mineralogica
73	Kunal Maharana	ENGG1G202201014	Study of Effect of Alteration on Unconformity and Fracture-Controlled Uranium Mineralisation in Madinapadu-Sarangapallitangeda Sector, Palnadu District, Andhra Pradesh
74	Chetan Eknath Kinkar	ENGG1G202201015	Provenance and Depositional Environments of Red Sediments of Badaputi- Basanputi Area, Ganjam District, Odisha- A Granulometric and Heavy Mineral Study with Geochemical Approach.
75	Shriya Mishra	ENGG1G202201016	Petro-Mineralogical and Mineral-Chemical Studies of U and REE Minerals in Mohuldih Deposit, Singhbhum Shear Zone, Seraikelakharsawan District, Jharkhan
76	Ayush Kumar	ENGG1G202201017	Petro-Mineralogical and Geochemical Studies of Sandstones and Mudstones and its Implication on Uranium Mineralisation in Motur Formation of Kalapani-Dharangmau Area, Betul District, Madhya Pradesh
BARCTS (NFC), Hyderabad			

77	Sanket Hegde	ENGG1A202201009	Studies on the Performance of Carbon Coatings as an Effective Barrier Against Pellet-Clad Interaction
78	Rapaka Nilesh	ENGG1A202201006	Studies on Design and Development of High Voltage Pulse Power Supply
IGCAR, Kalpakkam			
79	Mohanish Goel	ENGG02201901002	Study of Performance Characteristics of Hydrodynamic Bearing
80	Tarkesh Singh	ENGG02202101008	Effect of Directional Loading (Unequal) in Estimating Low Cycle Fatigue Life as per RCC-MRx
81	Bechra Jeet Pravinbhai	ENGG02202101010	Process Development for the Treatment of Ring Material ($MgCl_2$ + Mg + Zr) Generated in Zirconium Sponge Plant
82	Amit Prajapati	ENGG02202101019	Computational Model Development for Molten Corium Concrete Interaction
83	Netraj Vyankatesh Surnis	ENGG02202201004	Design, Analysis and Simulation of Tracked Mobile Robot
84	Rishabh Kumar	ENGG02202201006	Study of Effects of Transients on PFBR Fuel Pin Life
85	Sabarish R.	ENGG02202201007	Process Design of Sparger Type Contractor for Maximum Recovery of Actinides from Molten Salt Liquid Cd-Li Alloy
86	Debrup Paul	ENGG02202201030	Cesium Adsorption Studies on Zeolite for Molten Salt Treatment in Pyroprocessing
87	Neeraj Saini	ENGG02202201020	Slicing Strategy for Laser Additive Manufacturing Using Directed Energy Deposition of Tubular Bends
IPR, Gandhinagar			
88	Ayush	ENGG06202201001	A Novel Design of Ohmic Transformer Power Supply (OTPS) for Spherical Tokamaks
89	Aditya Naugraiya	ENGG06202201002	Electrostatic Field Analysis of High Voltage Ion Extraction and Acceleration Grid System for Neutral Beam Injectors

90	Vishal Verma	ENGG06202201006	Dynamic Analysis of Soft Catch for Electromagnetic Launcher System using ANSYS
91	Ayush Bhatt	ENGG06202201007	Development of Calorimeter for the Positive Neutral Beam System
92	Manish Tak	ENGG06202201008	Analytical and Simulation Study of Windowless Gas Target System for Neutronics Applications
93	Purvkumar Bachubhai Hansapura	ENGG06202201010	Signal Conditioning System for Cryogenic Temperature Measurement for NBI
94	Prashant Kumar	ENGG06202201004	Automated Control of Helicon Plasma Thruster System
95	Meddi Tharun	ENGG06202201009	Design of Modular Multilevel Converter based Power Supply for Accelerator Application
96	Jonnada Jayaram	ENGG06202201011	Development of Feedback Control System for Delta Robot
RRCAT, Indore			
97	Avantika Gautam	ENGG03202101001	Studies on Co Oxidation Catalyst and Theoretical Understanding of Gas Discharge Towards Development of Sealed-Off CO_2 Laser
98	Gaurav Yadav	ENGG03202101002	Experiments and Analysis on the Enhancement of Strain Sensitivity of Fiber Bragg Grating Sensor
99	Sachin Raturi	ENGG03202101003	Numercal studies on Tuning of a 325 MHz Drift Tube LINAC in Simlulation Environment
100	Krishnapada Maity	ENGG03202101004	Impact of Defects and Dislocations in GaN Epitaxial Layers on the Performance of Visible-Blind Ultraviolet Photodetectors
101	Ashwin Chalisgaonkar	ENGG03202101007	Development of Digital Control and Data Acquisition System for Pulsed Hydrogen Ion Source
102	Pokharkar Rahul Rohidas	ENGG03202101008	Studies on Modular Fast-Ramped, Switch-Mode Power Converters Energizing Series String of Electromagnets
103	Deeksha Vyas	ENGG03202101011	Design Studies and Development of RF Components for Solid State Amplifier

104	Deepak	ENGG03202201001	Design and Optimization of Fundamental Power Coupler for Superconducting Cavity
105	Shivangi Bidoliya	ENGG03202201002	Laser Driven Proton Acceleration with Controlled Preplasma Scale-Length and Development of Transport System Based on Magnetic Field Devices
106	Divyansh Pandey	ENGG03202201003	Physics Design Studies of Doubly Achromatic Energy Filtering systems of Electron LINACs for Different Applications
107	Kavita Bhatt	ENGG03202201004	Preliminary Studies on Candidate Double-Bend Achromat Structure for Low Emittance Booster Synchrotron of High Brilliance Synchrotron Radiation Source
108	Subhash Kesharwani	ENGG03202201009	Development Control, Protection and Automation Scheme for 132 kV Substation
109	Piyush Kumar	ENGG03202201011	Study, Design and Development of Digital Close Loop Control for Pulsed Nd:YAG Laser Power Supply
110	Ashok Kumar Sahoo	ENGG03202201012	Investigation and development of Raman Optical Fiber Distributed Temperature Sensor with Enhanced Features
111	Bonagiri Bhanuprakash	ENGG03202201013	Design and Development of Digitally Controlled Pulse Width Modulated Rectifier for Reduced Line Current Harmonic Pollution and 2-Way Utility Interface
112	Niklesh Kashyap	ENGG03202201014	Study and Investigation of Dynamic Control of Superconducting RF Cavity Resonance using Piezo Actuators Based Tuner
113	Tushar Dave	ENGG03202101005	Design and Development of a Single Cell S Band Pre-Buncher
114	Arkaprabha Bhowmik	ENGG03202201008	Assembly and Characterization of BF_3 based Multitube Position Sensitive Detector for Thermal Neutrons
115	Shivam Tiwari	ENGG03202201015	Studies on High Energy Laser Amplification in a 12 Disc Nd:Glass Amplifier

116	Venus	ENGG03202201018	Thermal Management in Semiconductor Laser Diode Arrays for High Power Applications
117	Bhawani Shankar	ENGG03202201019	Design and Development of an S-Band Pulsed 360° Phase Detection System for RRCAT FEL Facilities
118	Shivam Gupta	ENGG03202201020	Simulation and Optimization of Different Test Parameters for High Power RF Coupler Test Bench

HBNI Ranked 6 in Research Institution Category

HBNI Ranked 16 in University Category

HBNI Ranked 27 in Overall Category

Homi Bhabha National Institute
(HBNI)

Bhabha Atomic Research Centre
(BARC)

Indira Gandhi Centre for Atomic
Research (IGCAR)

Raja Ramanna Centre for
Advanced Technology (RRCAT)

Variable Energy Cyclotron Centre
(VECC)

Institute of Mathematical Sciences
(IMSc)

होमी भाभा राष्ट्रीय संस्थान
HOMI BHABHA NATIONAL INSTITUTE

Saha Institute of Nuclear Physics
(SINP)

Harish-Chandra Research Institute
(HRI)

Institute of Physics
(IoP)

होमी भाभा राष्ट्रीय संस्थान
Homi Bhabha National Institute

(An aided Institute of the Department of Atomic Energy and a Deemed to be University u/s 3 of UGC Act 1956)

www.hbni.ac.in

Institute for Plasma Research
(IPR)

Tata Memorial Centre
(TMC)

Mahamana Pandit Madan Mohan Malaviya
Cancer Centre & Homi Bhabha Cancer
Hospital (MPMMCC & HBCH)

National Institute of Science
Education and Research
(NISER)

Homi Bhabha Cancer Hospital &
Research Centre,
(HBCH & RC)

होमी भाभा राष्ट्रीय संस्थान
Homi Bhabha National Institute

ट्रेनिंग स्कूल परिसर /Training School Complex

अणुशक्तिनगर, मुंबई- 400094 / Anushaktinagar, Mumbai- 400094

www.hbni.ac.in / Email: offhbni@hbni.ac.in,

Phone No: 022-25597699, 022-25597625